INTERACTION OF FLAVONOIDS AND MITOXANTRONE WITH TETRAHYMENA G-QUADRUPLEX DNA SEQUENCE

Ph.D. THESIS

by

PRADEEP. T. P

DEPARTMENT OF BIOTECHNOLOGY
INDIAN INSTITUTE OF TECHNOLOGY ROORKEE
ROORKEE-247 667 (INDIA)
DECEMBER, 2014

INTERACTION OF FLAVONOIDS AND MITOXANTRONE WITH TETRAHYMENA G-QUADRUPLEX DNA SEQUENCE

A THESIS

Submitted in partial fulfilment of the

requirements for the award of the degree

of

DOCTOR OF PHILOSOPHY

in

BIOTECHNOLOGY

by

PRADEEP. T. P

DEPARTMENT OF BIOTECHNOLOGY
INDIAN INSTITUTE OF TECHNOLOGY ROORKEE
ROORKEE-247 667 (INDIA)
DECEMBER, 2014

INDIAN INSTITUTE OF TECHNOLOGY ROORKEE
ROORKEE

CANDIDATE'S DECLARATION

I hereby certify that the work which is being presented in the thesis entitled **"INTERACTION OF FLAVONOIDS AND MITOXANTRONE WITH TETRAHYMENA G-QUADRUPLEX DNA SEQUENCE"** is in partial fulfilment of the requirements for the award of the Degree of Doctor of Philosophy and submitted in the Department of Biotechnology of the Indian Institute of Technology Roorkee, Roorkee is an authentic record of my own work carried out during a period from July, 2009 to December, 2014 under the supervision of Dr. Ritu Barthwal, Professor, Department of Biotechnology, Indian Institute of Technology Roorkee, Roorkee.

The matter presented in this thesis has not been submitted by me for the award of any other degree of this or any other Institute.

(PRADEEP. T. P)

This is to certify that the above statement made by the candidate is correct to the best of my knowledge.

Dated: December, 2014

(RITU BARTHWAL)
Supervisor

Table of Contents

ABSTRACT

Telomeres are nucleoprotein regions found in the terminal ends of eukaryotic chromosomes. Their function is to stabilize and protect the ends of the chromosomes from degradation. In almost all eukaryotes, the telomeric repeat contains runs of Guanine bases. Some examples include the ciliates *Tetrahymena*, TTGGGG, and *Oxytricha nova*, TTTTGGGG; the plant, *Arabidopsis*, TTTAGGG; and the vertebrate repeat, TTAGGG. This G-rich telomeric overhang readily forms G-quadruplex structures; the basic unit of which is the G-quartet, a planar array of four guanines. DNA structures stabilized by G-quartets are variously referred to as G-quadruplex, G-tetraplex or G4 DNA. With each cell division some of the DNA is lost from the ends of chromosomes (telomere region) due to end replication problem. When telomeres reach a critical minimum length, cells cannot divide and cellular senescence and apoptosis is induced. Telomerase is a ribonucleoprotein complex, which preserves telomere length in stem cells, germ cells, and cancer cells by adding hexameric (TTAGGG) repeats to the ends of chromosomes. As stem cells, germ cells, cancer cells express the telomerase activity; adult somatic cells lack this enzyme. About 90% of cancer cells contain short telomeres, but exhibit high telomerase activity. Hence telomerase inhibition is a strategy to prevent cancer development and progression. There are several strategies to inhibit the activity of telomerase enzyme; an important one among them is stabilization of G-Quadruplex DNA structures, which act as substrate for the telomerase enzyme. Majority of the known G-quadruplex stabilizing ligands have an extended planar aromatic ring system and stack effectively on planar G-tetrad via π-π interaction.

In the present work we have carried out studies on the interaction of anticancer drug Mitoxantrone (MTX), flavonoids, Rutin and Quercetin, with *Tetrahymena* G-quadruplex DNA sequence which forms a tetramolecular parallel structure, by various biophysical techniques. Structures of these three compounds complexed to G-quadruplex d-$(TTGGGGT)_4$ have been determined using 2D NMR techniques followed by restrained Molecular Dynamics (rMD) simulations. The biological activity of these three compounds have been determined by 1-(4, 5-Dimethylthiazol-2-yl)-3, 5-diphenyl formazan (MTT) assay, Telomere Repeat Amplification Protocol (TRAP) assay.

The thesis is divided into six chapters. Chapter 1 gives the introduction about telomeres in general, G-quadruplex structures, telomerase and its relationship to cancer. It also explains the strategies involved in the inhibition of telomerase enzyme, in particular, by stabilizing the G-quadruplex

structures. The detailed literature survey of structural and functional aspects of ligands used to stabilize the G4 DNA structures is also discussed.

Chapter 2 gives the detailed materials and methodologies used in the present work, that is, UV-Visible Absorption, Fluorescence and Circular Dichroism (CD) spectroscopy as well as Surface Plasmon Resonance (SPR). The pulse programs of one and two dimensional Nuclear Magnetic Resonance (NMR) spectroscopy experiments and the steps for restrained Molecular Dynamics (rMD) simulations are also described. The procedure used to calculate binding constants and stoichiometry from the spectroscopic data, protocols for the, MTT, TRAP, PCR stop assays are also given in this chapter.

Chapter 3 describes the spectroscopic studies of interaction of flavonoids rutin, quercetin and mitoxantrone with G-quadruplex sequence d-$(TTGGGGT)_4$. Addition of increasing amounts of d-$(TTGGGGT)_4$ to MTX leads to the change in the absorbance spectra of the MTX molecule. The absorbance maximum of 659 nm of monomer MTX peak shifts towards the longer wavelength, 674 nm, upon binding to quadruplex DNA. At higher D/N ratios, the absorption maxima also show 50 % hypochromism. The Fluorescence emission spectra shows red shift of 12 nm, binding constant of $4.1x10^5$ M^{-1} and number of binding sites n = 2.4 . Job plot method of continuous variation analysis gives the inflection point at 0.66 and at 0.8 confirming thereby that two drug molecules bind to DNA. The CD results show that quadruplex structure is stabilized upon interaction with MTX. The Surface Plasmon Resonance (SPR) experiments yield dissociation constant of $8.75x10^{-5}$ M for the interaction of MTX with d-$(TTGGGGT)_4$.

Chapter 4 describes the detailed NMR study of binding of MTX with G-quadruplex DNA sequence d-$(TTGGGGT)_4$. A combination of both one dimensional ^1H and ^{31}P experiments along with two dimensional NOESY (τ_m = 100, 200, 250 ms), COSY, ^1H- ^{13}C HSQC, ^1H- ^{31}P HMBC experiments has been used to assign resonances of uncomplexed and complexed d-$(TTGGGGT)_4$ with MTX. The titration of MTX to quadruplex DNA d-$(TTGGGGT)_4$ results in the broadening of the proton resonances of T7 H6, G6 H8 and NH resonances upto D/N ratio 1.0, which get sharpened on further increase of D/N ratio to 2.0. The chemical shift data show upfield shift ~ 0.14-0.23 ppm in all G NH resonances. The aromatic ring proton 2/3H of MTX shifts upfield by 0.4 ppm, while alkylamine side chain protons of 13 CH_2 and 14 CH_2 shift by 0.11 ppm. Analysis of the NOESY spectra of MTX-d-$(TTGGGGT)_4$ complex at D/N ratio 2.0 shows existence of 35 intermolecular NOE cross peaks

between drug and DNA protons and 14 intra/inter molecular cross peaks within drug protons. The observed intermolecular peaks show proximity of MTX with terminal bases T1, T2 and G6, T7. The melting experiments show that G3 and G6 NH resonances disappear at 338 K in uncomplexed d-$(TTGGGGT)_4$, whereas in 2:1 complex, the G3 and G6 NH resonances are visible even at 363 K. The ^{31}P experiments shift upfiled by 0.146 and 0.125 ppm at G5pG6 and G6pT7 steps, respectively. The observed NOE restraints have been used to get the structure of complex.

Chapter 5 describes the NMR study of interaction of flavonoid quercetin with quadruplex DNA sequence d-$(TTGGGGT)_4$. Titration of quercetin with d-$(TTGGGGT)_4$ results in upfield shift of proton resonances. The NH resonances of all G tetrad forming Guanine residues show small upfield shift by 0.02 ppm. The melting studies show that d-$(TTGGGGT)_4$ gets stabilized upon complexation with quercetin. The intermolecular NOEs are observed between aromatic H2' and H6' of quercetin with T2 and G3 residues. The observed NOE restraints have been used to build the model of complex.

Chapter 6 describes the detailed NMR study of binding of flavonoid rutin with G-quadruplex DNA sequence d-$(TTGGGGT)_4$. Titration of rutin to d-$(TTGGGGT)_4$ G-quadruplex sequence results in shift of quadruplex resonances; all G NH proton resonances shift upfield, G6 NH shows maximum shift of 0.15 ppm and T7H6 shifts downfield by 0.20 ppm. The results of ^{31}P experiments suggest binding of rutin at G6pT7 step, which shows maximum downfield shift of 0.21 ppm. The two dimensional NOESY spectra show eight intermolecular cross peaks in 1:1 ruitn-d-$(TTGGGGT)_4$ complex, all of them being with G6 and T7 bases. The important intermolecular contacts are H6, H8, H6', H2 of rutin with G6 NH; H6' and H2' of rutin with G6 H1'. All rutin proton resonances shift upfield, maximum shift of 0.69 ppm observed for H6 proton. The melting studies show that d-$(TTGGGGT)_4$ gets stabilized upon complexation with rutin.

In conclusion, the present study shows that anticancer drug MTX, and naturally occurring flavonoids, rutin and quercetin interact with d-$(TTGGGGT)_4$ quadruplex sequence and stabilize it. Results of TRAP assay show, dose dependent inhibition of telomerase enzyme. The present results have major implications on the understanding of binding mode of G-quadruplex ligands and development of effective anticancer agents based on the strategy of stabilizing of G-quadruplex DNA sequence, there by inhibiting telomerase enzyme.

ACKNOWLEDGEMENTS

The pursuit of the Ph.D. degree has been a truly inspiring challenge for me and this thesis is the beginning of my journey as a professional researcher. During this five and half years, many people provided great help and contributed to the research. Here, I would like to thank all of them for helping me throughout these years.

First and foremost, I am grateful to my parents, for their endless love, moral support and encouragement. As we say home is the first school and parents are the first teachers, they taught me how to love the way of life and try to be a human in difficult situation. For an atheist like me, who doesnot believe in extra inhuman power, they are the only ray of hope in difficult situations in life. Without their love and care, I would not be who I am today. This thesis is dedicated to them, thank you Amma and Appa.

I would like to thank my advisor, Dr. Ritu Barthwal, Professor, Department of Biotechnology who not only taught me the necessary skills and showed me the way of critical thinking, and more importantly, taught me how to be a good academic researcher and how to communicate with people professionally. I am indebted to her for providing an opportunity to work in the 500 MHz NMR machine and other facilities at Central NMR facility, IIT Roorkee.

I thank Dr. R Prasad, Professor and Head, Department of Biotechnology for providing an opportunity to work in the department. I am also thankful to Prof. A.N. Tripathi, Prof. Petar M Mitrasinovic and Dr. Maya S. Nair for providing valuable suggestions during my initial days of Ph.D.

I take this chance to thank the Dr. Bhavani Shankar Joshi, Senior application scientist, Bruker India Pvt. Ltd., who has helped in setting NMR experiments smoothly.

I would also like to thank my SRC committee members, Prof. G. S Randhawa, Dr. A. K. Sharma and Prof. M. Malanath for their valuable suggestion during this work. I also thank Dr. Krishna Mohan Poluri for providing moral support and valuable help in preparation of thesis.

I take this opportunity to thank my good friends Sweta, Megha, Parmesh, Tapas, Padma, Tamogna, Selva, Bibekanad, Prabhat and all my MCC friends for their fun and support during my stay in Roorkee, without them it is impossible to complete this thesis.

I would thank my previous and present lab members Dr. Amit Kumar, Dr. Lata Chauan, Dr. Asif Hassan, Shilpa, Sweta Tripathi, Dhruv, Amit, Harshita, Padma, Poornima, Bharat, Ashish, Zia Tariq, Shailja…. And graduate and post graduate dissertation students Saurabh Bansal, Ashish Mittal, Rohit Kumar, Peeyush, Prashanth,Vishwa Prakash, Santhik, Kiran, Rohit, Kamala, Deepesh and Virender for their assistance in lab.

Finally, I would like acknowledge the University Grants Commission, Government of India for providing the funding to support my research.

22nd December 2014
Roorkee **(PRADEEP. T.P)**

List of publications

1. Research Papers

1. Mitrasinovic P M, **Palakshan. P T**, Tripathi. S and Tripathi. AN.

   On the affinity and specificity of quercetin to DNA. *Med Chem*. 2013 Mar; 9(2):193-202. Pubmed ID: 22779797.

2. Dogra. S, Awasthi. P, Tripathi. S, **Pradeep. TP**, Nair. MS and Barthwal. R.

   NMR-based structure of anticancer drug mitoxantrone stacked with terminal base pair of DNA hexamer sequence d-$(ATCGAT)_2$. *J Biomol Struct Dyn*. 2014 Jul; 32(7): 1164-83. Pubmed ID: 23808712.

3. Dogra. S, Awasthi. P, Tripathi. S, **Pradeep. TP** and Barthwal. R.

   Multispectroscopic methods reveal interaction of anticancer drug mitoxantrone with DNA henanucleotide sequence d-$(ATCGAT)_2$. (Communicated to *Spectrochimica Acta. A Molecular and Biomolecular Spectroscopy).*

4. **Pradeep T Palakshan**, Sweta Tripathi and Ritu Barthwal.

   Spectroscopic study on the binding of anti tumor anthraquinone drug, mitoxantrone with parallel $(TTGGGGT)_4$ G-Quadruplex DNA. (To be communicated).

5. **Pradeep T Palakshan**, Sweta Tripathi and Ritu Barthwal.

   Solution structure of anti-tumor drug Mitoxantrone - $(TTGGGGT)_4$ G-Quadruplex DNA. (To be communicated).

6. **Pradeep T Palakshan**, Sweta Tripathi and Ritu Bartrthwal.

   Structural studies of flavonol quercetin and flavonol glycoside, rutin with tetramolecular Quadruplex DNA. (To be communicated)

2. Papers in Conference and workshops:

1. **Pradeep T Palakshan**; Sweta Tripathi; Ritu Barthwal. Mitoxantrone inhibits telomerase enzyme by forming stable complex with G-quadruplex d-$(TTGGGGT)_4$. International Conference on Magnetic Resonance in Biological Systems (ICMRBS) XXVI, Dallas, Texas, USA. 24- 29th August 2014.
2. **Pradeep T Palakshan**; Sweta Tripathi; Ritu Barthwal.Stabilization of human G-quadruplex DNA by anticancer drug mitoxantrone leads to inhibition of telomerase enzyme. International Biophysics Conference by International Union for Pure and Applied Biophysics (IUPAB). Brisbance, Australia. 3-7th August 2014.
3. Ritu Barthwal**,** Rahul Yadav, Sweta Tripathi, **Tarikere Palakashan Pradeep**. NMR based structure of berberine bound to parallel stranded DNA quadruplex d-$(TTAGGGT)_4$ containing human telomeric repeat. Albany 2013, The 18th Conversation, State University of New York, SUNY at Albany, New York, USA, 11-15th June 2013.
4. **Pradeep T. P**, Sweta Tripathi, Maya S. Nair and Ritu Barthwal. Interaction of flavonoid, rutin with telomeric G-quadruplex sequence d-$(TTGGGGT)_4$, Symposium on New Developments in NMR and Conference of the National Magnetic Resonance Society (NMRS- 2012), Bangalore, February 5-8th 2012.
5. Sweta Tripathi, **Pradeep T.P**, Maya.S. Nair and Ritu Barthwal. Interaction of flavone, luteolin with Parallel stranded G-quadruplex sequence d-$(TTGGGGT)_4$, Symposium on New Developments in NMR and Conference of the National Magnetic Resonance Society (NMRS-2012), Bangalore, February 5-8th 2012.
6. **Pradeep T.P**, Amit Kumar, Nair Maya S, Ritu Barthwal. Spectroscopic studies of interaction of flavonoids, quercetin and rutin, with human telomeric d-$(TTAGGGT)_4$ quadruplex DNA, 7th Asian Biophysics Association (ABA) Symposium and Annual Meeting of the Indian Biophysical Society (IBS), New Delhi, 30th January – 2nd February 2011.
7. Sweta Tripathi, **Pradeep T.P**, Sayed Asif Hassan, Nair Maya S, Ritu Barthwal. Binding of Berberrubine Dimer To Minor Groove Of Promoter Sequence d$(CCAATTGG)_2$, 7th Asian Biophysics Association (ABA) Symposium and Annual Meeting of the Indian Biophysical Society (IBS), New Delhi, 30th January – 2nd February 2011.

Chapter 1

INTRODUCTION

1.1 Structure of Nucleic acids

1.1.1 Nucleic acids

Nucleic acids are the fundamental molecules of a cell. It occupies a critical role in cell survival events like replication, expression and conservation of genetic material, hence called as a master molecule. Chemical degradation studies shows that extract obtained from cell nuclei consists of high molecular-weight substance termed as nucleic acid. Nucleic acids upon degradation give four distinct nucleotide units, called as adenylic, guanylic, thymidylic and cytidylic acids. These individual nucleotide units can be further degraded into phosphate groups and four distinct nucleosides. The nucleosides can be further divided into one of the four nitrogenous heterocyclic bases and a pentose sugar. The phosphate group acts as a linker between two successive nucleosides, resulting in the formation of a polynucleotide chain. Therefore nucleic acids can be defined as a polynucleotide chain consisting of repeating unit of three basic blocks namely: phosphate group, a sugar, and one of the four bases. Basically nucleic acids are divided into two broad categories; like deoxyribose nucleic acids (DNA) and ribose nucleic acids (RNA). DNA consists of β-D-2'-deoxy ribose sugar with adenine, guanine, cytosine and thymine as nitrogenous bases, while RNA has β-D-ribose sugar with adenine, guanine, cytosine and uracil as nitrogenous bases.

1.1.2 Bases; chemistry and Base Pairing.

In its standard form nucleic acid bases of DNA consists of two purines (Pur or R); Adenine (Ade or A), and Guanine (Gua or G), each containing two planar fused rings made up of five and six atoms and two pyrimidines (Pyr or Y); thymine (Thy or T), and cytosine (Cyt or C), each containing a single six-atom ring. In case of RNA, thymine is replaced by uracil (Ura or U) which differs only in the lack of a methyl group at position 5. All the above mentioned bases are essentially planar and aromatic in nature, and they differ only in substituent groups. In addition to these standard bases, many other lesser known base forms are found in nucleic acids, especially in RNA (methyl-2-guanosine, methyl-7-guanosine, methyl-1-adenosine, methyl-5-cytosine, wybutine etc *Gefter and*

Russell, 1969) and chemical modification plays an important role in these non-standard base formation. For eg., base methylation prominently at C(C5) position in CpG islands, plays an important biological role of genetic control mechanism (*Bock et al. 2006*).

The nomencalture for the atoms of the nucleic acid bases as approved by the International Union of Biochemistry (IUB) is shown in Fig. 1.1

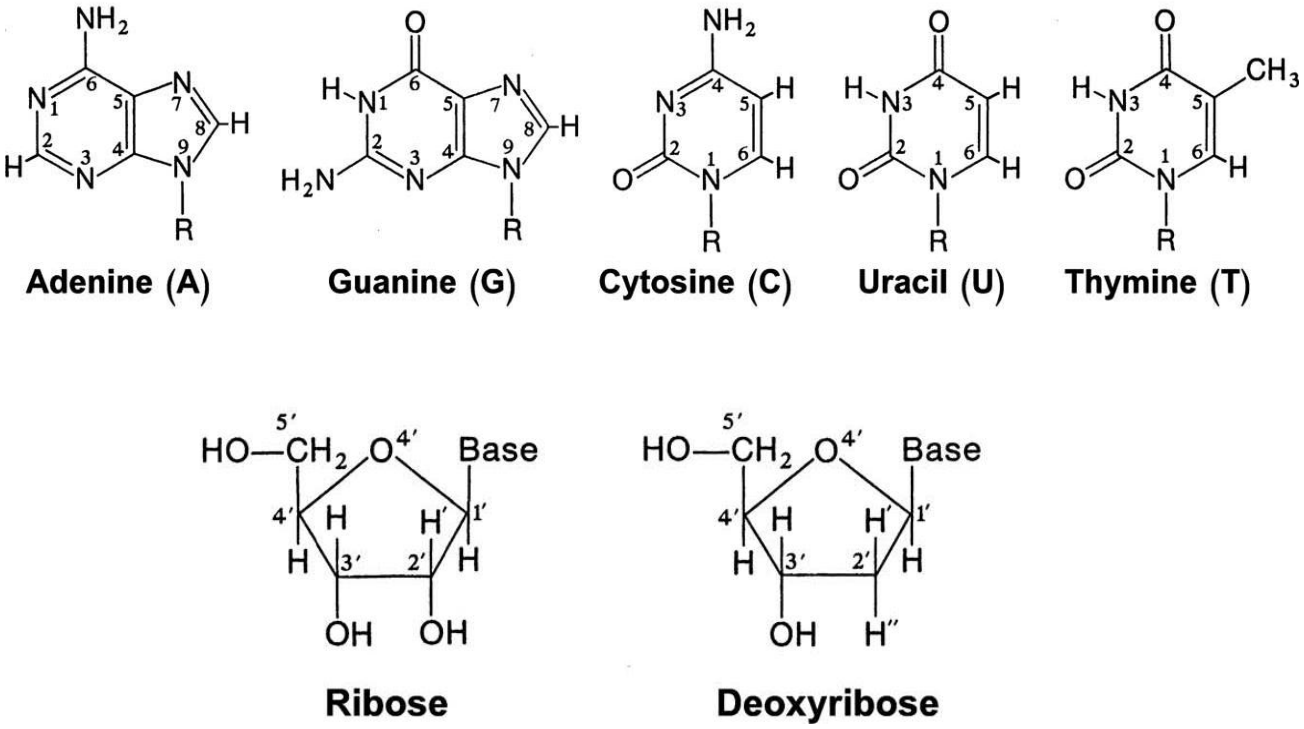

Figure 1.1: Chemical structure along with IUPAC numbering of common bases present in DNA and RNA structures, with pentose sugar present in these structures. R represents the point of attachment of aromatic base with the pentose sugar.

1.1.3 Sugar type and sugar conformation

Five membered furanose ring is an important constituent of the nucleotide; its configuration plays an important role in differentiating between DNA from RNA. DNA has β-D-2'-deoxy ribose sugar and RNA has β-D-ribose sugar. The basic difference is former lacks the hydroxyl (-OH) functional group at 2' position. This difference has important ramifications on the structure and property of these two nucleic acids. As a result of the replacement of 2'-OH group, DNA is less susceptible to hydrolysis and has more conformation flexibility. But the same 2'-OH group in RNA has some

important functions like extra hydrogen bonding capability, which gives greater possibilities for specific interactions.

A nucleoside is formed when nitrogenous base is attached to sugar in B-configuration at C1' of sugar. The pentose (deoxyribose in DNA and ribose in RNA) sugar ring in nucleic acids is non-planar because of sugar puckering. This non-planarity arises due to interaction between the substituents attached to the ring carbon atoms of a pentose sugar. The sugar attains a conformation such that substituents attached are present as far as possible. The puckering may be either in a chair or envelope conformation. The different sugar puckering can be correlated to the subtle structural differences between A-, B-, Z-type duplexes and G-quadruplexes.

The sugar pucker can be explained by five endocyclic torsional angles and conformation deduced from two parameters: pseudo rotation phase angle P, and puckering amplitude (the maximum degree of pucker) ν_M (Fig. 1.2). The pseudo rotation phase angle can be defined by five endocyclic torsion angles ν0-ν4 degree of pucker) ν_M (Table 1.1, Fig. 1.4)

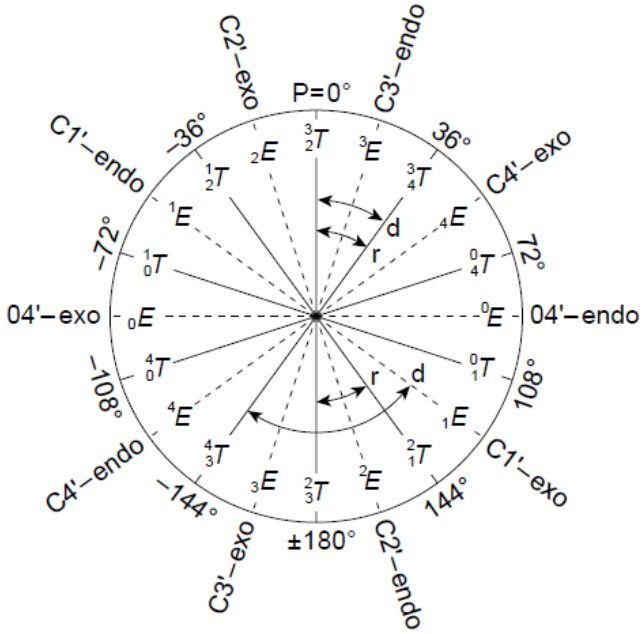

Figure 1.2: Pseudorotation cycle of furanose ring of nucleic acids.

1.1.4 Glycosyl torsional angle

Nitrogenous bases of the nucleic acids are essentially planar heterocyclic aromatic rings. The (deoxy) ribose pentose sugar is attached to aromatic planar nitrogenous base via a glycosidic bond, denoted by notation χ. This bond is formed between C1' of pentose sugar and N9 (Purines) or N1 (Pyrimidines) atom of nitrogenous base. Major conformation observed for glycosidic bond in numerous nucleic acids structure was β-stereochemistry, which means that the nitrogenous base will be in same orientation relative to the sugar ring's C4'-C5' exocyclic bond, while the C3'-O3' bond points in the opposite direction. This torsional angle χ is helpful in determining the rotation of the base relative to the sugar around the glycosidic bond. In purines the torsional angle (χ) can be determined by O4'-C1'-N9-C4 atoms and in pyrimidines it can determined by O4'-C1'-N1-C2 atoms. The structural data from various structural databanks of nucleic acids helps in analyzing the global average values of χ. The glycosyl bond can have any one of the two conformations, i.e *syn* and *anti*. The majority of nucleotides adopt the *anti* orientation, with χ between 180° and 300°, while the minority is in the *syn* orientation, with χ between 30° and 90°.

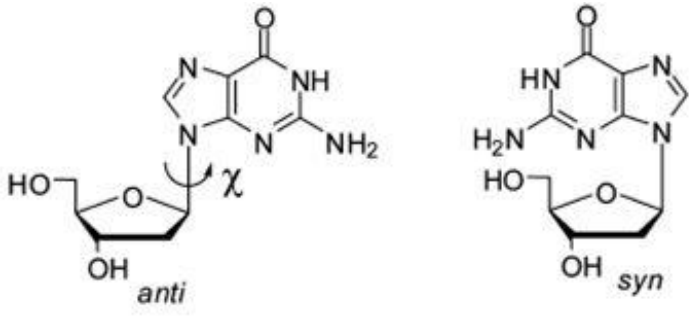

Figure 1.3: Guanine nucleosides showing *syn* and *anti* conformation around glycosyl bond.

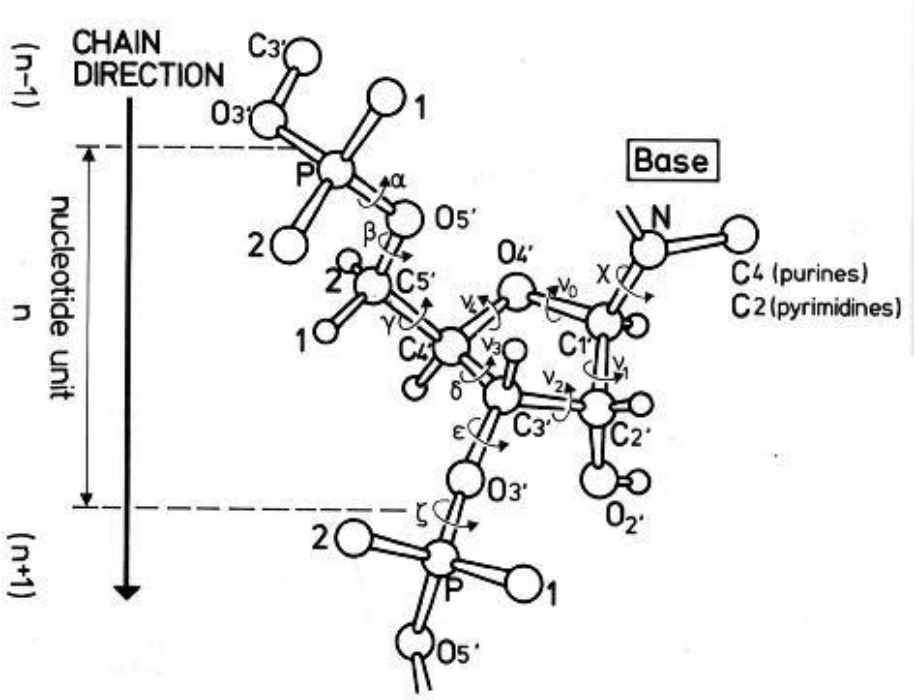

Figure 1.4: Backbone torsional angles of nucleic acids.

Table 1.1: Different backbone torsional angles in nucleic acids.

α	O-3'–P–O-5'–C-5'
β	P–O-5'–C-5'–C-4'
γ	O-5'–C-5'–C-4'–C-3'
δ	C-5'–C-4'–C-3'–O-3'
ε	C-4'–C-3'–O-3'–P
ζ	C-3'–O-3'–P–O-5'
χ(Pyrimidine)	O-4'–C-1'–N-1–C-2
χ(Purine)	O-4'–C-1'–N-9–C-4
Endocyclic sugar torsion angle	
$\nu 0$	C-4'–O-4'–C-1'–C-2'
$\nu 1$	O-4'–C-1'–C-2'–C-3'
$\nu 2$	C-1'–C-2'–C-3'–C-4'
$\nu 3$	C-2'–C-3'–C-4'–O-4'
$\nu 4$	C-3'–C-4'–O-4'–C-1

1.1.5 Base pairing and base stacking

The aromatic bases of nucleic acids are involved in two important mutual interactions; base pairing and base stacking. Nitrogenous bases of nucleotide units are held together by network of hydrogen

bonds, which are specific for each base pair. Hydrogen bonds are non covalent interactions between an electronegative acceptor atom (with a partial negative charge, in DNA it is C=O and N:) with a electropositive donor atom (with a partial positive charge, in DNA it is NH_2 and NH). H-bond forms when two interacting atoms are present at an angle of less than…in a distance range of 2.6 – 3.1 Å. As shown in Fig.1.5 adenine pairs with thymine via two hydrogen bonds, similarly guanine pairs with cytosine via three hydrogen bonds (*Donohue and Trueblood, 1960; Topal and Fresco, 1976*). This bonding scheme is called as Watson-Crick Base pairing. This base pairing requires both strands of DNA in anti-parallel direction, which provides the maximum stability by strong hydrogen bonds (*Germann et al. 1998, van de Sande et, al. 1988*).

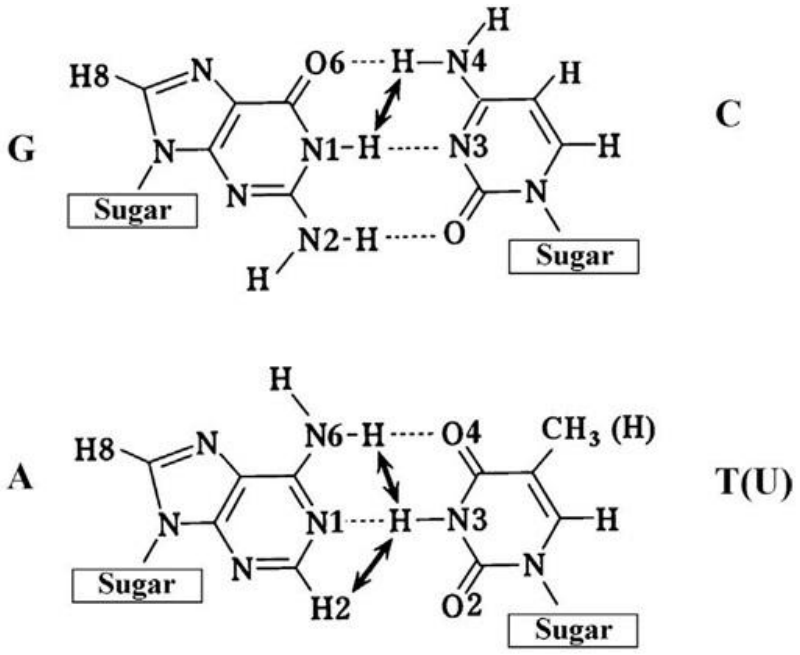

Figure 1.5: Watson and Crick base pairing between Guanine and cytosine and Adenine and thymine bases.

Apart from these canonical base pairing sites, nucleic acid bases show various potential hydrogen bonding donor and acceptor sites (Fig. 1.5). Due to the presence of these non-canonical H-bonding sites in bases, nucleic acids show various structural forms like triplex, quadruplex, pentaplex structrues.

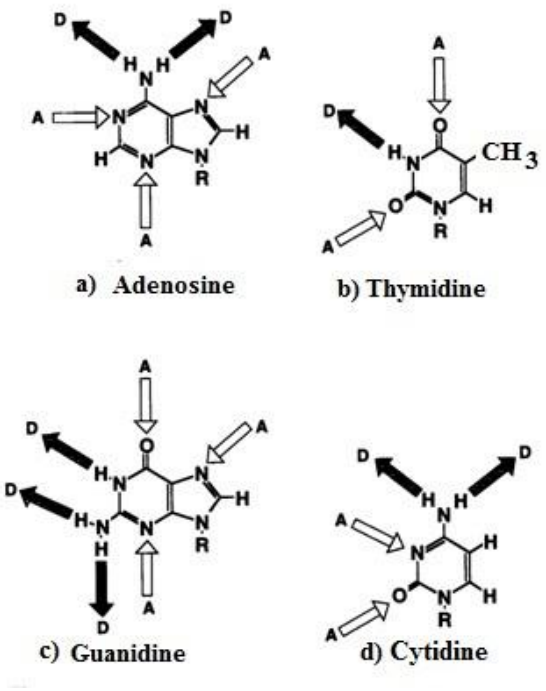

Figure 1.6: Hydrogen bonding sites in nucleic acid bases, a) adenosine, b) thymidine, c) guanidine and d) cytidine. Hydrogen donors are denoted by black arrows and by letter D, whereas hydrogen acceptors are denoted by white arrows with letter A.

1.2 DNA and polymorphism

Due to its inherent polyanionic character, nucleic acids adopt various isoforms depending upon solvent condition and base sequence present. The DNA polymorphism is broadly classified into two groups, namely canonical forms consisting of normal duplex forms like B-DNa, A-DNA and Z-DNA forms and non-canonical forms like triplex, quadruplex DNA etc.

1.2.1 Duplex DNA forms; A-DNA, B-DNA and Z-DNA

Using the x-ray diffraction studies James D. Watson, Francis H. Crick, and Maurice Wilkins with the major help from findings of Rosalind Franklin proposed the three dimensional structure of DNA (B-DNA) in 1953. B-DNA is the most common type of secondary structure present in DNA. This structure is formed by two anti-parallel polynucleotide chains running together along a common axis to form a right handed helix. The major structural features were summarized in Table 1.1 and depicted in Fig. 1.7. The diameter of the helix is 20 Å, with hydrogen bonded base pairs almost perpendicular to helical axis, and each base pair occupies a similar width, hence giving rise

to symmetry to this structure. The two anti-parallel helices are held together by hydrogen bonds between bases of the opposite strand. The aromatic bases are partially stacked on top of each other; the π electron delocalization on aromatic bases also confers to the stability.

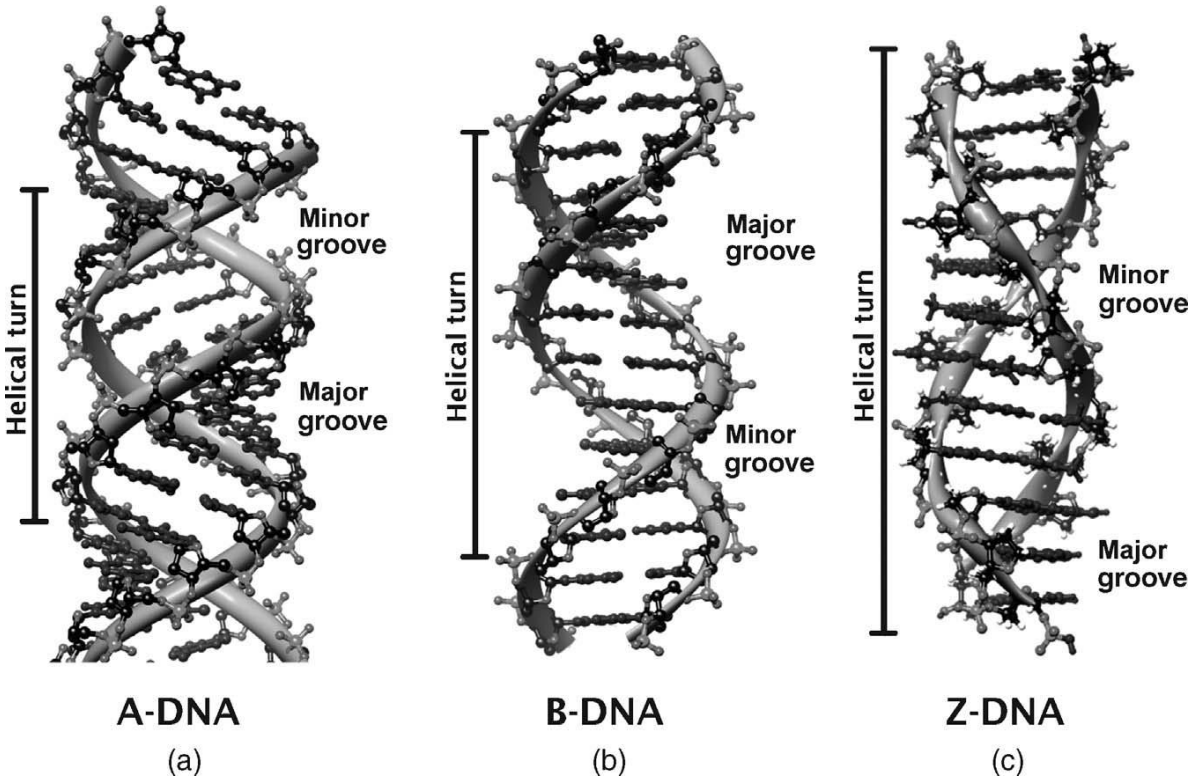

Figure 1.7: Different conformations of duplex DNA: a) A-DNA, b) B-DNA and c) Z-DNA.

1.2.3 Triplex DNA

Felsenfeld and Rich (*Felsenfeld and Rich 1957*) first explained the formation of triple helical nucleic acids under certain physiological conditions. This form of DNA is formed by association of three strands, in which third strand forms Hoogsteen or reverse Hoogsteen hydrogen bonding with the purine rich B-DNA duplex. This structure is stabilized by negative super coiling.

1.2.4 Quadruplex DNA

These are the structures formed by the arrangement of four strands, either in parallel or anti-parallel manner. Gellert (*Gellert et al. 1962*) in a classical work reported the formation of tetrad like structure by self-association of gaunosine molecules. G-quadruplex structures are the main focus of this thesis.

Table 1.2: Important structural features of A, B, and Z-DNA forms.

	DNA form		
Structural Characteristics	A	B	Z
Helical sense	Right-handed	Right-handed	Left-handed
Diameter of the helix	~ 26 A ˚	~ 20 A ˚	~18 A ˚
Rotation per repeating unit	32.7	35.9	-60
Base pairs per turn	11.6	10.5	12 (6 dimers)
Base tilt relative to helical axis	20^{o}	6^{o}	7^{o}
Helix rise per base pair	2.56 A˚	3.38 A˚	3.71 A˚
Pitch/turn of helix	34 A ˚	34 A ˚	44 A ˚
Mean propeller twist	+18	+16	0
Sugar pucker	C3’-*endo*	C2’-*endo*	G: C3’-*endo* C,T,A: C2’-*endo*
Glycosidic dihedral torsion angle	anti	anti	G: syn C, T, A: anti
Minor groove	Wide and shallow	Narrow and deep	Narrow and deep
Major groove	Narrow and deep	wide and deep	flat

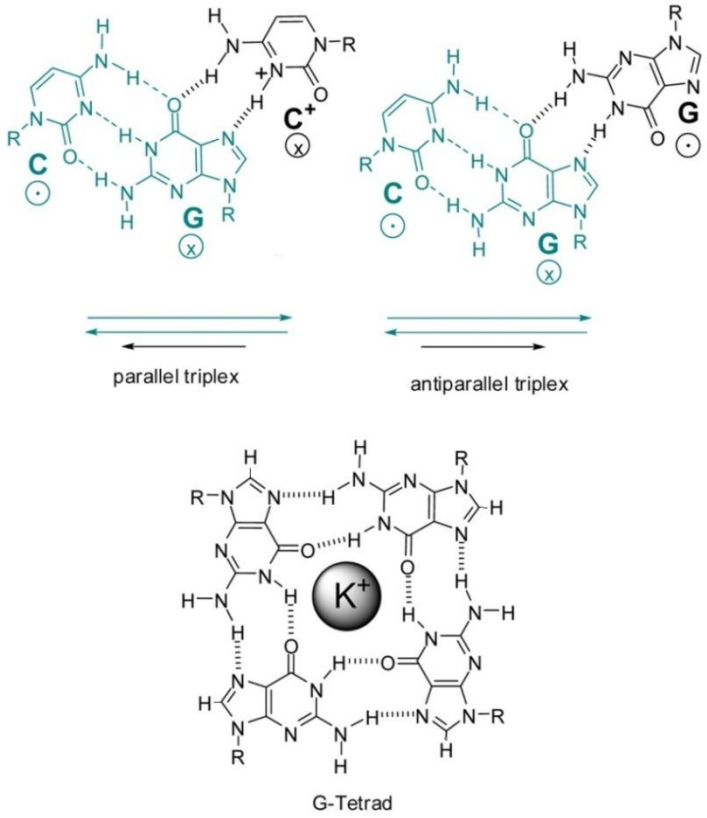

Figure 1.8: Base pairing scheme in base triplets and G-quartets.

1.2.5 Other higher forms: Pentaplexes

Apart from quadruplexes, higher order DNA structures like pentaplexes are formed by five nucleic acid strands (*Chaput and Switzer 1999*). These higher order structures are not found in natural conditions, but have application in supra-molecular studies.

1.2.6 I-motif DNA

I motifs are the quadruplex structures formed by the C-rich sequences in acidic pH condition. The cytosine rich sequences in acidic pH condition show protonation at C-5 position to form C+, which acts as a mismatch pairing in duplex DNA. The C:CH+ results in the formation of two parallel running duplex DNA, two such duplex DNA associate in head to tail to form an I motif. One of the important features of i-motif structures are systematic base intercalation. Solution NMR studies show these structures form higher order quadruplex structures. The human telomere $(C3TA2)_4$ sequence forms intra-molecularly folded i-motif quadruplex structure under acidic pH conditions (*Gehring et al. 1993*). In NMR spectrum the observation of imino proton resonances between 15-16 ppm is indicative of formation of C:CH+ mismatch pairs and the appearance of single set of resonances confirms the formation of quadruplex structure with four fold symmetry. The i-motif quadruplex contains a pair of opposing wide grooves and a pair of opposing narrow grooves.

1.3 Cancer; Biology and effects

Cancer is the most important disease in recent human history, the prevalence rate is increasing day by day due to fast changing human lifestyle and degrading environmental resources. It is one of leading causes of death due to a disease in humans. Cancer is defined as deregulated multiplication of cells resulting in the excessive and abnormal increase in number of cells in particular organs. Due to its importance in human health, the development and progression of cancer is a well studied and highly researched topic in science. During its initial development, cancer is confined to a specific organ of origin, while in later advanced stages it migrates to the surrounding tissues via the hematopoietic and lymphatic systems of our body, termed as *metastasis*. Numerous pathways have been put forward to explain cancer development and progression in human body, but most important among them was the one due to the damage of the cellular genome, either by cellular mechanisms like error during replication of DNA or those caused by environmental influences.

The major environmental factors are chemical carcinogens (e.g. aflatoxin B1 in liver cancer, tobacco smoke in lung cancer, radiation (UV radiation), viruses (such as hepatitis B virus in liver cancer, or human papilloma virus in cervical cancer).

Cancer development due to changes in genetic material attributed mainly to the mutation in genes involved in DNA replication and maintenance. It may be due to dominant mutations in oncogenes like, recessive mutations in tumor suppressor genes or by integration of viral DNA into the regulatory region of a cellular gene which is termed as viral insertion or integration. For e.g. insertion of retroviral region in the promoter site of *c-myc* proto oncogene results in the activation of the *c-myc* gene (*Hayward et al. 1981*)

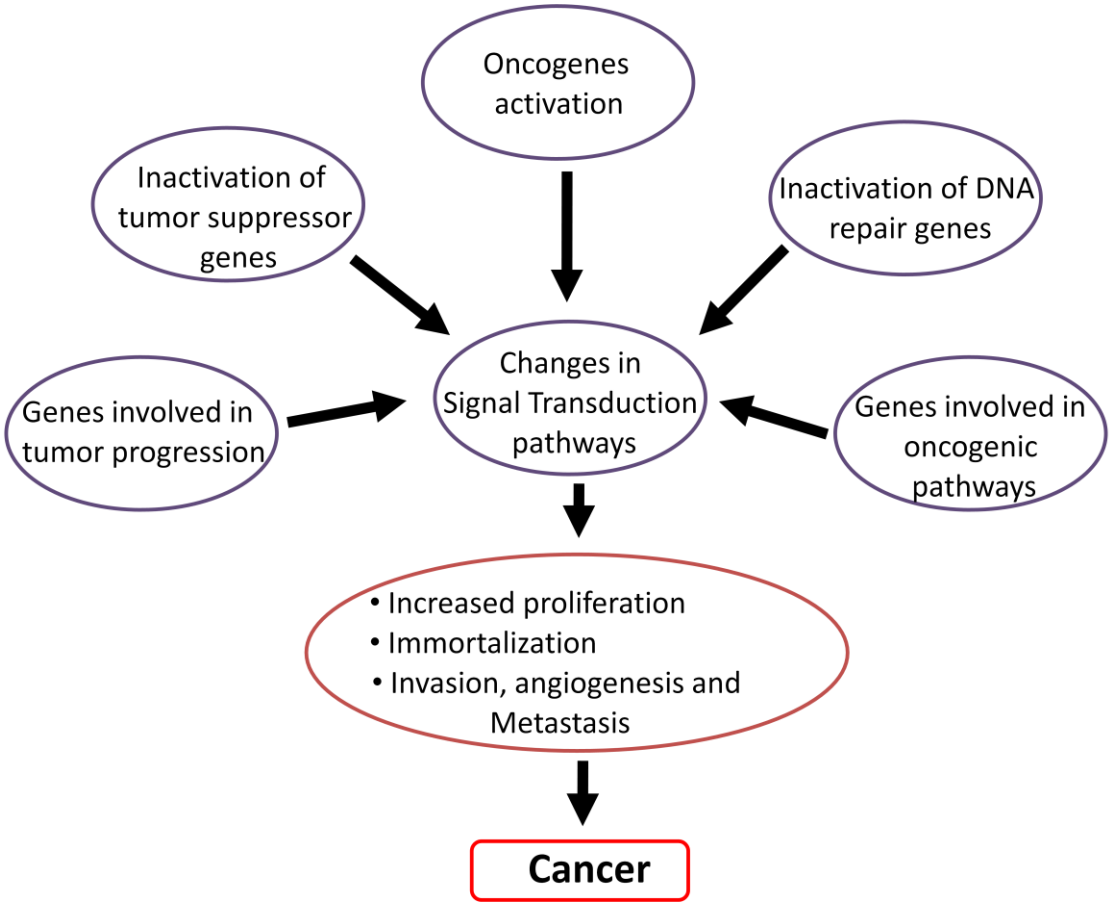

Figure 1.9: Important classes of genes involved in cancer development and progression which also shows DNA damage and response plays an important role in cancer development

1.4 Telomere, Telomerase and Cancer

DNA is the fundamental target for many small molecule drugs, as targeting this biomolecule at the first level of gene expression step, results in decrease in the type and number of target molecules to be targeted by drug molecules and more effective regulation of gene expression. DNA is the polymorphic molecule which adopts wide variety of secondary structures, like duplex, Holliday junction and quadrulpex structures in the telomeric regions. Telomeres are the specialized regions found in the termini of the eukaryotic chromosomes, which helps in the stability and protection of the chromosomes. The important function of telomeres includes the protection of chromosome from recombination, nuclease degradation and end-to-end fusion events. In almost all eukaryotes, the telomeric repeat contains runs of G's. Some examples include the yeast *S. cerevisiae*, $TG_{(1–3)}$; the ciliates *Tetrahymena*, TTGGGG; *Oxytricha nova*, TTTTGGGG; the plant, *Arabidopsis*, TTTAGGG and the vertebrate repeat, TTAGGG. This G-rich telomeric overhang readily forms G-quadruplex structures, which are characterized by the presence of G-quartets (*Williamson et al. 1989*). The basic unit of these structures is the G-quartet, a planar array of four guanines, in which each guanine pairs with two neighbors by Hoogsteen hydrogen bonding. G-quartets can promote inter- or intra-molecular interactions, between parallel or anti-parallel DNA strands. DNA structures stabilized by G-quartets are variously referred to as G-quadruplex, G-tetraplex, and G4 DNA.

With each cell division some of the DNA is lost from the ends of chromosomes, as conventional DNA polymerase cannot fully duplicate the 3' end of the lagging strands (end replication problem) (*Levy et al. 1992*). Hence after each round of replication telomere shortens and when telomeres reach a critical minimum length, cells cannot divide and cellular senescence and apoptosis is induced (*Counter et al. 1992*), which coincides with the activation of *p53, p21*, and *p16* pathways in cells (*Herbig et al. 2004*). The mechanism of apoptosis is the most common way for the destruction of cells in which apoptosis signals have generated. Human somatic cells have the potential to undergo about 60 to 70 divisions after which they experience growth arrest and enter senescence.

But sometimes this loss may be also due to deletion or exonuclease activity. Telomere region at the end is not blunt but have a 3' single stranded G-rich overhang. This feature is conserved in all eukaryotes and this overhang of 30-500 nucleotides (*Makarov et al. 1997; Wright et al. 1997*), involve in the formation of a secondary structure called as t-loop. The t-loop is formed by both duplex region and single stranded overhang, in which single stranded region folds back and associates with double stranded region by strand invasion to form D-loop (*de Lange, 2005*). The

stabilization of this loop structures is mediated by six telomere associated protein components; Telomere Repeat binding Factor (TRF) 1, TRF2, TRF Interacting Nuclear factor (TIN) 2, Repressor-Activator Protein (RAP) 1 (*Li et al. 2000*), TINF-2 Interacting Protein (TPP) 1 and Protection Of Telomeres (POT) 1. All these proteins are collectively termed as shelterin complex (de *Lange, 2005*). TRF1 (*Zhong et al. 1992*) and TRF2 (*Broccoli et al. 1997*) bind to the double stranded region of the telomere, while POT1 (*Baumann and Cech 2001*) binds to the single stranded TTAGGG repeats of 3' overhang. POT1 interacts with TRF1 and TRF2 with the help of other two proteins, TIN2 (*Kim et al. 1992*) and TPP1 (*Ye et al. 2004*). TIN2 binds to TRF1 and TRF2 independently and recruits TPP1 and POT1 complex. The TPP1 acts as connection between POT1 and TRF1-TRF2-TIN2 complex and its amino terminus contains a telomerase interacting domain. Hence TPP1 helps in recruiting the telomerase enzyme to the chromosome ends. The t-loop, D-loop along with associated proteins forms a cap like structure that protect chromosome ends from exonuclease activity and terminal fusion, which being recognized as DNA damage by cells.

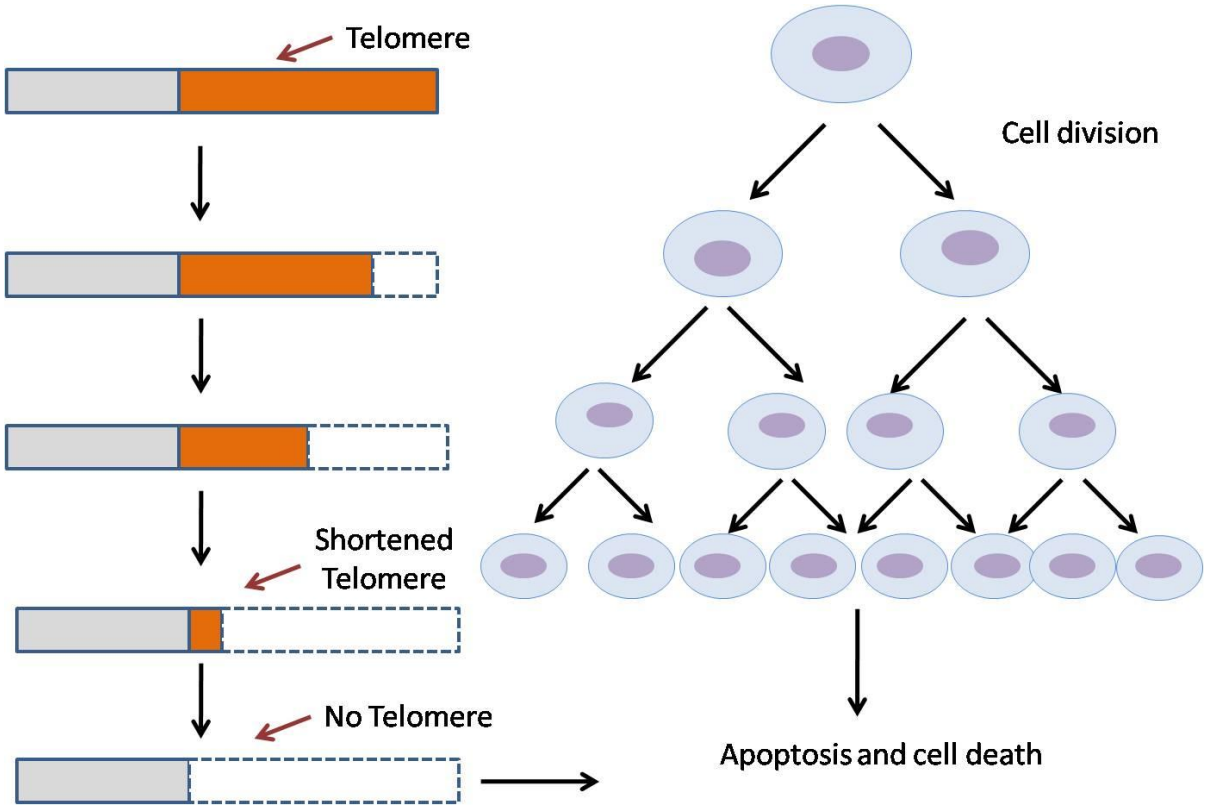

Figure 1.10: Importance of telomere length in cell cycle and cell life maintenance.

Apart from the participation in the formation of t-loop structure, the single stranded region of 3' end of telomere can also form the higher order structure called as G-quadruplex, which is formed by the square planar arrangement of two or more G-tetrads and consists of four backbone strands.

Telomerase is a ribonucleoprotein complex, which preserves the telomere length in stem cells, germ cells, and cancer cells by adding hexameric, TTAGGG repeats to the 3'-ends of chromosomes. This ribonucleoprotein consists of endogenous RNA template (*TR*) and a protein part called telomerase reverse transcriptase (*TERT*) which catalyses the process of telomere addition (*Blackburn, 2001*). Telomerase recognizes the G-rich strand of an existing telomere repeat sequence and elongates it in the 5´-to-3´ direction. Telomerase enzyme requires single stranded telomere as primer for its activity. As stem cells, germ cells and cancer cells express the telomerase activity, adult somatic cells lacks this enzyme activity; hence after certain number of cell divisions, telomere shortening results in Hayflick limit, leading to cell death and senescence. It has been shown that all somatic cells contain the RNA template (*TR*) but lack the reverse transcriptase part (*TERT*). About 90% of the known cancer cells contain short telomeric DNA, but they exhibit high telomerase activity. Several different cancer types were studied to demonstrate the correlation between short telomere length and high telomerase activity. For example, ~ 70% of oral carcinomas, ~ 90% of breast cancers, ~ 80% of lung cancer and ~ 95% of colorectal cancers show detectable amount of telomerase enzyme activity when compared to normal human somatic cells. Therefore telomerase enzyme acts as an important tumor marker.

Due to its importance in the tumor development and progression, telomerase and its components act as an important target for the anticancer drug targeting. Numerous strategies have been developed to inhibit the activity of telomerase enzyme, which has been broadly classified into two broad categories; a) directly inhibiting the components of telomerase and b) inhibition by indirectly stabilizing the secondary structures formed during replication in substrate telomeric DNA.

a) Inhibition of the components of telomerase

Direct inhibition of telomerase activity by targeting the components of telomerase like TR or TERT is major challenge due to the fact that only few molecules of telomerase enzyme was present at any given time in a cell (*Cohen et al. 2007*). As telomerase is a very robust enzyme, only few copies of it are necessary for cell survival. Structure based drug design requires the complete structural data of

a receptor. Therefore the lack of complete structural data of the telomerase enzyme complex also hinders this process.

i) Targeting the TERT component of Telomerase

As protein component of telomerase functions by reverse transcriptase (RT) activity, several known reverse transcriptase inhibitors were tested for their ability to inhibit the activity of telomerase enzyme. The substrate dNTPs can be replaced by dideoxynulceotides (*Strahl and Blackburn 1996*), and nonnucleosidic compounds like BIBR 1532 (*Damm et al. 2001*)

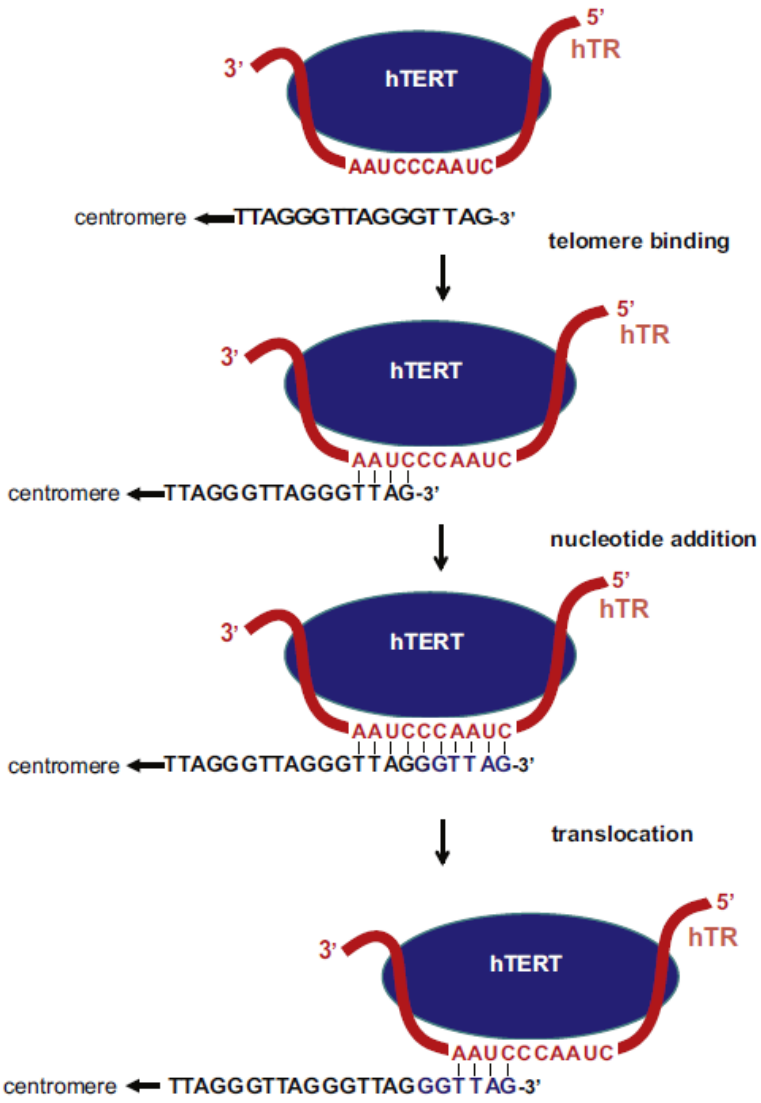

Figure 1.11: Telomerase function: Diagrammatic representation of telomere elongation process by telomerase enzyme.

ii) Targeting the TR portion of Telomerase:

Telomerase consists of a RNA component (TR) which acts as a template sequence for telomere extension step. The sequence and length varies depending upon organisms, but the template region is conserved among species (*Lin et al. 2004*). The best known telomerase inhibitor in advanced clinical trials is GRN 163L, an oligonucleotide, which inhibits the telomerase by binding with TR component through complementary base pairing (*Norton et al. 1996*).

b) Stabilization of G-quadruplex structures in telomere substrate

The most important strategy used for telomerase inhibition is by stabilizing the G-Quadruplex DNA structures which act as substrate for the telomerase enzyme. Zahler and co-workers demonstrated that formation of quadruplex structures inhibits the activity of telomerase enzyme in *Oxtryicha nova* cells (*Zahler et al. 1991*). This principle of telomerase inhibition has been utilized by other workers to develop small molecule ligands which can bind and stabilize quadruplex scaffold. The first report of inhibition of telomerase activity by stabilizing quadruplex structures was shown by Sun and co-workers. They showed that compound 2, 6- diamido anthraquinone binds to G-quadruplex structure and inhibits the telomerase enzyme activity *in-vitro* (*Sun et al. 1997*). Nowadays active research is going on in identifying/synthesizing compounds which show specificity and affinity for quadruplex structures when compared to other forms of nucleic acids exists in cells. Majority of the known G-quadruplex interacting ligands have an extended planar aromatic ring sysytem and stack effectively on planar G-tetrad via π- π inteaction. Many planar aromatic compounds have been identified which binds to quadruplex strcuture therby inhibiting the teloemrase activity. The list inclues macrocycle porphyrin derivatives like TMPyP4 (*Wheelhouse et al. 1998; Anantha et al. 1998; Seeniswamy et al. 2005*), PIPER (*Fedoroff et al. 1998*), RHPS4 (*Gavathiotis et al. 2003*), daunomycin (*Clark et al. 2003*)

Apart from aromatic ligands which tend to stack on G-quartet surface, numerous lignads which binds to grooves of quadruplex structres has been known. Groove binders like Distamycin-A and its analogues, netropsin, (*Martino et al. 2007; Randazzo et al. 2003; Cosconati et al. 2010*). Due to the variations in the structure of G-quadruplexes, recently few cyanine drugs have been used to distinguish between different quadruplex DNA (*Nanjunda et al. 2013*).

Apart from its importance as the target for anti-cancer strategies involving the inhibition of telomerase activity, there has been an increasing interest in the G-quadruplex structures in recent

years. This was due to their high prevalence in human genome. Recently it has been shown by extensive bioinformatics analysis of human genome that more than 3,50,000 potential quadruplex forming (QFOs) sequences exists in genome (*Huppert and Balasubramaniam, 2007*). In support of this, G-quadruplex forming regions and G-quadruplex structures have been shown to present in the 5'-UTR regions of important cancer causing genes, immunoglobulin switch regions, and in recombination hotspots. Their prevalence in different region of genome correlates to the important functional role of these quadruplex structures. For example, formation of G-quadurplex structures in the promoter region of oncogenes like *c-myc (Siddhiqui Jain et al. 2002), c-kit, bcl-2,* leads to the suppression of activity of the gene of interest and tight regulation of cancer genes. Promoter regions of various important genes and cancer causing genes have GC rich region like bcl-2 (*Nambiar et al. 2011*), *c-met, c-myc, c-kit,* etc. various ligands can be used to effectively stabilize the secondary structures formed by these promoter sequences (*Singhal and Rajeshwari, 2009; 2009; 2010*)

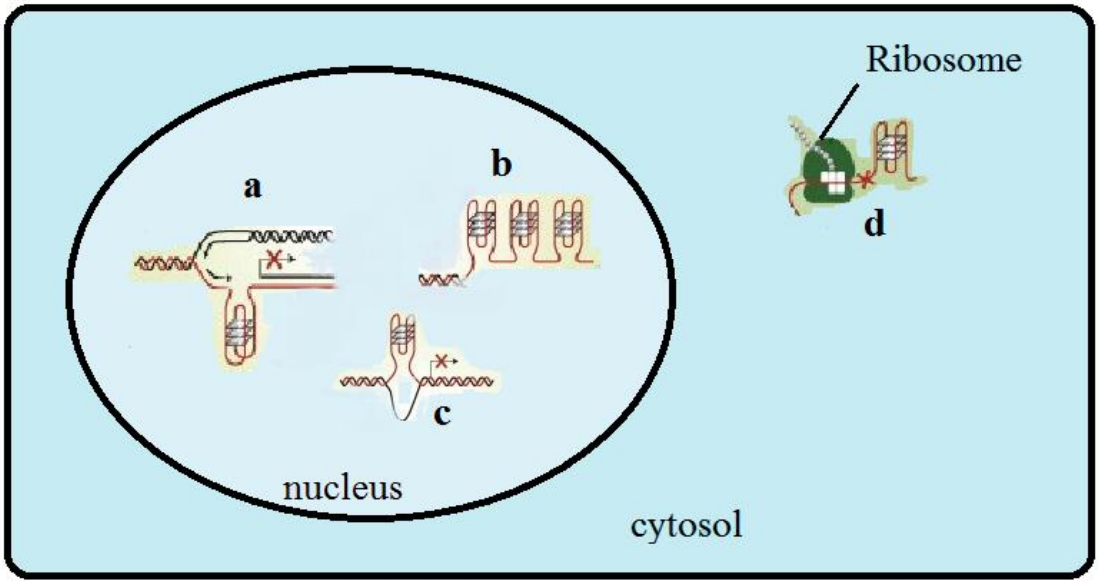

Figure 1.12: Quadruplex structures present in cell and its importance a) during replication, b) at the end of telomeres, c) tumor promoters and d) in 5' UTR region of important genes.

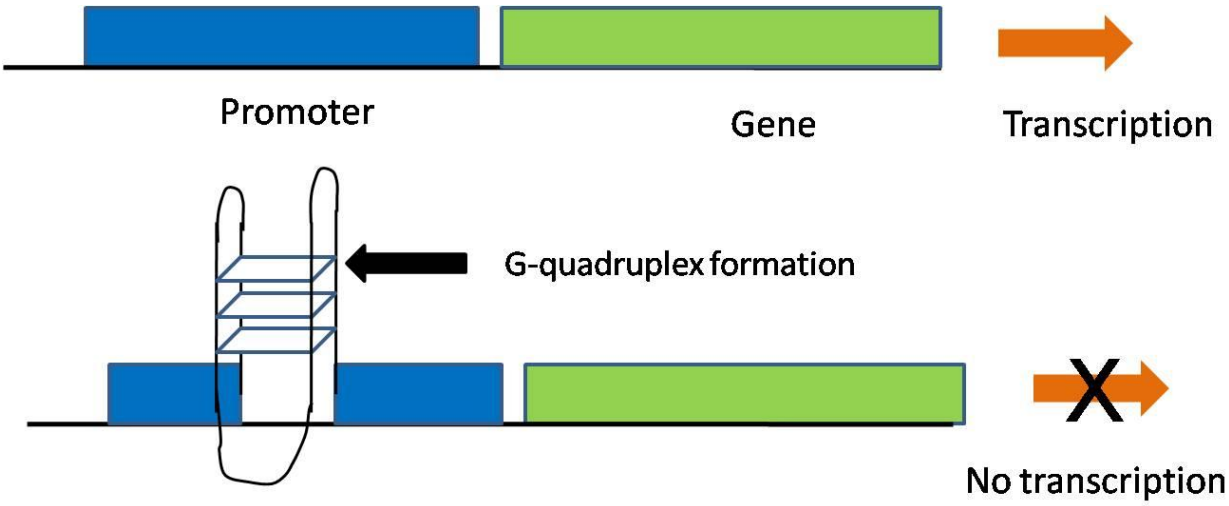

Figure 1.13: formation of G-quadruplex structures in promoter regions terminates the transcription.

1.5 Structure of G-quadruplex DNA

Depending upon the orientation of G-rich strands or polarity of strands, G-quadruplex structures have been broadly classified into parallel and antiparallel. Parallel stranded structures contain G-tetrad forming guanines in anti-glycosidic torsion angles (*Sen and Gilbert 1988*) and form in the presence of K+ ions (*Williamson et al. 1989*). In the other hand, antiparallel G-quadruplex structures contain G-tetrad guanines in both *syn* and *anti*-glycosidic torsion angles and formed in the presence of Na+ ion (*Williamson et al. 1989*). This generalization is applied only to the structures formed by one or two G-rich strands termed as unimolecular and bimolecular G-quadruplexes, respectively. Unimolecular structures contain four or more G-rich repeats, and bimolecular quadruplex consists of two G-rich repeats. But quadruplex structures formed by association of four single repeat G-rich strands called as tetramolecular G-quadruplexes contain all strands in one direction i.e 5'-3' with all anti glycosidic torsion angles (*Wang and Patel 1992; Wang and Patel 1993; Aboul-ela et al. 1994; Gavathiotis et al. 2003*) and formed in variety of monovalent cationic conditions like K+, Na+, NH_4+. Apart from G-tetrad structure, an intervening adenine, thymine and cytosine in the G-rich sequence can also form tetrad structure (*Patel et al. 2000; Patel and Hosur, 1999; Patel et al. 1999*)

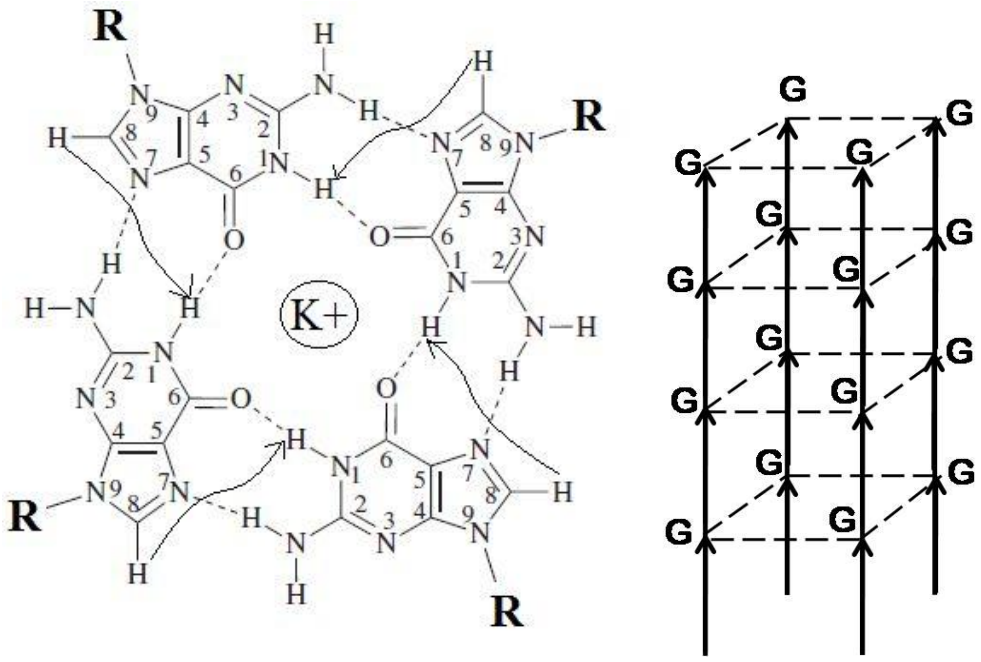

Figure 1.14: G-tetrad showing alignment of adjacent bases along with H8-NH connectivity between adjacent guanine bases, and parallel tetramolecular G-quadruplex formed by alignment of G-tetrads.

In unimolecular and bimolecular quadruplexes, the intervening connector sequences present in between successive G-rich tracts, adopt distinct topologies in the form of loops. Three principal types of loops are identified, namely diagonal, lateral and chain reversal or propeller. First two types are called as anti-parallel loops, as they present in quadruplex structures having G-rich strands in anti-parallel structure. The chain reversal or propeller loops results in quadurplex structures with parallel G-rich strands.

A diagonal loop connects the two adjacent anti-parallel G-rich strands, commonly found in bimolecular quadruplexes. For example diagonal loops were observed in quadruplex structures formed by *Oxytricha nova* telomere sequence d($G_4T_4G_4$) (*Smith and Feigon, 1993*) in which T_4 stretch forms a diagonal loop. Due to the diagonal loop the quadruplex structure has a twofold symmetry with one narrow, one wide and two medium grooves. A lateral loop connects joins the adjacent anti-parallel loops on the same quadruplex surface. The chain reversal or propeller loops connects the two parallel strands.

1.5.1 Quadruplex and metal ions

G-quadruplex structures containing G-quartet motif have unique central channel which can accommodate metal cations. The formation of type of G-quadruplex structure and its stabilization depends on the type of cation and its ionic radii. The O-6 atom of guanine G-tetrad which is present near central channel helps in the coordination of cation (*Arnott et al. 1974*). Due to its co-ordination geometry and size potassium ion (K+) stabilizes the G-quadruplex structure more effectively than any other known monovalent cation. Depending upon the radius of the central metal ion, G-quadruplexes adopt different polarity in strands (Fig. 1.16)

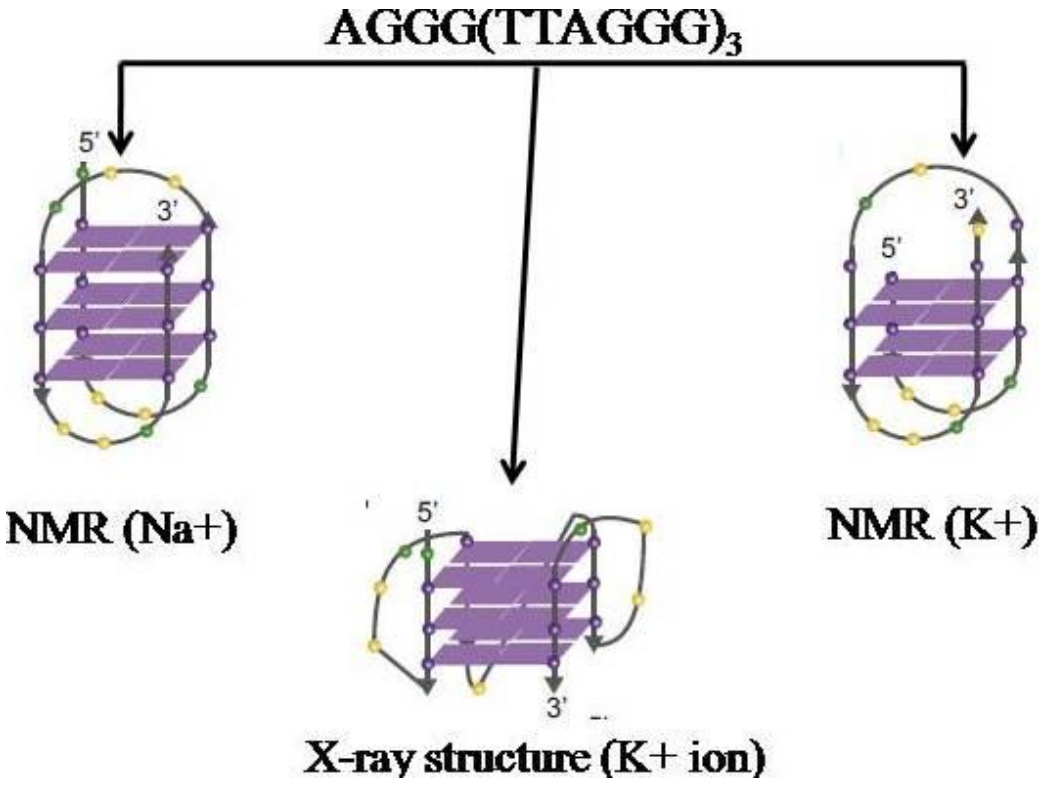

Figure 1.16: NMR and X-ray structure of human telomere repeat sequence at K+ and Na+ ion condition.

1.5.2 Methods to study structure of quadruplex DNA

After the isolation and identification of telomere and telomerase components, there is a wide spread interest in pharmacological and structural biology groups across the globe to define the structure and dynamics of telomere and related protein complexes.

Detailed knowledge of quadruplex-drug complex is essential for understanding the forces and type of quadruplex stabilization and to use this model as telomerase inhibition strategies and for anti-cancer drug design. Several methods have been used to study and identify the G-quadruplex structure formed *in-vitro* by oligonucleotide sequences and its stabilization by drug complexes. Circular dichroism (CD) spectra gives basic insights about whether the chosen sequence forms parallel, antiparallel or mixed type quadruplex structure (*Paramasivan et al. 2007; Randazzo et al. 2013*). Hence CD spectroscopy gives the strand orientation of the G-quadruplex structure.

The atomic resolution three dimensional structures of G-quadruplexes can be obtained by X-ray crystallography and solution NMR spectroscopy. Both of these techniques has positives and negatives in the structural elucidation of G-quadruplexes and its ligand complexes. Compared to X-ray crystallography NMR spectroscopy has an edge in understanding kinetics and dynamics of quadruplex as well as molecular interaction studies simultaneously. The other important limitation of G-quadruplex structure determination by X-ray crystallography over solution state NMR spectroscopy is because unimolecular and bimolecular G-quadruplex structures contains dynamic loops, which hinder the process of crystal packing during crystallization process, and exclude the subset of G-quadruplex conformations. Moreover the conformation adopted by G-quadruplex depends on the ionic and solvent conditions, collectively termed as molecular crowding conditions. The solvent content in the crystal used to determine the structure of G-quadruplex was estimated to be ~ 55%. Hence crystallization procedure generates highly crowded condition, which affects the structure of G-quadruplex formed by the DNA sequence. It is difficult to obtain the crystals for the G-quadruplex ligand complexes, as the system has low specificity and ligands can exchange easily among their variety of binding sites (*Wilson and Jones 1997*).

One of the important limitations of structure determination by solution state NMR is because of its poor resolution of structures above 10 kDa molecular weight. This was mainly due to overlapping of signals in two and three dimensional NMR. But oligonucleotides which form G-quadruplex DNA usually have molecular mass less than 10 kDa. Moreover recent developments in the area of high field NMR (upto 1000MHz), cryo probe usage along with site specific isotope labeling of ^{13}C, ^{15}N isotopes aids in the determination of three dimensional structures of unimolecular G-quadruplex by NMR spectroscopy. The ligand based approach like STD NMR, Water LOGSY (*Ramirez et al. 2014; Antanasijivec et al. 2014*) helps in the determination of type of interaction

between ligand and large molecule, without requiring complete knowledge of large molecule of interest.

1.5.3 Structural characterization of G-quadruplex using NMR spectroscopy

Nuclear magnetic resonance (NMR) studies provides precise three dimensional structure and analysis of the NMR data reveals several important structural information like exchangeable protons, kinetics of proton exchange rate which correlates to the environment of proton present, diffusion rate, temperature dependence kinetics etc (*Hosur et al. 1998*). As G-quadrulpex structures have been formed by single strand (unimolecular), two strands (bi-molecular) and four strands (tetramolecular); due to the folding back of strands numerous possibilities of loop formation exists in the first two types of quadruplex structures. The first step in the structural analysis of quadruplex is to correctly assign the frequency positions to corresponding proton nuclei of the given oligonucleotide. Apart from these, four guanines of a quartet resonate at the same frequency (*Gavathiotis et al. 2003; Wang and Patel 1993*). Due to the overlap of signals, complexities in the folding topologies and assignment of *syn* and *anti* nucleotides which exists in the unimolecular quadruplex DNA structure, these oligonucleotides have been used with partial or full isotopic label for NMR studies.

The ^{1}H spectrum in 90% H_2O/10% D_2O (buffered with 100 mM KCl) at room temperature provide information about both the exchangeable and non-exchangeable protons. The number of imino proton resonances in the Hoogsteen hydrogen bonded region (~ 10.5 -12 ppm) indicate/confirm the number of G-quartets present, stoichiometry of the strands and the symmetry of the quadruplex structure. The appearance of imino proton resonances resonating downfield to 12.5 ppm suggests the existence of Watson-Crick base paring (NH···H) scheme. Due to the square planar arrangement of G-quartets in quadruplex structure, the imino proton resonances of guanine bases appear in the range of 10.5 – 12 ppm, which shows the presence of Hoogsteen hydrogen (NH···O) bonding scheme. Similarly if T-tetrad is present, the imino protons resonates upfield to 9.6 ppm. The formation of A-tetrad has been reported (*Gavathiotis et al. 2003*). The amino protons resonate upfield of imino protons, and the chemical shift separation greater than 1.5 ppm between the two amino protons indicate the arrangement in which one proton is hydrogen bonded and other is exposed to solvent.

The rate of imino proton exchange with water can be used as an indicator to the location of imino proton in the quadruplex structure, since the slowest exchanging protons often belong to the inner quartets.

1.5.3.1 Solution structure of tetramolecular quadruplex structures:

Single repeat G-rich sequences forms tetramolecular quadruplex structure in solution conditions, with strands arranged in parallel orientation. The initial evidence for formation of quadruplex structure by single repeat guanine rich sequences were shown both in single repeat blunt end sequences having terminal 3'-guanine and those lack 3' terminal guanine. The solution studies of single repeat sequences d(T_2AG_3T), d(T_2G_4T) (*Wang and Patel, 1992, Wang and Patel, 1993*), d(TG_4T) (*Abouela et al. 1992;1994*), d(TG_3T) (*Jin et al. 1989*), d(T_4G_4) (*Gupta et al. 1993*) shows these sequences form tetramolecular parallel quadruplex structures with all residues adopting *anti*-glycosidic torsion angles. Hence all four guanines adopt *anti:anti:anti:anti* arrangement in a G-tetrad. These structures show right handed helical arrangement with deoxy ribose sugar in S-type (C2'-*endo*) pucker conformation. All four grooves are of equivalent width and depth. Four guanines exist as coplanar arrangement in a G-tetrad, without any base tilt. Apart from these reports, solution studies of single repeat blunt end sequences, that is a sequence which ends with terminal 3' guanine, tends to aggregate to form higher order structures like quadruplex dimers.

The single repeat tetramolecular quadruplex forming oligonucleotide sequences can be used without isotopic enrichment as the final kinetically stable quadruplex gives well separated proton resonances in the exchangeable and non-exchangeable region (*Wang and Patel 1993*).

1.6 Quadruplex-Ligand complexes

Interaction of ligands with various G-quadruplex forming sequences and structures have been widely classified into end stacking, intercalation and groove binding. If unimolecular or bimolecular G-quadruplex forming sequences are used, another type of binding mode that is external loop binding may be present. Ligands bind to quadruplex in any one of these characteristic binding modes and the type of binding, like in any other biomolecules can be elucidated by structural determination techniques like solution state NMR and X-ray crystallographic studies (*Ramirez et al. 2014*). Changes in absorbance and fluorescence characteristics of ligand (*Islam et*

al. 2009), energy terms obtained by ITC and SPR experiments can be used to support the binding mode obtained by structural determination methods.

During the past few decades important advances have been made in understanding the ligand binding to nucleic acids (*Kumar et al. 1998*). This is mainly attributed to the development in structural elucidation, quantum chemical computing and thermodynamic binding analysis techniques. The principles of ligand binding to duplex nucleic acids can be applied to quadruplex structures also, but quadruplex offers some new perspectives in drug DNA binding studies because of the following reasons;

First important aspect is size of G-quartet, a basic motif of G-quadruplex structures offers large extended aromatic surface when compared to duplex DNA. This structural feature in turn brings about changes in binding behavior of ligands. As due to the availability of large pi-pi surface area drugs tend to stack rather than to intercalate between G-quartet planes. Secondly, quadruplex nucleic acids are stabilized by centrally coordinated metal ion like K+ or Na+. Therefore intercalation of a ligand between G-quartet steps in energetically not favorable. Therefore most of the known ligands which have large aromatic surface tend to stack upon G-quartet surface rather than to intercalate. Thirdly, quadruplex structures differ from duplex DNA in width and type of grooves. Duplex DNA has major and minor grooves, but quadurplex grooves depend upon the type of quadruplex sequence and structure formed. For example groove structure in tetramolecular and unimolecular G-quadruplex structures differ in their width. Tetramolecular structures have all the four grooves of equal width, but unimolecular G-quadruplex structures show different groove widths depending upon strand orientation, and finally quadruplex structure offers extra binding pockets in the form of loops. In unimolecular and bimolecular quadruplex structures folding back of a strand results in the loop formation involving the intervening bases. Numerous ligands stabilize the quadruplex structure by binding in the loop region. Interestingly end-stack binding mode also involves the contribution from nucleotides present in the loop region.

NMR methods can be effectively applied to elucidate the binding mode and to obtain binding stoichiometry of drug-DNA complexes, along with this NMR studies also reveals kinetic behavior of the complex formed.

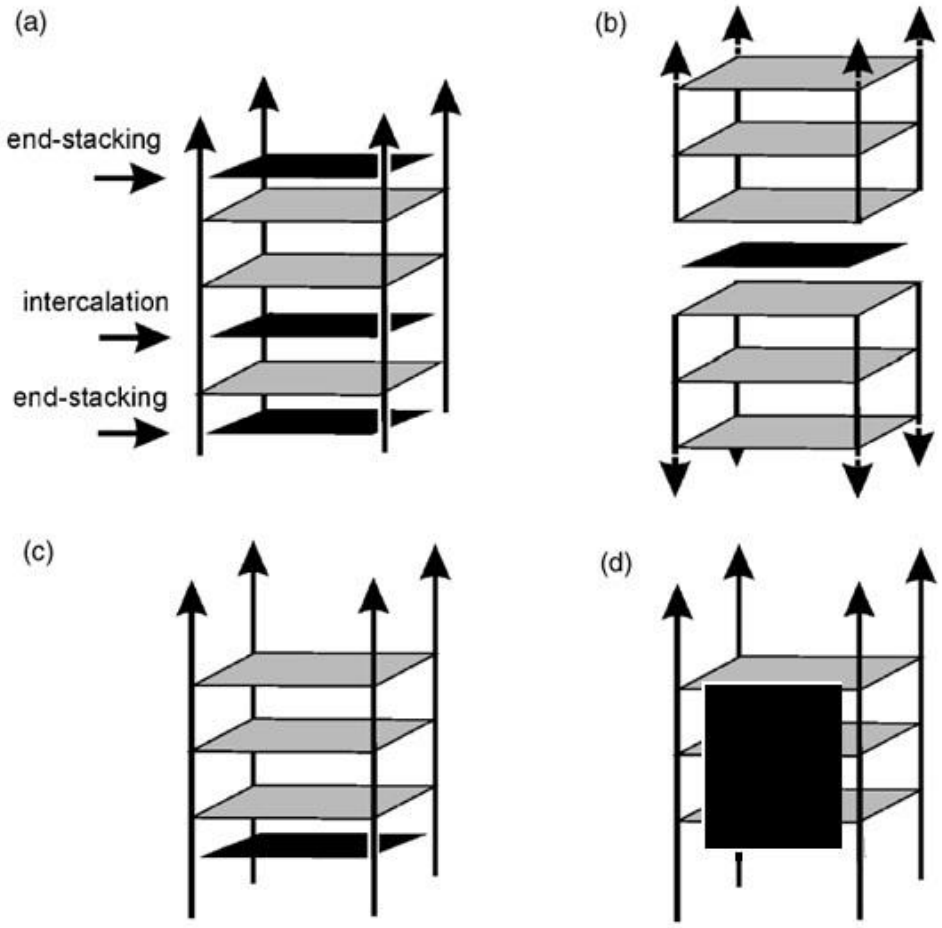

Figure 1.17: Types of interaction of ligands with G-quadrulpex structures. a) end stacking and intercalation in G-quadruplex structures, b) and c) showing end-stacking mode of binding in blunt end G-quadruplexes and d) groove binding.

The following part contains literature review of different class of G-quadruplex binding ligands.

Telomestatin is a macro cyclic natural product isolated from the bacteria *Streptomyces anulatus* strain 3533-SV4, by Kazuo Shin-ya and Co-workers. (*Shin-ya et al. 2001*). Due to its extended macrocyclic structure it shows specific inhibition of telomerase enzyme with IC-50 value in sub-micro molar range of 0.005 μM (5 nM). Telomestatin inhibits the activity of telomerase by interacting and stabilizing G-quadruplex structure in telomere region (*Kim et al. 2002*). A simulated annealing and docking method shows that telomestatin binds to intramolecular G-quadruplex structure by end stack mode forming 2:1 complex.

Cationic porphyrins are one of the important classes of ligands which are known to inhibit telomerase enzyme by stabilizing G-quadruplex structures. Because of their extended aromatic surface cationic porphyrin ligands have been shown to stabilize G-quadruplex structures and inhibit telomerase enzyme at effective concentrations. Using NMR and spectroscopic studies, Mita and Co-workers (*Mita et al. 2006*) showed that porphyrin TMPyP4 interacts and stabilizes the human tetramolecular G-quadruplex repeat sequence $(TTAGGG)_4$. Upon interaction with TMPyP4, the aromatic protons of quadruplex step A3pG4 show significant line broadening effect and up-field shifts. 200ms mixing time NOESY spectra shows specific intermolecular contacts exist between T2H4', A3H1', A3H4', G4H1' and G4H4' quadrulpex protons with *ortho* protons of TMPyP4 and A3H2 and A3H8 aromatic protons with beta protons of TMPyP4, confirms the ligand binding to A3pG4 step of quadruplex molecule. The up-field shift of imino protons of G4 and G5 is due to the ring current effect upon porphyrin binding to DNA. In a plausible model explained on the basis of NMR studies it was shown that planar TMPyP4 stacks on the A3pG4 step covering two or all four bases of adenine residue. The N-methyl pyrinidum side chain of TMPyP4 is present near the DNA backbone and this cationic side chain helps in the binding thermodynamics by forming electrostatic interaction with negatively charged phosphate backbone of quadruplex DNA. The spectroscopic studies show the affinity constant of 6.2×10^{-6} M^{-1}, and number of binding sites approximately equal to one. These above results are supported by UV-vis, fluorescence, CD and TCSPC studies on human tetramolecular TTAGGG repeat sequence, in which the titration of quadruplex DNA to fixed concentration of TMPyP4 show bathochromic shift of 8 nm and 35% hypochromism of 422 nm TMPyP4 peak. The apparent binding constant of 1.29×10^{-6} M^{-1} and number of binding sites 3 is observed for TMPyP4 –G4 DNA interaction (*Zhang et al. 2008*).

Acridines are natural occurring compounds found in coal tar, having anthracene heterocycle with nitrogen atom in the central ring. These molecules are planar and interact with quadruplex nucleic acids through intercalation of Pi-stacking. There are many known acridines like BRACO-19, RHPS4, BSU 6039, which are known to bind G-quadurplex structure.

BRACO, belongs to a group of 3, 6, 9-trisubstituted acridines, but it shows poor selectivity towards quadruplex structure when compared to duplex DNA. Hence BRACO-19, a 3, 6-di substituted acridine with 9-amino side chains shows enhanced quadruplex binding and telomerase activity inhibition and also results in chromosome end-end fusion in cancer cells (*Incles et al. 2004*). The interaction of BRACO-19 with bimolecular human telomere repeat sequence

d(TAGGGTTAGGGT) was studied at 2.5 Å using X-ray diffraction studies by Campbell et al., (*Campbell et al. 2008*). Binding model shows that single molecule of BRACO-19 sandwiches between two molecules of bimolecular quadruplexes at the 3' end. Hence, this shows that BRACO-19 binds as an end stacker. Drug stacks asymmetrically on the end of quadruplex stabilized by π-π stacking interaction with two terminal guanine bases. The substituents at 3- and 6- position of BRACO-19 extend into grooves of G-tetrad hence further stabilizing the complex. The cationic ring nitrogen present on the axis of K+ ion channel acts a stabilizing factor to hold two quadruplexes. Earlier the same group of researchers showed by molecular modeling studies that BRACO-19 stacks on G-tetrad with its side chains occupying the grooves. BRACO-19 shows less membrane permeability which needs to be addressed before its future clinical studies as an anti-cancer agent. Increase in the length of side chains from 3- to 6- results in the progressive decrease in quadruplex binding of BRACO-19 (*Moore et al. 2006*).

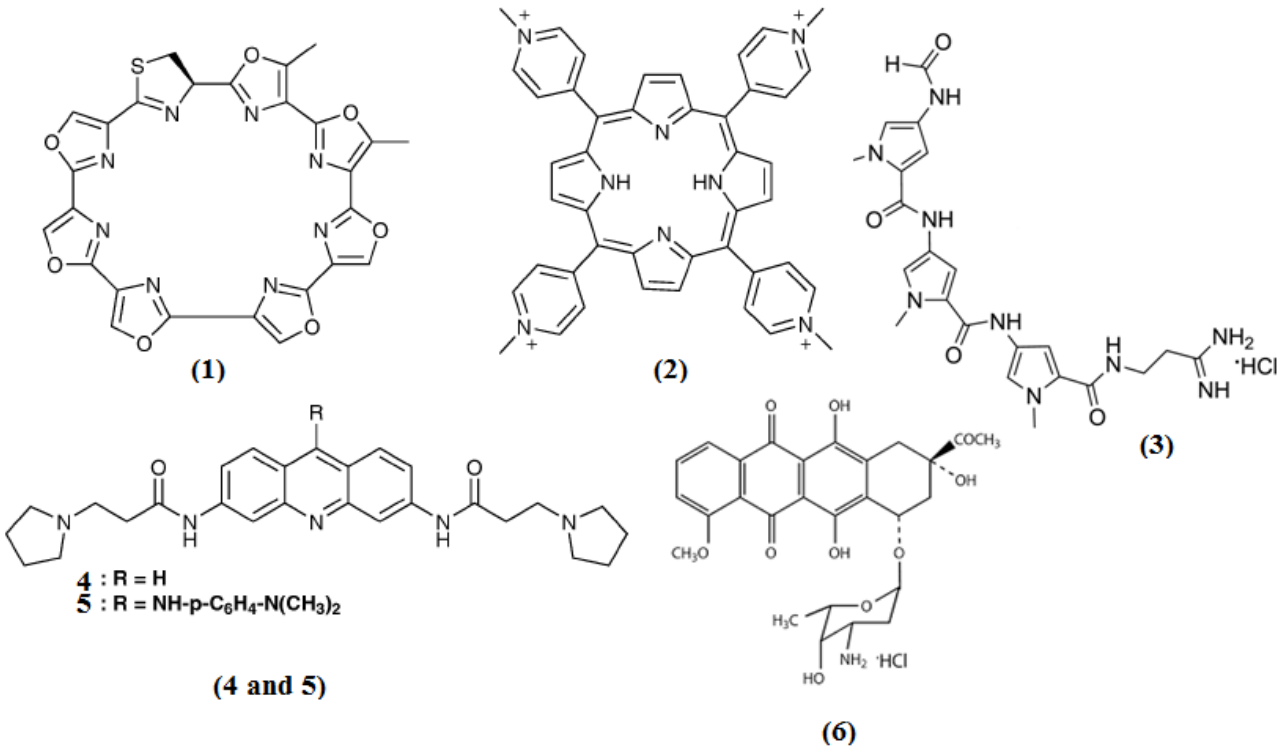

Figure 1.18: Chemical structure of different G-quadruplex ligands; (1) Telomestatin, (2) TMPyP4, (3) Distamycin A, (4) BSU-6039, (5) BRACO-19 and (6) Daunomycin.

RHPS4 is a five membered acridine derivative which shows quadruplex binding and stabilization. Initial studies using TRAP assay protocol shows RHPS4 inhibit activity of telomerase enzyme in sub micro molar range with an IC_{50} value of 0.33 ± 0.13 μM (*Gown et al., 2001*). Solution structure of parallel stranded human quadruplex d-$(TTAGGGT)_4$ with fluorinated pentacyclic quino[4,3,2-kl]acridinium cation, RHPS4 have been determined (*Gavathiotis et al. 2003*). ^{1}H and ^{19}F studies of the complex d-$(TTAGGGT)_4$-RHPS4 shows that drug is in fast exchange with quadruplex DNA. The titration data shows that line width broadens at drug/DNA ratio 0.5 and again sharpens as drug/quadruplex ratio increases to 2. This behavior shows that RHPS4 is in fast exchange with d-$(TTAGGGT)_4$. All the central G-tetrad core i.e G3-G4-G5 are intact, which clearly indicates that RHPS4 is not intercalating between any of G-tetrads. Proton chemical shift perturbations and 24 intermolecular NOE contacts with 5'-ApG step and 5'-GpT step indicates RHPS4 stacks on either side of G-tetrad. Restrained molecular dynamics based on the distance restraints obtained from NOESY and intermolecular peaks confirms the stacking of RHPS4 on either side of G-tetrad. Hence RHPS4 binds to quadruplex DNA by end-stacking mode. It is one of the most potent telomerase inhibitor under clinical trial.

The first NMR based quadruplex ligand complex structure was proposed by Laurence Hurley group in 1998 (*Fedoroff et al. 1998*). Both one dimensional two dimensional NOESY NMR technique was used to study the binding interaction of PIPER (3,4,9,10-perylenetetracarboyxlix diimide) with human tetramolecular repeat sequences. They used four different sequences like d-$(TTAGGGTT)_4$, d-$(TTAGGGTTA)_4$, d-$(TTAGGG)_4$ and d-$(TAGGGTTA)_4$, to distinguish between end-stacking and intercalation mode of binding. Addition of PIPER to d-$(TTAGGGTTA)_4$ results in gradual disappearance of GNH resonances and gradual appearance of new resonances in the corresponding up-field region. Due to the broadening of resonances after addition of PIPER, only two complexes namely d-$(TTAGGG)_4$ and d-$(TAGGGTTA)_4$ were further studied to get the structure through NOESY correlations. Based on the chemical shift perturbation and NOEs it was shown that PIPER binds on the terminal G-quartet plane of d-$(TTAGGG)_4$ by end-stacking mode. A single molecule of PIPER stacks between the two molecules of quadruplex, with two quadruplex structures arranged in head-to-tail fashion. But a different type of binding was observed when PIPER interacts with quadruplex sequence with 3' overhang sequences, like in d-$(TAGGGTTA)_4$. The presence of NOEs with G5pT6 step protons shows that PIPER binding site, as the $(GGG)_4$ core

remains intact it was predicted that drug binds to d-$(TAGGGTTA)_4$ quadruplex sequence by threading intercalation mode.

BSU6039, an acridine derivative with di-substitutions at the 3 and 6 positions with 3-pyrrolidinopropionamide (aminoalkylamido side chains) side-chains have shown to inhibit the activity of telomerase enzyme (*Perry et al. 1999; Read et al. 2001*). In 2003 Haider and co-workers of Stephen Neidle group (*Haider et al. 2003*) solved the crystal structure of 3,6-bis-[3-pyrrolidino-propionamide] acridine (BSU6039) with *Oxytricha nova* telomeric DNA sequence d(GGGGTTTTGGGG) at 1.75 Å resolution in the presence of K+ condition. This sequence forms a hairpin dimer with thymine loops present diagonally across the top and bottom G-tetrad with alternating *syn-anti* guanines. BSU6039 forms a 1:1 complex with this quadruplex structure, with acridine ring stacking on the terminal G-tetrad. Pi-pi interaction between terminal two guanine bases and acridine chromophore acts a stabilizing force for the binding interaction. BSU6039 contains two aminoalkylamido side-chains, both of which position themselves near the quadruplex grooves. The O2 atom of the loop thymine T2 forms a hydrogen bond with the acridine ring nitrogen, which is protonated at pH > 7.0.

Well studied DNA minor groove binding ligands like distamycin A and netropsin have been shown to interact with G-quadruplex DNA. In one such study Martino and his Co-workers (*Martino et al. 2007*) reported the detailed NMR structure of distamycin A binding to a parallel G-quadruplex structure d-$(TGGGGT)_4$. Chemical shift perturbation and intermolecular NOE peaks shows that distamycin A exists as dimer in head to tail fashion and binds to two opposite grooves of d-$(TGGGGT)_4$. The BMI values obtained by saturation transfer difference (STD)-NMR study also supports the binding of distamycin A to d-$(TGGGGT)_4$. To prove that distamycin A is interacting in groove region they also used modified DNA sequence 8-bromo gaunosine in the second G of G2-G3-G4-G5 stretch, d-$(TGG\text{-}BrGGT)_4$. This modified oligonucleotide forms a parallel quadruplex sequence but bulky Br protrudes out in the groove region, which prevents the binding of distamycin A to this quadruplex DNA.

Based on Distamycin structure, various analogues have been synthesized which can bind and stabilize G-quadruplex structures. In one such study Cosconati and co-workers (*Cosconati et al. 2010*) replaced amidinium group by an uncharged N-methyl amide group in distamycin molecule. GNH and GH8 proton signals of all four G-tetrad steps show upfield shift upon interaction with the

ligand. On the contrary both terminal TH6 and CH_3 signals show downfield shift. 12 drug head-to-tail dimer NOEs were observed similar to distamycin molecule (Martino et al. 2007) and 14 NOEs were observed between Dist-A analogue with d-$(TGGGGT)_4$ quadruplex. Hence it was evident that Dist-A analogue binds to groove and 3' end of quadruplex d-$(TGGGGT)_4$ quadruplex structure as head-to-tail dimer.

Clark G. R et al., (*Clark et al. 2003*) solved the high resolution crystal structure of anti-cancer anthracycline daunomycin with tetramolecular quadruplex forming sequence from *Tetrahymena* telomere, d-$(TGGGGT)_4$ in a Na+ ion condition. The crystal data showed that daunomycin binds to the G-quadruplex structure in end stacking mode. Six daunomycins arrange in two layers of three molecules each and stacks into the terminal 5'-GT segment of the two end to end stacking quadruplexes. Hence the binding stoichiometry is three daunomycin molecules end stack to a quadruplex structure, which is stabilized by pi-pi interaction between daunomycin-daunomycin and daunomycin-quadruplex. The sugar moiety of daunomycin molecule interacts with the groove of quadruplex through hydrogen bonding or Van der Waals interaction. Therefore three of the four quadruplex grooves were occupied by sugar moiety of three daunomycin molecules. In a similar study Clark and Co-workers (*Clark et al. 2012*) shows the effect of terminal thymine nucleotide on daunomycin interaction to tetramolecular quadruplex structure. The crystal studies of d-$(GGGG)_4$-daunomycin in the presence of Na+ ions shows that daunomycin binds in end stacking mode, but with a higher order aggregation structure. The four daunomycin molecules arrange in a plane with nose to nose arrangement, four such daunomycin layers stack between the two GGGG quadruplex layers. The binding arrangement shows d-$(3'$-GGGG-$5')_4$-Dau-Dau-Dau-Dau-d-$(5'$-GGGG-$3')_4$. 'Dau' denotes a layer of four daunomycin molecules. The stability of this complex structure stems from the extensive pi-pi stacking between daunomycin-daunomycin aromatic chromophore layer and between daunomycin-terminal gaunosine bases. The complex shows the perfect 4-fold symmetry. The 5'-terminal guanine shows glycosyl orientation of *syn* due to the square prim orientation of Na+ ion.

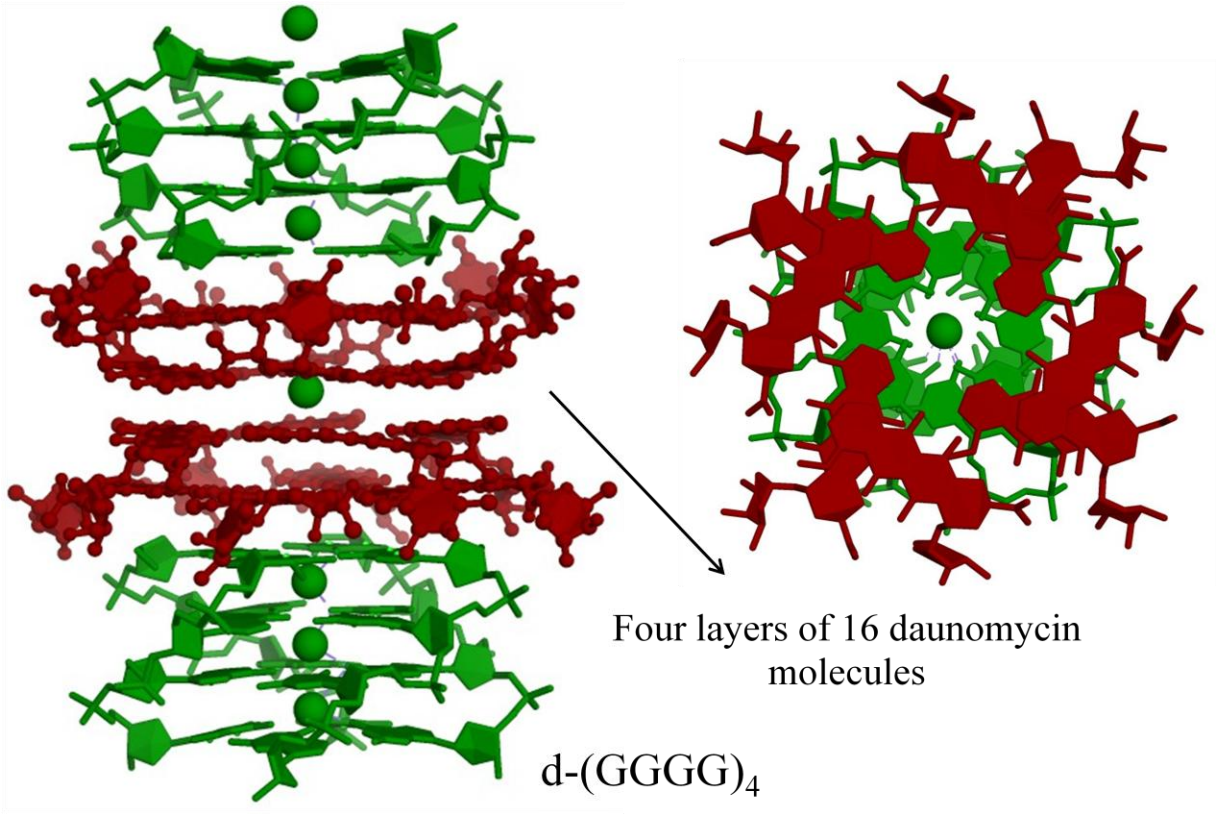

Figure 1.19: Binding of daunomycin to d-$(GGGG)_4$ tetramolecular quadruplex structure; PDB ID (Clark et al., 2012)

Wei Gai and Co-workers (*Gai et al. 2013*) showed that cyanine dye 2,2'-diethyl-9-methyl-selenacarbocyanine bromide (DMSB) binds to d-$(TGGGGT)_4$ in a dual mode; while in one site drug binds as dimer and as a monomer in the second site. Initial addition of DMSB to d-$(TGGGGT)_4$ i.e D/N ratio 0.5 to 2, results in the broadening of aromatic and methyl protons of G5pT6 step. DMSB binds to quadruplex DNA in monomer mode (M-mode) in this D/N ratio. G6-NH show up-field shift and T6-H6 and T6-CH_3 show downfield shift (> 0.1 ppm), hence DMSB stacks as monomer between G5 and T6 residues by end stacking mode. Further increase in D/N ratio from 3:1 to 8:1 results in the sharpening of G5-NH, G5-H8, T6-CH_3, T6-H6 resonances and show little change in chemical shift position in this D/N range. This clearly indicates the filling up of this site, but proton resonances of T1 and G2 step shows dramatic shift, and broaden remarkably. G2-NH proton shifts maximum downfield (~0.3ppm). This clearly shows the different binding behavior, as drug binds other than stacking, as it involves T1, G2 and G3 steps. Based on these observations the authors propose the structure of DMSB bound d-$(TGGGGT)_4$ tetramolecular

quadruplex. One drug binds to G5pT6 step as a monomer by external stacking, and a head to tail dimer DMSB molecule binds to T1pG2pG3 step in groove region.

Quin Li and Co-workers (*Li et al. 2009*) in their study of interaction of non-planar alkaloids peimine and peiminine, with human tetramolecular quadruplex forming sequence d-$(TTAGGGT)_4$, showed that drug binds as a monomer in two separate grooves. Addition of peimene/peiminine to d-$(TTAGGGT)_4$ results in downfield shift of G4, G5 proton resonances and upfield shift of G6 proton resonances. Apart from these, T2H6, $T2CH_3$, A3H8, A3H2, G5H8, $T7CH_3$ proton resonances also show downfield shift. The 2:1 NOESY spectra acquired at 100 ms and 300 ms show very few intermolecular peaks due to signal overlapping, the important among them are peiminine 23- positioned methyl protons with T2H2', T2H2", A3H2' protons, and 19-positioned methyl group with T2H2' proton. These two studied alkaloids lack extended planar aromatic ring structure for π-π stacking on G-quartets and based on the obtained intermolecular peaks between peiminine and d-$(TTAGGGT)_4$, the authors clearly conclude the two alkaloid molecules binds as a monomer in the two grooves of G-quadruplex structure. The thermal stabilization experiments based on CD spectroscopy, peimine and peiminine stabilize d-$(TTAGGGT)_4$ quadruplex melting by $14\pm 2\ ^{o}C$ and $13\pm 2\ ^{o}C$, respectively.

Interaction between heme and parallel G-quadrupelx DNA TTAGGG was studied using NMR techniques (*Saito et al. 2012*). The heme (Fe^{3+}) is sandwiched between the two terminal G-quartets of the d-(TTAGGG) G-quadurplex DNA. Intermolecular NOEs between heme (methyl and vinyl) and G6 (H8, H1', H2', H2", H3' and H4') protons of the G-quadruplex shows that heme stacks on terminal G-tetrad.

Spectroscopic studies like UV-visible, fluorescence, circular dichroism spectroscopy, ESI MS, ITC, DSC and SPR studies along with molecular modeling approaches were used to study the mode of interaction, stoichiometry of the ligand binding, energetics of the binding interaction of numerous ligands to different quadruplex structures. Importance of telomerase inhibition by quadruplex stabilization made numerous research groups across the world to do work on both natural and synthetic analogues of small molecule compounds as G-quadruplex binding/stabilizing agents. One such well known anti-tumor drug is mitoxantrone.

Table 1.3: Some important PDB structures reported for solution NMR and X-ray crystal structures of quadruplex-ligand complexes with important binding characteristics.

PDB ID (method of study)	Ligand	Sequence	Binding mode and other features	Reference
Parallel tetramolecular complexes				
1NZM (NMR)	RHPS4	Tetramolecular parallel quadruplex d-$(TTAGGGT)_4$	End stacking on both sides of G-quartets, i.e at A3pG4 step and G6pT7 step	*Gavathiotis et al. 2003*
1O0K (X-ray)	Daunomycin	Tetramolecular parallel quadruplex d-$(TGGGGT)_4$	End-stacking, with two layers of three daunomycin in one plane sandwiching between two quadruplex molecules	*Calrk et al. 2003*
2JWQ (NMR)	Quinacridine based ligands	Tetramolecular parallel quadruplex d-$(TTAGGGT)_4$		*Hounsou et al. 2007*
2JT7 (NMR)	Distamycin	Tetramolecular parallel quadruplex d-$(TGGGGT)_4$	Two distamycin molecules as head-to-tail dimer in two opposite grooves of quadruplex.	*Martino et al. 2007*
2KVY (NMR)	Distamycin analogue	Tetramolecular parallel quadruplex d-$(TGGGGT)_4$	Dimer both end stacking and groove binding	*Cosconati et al. 2010*
3TVB (X-ray)	Daunomycin	Tetramolecular parallel quadruplex d-$(GGGG)_4$	End-stacking, with four layers of four daunomycin sandwiching between two quadruplex molecules	*Clark et al. 2012*
Bimolecular complexes				
3CE5 (X-ray)	BRACO-19	Bimolecular, human telomere d(TAGGGTTAGGGT)	End stacking	*Campbell et al. 2008*
Unimolecular complexes				
2MB3 (X-ray)	Telomestatin	Unimolecular human telomere d$[T_2G_3(T_2AG_3)_3]$	End stacking,	*Chung et al. 2013*

1.7 Mitoxantrone

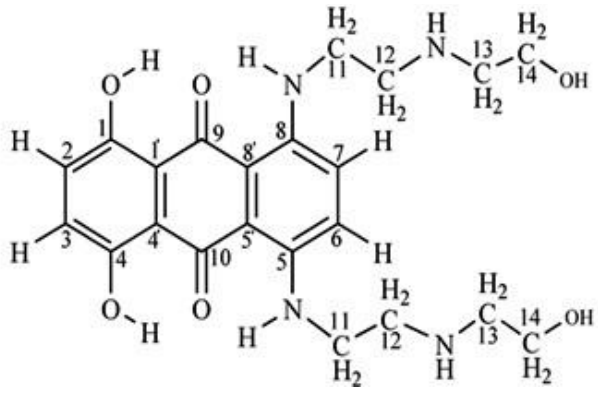

Figure 1.20: Chemical structure of Mitoxantrone.

Mitoxantrone (IUPAC: 4-dihydroxy-5,8-bis[[2-[(2-hydroxyethyl) amino)ethyl]amino]]-9,10-anthracendione) is a synthetic antitumor (antineoplactic or cytotoxic) derivative of anthracenedione or dioxoanthrcene (anthraquinone). The basic structure of mitoxantrone consists of three planar aromatic rings with two keto groups at 9 and 10 position (9,10-anthraquinone), and aminoethylamino side chains at position 5 and 8 (Fig. 1.20). Mitoxantrone (MTX) acts as an effective synthetic substituent to naturally occurring anthracycline drugs which were used as antitumor agents. Mitoxantrone has planar anthraquinone rings but differs from anthracyclines (e.g. doxorubicin) owing to lack of sugar and tetracycline ring (ring A). These anthracycline dugs show toxicity and cause irreversible damage to the cardiac muscles after prolonged therapy. In contrast, the clinical trials of mitoxantrone shows significant clinical activity in patients with solid tumor like breast cancer, acute leukemia and lymphoma with less cardio-toxicity.

1.7.1 Structure and activity relation

The clinical studies of mitoxantrone began in1979 (*Murdock et al. 1979*), in these studies mitoxantrone show anti-cancer activity in patients with acute leukemia and breast cancer. Along with its important anti-cancer function MTX also pocesses antiviral, antibacterial, antiprotozoal, immuno modulating, and anti-neoplastic properties. The major mechanism of action of MTX involves the DNA intercalation/end stacking and electrostatic interactions of its side chains along the grooves of DNA (*Kotovych et al. 1986*). MTX also efficiently inhibits the activity of human topoisomerase II enzyme (*Errington et al. 1999*), which is over-expressed in cancer cells. The gastrointestinal and cardiac effects are less severe and less frequent than that with the anthracycline

anticancer drugs. Due to its low incidence of harmful toxicities, serious side effects and its effectiveness in treating solid tumors and leukemias, mitoxantrone is a promising agent in the treatment of cancer.

The initial study of structure based approach to develop amido anthraquinone derivatives to inhibit the activity of telomerase enzyme by stabilizing G-quadruplex structure was done by Sun and Co-workers of Stephen Neidle and L H Hurley group (*Sun et al., 1997*). The 2,6-diamidoanthraquinone inhibits human telomerase enzyme by stabilizing G-quadruplex structure. NMR experiments and TRAP assay was used to determine the binding behavior of 2,6-diamidoanthraquinone to d-[T_2AG_3T] quadruplex DNA. Complex formation results in upfield shift of NH resonances of all three quartet forming guanines. Presence of imino-imino sequential walk in the 2D-NOESY of the 2,6-diamidoanthraquinone: d-[T_2AG_3T] complex suggests ligand is not intercalating between G-steps. But the obtained upfield shifts of Guanine imino proton suggests that 2,6-diamidoanthraquinone may be interacting with 5'-AG step. The ^{1}H-NMR thermal denaturation experiments shows stabilization of G-quadruplex structure by 2,6-diamidoanthraquinone. The increase in *Tm* by about 20 ^oC at 4:1 ratio 2,6-diamidoanthraquinone: d-[T2AG3T] complex compared to the alone d-[T2AG3T] clearly show the stabilization of G-quadruplex structure by the ligand.-TRAP assay results show the EC_{50} value of 23 μM.

Numerous spectroscopic studies have established that MTX binds to DNA via intercalation/stacking mode of binding (*Kotovych et al. 1986; otter et al. 1986; otter et al. 1996*). Kapunsciski and Co-workers (*Kapunsciski et al. 1981*) showed that MTX forms intercalation complex with both A-DNA and B-DNA forms, aided by electrostatic interaction of aminoalkyl side chain with DNA phosphate groups. Upon interaction with DNA the MTX monomer and dimer peaks shows red shift and the binding constant was found to be 1.8×10^6 M^{-1}, the unwinding angle of 26.5^o which was comparable with other intercalating drugs like EtBr and proflavine binding to DNA.

1.8 Flavonoids

Evolution and existence of every organism on this planet Earth depends on the photosynthesis, in-turn plants are the reservoir of this energy storage mechanism. Plant extracts or its active constituents are the primary source for majority of traditional medicininal practices around the world. In fact, World Health Organization (WHO), a premier institute of United Nations (UN)

estimates that traditional medicines from plants constitute the primary health care needs for more than half of world's population. Numerous modern medicines were developed directly or indirectly from natural products. Moreover, the exact mode of action and target organs/tissues for most of the traditional medicines has not been fully elucidated due to lack of research and knowledge about these plants.

Flavonoids are one such major traditional medicine used from time immemorial in various traditional practices around the world. Flavonoids are the naturally occurring plant secondary metabolites and serves as a major component of our diet. Flavonoids are not reported to occur naturally in animals. They belong to the large class of plant metabolites called polyphenols. The chemical structure of flavonoids is characterized by carbon skeleton of three units C6-C3-C6, in which two aromatic rings are linked through an oxygenated heterocycle, the three rings are designated as A, B and C. Rings A and B are aromatic in nature. The A and B ring have different metabolic source, the B ring is formed by the shikimate pathway, and A ring through condensation of three units of malonyl Co-A.

Flavonoids are classified based on the degree of oxidation of three carbon central C ring, into flavonols, flavones, isoflavones, flavanones and flavanals. There are more than 4000 flavonoids discovered from variety of plant sources and known to play various important roles in plants. They are also known to occur with variety of modifications like glycosylation, methoxylation, hydroxylation etc.

Primarily, flavonoids functions as a plant coloring agents (pigmentation) and helps in plant protection from predators. But, flavonoids are well known for their biological effects on animals, particularly humans. They possess various health benefits due to their antioxidant properties.

Apart from their numerous biological activities like anti-oxidant, anti-inflammatory activities, flavonoids show anticancer activity. This significant property of flavonoids is through the induction of apoptosis by modulating proliferation pathways and inhibition of the ubiquitin–proteasome pathway. Several flavonoids like apigenin, luteolin, quercetin, and chrysin have been shown to inhibit proteasome activity and induce apoptosis in human leukemia cells (*Chen et al. 2005; 2007*. Flavonoids are diverse group of pro-beneficial secondary metabolites, having numerous structural variations. These structural variations aids in identifying variety of biological receptor molecules. For example quercetin and luteolin were known to inhibit topoisomerase I (*Webb and Ebeler,*

2004), while genistein, a major soy isoflavone was reported to inhibit the activity of topoisomerase II enzyme (*Bandaele and Osheroff 2007*.). Topoisomerase inhibition supports the proposed anti-cancer property of flavonoids along with inhibition of protein tyrosine phosphyrlation (Ref). But the main cellular target for the flavonoids remains elusive yet.

Numerous studies exist explaining the mode of interaction of flavonoids with duplex, triplex and quadruplex DNA molecules. The first report of flavonoid binding to DNA structure was of quercetin binding to calf thymus DNA (*Alvi et al. 1986*). Melting studies shows quercetin stabilizes the DNA by about 4 ^{o}C. Quercetin and luteolin are the two the most widely studied flavonoids, which binds duplex DNA by intercalation or external binding (*Solimani, 1995; Chowdhury et al. 2002*).

Nerdal and Co-workers (*Nerdal et al. 1993*), showed the interaction of flavonoid glycoside kampeferol 7-O-neohesperdioside with *Escherichia coli* lac promoter dodecamer sequence d-(GCGTATGTTGCG) using solution state NMR studies. Binding of kampeferol 7-O-neohesperdioside to DNA sequence shows line broadening of flavonoid resonances. NOESY spectra (100, 180, 250 ms at 296 K and 180 ms at 315 K) of kampeferol 7-O-neohesperdioside- d-(GCGTATGTTGCG) complex shows both kampeferol 7-O-neohesperdioside intramolecular cross peaks and kampeferol 7-O-neohesperdioside-DNA intermolecular cross peaks. The presence of sequential walk between base (H6/H8) protons with sugar (H1' and H2'/H2") protons proves that kampeferol 7-O-neohesperdioside binds to DNA through non-intercalative mode. Kampeferol 7-O-neohesperdioside H5' and H3' protons shows NOEs with A5 sugar H1' and H6' and base H2 protons of DNA. Model building using NOEs shows the mode of binding of kampeferol 7-O-neohesperdioside to DNA dodecamer sequence as groove binding type, with aglycone flavonoid moiety interacting with DNA groove protons and sugar moiety present outside this groove region due to steric hindrance. This clearly proves that kampeferol-7-neohesperdioside binds to duplex DNA by groove binding mode.

Flavonoids were also shown to bind to triplex DNA structures. Wan et al. (*Wan et al. 2009*) showed that flavonoid aglycones like quercetin, luteolin, kampeferol binds to duplex DNA more strongly than triplex DNA structures.

In this part of literature review, we mainly focus on studies on the interaction of flavonoids with quadruplex DNA.

The first report on the interaction of flavonoid with quadruplex DNA was provided by Sun. H and Co-workers (*Sun et al. 2006*). They studied the interaction of quercetin with monomeric and dimeric tetramolecular G-quadruplex DNA using absorption, fluorescence, CD and one dimensional NMR spectroscopy. The UV-visible study shows red shift of 371 nm band of quercetin to 380 and 376 nm upon interaction with monomeric and dimeric G-quadruplexes, respectively. The 371 nm peak is attributed to the benzoyl and cinnamoyl ring system of quercetin. The fluorescence spectral study shows increase in the intensity of emission peak at 533 nm more than 422 nm peak, when bound to monomeric G-quadruplex. But when bound to dimeric form the intensity of 422nm peak increases more than 533nm peak. Based on the proton transfer process in quercetin at different environments, authors predict quercetin binds to monomeric form of G-quadruplex structure through intercalative mode of binding and dimeric G-quadruplex structure by groove binding.

In another major study, interaction of flavonoid glycoside, rutin with extended tetramolecular human G-quadrulpex structures d-$(TTAGGG)_4$, d-$(TTAGGGG)_4$ and d-$(GGGT)_4$ has been reported (*Sun et al. 2007*). Rutin also called as vitamin P, in conjugation with backbone flavonone planar 15 member ring, rutin has non planar substituent group of β-D-rutinoside at C (3)-O position. Structurally rutin resembles the structure of an axe, with planar flavonone ring acting as blade and non-planar rutinose sugar as hammer. Upon interaction with G-quadruplex structure, the 356 nm absorption band of rutin shows bathochromic shift and fluorescence emission intensity increases. The bathochromic shift and increase in emission intensity is more for blunt end stacked d-$(TTAGGG)_4$ and d-$(TTAGGGG)_4$ structures when compared to interlocked d-$(GGGT)_4$ G-quadruplex structure. The proton NMR studies shows addition of rutin results in the decomposition of blunt end stacked G-quadruplex structures to its monomer from. The imino proton resonance of terminal G-quartet residue in d-$(TTAGGG)_4$ and d-$(TTAGGGG)_4$ structures show upfield shift, but the terminal imino proton resonances of interlocked d-$(GGGT)_4$ sequence show no shift in position. These results clearly explain that rutin binds to terminal G-quartet via stacking interaction.

Apart from above mentioned flavones, daidzin, an important isoflavone present in soy compounds also shows stabilization of G-quadruplex structure (*Li et al. 2006*). Daidzin is a 7-O-glucoside of isoflavone daidzein. ESI-MS studies shows that daidzin interacts with human telomeric antiparallel G-quadruplex structure $dAG_3(T_2AG_3)_3$ under molecular crowding condition in the stoichiometric

ratio of 1:2. The electrophoretic mobility shift assay also confirms the formation of daidzin-d[$AG_3(T_2AG_3)_3$] complex. Circular Dichroism and thermal melting studies show stabilization of antiparallel quadruplex structure by daidzin. The CD spectra shows increase in intensity with blue shift of 295nm positive CD band of antiparallel d[$AG_3(T_2AG_3)_3$] quadruplex structure, with increase in T_m from 62^{o}C to 66.5^{o}C at D/N ratio 2.0. Molecular docking studies shows binding of daidzin molecule to d[$AG_3(T_2AG_3)_3$] quadruplex structure in diagonal loop, with π-π interaction with G10 and T12 residues and formation of three hydrogen bonds between daidzin and quadruplex structure.

Daidzein and genistein comprises the major class of soy isoflavones and they show anticancer activity at the earlier stage of cancer development. The anticancer activity of genistein in prostate cancer cells was due to inhibition of telomerase enzyme activity through repression of hTERT transcription via *c-Myc* and also by altering posttranslational modification of hTERT through *Akt* (*Guo et al. 2004; Ravindranath et al. 2004*).

The knowledge that isoflavones acts as G-quadruplex ligands were also supported by the work of Jin-li Zhang (*Zhang et al. 2009*). The interaction of isoflavones daidzein and genistein and their glycoside form daidzin and genistin, with human G-quadruplex sequence d[AG3(T2AG3)3] and duplex DNA was studied through spectroscopic techniques like UV-vis, fluorescence, CD, ESI MS and molecular modeling. Upon interaction, 294 nm positive CD peak of d[AG3(T2AG3)3] quadruplex shows increase in intensity for glycosidic forms daidzin and genistin, when compared to their aglycosidic forms. Thermal melting profiles show increase in ΔTm by about 4-5 ^{o}C for glycosidic forms and 2-3 ^{o}C for aglycosidic forms. The fluorescence intensity of glycosides quenches due to static quenching upon formation of complex with quadruplex DNA. Moreover glycosides show destabilizing effect on 22 mer duplex DNA. ESI MS results show formation of both 1:1 and 2:1 complex in the case of glycosides daidzin and genistin with AG22 quadruplex DNA. The molecular docking studies shows genistin and daidzin interacts with G-quadruplex DNA in the diagonal loop region with aglycone ring shows π-π interaction with 5'- terminal G-quartet accounting for stabilization of G-quadruplex structure.

Sengupta et al. (*Sengupta et al. 2013*) showed the interaction of medicinally important plant flavonoid fisetin with unimolecular DNA sequence d(T2AG4)$_4$ using spectroscopic and chromatographic studies. d(T2AG4)$_4$ forms an anti-parallel G-quadruplex structure in the 25 mM

NaCl containing Tris buffer. Thermal difference spectra shows induced positive band at 345 nm with a shoulder at 312 nm along with the trough at 390 nm which suggests the interaction of fisetin with DNA quadruplex structure. Addition of quadruplex DNA (0 to 20 μM) to fisetin shows enhancement of fluorescence intensity of the 530 nm band along with red shift of 15 nm. This drastic changes in the fluorescence behavior of fisetin in the presence of G-quadruplex structure indicative of changes in the environment of flavonoid molecule from aqueous buffer to aprotic quadruplex DNA. This in turn was confirmed by time resolve fluorescence spectroscopic studies, which shows increase in average lifetime (τ) of fisetin molecule by six to seven times and by ~ 14% when DNA concentration increased by 7.5 μM to 27 μM. The mode of binding of fisetin to anti-parallel G-quadruplex is along the face of G-quartet along the diagonal loop, confirmed by competitive ethidium displacement experiments. Ethidium bromide (EtBr) is known to bind G-quadruplex structure by intercalation or by end stacking mode. Fisetin does not show reduction in the emission intensity, in the presence of EtBr, which clearly shows that binding sites of EtBr and fisetin are different from each other. Hence the fisetin binds to anti-parallel G-quadruplex along the face of G-quartet along the diagonal loop. This binding mode is also supported by the absence of induced CD band in circular dichroism spectroscopic studies and no significant increase in the T_m of $d(T2AG4)_4$ in the presence of fisetin by UV thermal melting studies.

1.9 Importance of sequence and ligands used in present work

The sequence used in present work d-(TTGGGGT) is related to telomere sequence of ciliate *Tetrahymena* which has repeating unit of TTGGGG. The freshwater ciliated single celled protozoan *Tetrahymena thermophila* is used as model organism in various molecular biology experiments. It is found in various freshwater habits like streams, ponds and lakes and in range of climates. As blunt end G-quadruplex structures tend to stack between themselves to form higher order dimer structures, we have chosen a sequence with 3' terminal thymine (T7), which results in formation of stable tetramolecular parallel quadurplex structure.

1.9.1 Mitoxantrone

Mitoxantrone is an important anticancer drug used against variety of cancer forms. It is a well known duplex binder, binds by external stacking or by intercalation mode to duplex DNA and RNA.

1.9.2 Quercetin

Quercetin is an important flavonoid representative, as it shows numerous health benefits like antioxidant activity, anti-inflammatory effect, cardio-vascular protection, anti-tumor activity, anti-allergic activity, anti-bacterial, anti-viral, anti-helminthes activity. Important structural features of quercetin includes the presence of 3-OH group, 2, 3 position double bond in conjugation with 4-keto function group in the C-ring. It also possess 3', 4'-dihydroxy group in the B-ring. All these structural features are essential for maximum radical scavenging (anti-oxidant) activity of flavonol quercetin. The crystal and solution structure along with molecular modeling studies shows quercetin is a planar molecule, as the exocyclic B-ring exists in planar conformation with respect to the A and C ring. The planarity results in the extended delocalization and conjugation of pi-electrons. This characteristic planarity helps in the reported intercalation binding of quercetin to nucleic acids. In addition to this, presence of 3, 5, 7, 3', 4' -OH groups in quercetin plays an important role in stabilizing the quercetin-biomolecule interactions.

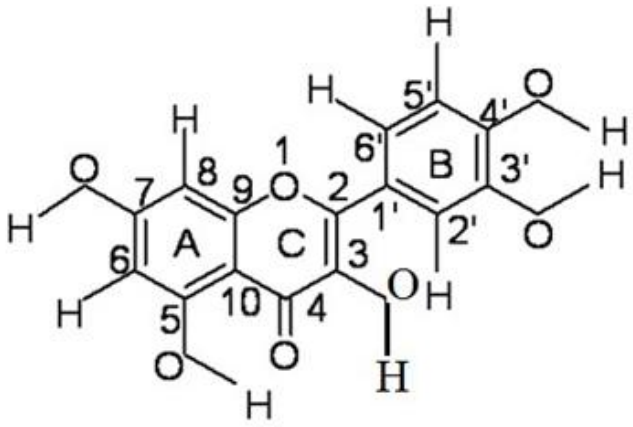

Figure 1.21: Chemical structure of quercetin.

1.9.3 Rutin

Rutin also known as vitamin P is the major flavonoid glucoside present in plants. Rutin is widely present in plant kingdom, like *Ruta graveolens*, buckwheat plant (*Fagopyrum exculentum*) contains ~ 3% (w/w) of rutin in the dried sample. Chemical structure of rutin consists of rutinose sugar attached to 3' OH of quercetin. Hence rutin is the 3'-β-rutinoside of quercetin. The rutinose is a disaccharide sugar consists of α-L-rhamnopyranoside-(1 → 6)-D-glucose. This rutinose moiety attaches to the flavonol backbone at anomeric C1' group of glucose residue. Most of the naturally

occurring sugars are in D-form, but rutinose contains rahmnose in L-from. The important biological activity of rutin includes antioxidant activity, superoxide dismutase activity with metal complexes (*Kostyuk et al. 2004*), cell-dependent reduction of extracellular oxidants (oxido reductase activity) (*Fiorani and Accorsi 2005*). Rutin was shown to bind to G-quadurplex DNA structure by Sun and Co-workers (*Sun et al, 2009*).

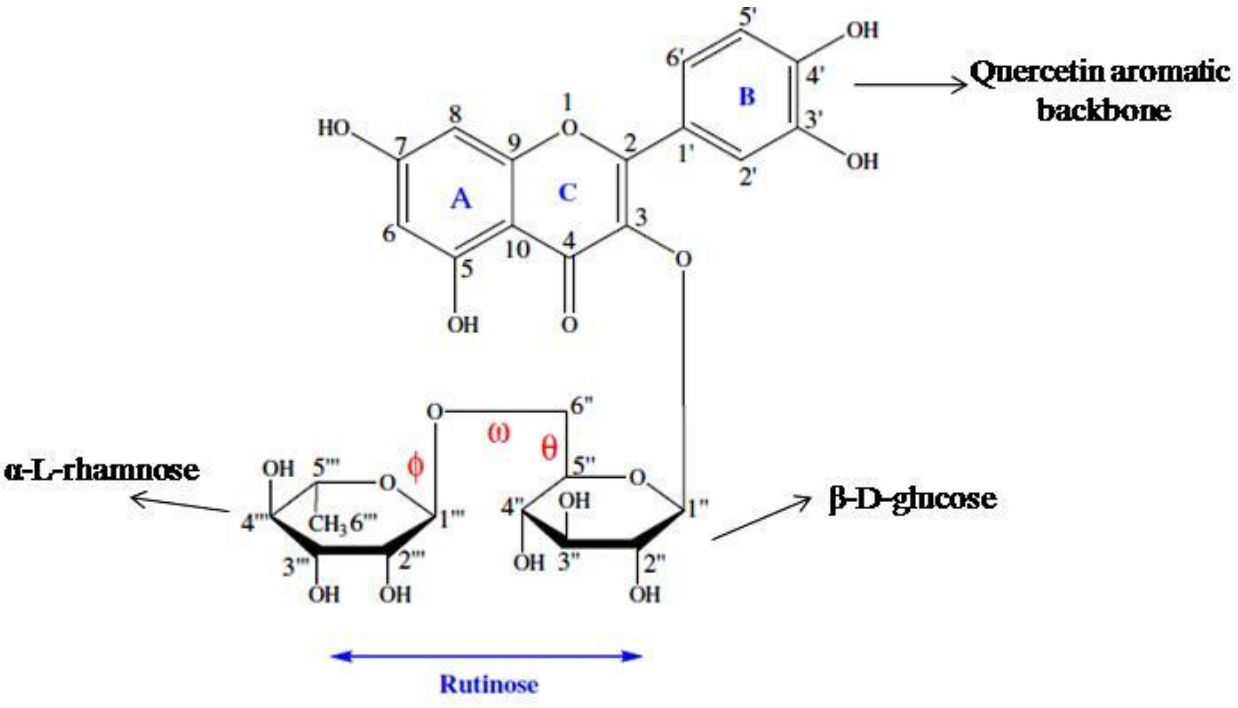

Figure 1.22: Chemical structure of rutin.

1.10 Scope of the thesis

Almost all of the processes in cellular biology and molecular biochemistry depend upon the phenomenon of molecular recognition between receptors and ligands. These processes are critical to the survival of cells and hence the organs and organisms. To name a few, these interactions include enzyme-substrate, transcription factor and DNA interaction, cell receptor and signaling molecules interactions and many more. Majority of these biomolecular interactions are of non-covalent type and often are reversible process governed by basic thermodynamic principles. Generally the receptor or substrate molecule is bigger biomolecule like proteins, DNA and RNA, and ligand are small molecules. Chromosome of eukaryotes consists of terminal telomere region which is made up of G-rich repetitive DNA and associated proteins. These G-rich repeats have been reported to form G-quadruplex structure, which inhibits the activity of telomerase reverse

transcriptase enzyme. Telomerase is an important cancer marker, over expressed in cancer cells, helps in maintenance and elongation of telomeric DNA thus preventing cells from undergoing cell death by apoptosis pathways. Hence stabilization of G-quadruplex DNA thereby inhibiting telomerase enzyme is an attractive strategy for development of anticancer agents.

Being an important anti-cancer agent since past three decades, there is no detailed solution or crystal structure reported for mitoxantrone and its interaction with biologically relevant telomeric G-quadruplex sequence. Flavonoids are the important components of our daily diet, with numerous beneficial properties for humans like anti-oxidant, anti-inflammatory etc. These molecules have been reported to interact with quadruplex structures, but detailed three dimensional structures are not available in any of the structural data banks like PDB of BMRB/NDB. This prompted us to study interaction of these three ligands namely mitoxantrone, quercetin and rutin with quadruplex DNA. In the present work we focus mainly on the interaction of small molecule ligands: one is well known anticancer drug mitoxantrone and other two are major flavonoids in our daily diet, i.e. quercetin and rutin with tetramolecular parallel G-quadruplex DNA.

The current work in thesis is divided into six chapters. Chapter 1 contains introduction about the subject and a detailed review of literature. Chapter 2 consists of materials and methodology used in the present study. Chapter 3 deals with the spectroscopic studies of interaction of mitoxantrone with d-$(TTGGGGT)_4$ parallel quadruplex structure. UV-visible, Fluorescence, CD spectroscopy along with SPR techniques were used to deduce the binding affinity and thermodynamic parameters for interaction of MTX with quadruplex DNA. Chapter 4 consists of solution studies of interaction of MTX with d-$(TTGGGGT)_4$ using one and two dimensional NMR techniques. This chapter also deals with the restrained molecular dynamics simulations of MTX- d-$(TTGGGGT)_4$ complex using NOE restraints. Chapter 5 includes NMR solution studies of interaction of major flavonol, quercetin with d-$(TTGGGGT)_4$ quadruplex structure. And final chapter 6 explains the solution studies of interaction of quercetin glycoside, i.e. rutin with d-$(TTGGGGT)_4$ quadruplex DNA.

Chapter 2

Materials and Methods

2.1 Material and methods

Desalted oligonucleotide sequence d-$(TTGGGGT)_4$ and 5' biotin labeled d-TTGGGGT were purchased from Sigma Aldrich Chem. Co. USA. Mitoxantrone, quercetin and rutin were purchased from Sigma Aldrich Chem. Co. USA. Mitoxantrone was purchased as mitoxantrone hydrochloride, quercetin as quercetin dihydrate and rutin as rutin hydrate. NMR standard reference compounds like DSS and TSP, TMS were purchased from Sigma Aldrich Chem. Co. USA. Chemicals required for buffer preparation like EDTA, K_2HPO_4 and KH_2PO_4 were purchased from Merck chemicals. TRAP assay kit and reagents were purchased from Merck Millipore.

2.2 Preparation of buffers, ligands and DNA solutions

All the spectroscopic experiments were performed in 20 mM KBPES buffer (pH 7.0) containing 100 mM KCl, 10 mM K_2HPO_4 and 1 mM EDTA. 100 mM KCl was required for the formation of parallel stranded quadruplex and the presence of EDTA suppress paramagnetic impurities responsible for line broadening in NMR experiments. All the experiments except melting studies were conducted at 25 ºC. The oligonucleotide sequence d-(TTAGGGT) was dissolved in 20 mM KBPES buffer (pH 7.0), and heated at 90 ºC for 5 minutes and was allowed to cooled overnight at room temperature. The sample was stored at 4 ºC and shaken gently at regular intervals to ensure its homogeneity. The stock solution of MTX was prepared by dissolving 1 mg of MTX into 1 mL of KBPES buffer (pH 7.0) while flavonoids (quercetin and rutin) were dissolved in DMSO.

2.3 Determination of concentration of DNA and ligands

The concentration of oligonucleotide, ligands mitoxantrone, quercetin and rutin were determined spectrophotometrically using the formula

$$A = \varepsilon c l$$

Where, A is the absorbance of the oligonucleotide or ligands at particular wavelength (λ_{max}) as given in the table 1, ε is the molar extinction co-efficient (M^{-1} cm^{-1}) of the oligonucleotide and ligands at λ_{max}, c is the concentration in molar (M) and *l* is the pathlength of the cuvette in *cm* (usually standard pathlength is 1cm).

Table 2.1: Molar extinction co-efficient of the oligonucleotide and ligands along with their respective absorption maxima used.

Sample	**λ (nm) used for ε calculation**	**ε (M^{-1} cm^{-1})**
TTGGGGT	260	65,900
Mitoxantrone	660 (Monomer)	20,900
Quercetin	380	14,920
Rutin	368	19,700

2.4 UV-Visible absorption spectroscopy

UV-Visible absorption spectroscopy measurements were carried out using Carry^{TM} Bio 100 UV-visible spectrometer attached with thermal peltier system. For absorption spectroscopic studies fixed concentration of mitoxantrone (drug) was taken in 1cm pathlength quartz cuvette, and increasing amount of d-$(TTGGGGT)_4$ from stock solution was added to attain the fixed drug/DNA ratio. After adding DNA the samples were mixed well and kept for five minutes before taking reading. The samples were scanned from 200 nm to 800 nm at temperature 25^{o}C to get the absorbance peaks. Mitoxantrone monomer peak at 658 nm was monitored throughout the experiment as it is more susceptible to changes upon binding and aggregation. In order to get an idea about the interaction between G-quadruplex and ligand the maximum peak position (λ_{max}) of ligand was monitored in the absence and presence of G-quadruplex sequence. The extent of binding was determined by the magnitude of this shift. Titration experiments were conducted to get information regarding binding constant and stoichiometry. For titration studies the concentration of MTX was kept constant (4.4 μM) and the quadruplex sequence was added progressively from stock solution into it in order to achieve Drug to quadruplex Nucleotide (D/N) ratio ranging from 0.08 to 6.7. The samples were incubated for one hour at 25 ºC and the spectra were recorded in the wavelength range of 200 nm to 800 nm. The absorbance obtained at λ_{max} = 659 nm was used to calculate the intrinsic binding constant since it's more sensitive to the change in mitoxantrone concentration and DNA doesn't have any absorbance in this region, using the following equation

(*Benesi and Hildebrand, 1949*):

$$\frac{[DNA]}{\varepsilon_a - \varepsilon_f} = \frac{[DNA]}{\varepsilon_b - \varepsilon_f} + \frac{1}{K(\varepsilon_{b-} \varepsilon_f)} \quad \ldots\ldots\ldots\ldots (1)$$

where [DNA] = N, the concentration of d-$(TTGGGGT)_4$, *K* is the equilibrium constant for binding, ε_a is the apparent extinction coefficient obtained by calculating ratio of observed absorbance of drug-DNA complex to the drug concentration (A_{obs}/[D]), ε_f corresponds to the extinction coefficient of the drug in its unbound form and ε_b refers to the extinction coefficient of drug in bound form. The binding constant *K* was obtained from the intercept-to-slope ratios of the plot of [DNA]/ε_a-ε_f vs. [DNA].

2.5 Fluorescence spectroscopy

Fluorescence spectra were recorded using Horiba Jobin Yvon Fluorolog^{TM} spectrofluorimeter. The samples used for UV absorption spectroscopic measurements were used to get fluorescence measurements. The samples were mixed well and care should be taken to prevent the formation of air bubbles inside the cuvette. Samples were taken in quartz cuvettes with all its four sides polished. Emission scan were acquired by exciting the mixture at λ_{exc} = 610 nm, and measuring emission from 630 nm to 800 nm. The mitoxantrone gives emission maxima at 678 nm when excited at 610 nm, peak at 678 nm was monitored for further studies. Most of the ligands exhibit fluorescence due to presence of aromatic rings and function groups present on it. Such compounds when excited at a particular wavelength emit light in the form of fluorescence. Since the intrinsic fluorescence of G-quadruplex sequence is too low to be detected the fluorescence property of mitoxantrone was used to monitor the changes upon interaction with quadruplex sequence d-$(TTAGGGT)_4$. Wide range of interaction affect emission spectrum as this process occur at a slower time scale (10^{-8}) and both shift and shape of the band give information about the binding mode and orientation of ligand, which can be measured by fluorescence quenching. The fluorescence quenching constant, K_{sv}, was evaluated using Stern-Volmer equation (*Lakowicz, 2006*):

$$F_0/F = 1 + K_{sv}[DNA] \quad \ldots\ldots\ldots\ldots\ldots\ldots (2)$$

Where F_0 and F are the intensity of fluorescence in the absence and presence of DNA, respectively, and K_{sv} is the Stern-Volmer quenching constant, which is a measure of quenching efficiency of DNA. K_{SV} was obtained from the slope of the plot of F_o/F vs. [DNA] using titration

data. Depending upon the quenching mechanism binding constant and stoichiometry can be calculated.

When quenching phenomenon is static and the ligand binds to independent equivalent sites the binding constant K_b and binding stoichiometry (n) of the complex can be determined using the following equation (*Liu et al. 2012*):

$$\log [(F_0 - F)/F] = \log K_b + n \log [Q] \quad \text{..... (3)}$$

Where quencher concentration [Q] = [DNA] = N, K_b is the binding constant and n is number of ligands binding to DNA. Plot of log $[(F_0 - F)/F]$ vs. Log [DNA] yielded K_b and n.

2.6 Time Resolved Fluorescence spectroscopy

Time resolved fluorescence measurements were performed using FluoroLog®-TCSPC, (make HORIBA Jobin Yvon Spex®) using a 10 mm path length quartz cuvette operating in time correlated single photon counting (TCSPC) mode and ready to perform time domain lifetime spectroscopy building up a histogram of the sample's fluorescent decay. Fluorescence life time of free and bound chromophore differs which can be resolved on experimental time scale. Time–Resolved fluorescence studies can give an idea of the binding modes of ligand-DNA complex depending upon their fluorescence decay profile. The samples were excited by a fixed-wavelength Nano LED of 635 nm with a pulse duration of <200 ps. All decay traces were measured using 2048 channel analyzer. Typical parameters for these experiments were: time resolution = 0.2 nm, accuracy = ± 0.5 nm, speed = 150 nm/s, TAC range = 100 ns. The data were fitted using a re-convolution method of the instrument response function producing best chi square fitting values and errors were given as standard deviation obtained from the fits. All the measurements were carried out three times to check the reproducibility and to obtain the average values of the life time for MTX and its complex with 7-mer DNA quadruplex

2.7 Circular Dichroism spectroscopy

Circular dichroism experiments were performed using Applied Photophysics Circular Dichroism spectrometer model Chirascan, equipped with Quantum Northwest temperature controller (temperature accuracy $\pm$ 0.01 ^{o}C). A pure nitrogen gas of 99.99 % was purged throughout the

course of experiment. Spectra were recorded between 200-750 nm with 1mm pathlength rectangular quartz cuvette and final data represents averaging of three scans. During data collection mono-chromator bandwidth of 1 nm, 1-nm step and spectral averaging time of 0.35 seconds were used. The concentration of DNA was fixed at 8.2 μM, and required amount of MTX added to reach the desired D/N ratios 0.13 to 6.0. After each addition of MTX, the drug-DNA mixture was mixed well, and allowed to equilibrate for 5 min before taking the reading. Each reading was subtracted with buffer baseline and smoothened to desired level.

2.8 Surface Plasmon Resonance (SPR)

Samples of DNA dissolved in HEPES buffer (0.01 M HEPES, 3mM EDTA, 0.005% surfactant P20, 100 mM KCl) at 50 nM concentration were applied to flow cells in streptavidin derivatized sensor chips (BIACORE SA) by direct flow at 5 μL/min in a BIACORE 2000 Surface Plasmon Resonance (SPR) instrument, available at John F. Welsh Technology Centre, GE Healthcare Life sciences, Bangalore, India.

Steady state binding analysis was performed with multiple injections of different concentrations of mitoxantrone in the range 15-360 μM (prepared by serial dilutions from a stock solution prepared in HEPES buffer containing 100 mM KCl) over the immobilized DNA surface at a flow rate of 30ul/min at 25 ^{o}C. Solutions of known ligand concentrations were injected through the flow cells until a constant steady state response is obtained, where the rate of association and dissociation are equal. The ligand (mitoxantrone) solution was then replaced by buffer flow resulting in dissociation of the complex. Flow cell 1 was kept blank as control to account for any signal generated to bulk solvent effects or any other effect not specific to MTX-DNA quadruplex interaction.

A set of sensogram at different concentration for binding of MTX to d-$(TTGGGGT)_4$ was obtained. The average of the data in the steady state region of each sensogram (RU avg) was determined by linear averaging one selected time span and is plotted as a function of analyte/ligand (mitoxantrone) concentration.

2.9 TRAP Assay

Inhibition of telomerase enzyme by mitoxantrone, quercetin and rutin was evaluated by using TRAP assay. The assay was performed using TRAPeze XL Telomerase Detection Kit (S7707)

supplied by Merck Millipore, assay conditions and protocols are followed as provided by manufacturer kit.

2.9.1 Telomerase enzyme isolation

MCF-7 breast line cancer cells (passage 15) were harvested and approximately 100,000 cells were pelleted, to remove media. The pellet was washed thrice with PBS and freshly used for enzyme isolation or stored at -80^{o}C for further use. For enzyme isolation cell pellets were resuspended in 200ul of CHAPS Lysis buffer (0.5 % CHAPS, 10mM Tris-HCl, 1mM MgCl2, 1mM EGTA, 5mM β-mercaptoethanol, 0.1mM Benzamidine, 10% Glycerol) and incubated in ice for 30 minutes. The lysate was centrifuged at 10,000 rpm for 20 minutes at 4 ^{o}C supernatant was transferred to fresh tube and the protein concentration was determined using Bradford's method of protein estimation. The supernatant was divided into aliquots and stores at -80^{o}C or used directly.

2.9.2 Assay procedure

50 uL of TRAP reaction mix consists of 100mM Tris-HCl (pH 8.3), 7.5 MgCl2, 315 mM KCl, 0.25 % Tween-20, 5 mM EGTA, 0.5 mg/mL BSA, 60 μM of dATP, dGTP, dTTP, dCTP, and the oligonucleotides TS primer (5'-AATCCGTCGAGCAGAGTT-3'), RP Amplifluor primer [5'-$(CCCTTA)_3$CCTAA-3'], K2 Ampliflour primer (5'-ATCGCTTCTCGGCCTTTT-3') and TSK2 template (5'-AATCCGTCGAGCAGAGTTAAAAGGCCGAGAAGCGAT-3'), 2 units of Taq Polymerase, 500ng/μL (2 μL) of cell extract. The reaction mix with enzyme was incubated at 30^{o}C for 30 minutes. Then required concentration of MTX/quercetin/rutin was added to the reaction mix and a 4 step PCR reaction was carried out as follows, 94 ^{o}C / 30 seconds, 59 ^{o}C / 30 seconds, 72 ^{o}C / 1 minute this step is repeated for 36 cycles, this followed by a 72 ^{o}C / 3 minute extension step and then at 55 ^{o}C / 25 minutes.

The assay products are examined by directly running on 15% non-denaturing PAGE gel electrophoresis (100 volts for 1 h) and stained with EtBr for 10 min and destained with deionized water for 15 min. The Gel was illuminated in UV region and pictures are taken using Biorad Gel documentation system. TRAPeze XL Telomerase Detection Kit (S7707) is a advanced Amlifluor primer containing kit, hence PCR products can be directly quantified using spectrofluorimeter (Horiba Jobin Yvon). 20uL of assay mixture was diluted to 600uL with 10 mM Tris-HCl pH 7.4, 0.15 M NaCl and 2 mM $MgCl_2$ containing buffer. The fluorescence of sample was measured in 1

cm pathlength cuvette by collecting emission scan after exciting fluorescein at 495nm and sulphorhodamine at 600 nm, respectively. The relative fluorescence intensity was measured using,

$\Delta F/\Delta R = FL_0 - FL_{neg}/R_0 - R_{notaq}$,

Where, $\Delta F/\Delta R$ net fluorescence increase or decrease, FL_0 and R_0 are fluorescence intensity of fluorescein and sulforhodamine of each samples, FL_{neg} fluorescence intensity of the telomerase negative control and R_{notaq} fluorescence intensity of the Taq negative control.

2.10 Sample preparation for NMR

The parallel tetramolecular quadruplex forming DNA sequence d-$(TTGGGGT)_4$ and Mitoxantrone were prepared by dissolving in 90% H_2O and 10% D_2O containing 20 mM potassium phosphate buffer (pH = 7.2) and 100 mM KCl, 0.1mM EDTA was added to suppress paramagnetic impurities which cause line broadening during NMR experiments. Flavonoids quercetin and ruitn were prepared by dissolving in DMSO-d_6 containing 20 mM potassium phosphate buffer and 100 mM KCl. 0.1µl of 0.1 M TSP (TSP) was added as the standard reference for aqueous samples, and 0.1µl of 0.1 M TMS (TMS) was used as reference for non aqueous samples. Quadruplex forming oligonucleotide, d-(TTGGGGT) was dissolved in 90% H_2O and 10% D_2O containing 100 mM KCl and 20 mM potassium phosphate buffer. The sample was heated at 95 ^oC for 5 min and annealed overnight at room temperature to form quadruplex structure. The final concentration was determined spectrophotometrically before the NMR titration.

2.10.1 Preparation of d-$(TTGGGGT)_4$ and mitoxantrone (MTX) complex:

To prepare d-$(TTGGGGT)_4$-mitoxantrone complex, 500 µl of 2.1 mM quadruplex strand concentration of d-$(TTGGGGT)_4$ in 90% H_2O and 10% D_2O buffer was taken in a clean NMR tube and required volume MTX from 65.5 mM stock was added in step by step to reach the desired D/N ratios. Total of 64 µl of MTX was added to reach the final D/N ratio of 4.0. The exact concentration of quadruplex DNA and required MTX in each step of titration was calculated as follows,

i) The concentration of d-$(TTGGGGT)_4$ (N_1) in total volume of 504 ul is determined by

$$N_1V_1 = N_2V_2$$

$$N_1 \times 504 = 2.1mM \times 500$$

$$N_1 = 2.08mM$$

ii) The concentration of mitoxantrone (N_3) in the complex is determined as follows:

$$N_3V_3 = N_4V_4$$

$$N_3 \times 504 = 65.5\ mM \times 4$$

$$N_3 = 0.52\ mM$$

This method of calculation is repeated for reach other D/N ratios. The concentration of d-$(TTGGGGT)_4$ (N) and mitoxantrone (D) at each successive D/N ratios were given in Table 2.2.

Table 2.2: Concentration of mitoxantrone (D), d-$(TTGGGGT)_4$ (N) in mitoxantrone-d-$(TTGGGGT)_4$ complex at different D/N ratios.

Concentration of d-$(TTGGGGT)_4$(mM) = N	Concentration of mitoxantrone (mM) = D	D/N
2.1	0.00	-
2.08	0.52	0.25
2.06	1.03	0.50
2.05	1.53	0.75
2.03	2.03	1.0
2.01	2.52	1.25
1.99	2.99	1.5
1.98	3.46	1.75
1.96	3.92	2.0
1.93	4.82	2.5
1.9	5.7	3.0
1.87	6.54	3.5
1.84	7.36	4.0

2.10.2 Preparation of d-$(TTGGGGT)_4$ and quercetin complex

500 µl of 2.2mM quadruplex strand concentration of d-$(TTGGGGT)_4$ in 90% H_2O and 10% D_2O buffer was taken in a clean NMR tube and required volume quercetin from 68.67 mM stock was added in step by step to reach the desired D/N ratios. Total of 32µl of quercetin was added to reach the final D/N ratio of 2.0. The exact concentration of quadruplex DNA and required quercetin in

each step of titration was calculated using the methodology explained in the above section, The concentration of d-$(TTGGGGT)_4$ (N) and quercetin (D) at each successive D/N ratios were given in Table. 2.3

Table 2.3: Concentration of quercetin (D), d-$(TTGGGGT)_4$(N) in quercetin-d-$(TTGGGGT)_4$ complex at different D/N ratios.

Concentration of d-$(TTGGGGT)_4$(mM) = N	Concentration of quercetin (mM) = D	D/N
2.2	0.00	-
2.18	0.54	0.25
2.16	1.08	0.50
2.14	1.60	0.75
2.12	2.12	1.0
2.04	4.08	2.0

2.10.3 Preparation of d-$(TTGGGGT)_4$ and rutin complex

500 µl of 2.15 mM quadruplex strand concentration of d-$(TTGGGGT)_4$ in 90% H_2O and 10% D_2O buffer was taken in a clean NMR tube and required volume rutin from 68.67 mM stock was added in step by step to reach the desired D/N ratios. Total of 32 µl of rutin was added to reach the final D/N ratio of 2.0. The exact concentration of quadruplex DNA and required rutin in each step of titration was calculated using the methodology explained in the earlier in the chapter (section 2.10.1). The concentration of d-$(TTGGGGT)_4$ (N) and rutin (D) at each successive D/N ratios were given in Table 2.4

Table 2.4: Concentration of rutin (D), d-$(TTGGGGT)_4$(N) in rutin-d-$(TTGGGGT)_4$ complex at different D/N ratios.

Concentration of d-$(TTGGGGT)_4$(mM) = N	Concentration of rutin (mM) = D	D/N
2.15	0.00	-
2.13	0.53	0.25
2.11	1.05	0.50
2.09	1.56	0.75
2.07	2.07	1.0
1.99	3.98	2.0

2.11Nuclear Magnetic Resonance Spectroscopy

All NMR were recorded using Bruker Avance 500 MHz Fourier Transform NMR spectrometer with Triple channel inverse (TXI) probe, Broad band (BBO) probe and Cryo TXI probe at the Central NMR Facility, Indian Institute of Technology Roorkee, Roorkee. Bruker variable temperature unit (BVTU) was used to regulate the temperature changes during experiments. The samples were allowed to equilibrate at particular temperature for 20 min before any experiment.

2.11.1 NMR experimental parameters:

2.11.1.1One dimensional NMR:

The first step of any NMR assignment of molecule is the acquisition of good one dimensional NMR spectrum; through which parameter optimization was done for further two dimensional studies. As nucleic acids and ligands used in the present work contains important NMR detectable nucleus like ^{1}H, ^{13}C and ^{31}P.One dimensional experiment of these nucleuses were recorded using standard parameters mentioned below.

^{1}H experiments were recorded by using two pulse programs, *zg30* and *zgpr*. Pulse program z*g30* is used to record proton resonances which doesnot require solvent suppression. Hence 1H experiments of flavonoids quercetin and rutin dissolved in DMSO-d_6 were recorded using this pulse program. For d-$(TTGGGGT)_4$ and mitoxantrone were dissolved in 90% H2O :10% D2O solution requires suppression of solvent water to observe the other proton signals. Hence *zgpr*, which uses presaturation hard pulse to suppress solvent peaks were used for d-$(TTGGGGT)_4$ and its complex one dimensional proton experiments. The experiments were acquired with 128 scans with 64K data points using spectral width of 20 ppm. For solvent suppression experiment, *gs* mode was used to detect the exact O1P value for solvent peak suppression. The proton signals were referenced to the standard reference signals.

^{13}C and ^{31}P experiments were recorded using *zgpg30* pulse program, which uses proton decoupling to transfer magnetization to the X nucleus of interest *Cpdg* pulse was used for decoupling purpose. Spectral width of 260 ppm and 10 ppm were used for 13C and 31P experiments, respectively. The 128 scans (ns) were acquired with 64 K data points.

2.11.1.2 Two dimensional NMR

Transfer of magnetization through bond (scalar) and space (dipolar) acts as an important mode of magnetization relaxation process in molecules. Chemical bond between two atoms acts a bridge through which nuclear magnetic dipole of one atom can interact with neighboring atom through their shared electrons. This relaxation process is called as T_2 relaxation and numerous NMR experiments have been developed to utilize this process and provide information about structure of a molecule of interest. By using a variety of such pulse sequences, it is possible to take advantage of theseT_2 relaxation processes in order to transmit magnetization information along a chain of atoms of two bonds, or more. Hence the group of atoms which are chemically connected with each other can be easily identified. Common two-dimensional experiments that measure this are COSY, TOCSY, HMBC, HSQC, HMQC, and HETCOR (or heteronuclear COSY). The first two of these are homonuclear experiments that establish through-bond connectivities between protons. The remaining four experiments establish through-bond connectivities between protons and hetero atoms (e.g., ^{13}C, ^{15}N, and ^{31}P).

2.11.1.2.1COSY

The COSY experiment (homonuclear *Co*rrelated *S*pectroscop*Y*) is one of the most powerful and important two-dimensional NMR experiment, originally developed by Jeenar (*Jeenar, 1979*). The spin ½ nuclei which are connected by a scalar coupling with a coupling constant of *J* Hz shows two doublets in a one dimensional experiments, but in two dimensional COSY spectrum will show a pair of symmetrical cross peaks between the diagonal peaks of two spins. In biomolecules many spin systems have a variety of coupling constants ranging from large geminal couplings of 15 *Hz* or more, through typical vicinal couplings of a few Hz, down to long-range couplings of a fraction of a 10 - 20 Hz.

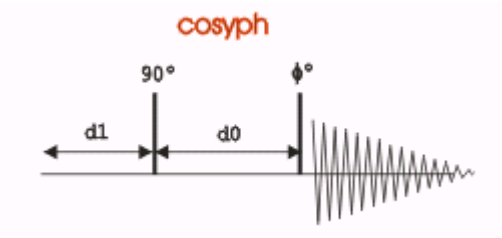

Figure 2.1: Pulse program scheme for COSY experiment

The simple COSY experiment consists of an four important steps, they are excitation pulse (90°), an evolution time (t_1), a mixing pulse, and then detection (Fig.2.1). Before the start of the experiment the spin system should reach equilibrium. The first 90° pulse rotates the equilibrium magnetization to the transverse plane and generates single-quantum coherence. During the evolution time t_1, the single-quantum coherence evolves, resulting in F_1 frequency labeling of the detected coherence. The last pulse transfers the magnetizations between spins via the scalar coupling between them. Finally, the correlated coherence is detected as the FID in the detection period. The coherence selection is achieved by the gradient pulses following each RF pulse. The cross peaks appear as symmetrically placed pairs above and below the main diagonal.

Experimental parameters: The pulse program used was *cosygpqf*, which uses gradient pulses for coherence transfer. Quadrature detection (QF) method was used in F1 direction, with a spectral width of 20 ppm. The size of the FID consists of 2048 data points in F2 direction at 256 steps in F1 direction, acquired for 56 scans. Pre-scan delay (d1) 1.5 seconds was used between each experiment. The time domain data was converted into frequency domain and following processing parameters were used. Sine bell window function was used, with a line broadening factor of 0.3 Hz in F_1 direction and 1 Hz in F_2 direction. Nucleic acids show important through bond ^{1}H-^{1}H couplings, especially between the sugar ring protons, which help in identifying numerous resonances and puckering pattern of sugar ring. Table 2.5 lists the through bond correlation expected in nucleic acids (A-DNA / B-DNA).

Table 2.5: ^{1}H-^{1}H through bond correlation in Nucleic acids.

Bond correlations	Aromatic bases
^3J	H5-H6 (Cytosine)
^4J	CH_3-H6 (Thymine)
	Sugar
^3J	H1'-H2', H1'-H2"
^2J, ^3J	H2'-H2", H2'-H3'
^3J	H2"-H3'
^3J	H3'-H4'
^3J	4'H-5'H, 4'H-5"H
^2J	5'H-5"H

2.11.1.2.2 NOESY:

NOESY (*N*uclear *O*verhauser *e*ffect *s*pectroscopy) is one of the most commonly used two dimensional technique applied to the assignment of protons and structural determination of biological macromolecules like nucleic acids, proteins and carbohydrates. Its basic principle is based on Nuclear Overhauser Effect or NOE, which is a relaxation phenomenon used to derive information on short internuclear distances. These distances can be used to derive three dimensional structural details. The origin of NOE can be explained by the knowledge of Solomon equations and relaxation of molecular relaxation mechanisms, apart from dipole-dipole interactions.

Fig. 2.2 shows the NOESY pulse sequence used in the present work which consists of three $\pi/2$ (90°) pulses separated by certain delay times (d). The first delay time d_1 is the recycling delay between two experiments/scans in which the precessing magnetization relaxes to the equilibrium ground state. The first $\pi/2$ pulse (p1) converts longitudinal *z* magnetization into transverse spin magnetization. This is followed by second delay period (d_0), during which the transverse magnetization precesses around the *z* axis, so that at the end of t_1 each nucleus has precessed through an angle ωt 1, where ω is the angular frequency of the nucleus compared with the reference frequency, or in other words its chemical shift difference from the carrier, which in a quadrature detection experiment is in the center of the spectrum. The second *π/2* pulse (p1) rotates this transverse magnetization to the longitudinal one in the pulse direction i.e in the *xz* plane. The phases of the pulses are cycled in subsequent pulse sequences so that any residual transverse magnetization following the second pulse is canceled out. Thus, the only magnetization that is added constructively as a result of the complete phase cycle is that resulting from the magnetization that is along the z axis after the second pulse. The first two pulses have therefore achieved a frequency labeling of magnetization, in which each magnetization vector now has an intensity modulated both byt1 and by its frequency. The period between the second and third pulses is the mixing period (*d8* in Bruker instrument) τ_m during which the NOE build up occurs. By the end of this mixing period, magnetization in the *z* direction has modified by NOE cross relaxation. The final *π/2* pulse (p1) reads the magnetization present in z direction and converts it into a transverse magnetization, which is then detected. This experiment is repeated for a series of regularly incrementedt1 values and stored as a matrix of points.

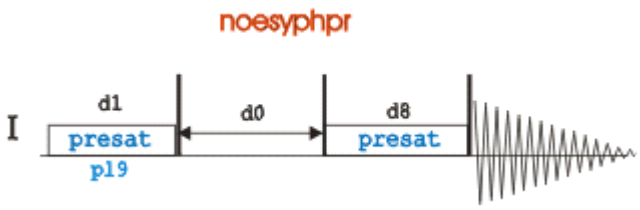

Figure 2.2: Pulse program scheme for NOESY experiments.

In common with most other two-dimensional experiments, NOESY spectra are normally presented as square plots containing a line of diagonal peaks and symmetrically placed cross peaks. The two dimensions in NOESY experiment were labeled as F_1, F_2 ($\omega 1$, $\omega 2$) where 1and 2 refer respectively to the indirectly and directly detected dimensions.

In NOESY experiments, cross connectivities originate from cross relaxation between two nuclei that are close to each other in space, hence called as dipolar-dipolar coupling. Therefore appearance of a NOE cross peaks is interpreted as a short distance between the two nuclei at the chemical shifts of the cross peak. The appearance of NOE cross connectivity for a pair of proton within a molecule under study depends upon the proximity of the two protons, generally less than the5A°, mixing time (τ_m) and sensitivity of the instrument. In some cases spin diffusion results in the appearance of connectivities between protons which are at distance longer than 5A°. To minimize this lower mixing time values in the range of 50-200 ms were used.

Experimental parameters: The Pulse program used was *noesyphpr*, which uses phase sensitive detection with pre-saturation pulse for water suppression. States TPPI method of detection was used in F_1 direction, with a spectral width of 20 ppm. The size of the FID consists of 2048 data points in F_2 direction at 256 steps in F_1 direction, acquired for 56 scans. Pre scan delay (d1) 1.5 seconds was used between each experiment. One of the important parameter taken care of before NOESY experiment is mixing time (τ_m), which is D8 of 100, 200 and 250 ms was used in the present study. Exact transmitter offset position (O1P) for suppression of solvent water peak was determined by gs mode.

The data was processed using the Bruker Topspin 2.1 processing software. The time domain data was converted into frequency domain and following processing parameters were used. Quadrature Sine bell window function was used, with a line broadening factor of 0.3 Hz in F_1 direction and 1 Hz in F_2 direction.

Table 2.6: Short interproton distances in regular B-DNA in Å.

	Residue n		Residue n+1			
Residue (n)	H2"	H6/H8	H6/H8	H5	CH_3	NH
H1'	2.6	3.8	3.1		3.8	
H2'	1.75	2.1	3.9	3.2	2.8	
H2"	-	3.5	2.3	2.8	2.4	
H6/H8		-			3.2	
NH						3.8

Table 2.7: Short interproton distances in regular A-DNA in Å.

	Residue (n)		Residue (n+1)		
Residue (n)	H2"	H6/H8	H6/H8	H5	CH_3
H1'	2.3	3.8	4.0		
H2'	1.75	3.8	1.6	3.0	2.8
H2"	-	3.5	3.2		
H6/H8		-		3.7	3.1

2.11.1.2.3 ROESY:

ROESY (*R*otating frame nuclear *O*verhauser *e*ffect *s*pectroscop*y*) is an alternative to the NOESY experiment used for the determination of dipolar coupling in molecules with intermediate molecular weight. The pulse program used for ROESY experiment was *roeyphpr*. Acquisition and processing parameters were similar to NOESY experiment except for mixing time which can be set by changing p15. ROESY experiment was used to determine the conformation ligands i.e. mitoxantrone, quercetin and rutin used in the present studies.

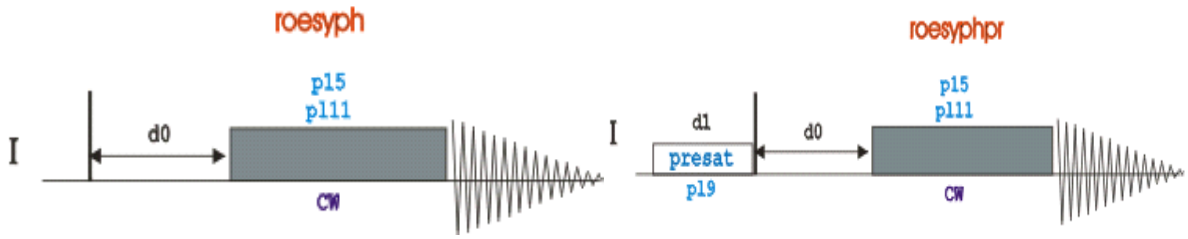

Figure 2.3: Pulse program scheme for ROESY experiments.

2.11.1.2.4 TOCSY:

TOCSY (*To*tal *c*orrelation *s*pectroscop*y*) is also called as two dimensional HOHAHA (homonuclear Hartmann-Hahn) experiment. This experiment reveals both scalar and relayed scalar coupling connectivities (*Davis and Bax, 1985*).The proton of interest show correlations with all other protons in that spin system, which results in a 2D correlation map. This experiment plays an important role in identifying sugar protons in DNA, RNA and sugar systems present in various flavonoid glycosides. Due to the presence of glycosidic bond, TOCSY correlation breaks between two sugars or between sugar and nitrogenous base in DNA.

The basic pulse sequence of the TOCSY experiment (Fig.2.4) follows the same principles of the other homonuclear 2D experiments like COSY and NOESY. After a excitation with 90º ^{1}H pulse, transverse magnetization evolves during a free variable evolution t_1 period, then isotropic mixing sequence or TOCSY mixing pulse (*d9* in Bruker instrument) typically 50-100 ms was used to transfer magnetization between spins via the strong scalar coupling, which results in transfer of magnetization to the several spin coupled proton during the mixing time. The isotropic mixing is usually performed applying a WALTZ, MLEV or DIPSI pulse train and it was performed on the longitudinal magnetization. The TOCSY pulse sequence is combined with solvent suppression pulses, when used for biological systems.

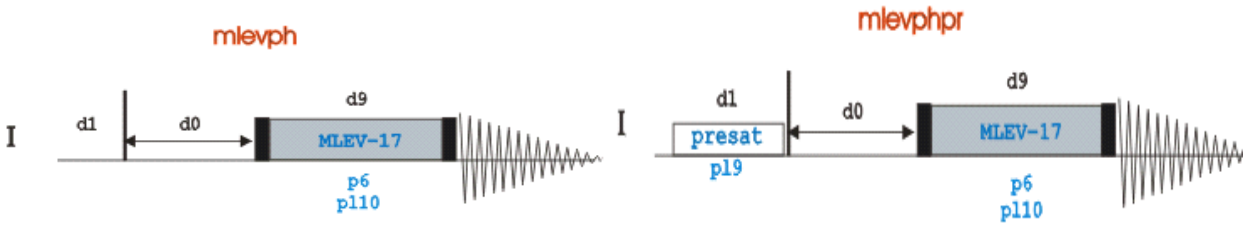

Figure 2.4: Pulse program scheme for TOCSY experiments.

Experimental Parameters:

In the present study *mlevphpr* (Fig. 2.4) pulse program was used to get the TOCSY correlation map. STATES-TPPI method of detection was used in F1 direction, with a spectral width of 20 ppm. The size of the FID consists of 2048 data points in F2 direction at 256 steps in F1 direction, acquired for 56 scans. Pre scan delay (d1) 1.5 seconds was used between each experiment. The

time domain data was converted into frequency domain and following processing parameters were used. Sine bell window function was used, with a line broadening factor of 0.3 Hz in F_1 direction and 1 Hz in F_2 direction.

2.11.1.2.5 HSQC:

The HSQC (*H*etero *s*equential *q*uantum *c*oherence) is a heteronuclear experiment used to determine the proton coupled directly to the heteroatom (X nucleus like spin½, ^{13}C, ^{15}N or ^{31}P).In an ^{1}H-^{13}C HSQC experiment all the protons attached directly to carbon (^{13}C) nucleus through one bond (C-H) produces a correlation map consists of ^{13}C (hetero nucleus, X in F_1 dimension) and ^{1}H (proton in F_2 dimension) via the direct heteronuclear coupling 1*J*(X-H). This gives chemical shift of each bonding pair atoms and hence information about the coupling constant between them.

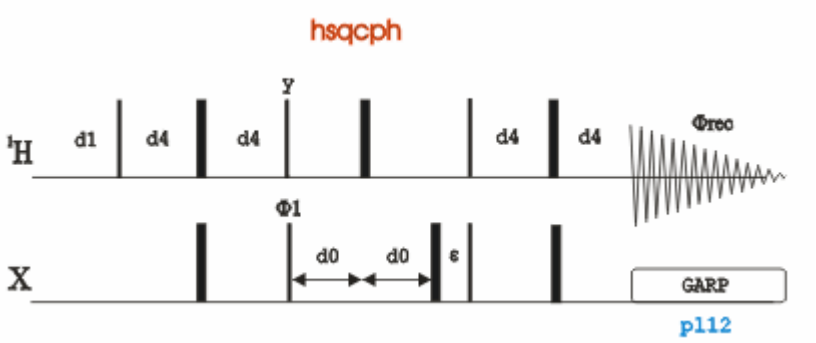

Figure 2.5: Pulse program scheme for HSQC experiments.

Experimental Parameters:

The natural abundance ^{1}H-^{13}C HSQC experiment was done by using pulse program *hsqcetgpsi* with an acquisition mode of echo-anti echo in *F1* direction, size of the FID is 1024 data points in F2 direction with 400 scans in F1 direction. The spectral width of 200 *ppm* in F1 direction and 16 *ppm* in F2 direction was used. Delay (d1) of 1.5 seconds was used between each acquisition. 56 scans with 16 dummy scans were used. Q-Sine window function was used for window function in both dimensions, with line broadening factor of 1*Hz* in F2 and 0.3*Hz* in F1 direction. Shifted square sine bell (SSB) function of 2 was used.

2.11.1.2.6 HMBC:

The HMBC (*H*etero *m*ultiple *b*ond *c*orrelation) is a heteronuclear two dimensional experiment, which provides correlation between 1H and any X nuclei (X nucleus like spin½, ^{13}C, ^{15}N or ^{31}P) which are separated by two, three or four bond away (^{3}J, ^{4}J). The direct one bond correlation that is HSQC type correlation is suppressed. The coupling between the nucleus directly relates to the intensity of the observed correlation.

Along with the HSQC experiment, HMBC is one of the widely used technique for the structural determination for natural compounds. In flavonoid glycosides like rutin, this experiment provides valuable wealth of information in identifying the proton resonance of hydroxyl groups.

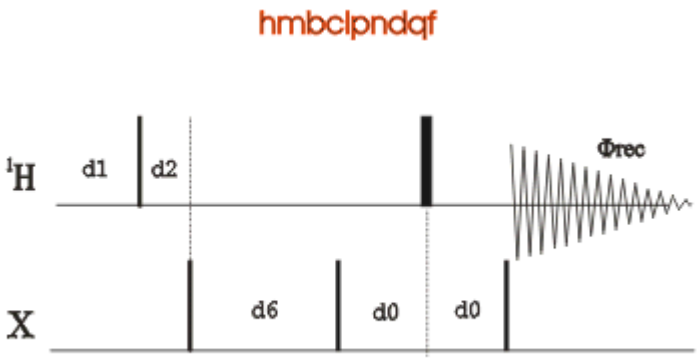

Figure 2.6: Pulse program scheme for HMBC experiments.

Experimental Parameters:

The natural abundance ^{1}H-^{13}C and ^{1}H-^{31}P HMBC experiment was done by using pulse program *hmbcgpndqf*, which uses gradient pulses for coherence selection, with an acquisition mode of quadrature (QF) in F_1 direction, size of the FID is 2048 data points in F_2 direction with 256 scans in F1 direction. The spectral width of 200 *ppm* in F1 direction and 16 *ppm* in F_2 direction was used for ^{1}H-^{13}C HMBC experiments and for ^{1}H-^{31}P HMBC experiments spectral width of 40 ppm in F_1 and 20 ppm in F_2 direction and delay (d1) of 1.5 seconds was used between each acquisition. 56 scans with 16 dummy scans were used. Q Sine window function was used for window function in both dimensions, with line broadening factor of 1 *Hz* in F_2 and 0.3 *Hz* in F_1 direction. Shifted square sine bell (SSB) function of 2 was used.

2.12 NMR study of nucleic acids and ligands.

Following the current paradigm that biological function is encoded in three-dimensional molecular structure, the last four decades have seen great efforts in the determination of well-defined solution structures of DNA using high resolution nuclear magnetic resonance (NMR) methods and modeling tools. Since the 1970s, NMR has emerged as the method of choice for the study of biomolecules under more physiological conditions that can be created in the crystalline state. Initially, it was successfully applied to the study of nucleic acids to yield only 'low-resolution' structural insights, such as secondary structure information or qualitative differences between similar samples. With large improvements in magnetic field strengths and development of sensitive two-dimensional (2D) NMR experiments, as well as the development of large-scale synthetic methods for nucleic acids, high resolution structures of DNA could finally be achieved.

The complete three dimensional structure of nucleic acids can be obtained by complete assignments of exchangeable and non-exchangeable protons of nucleic acids (4); (ii) converting spectral observables, i.e. intensities from quantitative 1D and 2D NOE spectroscopy or coupling constants from correlated spectroscopy into structural information; and (iii) building adequate models using the NMR-derived structural information.

Structural information used for DNA structure determination is typically in the form of distance restraints extracted from multidimensional homonuclear NOE spectra. The NOE cross-peak volumes are converted into distance restraints to provide quantitative information. Distance data are often augmented by scalar coupling constant-derived $^{1}H^{1}H$ or ^{1}H-^{31}P torsion angles, available from various correlated spectroscopy experiments (e.g. COSY, HETCOR). For the present purpose, it is important to realize that the NMR-derived parameters largely represent local information, where coupling constants usually extend over three bonds and NOEs reflect distances of > 5 Å, with the higher values only in the more auspicious case of methyl groups.

The chemical shift dispersion in sugar varies depending on the configuration, like deoxyribose sugar show more chemical shift dispersion of approx 4.5 ppm, whereas ribose sugar proton shifts concentrated in range approx 2.5 ppm. The base aromatic protons resonate between 6 and 8.5 ppm.

In base protons scalar coupling was observed only between H5 and H6 protons of cytosine (^{3}J = 8 Hz) and H6 and CH_3 of Thymine (^{4}J = 1-2 Hz), whereas no other exchangeable and non-

exchangeable base protons show scalar coupling. But deoxyribose sugar protons show scalar coupled system, which can be identified by magnitude mode or phase sensitive COSY correlation method. Both one dimensional and two dimensional NMR techniques can be effectively used to determine the structure of ligand molecules. Rutin is a flavonoid glycoside, it contains two sugar moieties, glucose and rahmnose, hence TOCSY and COSY techniques can be effectively used to determine the position of protons, and ultimately the structure of ligands (*Chakraborty et al. 1998; 2000; 2002; Sidhu et al. 2011; Khetrapal et al. 1984*)

Table 2.8: Chemical shift (ppm) ranges observed in nucleic acids

Deoxyribose	^{1}H (δ ppm)	^{13}C (δ ppm)
H1'	5.2–6.7	84–91
H2' and H2"	0.9–3.9	37–44
H3'	4.1–5.6	72–82
H4'	3.8–5.0	84–89
H5' and H5"	3.3–4.6	62–72
Nucleoside		^{13}C
AH2	7.3–8.4	153–155
CH5	4.5–6.5	92–99
CH6 and TH6	6.5–8.1	139–143
TCH_3	0.8–1.6	13.5–15
AH8 and GH8	7.4–8.5	137–142
		^{15}N (δ ppm)
A, C and G NH_2 (b and nb)	6.2–9.0	79–81(A), 74–76 (G), 96–98 (C)
NH imino proton of GNH and TNH	10–15	145_147 (G), 158–160 (T)

2.13 Determination of interproton distances using NOE data

NOESY experiments were recorded at different mixing times in order to get NOE build up curve, which will help to distinguish between cross peaks generated from direct dipolar interaction (the NOE) or as a result of spin diffusion (*Hosur et al. 1988*). At the lower mixing time spin diffusion rate is slow and the observed cross peaks are the one whose distances are shorter that is two protons are close through space. Initially the intensity of cross peaks increase with mixing time, but later at a higher mixing time due to multi spin relaxation, diffusion rate is fast and distance based NOE cross peaks does not exist and the intensity of all the cross peaks are same. Inter protons

distances were achieved by measuring the intensities of cross peaks in the "linear regime" through two-spin approximation, where only the rates of dipolar magnetization transfer between proximal spins i and j was monitored as follows:

$r_{ij} = r_{ref}(I_{ij}/ I_{ref})^{1/6}$ …… (4)

Where r_{ij} = distance between two protons i and j, r_{ref} = reference distance, I_{ij} = intensity of i and j and I_{ref} = reference intensity.

Cross peaks in the NOESY spectra were integrated and intensities were translated into inter-proton distances using thymine H6-CH_3 as the reference distance (3.00 Å) using the SPARKY software (*Goddard and Knell, University of California, San Francisco, USA 2004*). A range of ±0.5 Å was provided to avoid any errors in integration. The NOEs were categorized as very strong (ss), strong (s), medium (ws), weakly and very weakly intense with corresponding distances set range set in the range of ss = 2.0–2.5 Å, s = 2.5–3.0 Å, m = 3.0–3.8 Å, w = 3.8–4.5 Å, ww = 4.5–5.0 Å for the respective protons.

2.14 Restrained molecular dynamics simulations

Once the distances were calculated from NOESY cross peaks, these distances were used as distance restraints for restrained molecular dynamics (rMD) and simulations protocol. It is the final step of the determination of three dimensional structure using NOESY NMR data.

2.14.1 Restrained molecular dynamics simulation of ligand-d-$(TTGGGGT)_4$ complexes.

Structures of all three ligands MTX, quercetin and rutin were generated using builder module of INSIGHT II, Accelrys software (San Diego). The structures were energy minimized using biopolymer module, with restraints obtained from uncomplexed ligand 200ms ROESY spectra. Based on the distance ranges, the restraints were divided into strong (2.5-3.2 Å), medium (3.2-3.8 Å) and weak (3.8-5Å).

To build the complex structure, first the distances obtained from integrating the cross peaks of 200 ms NOESY spectra of complexes were used as restraints. Ligands were energy minimized using restraints obtained from complex NOESY spectra at D/N 2.0. The uncomplexed quadruplex structure of d-$(TTGGGGT)_4$ reported by Wang and Patel (PDB ID 139 D) (*Wang and Patel, 1994*) was used as a starting structure for tetramolecular quadurplex. The potential set up of this initial

structure was changed by replacing aromatic bases using Biopolymer module of INSIGHT II software.

Once the ligand molecule was placed in a binding site, all the intramolecular ligand-ligand, quadruplex-quadruplex, ligand-quadruplex restraints were incorporated. The planar constraints for G-quartet planes were used to keep G-quartets intact during the simulation. A force constant of 25 Kcal mol^{-1} was strong distances, 15 Kcal mol^{-1} for medium distances and 10 Kcal mol^{-1} for weak distances was used. The energy of the molecule was minimized using 1000 steps each of Steepest Descent and Conjugate Gradient to remove any internal strain due to short contacts in starting structure using a CFF91 force field in discover software version 2005 (Accelrys Inc., San Diego, California). Dielectric constant was fixed at 1.0 for calculation of electrostatic interactions. Conformational search was performed using the following simulated annealing restrained molecular dynamic protocol. The molecule was heated to a temperature of 800 K in steps of 100 K so that the chances of the molecule being trapped in local minima become lost and it can reach global minima. Molecular dynamics were carried out for 100 ps (1000 iterations with time step of 1 fs) at 800 K during which 100 structures were saved at regular intervals of 1 ps. Each of them was then slowly cooled at 300 K in steps of 100 K. The force constants for NOEs for strong, medium and weak peaks were held constant as 25, 15 and 10 kcal mol^{-1} $Å^{-2}$, respectively. At the end of simulated annealing all the structures were minimized by 1000 steps of Steepest Descent until a predefined convergence limit of root mean square derivative of <0.001 kcal mol^{-1} $Å^{-1}$ was reached.

Chapter 3

Spectroscopic studies on interaction of anti-cancer drug mitoxantrone with tetramolecular parallel telomeric sequence d-$(TTGGGGT)_4$.

Formation of G-quadruplex structures in the guanine rich telomere region of the chromosome, results in the inhibition of telomerase activity, which is over expressed in majority of cancer cells. Hence inhibition of this enzyme by stabilization of G-quadruplex structures acts an important anti-cancer strategy. Numerous different classes of small molecule ligands have been shown to bind and stabilize this important secondary structure. Mitoxantrone (MTX) is an important synthetic anti-neoplastic drug, known to inhibit the activity of topoisomerase II enzyme. Its anti-cancer activity was also attributed to its interaction with DNA. MTX interacts with duplex DNA molecule by end stacking/intercalative mode of binding with its alkylamino side chains occupying grooves forming electrostatic interaction. In the present chapter we studied the interaction of MTX with tetramolecular d-$(TTGGGGT)_4$ quadruplex DNA using various spectroscopic techniques like UV-Vis, fluorescence, CD, Fluorescence life time and SPR studies along with cell based TRAP assay.

3.1 Results and Discussion

3.1.1 Absorption (UV-Visible) spectroscopy

The mitoxantrone shows four distinct absorption bands at 242, 276, 610 and 658 nm. We have monitored titrations by measuring absorbance in the visible region since DNA absorbs efficiently in the UV region. We have monitored the binding behavior of MTX by adding different concentration of G-quadruplex to a fixed concentration (4.4 μM) of MTX. It is observed that intensity of both the bands, 610 and 658 nm, decreased by about 42 % at D/N = 4.3. On further progressive addition of nucleic acid quadruplex to MTX, a decrease in absorbance accompanied by red shift of 6 nm is observed till D/N ~2.0 (Fig. 3.1a). The absorbance showed a reverse trend and continuously increased on further addition of DNA at D/N = 1.0-0.08 (Table 3.1b) accompanied by red shift $\Delta\lambda$ = 15 nm at D/N = 0.08 (Fig. 3.1b), when most of the drug is apparently bound to DNA. In case of duplex DNA where end stacking is not significant a red shift ≥ 15 nm and

hypochromicity ≥ 35% is indicative of intercalative binding (*Pasternack et al. 1983; Krugh et al. 1975*). The predominant mode of binding in quadruplex DNA is end-stacking and groove binding. Hence this red shift (due to decrease in π-π* transition energy) is characteristic of end stacking interactions of the aromatic chromophore of MTX with base pairs of DNA, which prevents it from forming an H-bond with solvent water (*Lee and Dutta, 1989; Yang et al. 2005*). The plot of absorbance, A versus D/N (Fig. 3.2a, b) and 1/A versus D/N (Fig. 3.3a, b) shows an inflection point at D/N = 2 with a sudden change in slope of the curve. The plot of $\Delta\lambda$ vs D/N (Fig. 3.4, Table 3.1) shows that $\Delta\lambda$ levels off as D/N approaches values of 1.0, 2.0 and 4.0; and finally levels off to zero at D/N > 4.0. The hypochromism (from D/N = 4 to 2) followed by hyperchromism (from D/N = 1 to 0.08) shows at least two different modes of binding mechanisms, as well as points towards a likely stoichiometry of 2:1 and 1:1 in MTX-DNA complex. We note the absence of a sharp isobestic point, which shows the existence of multiple conformations in the MTX-DNA complexes or alternately, existence of several MTX-DNA complexes with different stoichiometric ratios. This is consistent with the observation of several slope changes between approximately linear regions in the Job plot, in which inflection point corresponds to stoichiometric ratio of 2:1 and 4:1 mol MTX/ mol of DNA quadruplex. The stoichiometric ratio saturation at 4:1 is consistent with the fact that no red shift occurs when D/N is increased beyond 4.0 to 4.3 and 8.7.

The intrinsic binding constant is evaluated by using the following equation,

$$\frac{[DNA]}{\varepsilon_a-\varepsilon_f} = \frac{[DNA]}{\varepsilon_b-\varepsilon_f} + \frac{1}{K(\varepsilon_b-\varepsilon_f)} \qquad \text{……..(1)}$$

where [DNA] = the concentration of DNA quadruplex, K is the equilibrium constant for binding, ε_a is the apparent extinction co-efficient obtained by calculating ratio of observed absorbance of drug-DNA complex to the drug concentration (A_{obs}/[D]), ε_f isthe extinction coefficient of the drug in its free form, and ε_b refers to the extinction coefficient of drug in bound form. The data fit into a straight line yield equilibrium constant for binding as K = 3.53 x 10^6 M^{-1} , and 3.73 x 10^6 M^{-1} (Fig. 3.5) for D/N = 0.5 to 2.0 and D/N = 2.0 to 4.0, respectively. Considering absorbance at λ = 659 nm for D/N = 0.08 to 0.5, we get K = 0.57 x 10^6 M^{-1}.

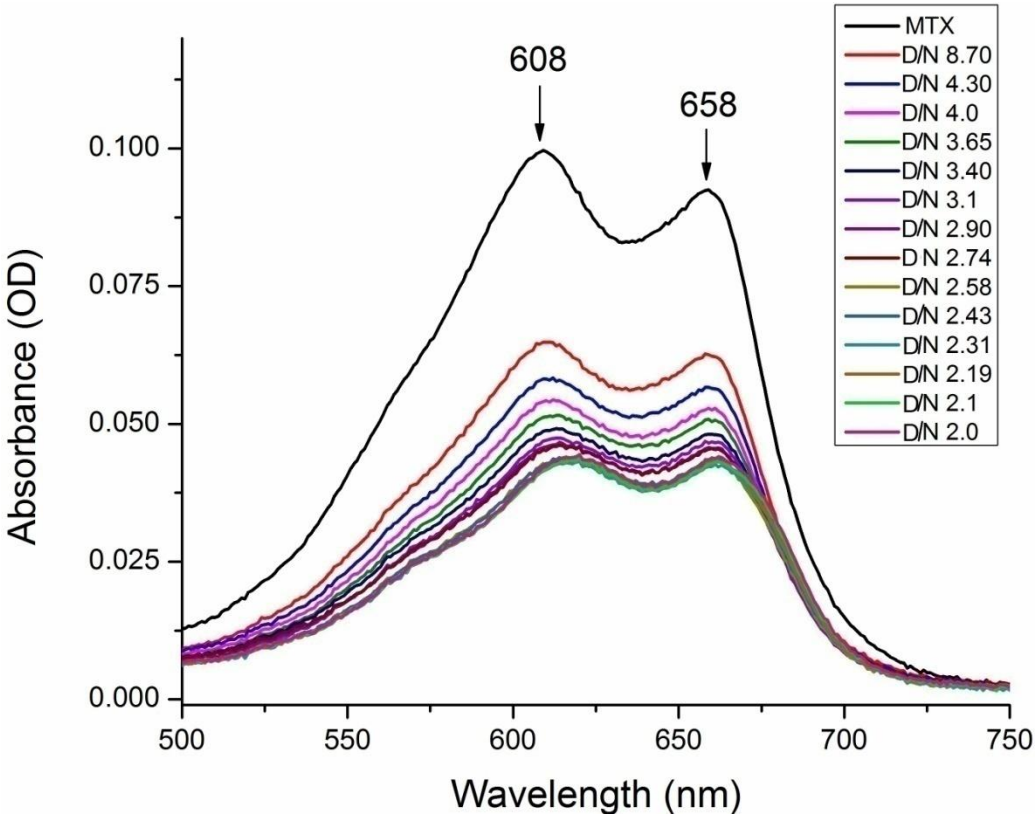

Figure 3.1(a) The absorption spectra of 4.4 µM MTX in the increasing concentration of d-(TTGGGGT)$_4$ at 298 K at higher D/N (MTX/d-(TTGGGGT)$_4$) of 8.7 -2.0.

Existence of multiple binding sites resulting in absence of clear isobestic point have earlier been reported in literature on binding of TMPyP4 and TPrPyP4 to parallel G-quadruplex (*Wei. C et al. 2010, Kovaleva. O. A et al. 2013, Freyer. M. W. et al. 2007*)

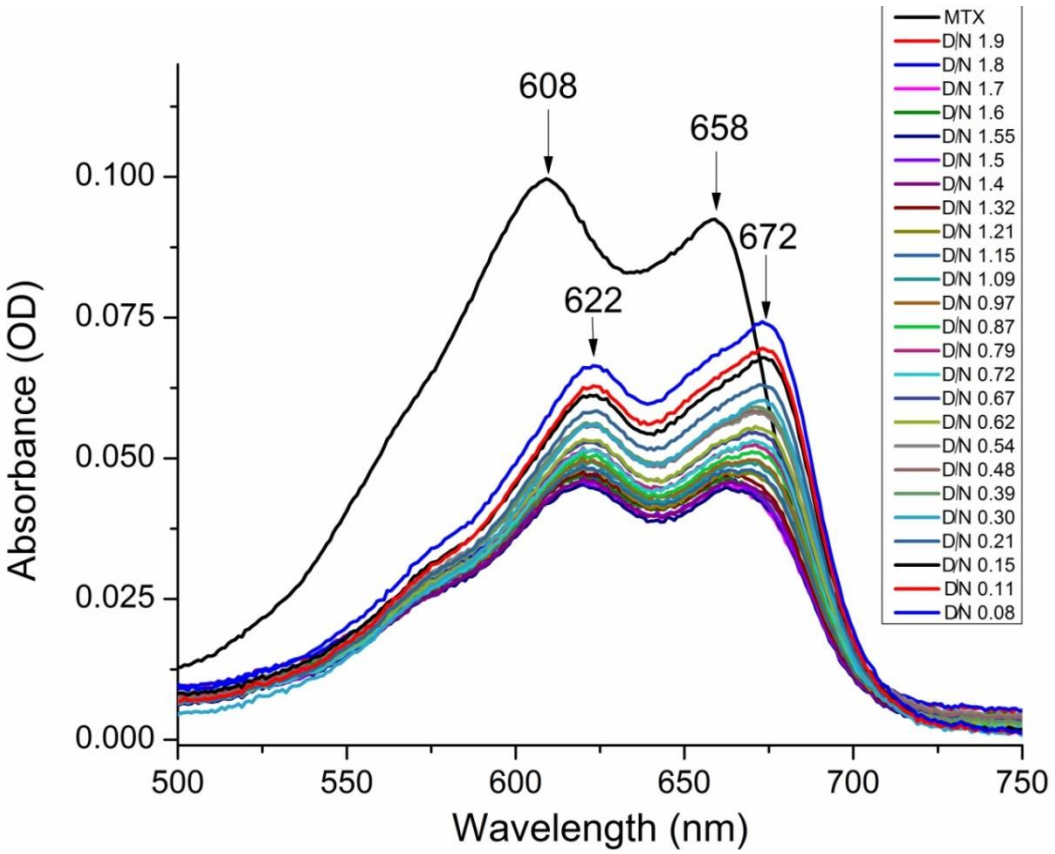

Figure 3.1(b) The absorption spectra of 4.4 µM MTX in the increasing concentration of d-(TTGGGGT)$_4$ at 298 K at lower D/N (MTX/d-(TTGGGGT)$_4$) of 1.9 -0.08.

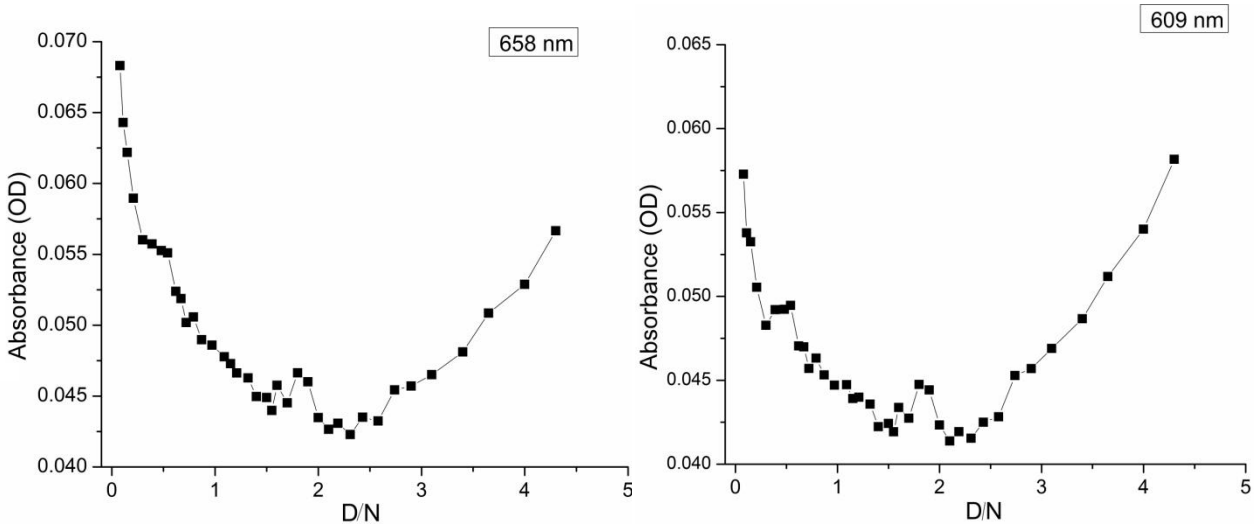

Figure 3.2 Plot of absorbance (A) versus D/N ratios at (a) 658 nm band and (b) 609 nm band.

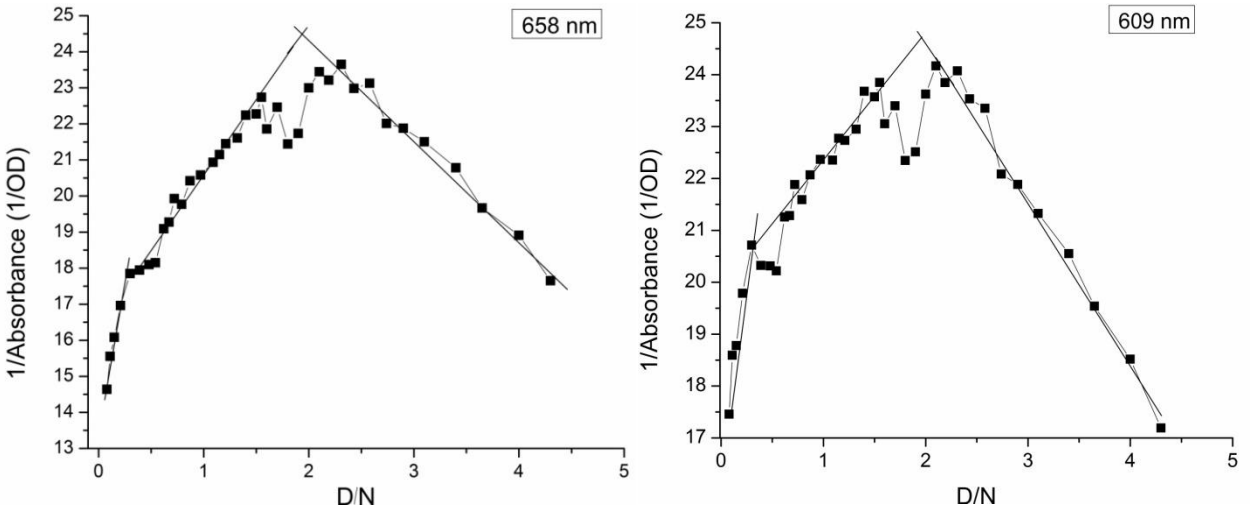

Figure 3.3 Plot of 1/absorbance versus D/N ratios at (a) 658 nm band and (b) 609 nm band.

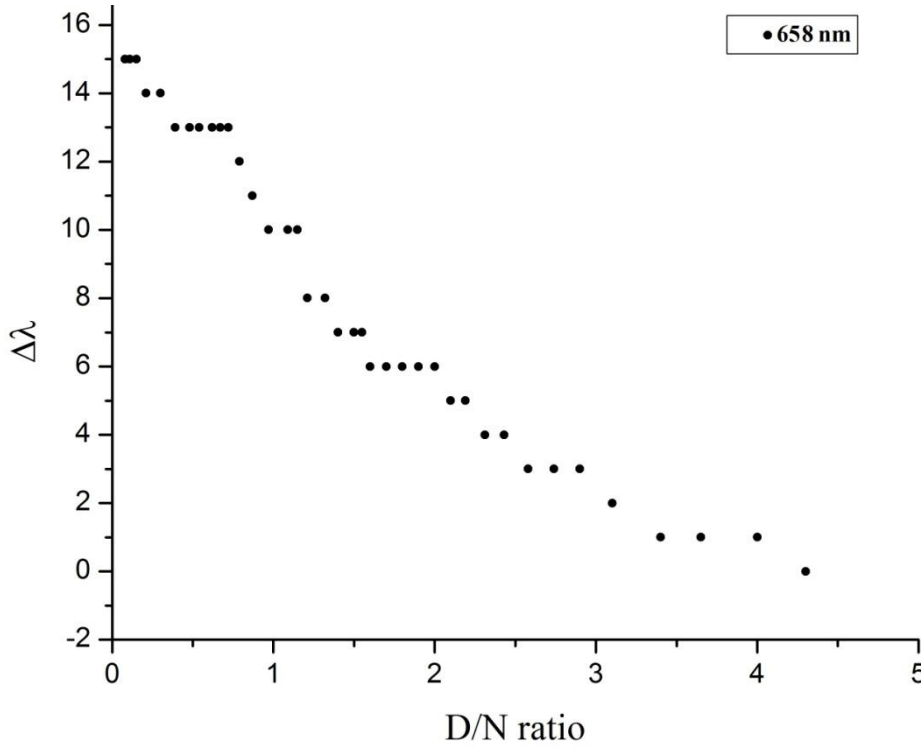

Figure 3.4 Change in the λ_{max} (Δλ) of 658 nm band at varying D/N ratios of MTX-d-(TTGGGGT)$_4$ complex.

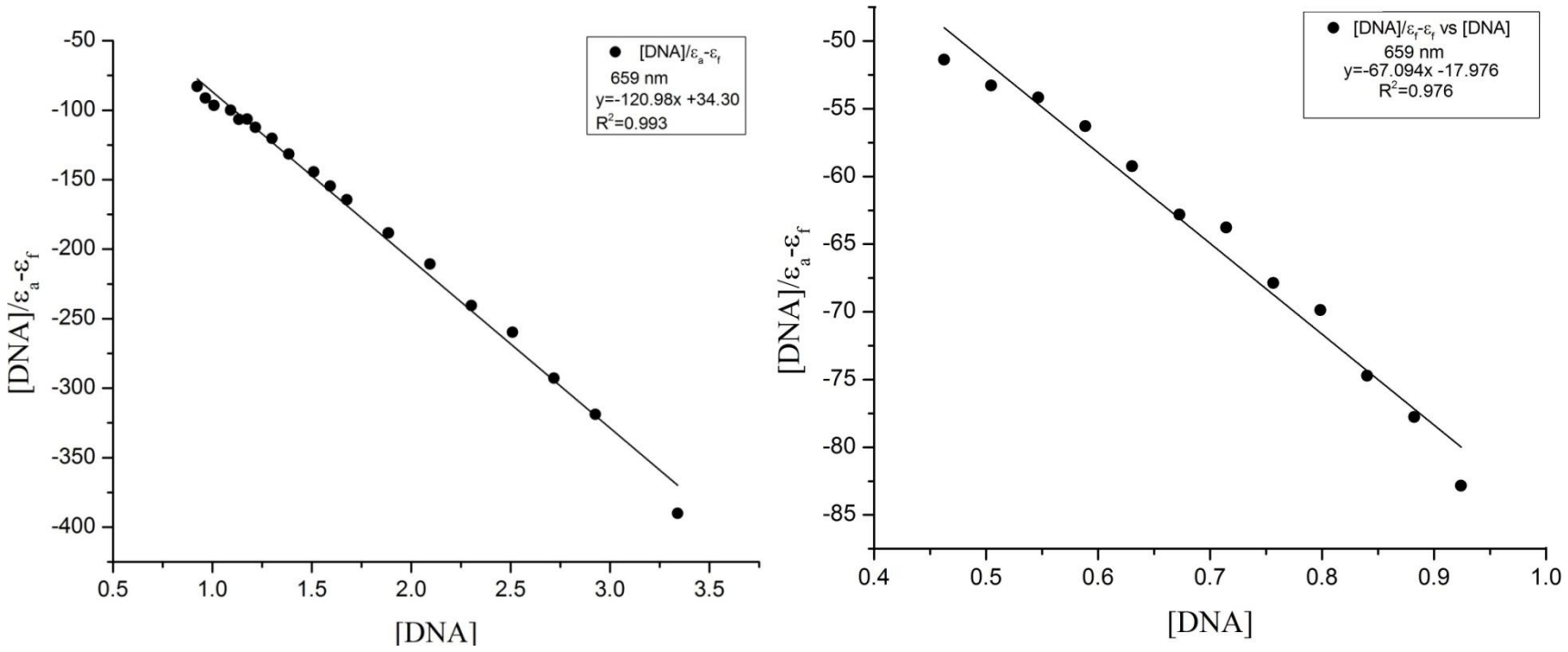

Figure 3.5 Plot of [DNA]/ε_a-ε_f versus [DNA] at 658 nm band for DNA concentrations at D/N ratio 0.5 – 2.0 (left) and for DNA concentrations at D/N ratio 2.0 - 4.0.

Table 3.1 Change in the absorption maxima (λmax), O.D, and M (659 nm band) on interaction of MTX with $(TTAGGGT)_4$ at varying D/N ratios.

D/N	Abs (OD) at 658 nm	λmax M	Abs (OD) of monomer at λmax	Δλmax
∞	0.092	658	0.092	0
8.7	0.0625	658	0.0625	0
4.3	0.062	658	0.062	0
4	0.052	659	0.056	1
3.65	0.050	659	0.053	1
3.4	0.048	659	0.0508	1
3.1	0.046	660	0.0481	2
2.9	0.045	661	0.0467	3
2.74	0.045	661	0.0456	3
2.58	0.043	661	0.0454	3
2.43	0.043	662	0.0431	4
2.31	0.042	662	0.0438	4
2.19	0.043	663	0.0425	5
2.1	0.042	663	0.0431	5
2	0.043	664	0.044	6
1.9	0.046	664	0.0463	6
1.8	0.046	664	0.0468	6
1.7	0.044	664	0.0449	6
1.6	0.045	664	0.0465	6
1.55	0.043	665	0.0447	7
1.5	0.044	665	0.0457	7
1.4	0.045	665	0.047	7
1.32	0.046	666	0.0474	8
1.21	0.046	666	0.0474	8
1.15	0.047	668	0.0479	10
1.09	0.047	668	0.0492	10
0.97	0.048	668	0.0497	10
0.87	0.049	669	0.0512	11
0.79	0.050	670	0.0524	12
0.72	0.050	671	0.053	13
0.67	0.051	671	0.0546	13
0.62	0.052	671	0.0556	13
0.54	0.055	671	0.058	13
0.48	0.055	671	0.0583	13
0.39	0.056	671	0.0591	13
0.3	0.056	672	0.0609	14
0.21	0.059	672	0.063	14
0.15	0.0621	673	0.0679	15
0.11	0.0642	673	0.0695	15
0.08	0.0683	673	0.0743	15

3.1.2 DNA Thermal Melting (T_m) studies

The results of thermal melting analysis are shown in Fig. 3.6, Table 3.2. The uncomplexed DNA melting at 54^{o}C gets stabilized to 62 ^{o}C at D/N ratio of 1. Further progressive addition of drug increases T_m linearly which finally appears to level off when D/N ratio of 4.0 is reached (Fig. 3.7). The total increase in T_m at saturation is = 25 ^{o}C and confirms 4:1 stoichiometry of the complex (*Wang et al. 2000*). Similar results have independently been monitored by NMR spectroscopy, which is discussed in chapter 4. The melting curves at D/N = 4.0-4.5 appear to be biphasic or triphasic with a high temperature phase (~79 ^{o}C) corresponding to a 4:1 stoichiometry of complex and two lower temperature phases near the T_m = 54 ^{o}C and 62 ^{o}C, that is of free DNA and 1:1 drug/DNA complex. On the other hand, the melting curve at D/N = 1.0 with T_m = 62 ^{o}C shows a high temperature phase melting at a temperature >74 ^{o}C, presumably corresponding to 2:1 stoichiometry in complex. This result is significant and shows that on adding 1 mole equivalent of drug to quadruplex, the stoichiometry of 2:1 exists in MTX-DNA complex, implying thereby that the drug binds as a dimer. Two drug molecules aligned in head to tail arrangement, have been clearly visualized in NMR spectra of complex at D/N =1.0, discussed in the chapter 4. Stability of quadruplex by ligand binding in groove and end stacking results in increase of T_m by 13-14 $^\circ$C on the binding of peimine and its analogue peiminine to human telomeric DNA (*Li et al. 2009*) and 11^{o}C on the stacking of Actinomycin D on the terminal G-tetrad (*Husdson et al. 2009*) while intercalating drug RHPS4 shows an increase of T_m by 20°C. Hence we can say that the observed stability lies in the range of groove binding and end stacking.

Table 3.2 Absorbance melting temperature (T_m) of d-(TTGGGGT)$_4$ and its complex with MTX at D/N ratios 1.0-5.0 and its corresponding ΔT_m

D/N	T_m °C	ΔT_m
0	54	0
1	62	8
2	69	15
2.5	71	17
3	75	21
3.5	77	23
4	79	25
4.5	80	26
5	80	26

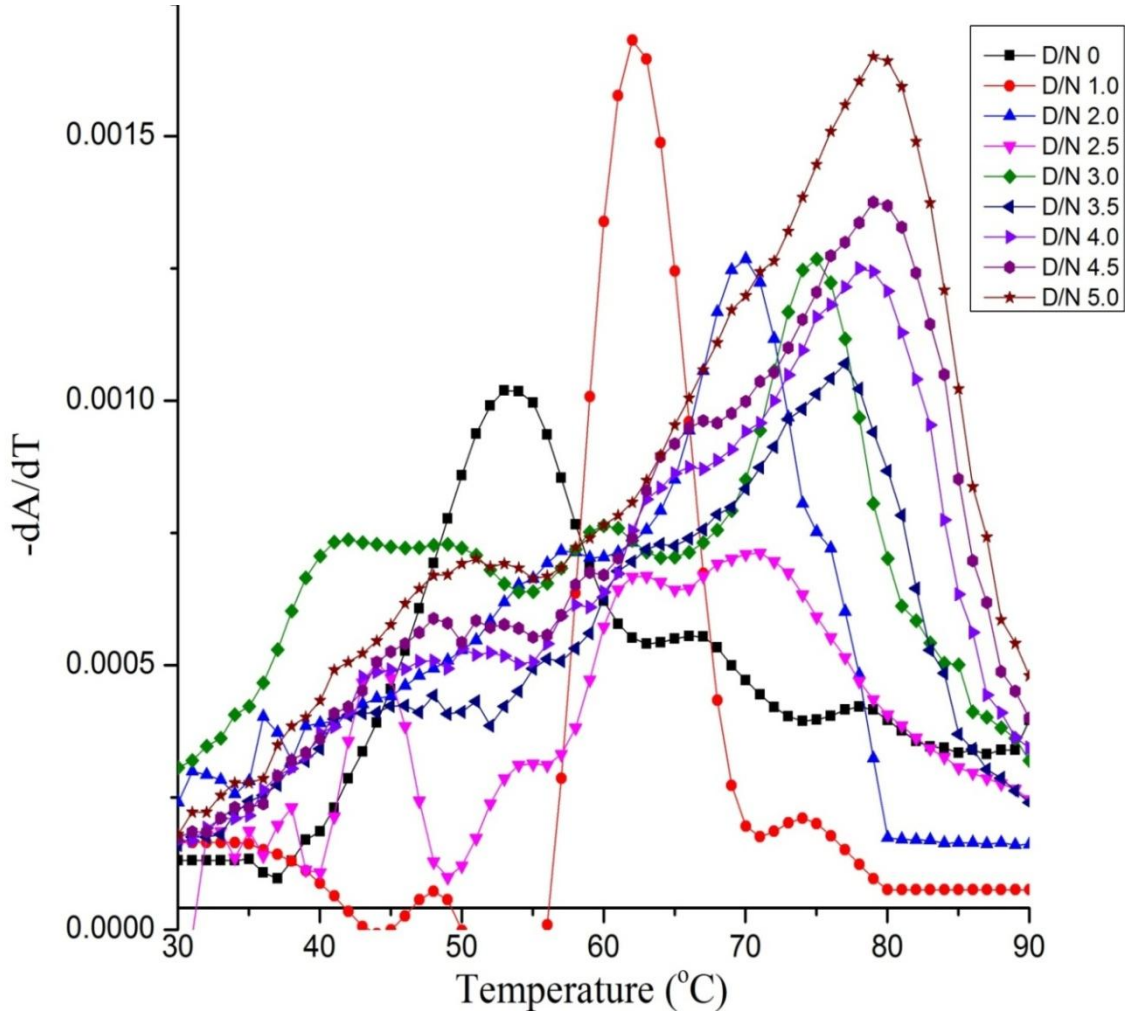

Figure 3.6 Derivative plot of thermal melting of d-(TTGGGGT)$_4$ alone and complex with MTX at various D/N ratios.

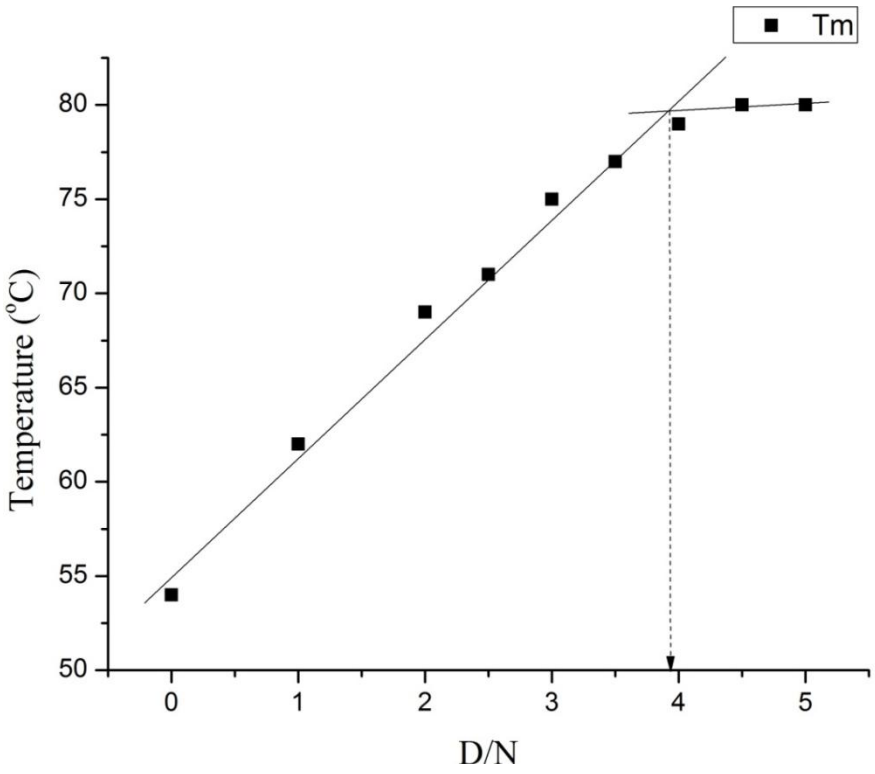

Figure 3.7 Plot of observed T_m changes with increasing MTX-d-(TTGGGGT)$_4$ (D/N) ratios.

3.1.3 Fluorescence spectroscopy studies

Fluorescence spectroscopy is a useful technique to probe the interaction of chromophore ligand with DNA, as fluorescence spectra provide important information about the changes in the local environment of the drug. The interaction of MTX with d-(TTGGGGT)$_4$ quadruplex DNA was evaluated by adding an increasing concentration of quadruplex DNA to a fixed 4.4 µM concentration of MTX and monitoring the changes in the fluorescence emission of MTX in the wavelength range 620-770 nm. We observed large changes in the emission spectra which may be due to changes in the environment of MTX upon binding to quadruplex DNA. On adding DNA, the fluorescence first decreased (D/N = 8.7-2.19) and then increased continuously (D/N = 2.19-0.08) accompanied by a red shift in emission maxima (Fig. 3.8a-c, Table 3.3). The maximum red shift was observed at D/N=0.97, which did not shift any further until apparently whole of drug was bound at D/N=0.08. This suggests the presence of multiple modes of binding, similar to that obtained by absorbance data. The absence of sharp isoemissive point also indicates the existence of multiple mode of binding between MTX and d-(TTGGGGT)$_4$ quadruplex DNA. The plot of

fluorescence intensity, versus N/D (Figs. 3.9a, b) at two different wavelengths of 678 and 686 nm shows an inflection point at D/N = 2.1(N/D=0.5), due to a sudden change in slope of the curve. The plot of Δ λvs D/N shows that Δλ is constant at D/N=0.08-0.97, being maximum $\Delta\lambda_{em}$= 8 nm and levels off to nearly zero at D/N = 4.0 (Fig. 3.10). These observations on shift in emission wavelength and emission intensity clearly point towards a stoichiometry of 1.0 and 2.0 in the MTX-DNA complex. The fluorescence quenching constant K_{sv} is evaluated (Figs. 3.11a, b) using the following equation (*Li et al. 2005, Chai et al. 2012)*:

$$F_0/F = 1 + K_{sv}\,[DNA] \quad \ldots\ldots\ldots \quad (2)$$

Where, F_0 and F are the fluorescence intensities in the absence and presence of quadruplex DNA at 678 nm, [DNA] = N, the concentration of nucleic acid quadruplex and K_{sv} is the Stern-Volmer quenching constant. We obtained K_{sv} = 7.1 x 10^5 M^{-1} for D/N = 4.0- 2.1. Using a typical value of fluorescence life time 0.2 x 10^{-9} s, an estimate of bimolecular quenching constant, K_q is 3.5 x 10^{15} $M^{-1}s^{-1}$. The binding constant *K* and binding stoichiometry (*n*, number of ligands binding to DNA) of the complex has been determined (Figs. 3.12-3.13a, b) using the equation (*Chai et al. 2012*):

$$\log [(F_0 - F)/F] = \log K + n \log [Q] \quad \ldots\ldots\ldots \quad (3)$$

in which quencher concentration [Q] = [quadruplex DNA] = N. We obtained a value of *K* = 6.6 x 10^5 M^{-1} and *n* = 0.9 for D/N ratio in the range 2.1- 4.0. For lower D/N values of 0.79 - 2.1, *K* = 5.4 x 10^5 $M^{-1}$and n = 1.89.

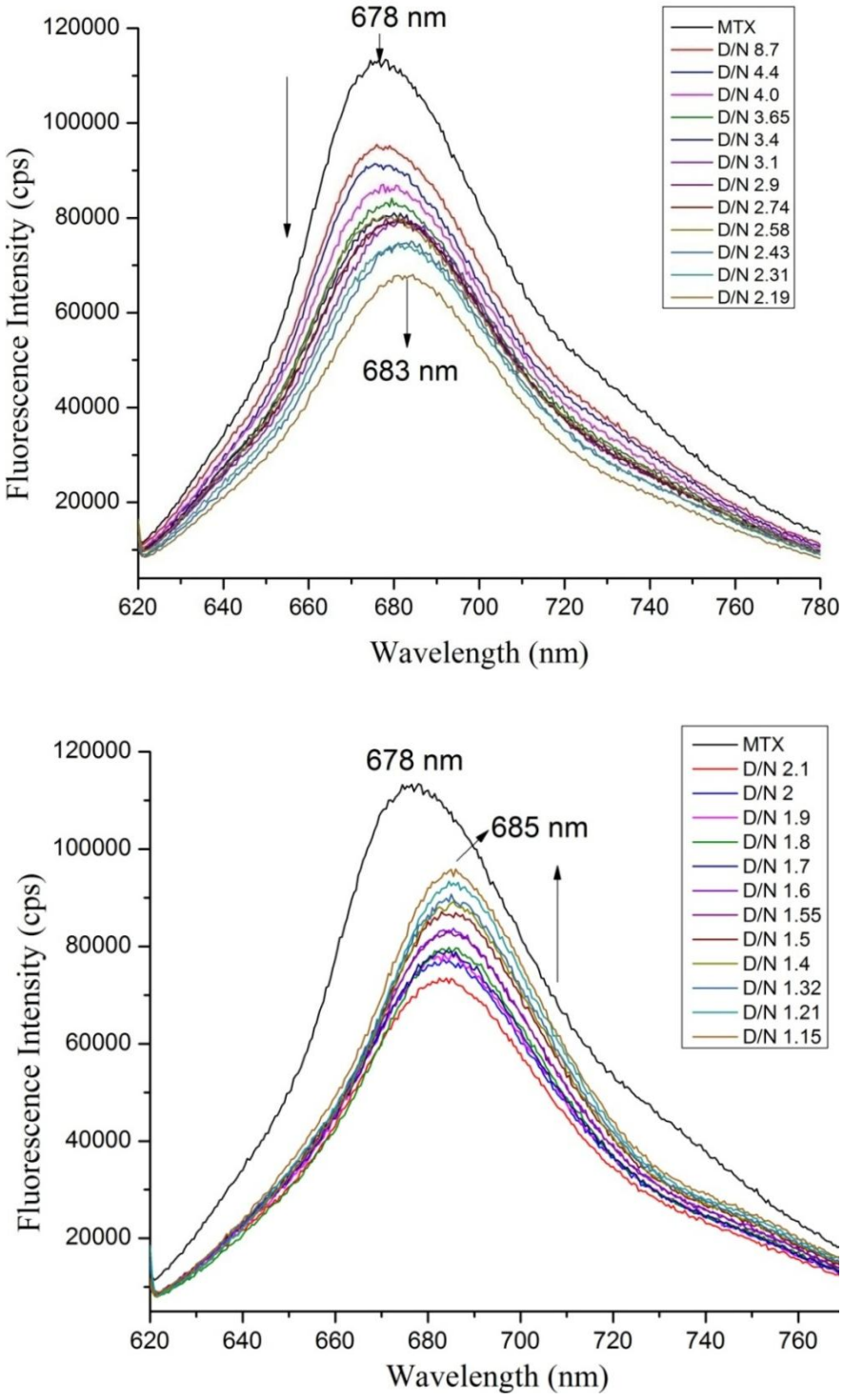

Figure 3.8(a) and (b) Fluorescence spectra of MTX in the increasing concentration of d-(TTAGGGT)$_4$ at 298 K at higher D/N ratios of 8.7 -2.19, (b) D/N ratios of 2.1 -1.15 also shown spectra of uncomplexed MTX.

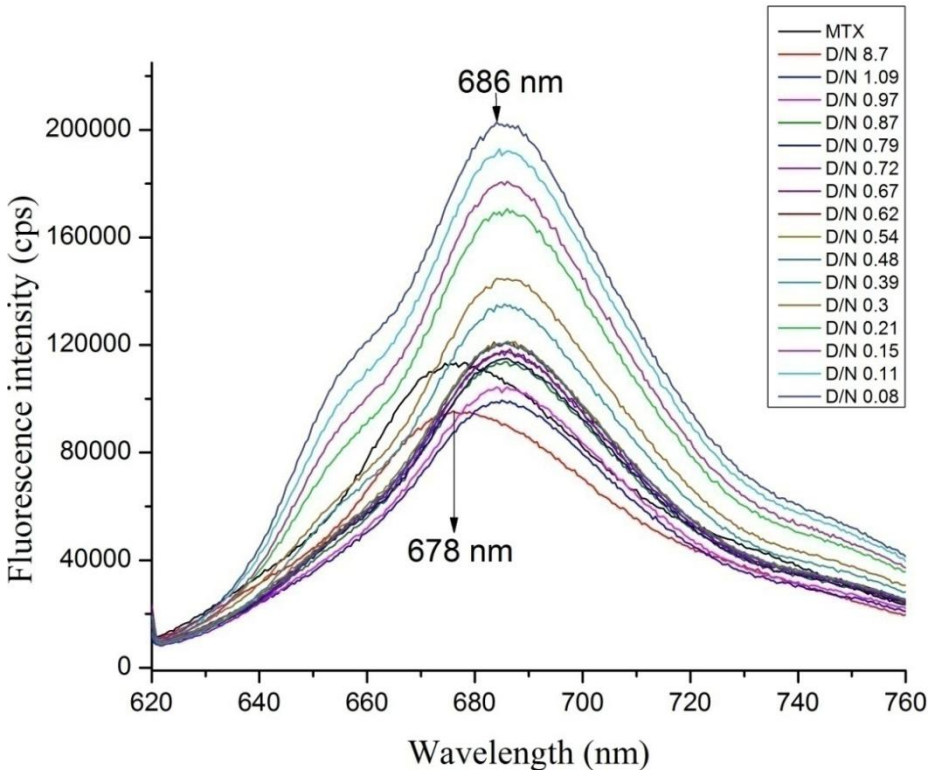

Figure 3.8(c) Fluorescence spectra of MTX in the increasing concentration of d-(TTAGGGT)$_4$ at 298 K at, and D/N ratios of 1.09– 0.08, also shown spectra of uncomplexed MTX.

Table 3.3 Change in the Fluorescence emission maxima (λ_{max}) of emission at 685 nm on interaction of MTX with $(TTAGGGT)_4$ at varying D/N ratios.

D/N	Fluorescence emission (cps) at 685 nm	λ_{max} (nm)	Fluorescence emission at λ_{max}	$\Delta\lambda_{max}$
∞	107646	678	113416	0
8.7	90178	679	95240	1
4.3	86756	679	91038	1
4	83848	679	86082	1
3.65	80596	679	84160	1
3.4	78778	680	80936	2
3.1	78480	681	79732	3
2.9	78366	681	79300	3
2.74	77648	682	79430	4
2.58	77378	682	80500	4
2.43	73978	682	75300	4
2.31	73006	682	75467	4
2.19	66998	682	67832	4
2.1	73420	683	73578	5
2	76632	683	77542	5
1.9	78264	683	78458	5
1.8	78880	684	79812	6
1.7	79030	684	79804	6
1.6	82990	684	83324	6
1.55	82878	684	83225	6
1.5	86428	684	86606	6
1.4	88904	685	88904	7
1.32	90688	685	90688	7
1.21	92456	685	92456	7
1.15	95826	685	95826	7
1.09	99522	685	99522	7
0.97	102338	686	104430	8
0.87	112936	686	113742	8
0.79	114780	686	114964	8
0.72	117554	686	117566	8
0.67	117824	686	117890	8
0.62	119724	686	120378	8
0.54	120190	686	121292	8
0.48	120332	686	120898	8
0.39	134020	686	134404	8
0.3	144530	686	144684	8
0.21	168066	686	170642	8
0.15	180506	686	180812	8
0.11	190488	686	192134	8
0.08	202090	686	202048	8

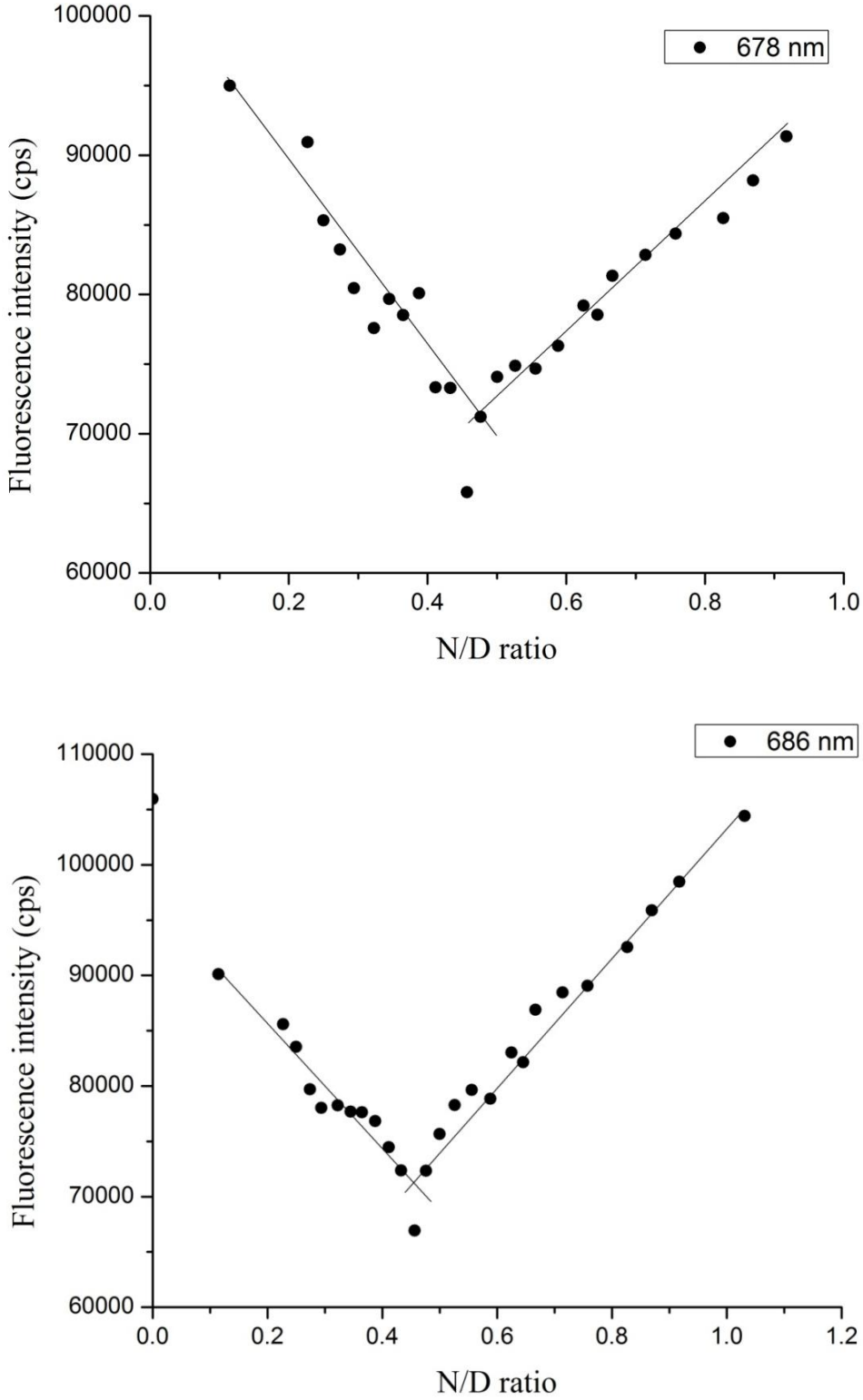

Figure 3.9 (a) and (b) Plot of change in the fluorescence intensity on varying N/D ratios.

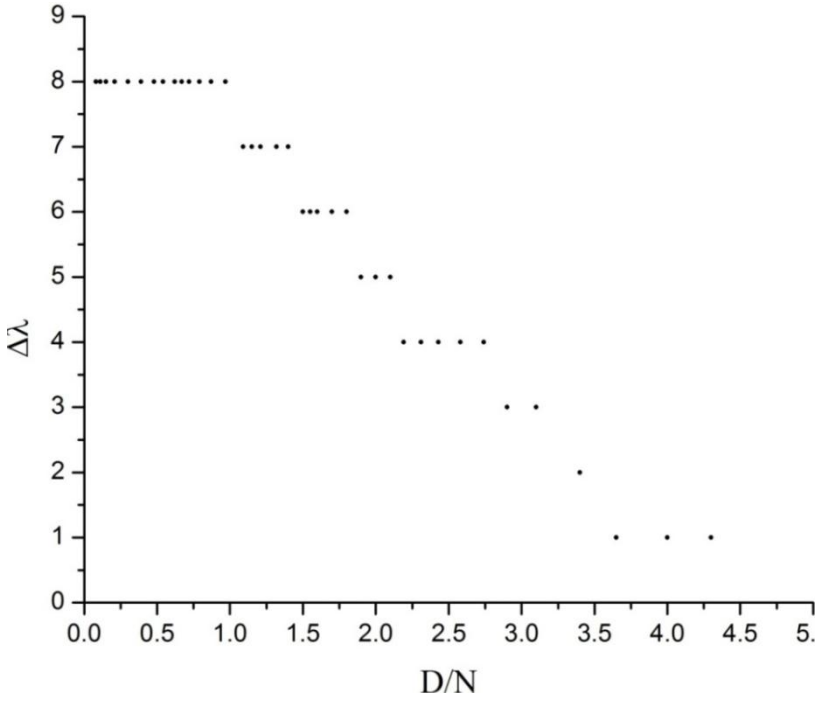

Figure 3.10 Change in the emission λ_{max} (Δλ) of 678 nm band at varying D/N ratios of MTX-d-(TTGGGGT)$_4$ complex.

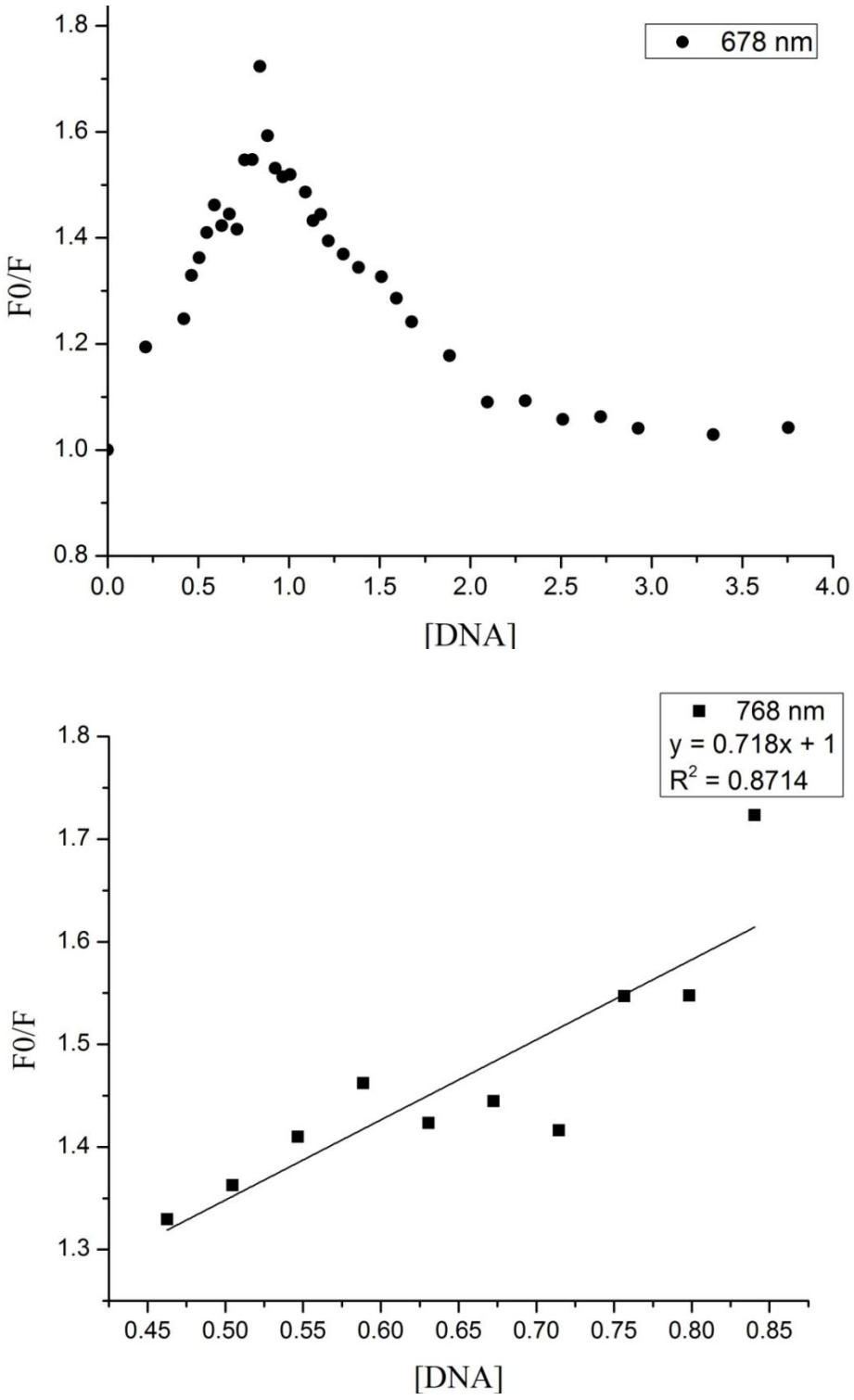

Figure 3.11 The Stern-Volmer quenching plot of 4.4 µM MTX with d-(TTGGGGT)$_4$ concentrations (a) full range of [DNA] i.e. 0.2-19.2µM (D/N 8.7-0.08) and (b) [DNA]= 0.48-2.19µM (D/N 4 -2.1).

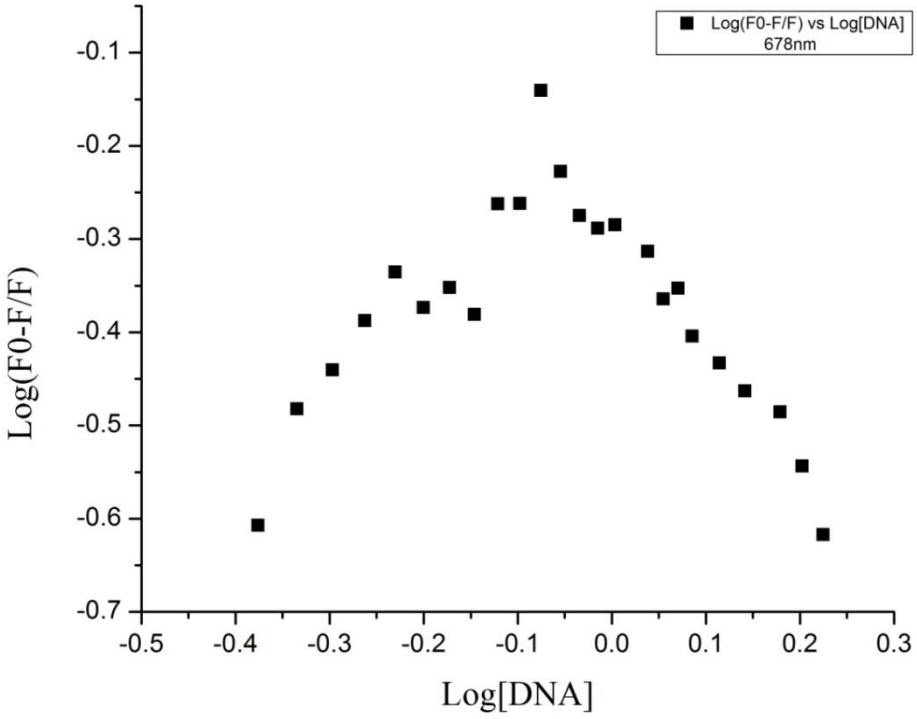

Figure 3.12 Plot of log (F_0-F)/F versus log [DNA] for full DNA concentration range.

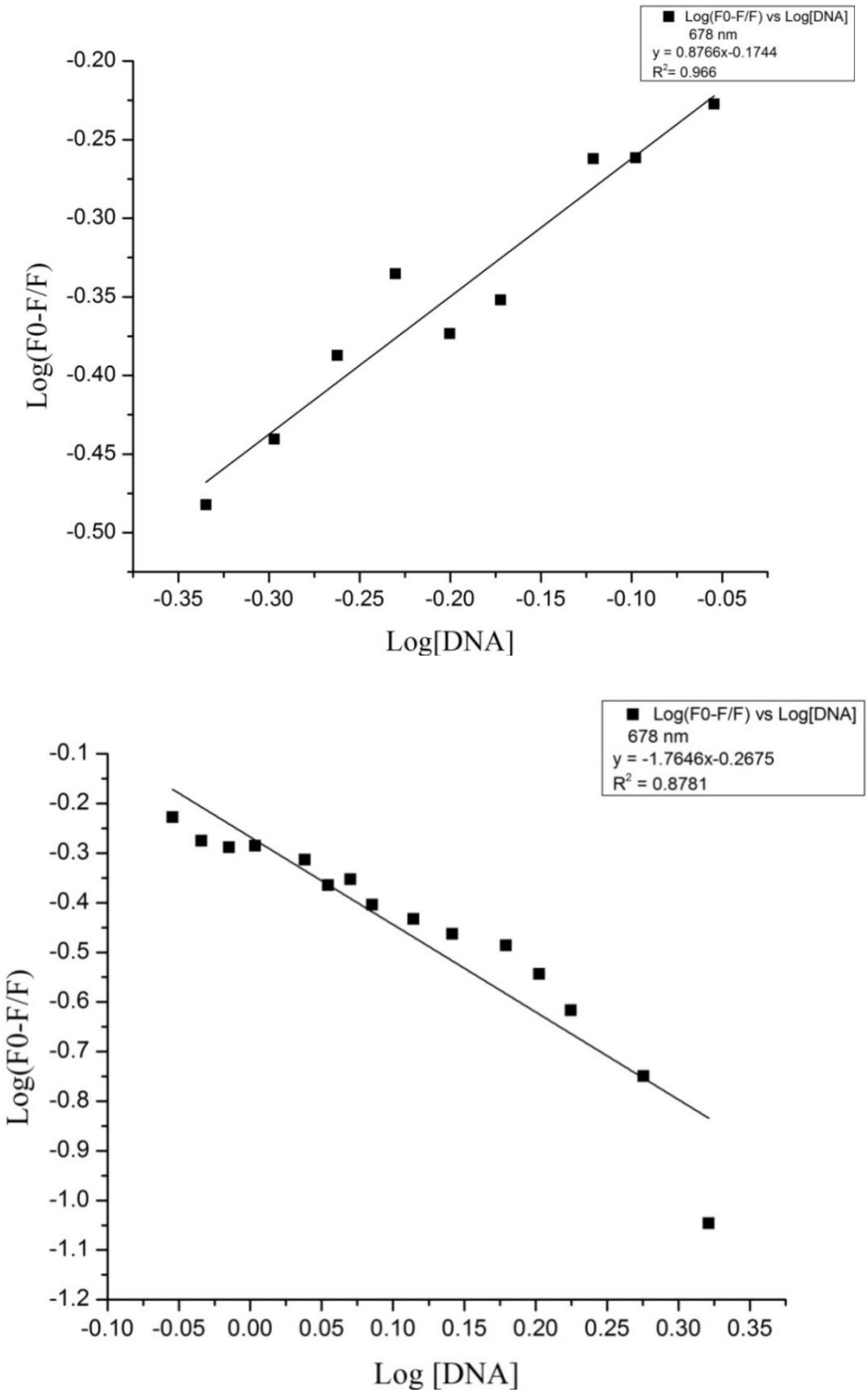

Figure 3.13 Plot of log (F0-F)/F versus log[DNA] for DNA concentrations (a) 0.46 – 0.88 µM (D/N 4 .0 – 2.1) and (b) 0.88 – 2.3 µM (D/N 2.1 – 0.79).

3.1.4 Job Plot

In order to establish the binding stoichiometry of mitoxantrone with G-quadruplex sequence d-(TTGGGGT)$_4$, the results of difference in emission intensity of MTX, $\Delta F = F\text{-}F_o$, in the presence (F) and absence (F_0) of DNA quadruplex, is plotted as a function of mole fraction of MTX in Fig. 3.14. Examination of Job plot shows several slope changes between approximately linear regions. The last two end points of slope change clearly yield stoichiometric ratios of 2:1 and 4:1 moles of MTX/mole equivalent of d-(TTGGGGT)$_4$ quadruplex corresponding to mole fraction of MTX = 0.66 and 0.80, respectively in the plot. However slope change at mole fractions of 0.33 and 0.50 is also evident from the plot, which yields a stoichiometric ration of 0.5:1 and 1:1 in the complex. Thus apparently multiple complexes with different stoichiometric ratios are being formed.

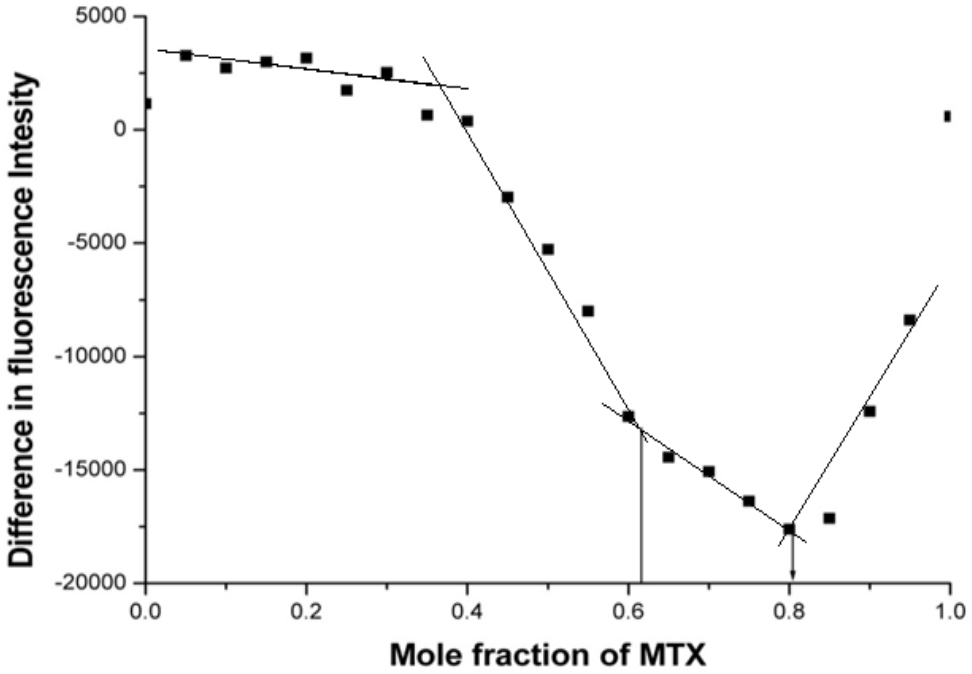

Figure 3.14 Job plot (Continuous variation plot) for the binding of MTX to (TTGGGGT)$_4$.

3.1.5 Fluorescence Lifetime measurements

Fluorescence life time of free and bound chromophore differs which can be resolved on experimental time scale. Time–Resolved fluorescence studies can give an idea of the binding modes of ligand-DNA complex depending upon their fluorescence decay profile. The fluorescent

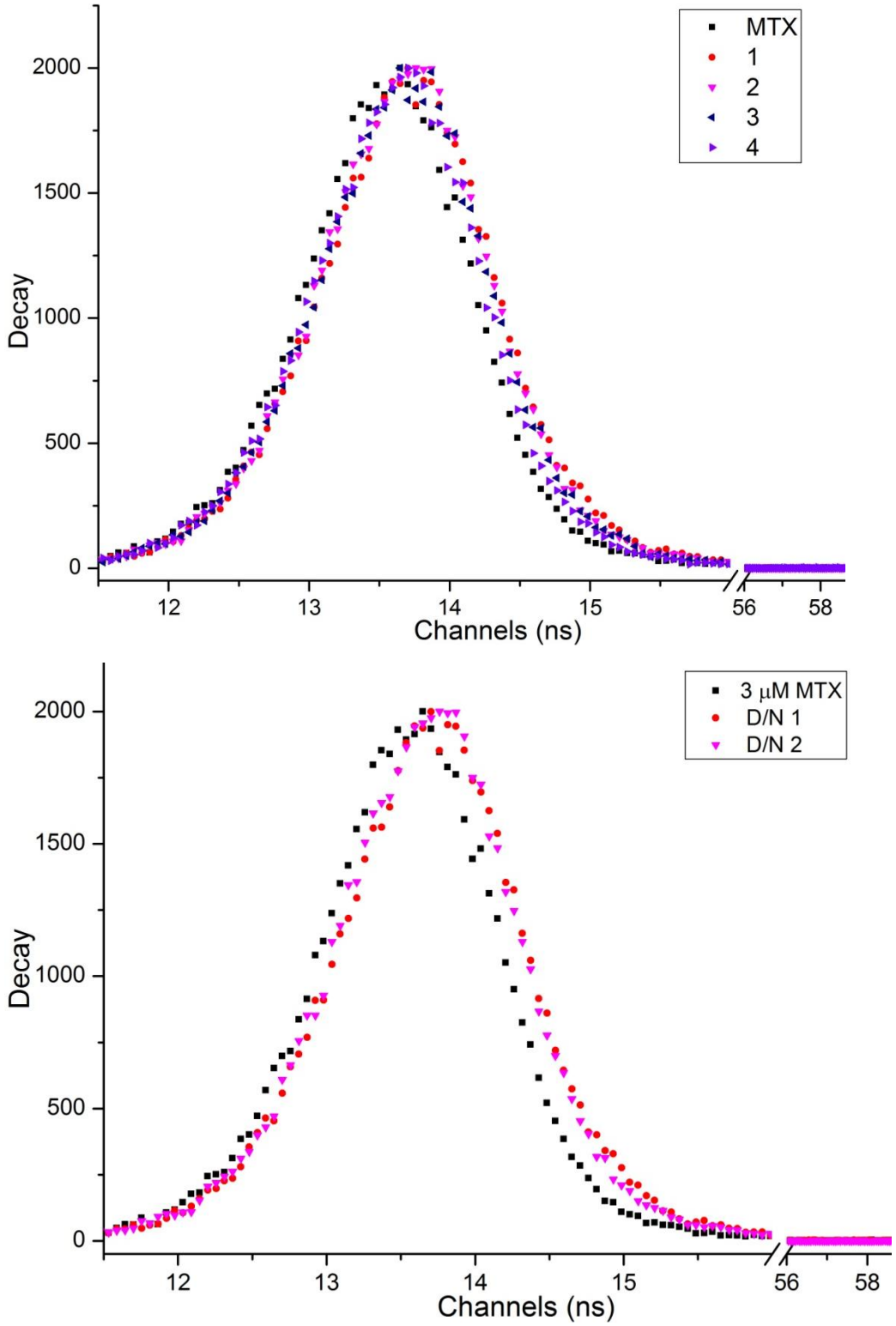

Figure 3.15 (a and b): Time resolved fluorescence decay curves of free MTX and MTX-d-(TTAGGGT)$_4$ complexes at varying D/N ratios in KBPES buffer (pH 7.0) at 298 K.

decay of 3 μM uncomplexed MTX is essentially monoexponential giving a life time value of 0.140 and 0.135 ns in separate experiments, which compares well with that reported in the literature (*Lin and Struve, 1991; Koningstein et al. 1992*). The fluorescence decay profiles of MTX-d-$(TTGGGGT)_4$ complexes at varying D/N ratios (Figs. 3.15a,b) showed that the lifetime of MTX increases on binding to quadruplex. This increase in the life time is due to shielding of the MTX chromophore from solvent, which resembles to its life time of aprotic solvent (*Lin and Struve, 1991*). The decay profiles are biexponential and yield two sets of average values of a life time, that is, $\tau = 0.46$ ns and $\tau = 0.19$ ns at D/N = 0.5-4.0 (Table 3.4), which can be attributed to the presence of two species. The amplitude of longer life time decreases with D/N. Since the higher stoichiometries complex is expected to be the dominant species at D/N ~ 4, it may be inferred that the complex having $\tau = 0.52$ ns is 4:1 MTX-DNA complex with a relative abundance of 91.15%. This life time is attributed to the externally bound MTX to quadruplex because on intercalation the life time increases about three to four times to that of free ligand. Ethidium bromide a classical intercalator shows an increase in life time $\tau = 22.2$ ns to that of free $\tau = 1.6$ ns upon binding to duplex DNA (*Malathi et al. 2003*).

Table 3.4 The fluorescence lifetimes of MTX in the presence or absence of d-$(TTGGGGT)_4$ at 298 K (where τ denotes fluorescence lifetimes and α denotes amplitude).

	τ_1 (ns)	τ_2 (ns)	α_1	α_2
MTX	0.14	-	100	-
D/N 0.5	0.42	0.19	35.21	64.79
D/N 1	0.36	0.15	54.68	45.32
D/N 1.5	0.46	0.17	21.06	78.94
D/N 2	0.48	0.19	21.92	78.08
D/N 3	0.42	0.15	23.78	76.22
D/N 4	0.52	0.17	8.85	91.15

3.1.6 Circular Dichroism spectroscopy studies

Circular dichroism (CD) spectroscopy is used to study changes in conformation of DNA due to binding of MTX. CD spectra of uncomplexed d-$(TTGGGGT)_4$ (Fig. 3.16) shows two well defined peaks, a maxima at 264 nm and a minima 243 nm. These are signature peaks of existence of parallel G-quadruplex structure (*Spada et al. 2010; Kypr et al. 2012; Ellestad, 2012*). Uncomplexed MTX does not show any optical activity. Upon complexation, the positive band at 264 nm decreases slowly till D/N 2.0 without any observable shift in the peak position (Figs. 3.16a-e, Table 3.5) and further increase in D/N ratio results in drastic decrease in the intensity of the positive CD band. The negative CD band, at 246 nm shows significant decrease in intensity from 2.25 to -1.77 mdeg at D/N ratio 0.13. Further increase in D/N has little effect on this band but it shows large decrease in intensity after D/N ratio 3.2. Upon complexation, there is no shift in the positive (264 nm) or negative (244 nm) CD band till D/N ratio 3.8. At higher D/N ratios, beyond 3.8, there is a red shift of 7 nm and 4 nm in positive and negative CD bands, respectively. Besides, a new positive CD band starts appearing at D/N > 3.8 at 289-300 nm which grows in intensity with D/N (Table 3.5). Fig. 3.17a, b shows the plot of change in CD signal versus D/N ratio where there is a sudden change in the slope after D/N > 3.8. When an achiral ligand binds to chiral DNA induced CD (ICD) bands are observed within the absorption region of bound ligand. In order to observe induced bands due to binding of MTX to DNA, a different set of experiment was conducted. In this set of titrations, MTX concentration is kept constant and d-$(TTGGGGT)_4$ was varied. The induced CD bands of MTX appeared in the wavelength region 620-720 nm, the absorbance region of MTX. Presence of positive induced CD bands indicates the binding of MTX into the grooves of quadruplex. Due to the problem in the baseline and noise, we cannot clearly ascertain the variations in induced CD bands, but we can identify quadruplex DNA induced MTX bands (Fig. 3.18) around 625, 648, 681 and 716 nm. The maximum CD signal is observed at D/N = 0.6 in 716 nm induced band, when maximum concentration of drug may be bound to DNA. The plot of variation in induced CD versus D/N concentration shows the inflection points (Figs. 3.19) at D/N = 1, 2 and perhaps 3.8, which once again clearly shows that MTX binds to with d-$(TTGGGGT)_4$ with multiple binding modes.

Table 3.5 Change in the ellipticity (Θ) and λ_{max} for positive CD band (264 nm) and negative CD band (246 nm) of uncomplexed and MTX complexed d-$(TTGGGGT)_4$.

D/N	CD (mdeg) at 264 nm	CD (mdeg) 246 nm	Positive CD λ_{max} nm	CD (mdeg)at λ_{max}
d-$(TTGGGGT)_4$	7.62	-2.25	264	7.626
0.13	7.36	-1.77	264	7.360
0.26	7.31	-1.80	264	7.311
0.4	7.18	-1.61	264	7.181
0.53	7.25	-1.41	264	7.255
0.67	7.06	-1.55	264	7.064
0.8	6.68	-1.64	264	6.686
0.94	6.72	-1.39	264	6.725
1.07	6.44	-1.66	264	6.441
1.2	6.65	-1.62	264	6.654
1.4	6.65	-1.62	264	6.653
1.6	6.6	-1.62	264	6.603
1.8	6.54	-1.64	264	6.553
2.1	6.48	-1.68	264	6.483
2.4	6.34	-1.60	264	5.783
2.7	6.16	-1.05	264	6.164
3.2	5.02	-2.62	264	5.264
3.8	4.24	-4.81	264	4.664
4	3.22	-7.11	266	3.729
4.7	0.59	-11.73	268	1.77
5.4	-2.7	-15.2	271	-0.305
6	-4.88	-17.1	271	-2.48

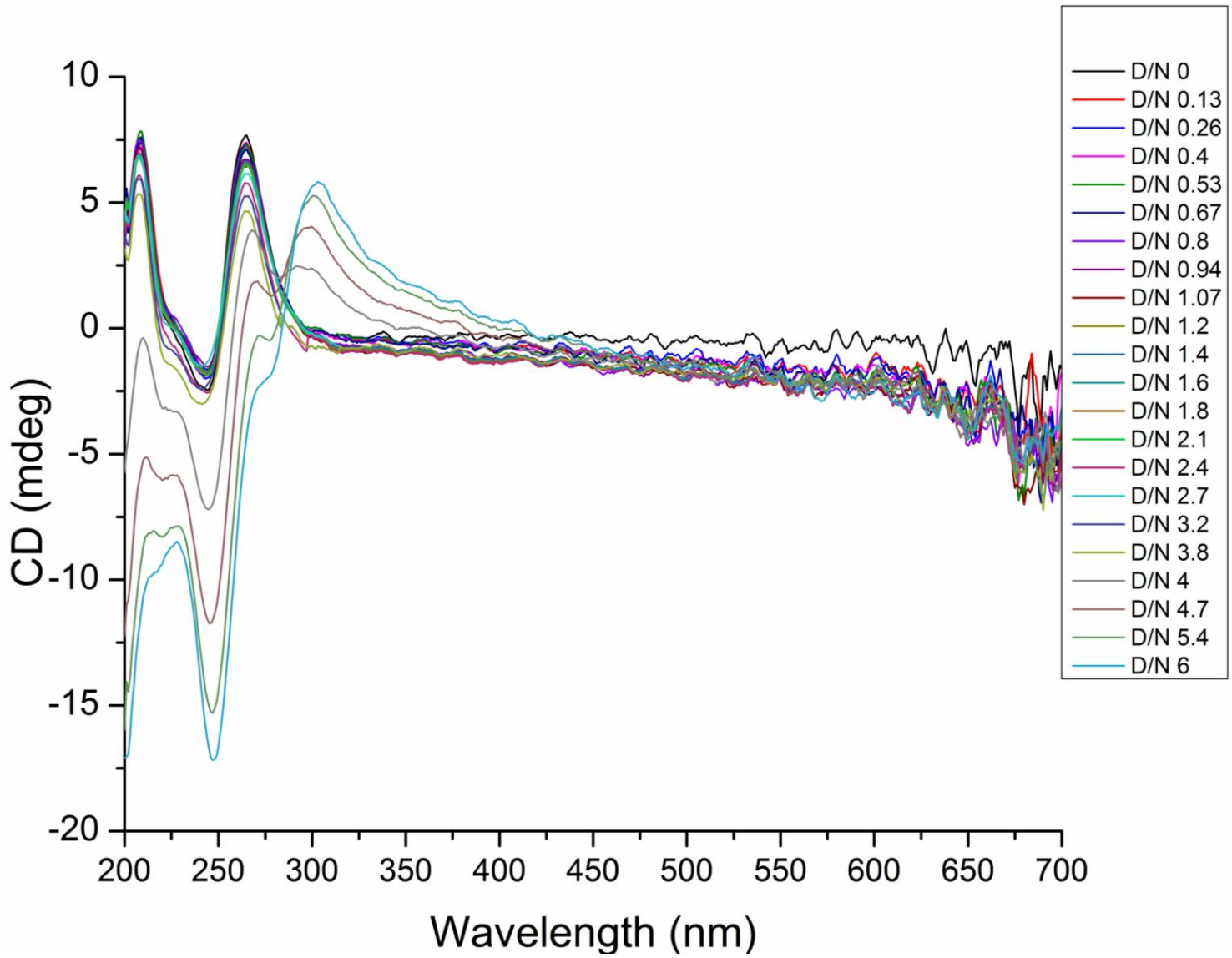

Figure 3.16(a) Circular Dichroism (CD) spectra of 8μM d-$(TTGGGGT)_4$ in the absence and presence of MTX at 298 K at varying D/N ratios.

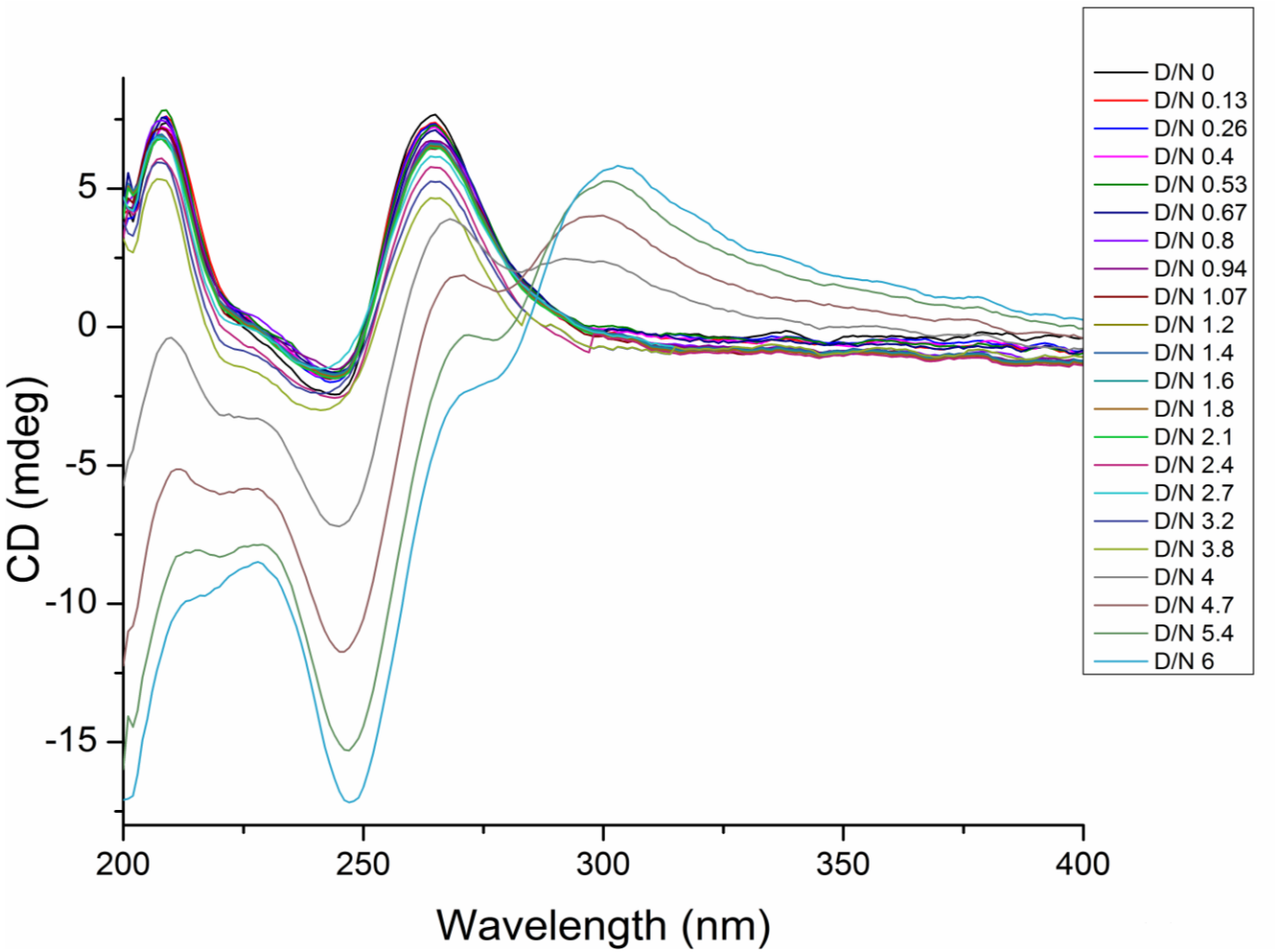

Figure 3.16 (b) Expanded region from 200 – 400 nm of Circular Dichroism (CD) spectra of 8µM d-(TTGGGGT)$_4$ in the absence and presence of MTX at 298 K at varying D/N ratios.

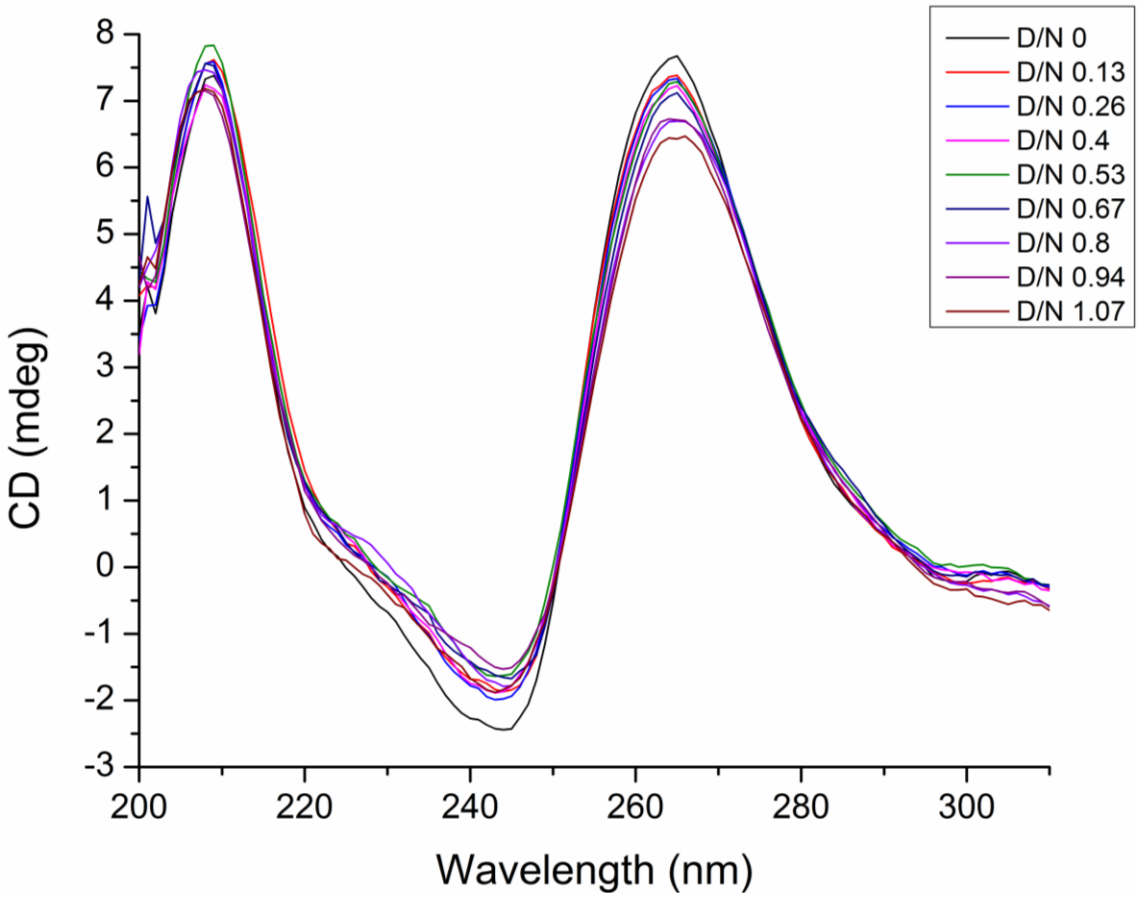

Figure 3.16(c) Expanded region Circular Dichroism (CD) spectra at varying D/N ratios (D/N 0.13-1.07), also shown uncomplexed d-(TTGGGGT)$_4$ (8 μM).

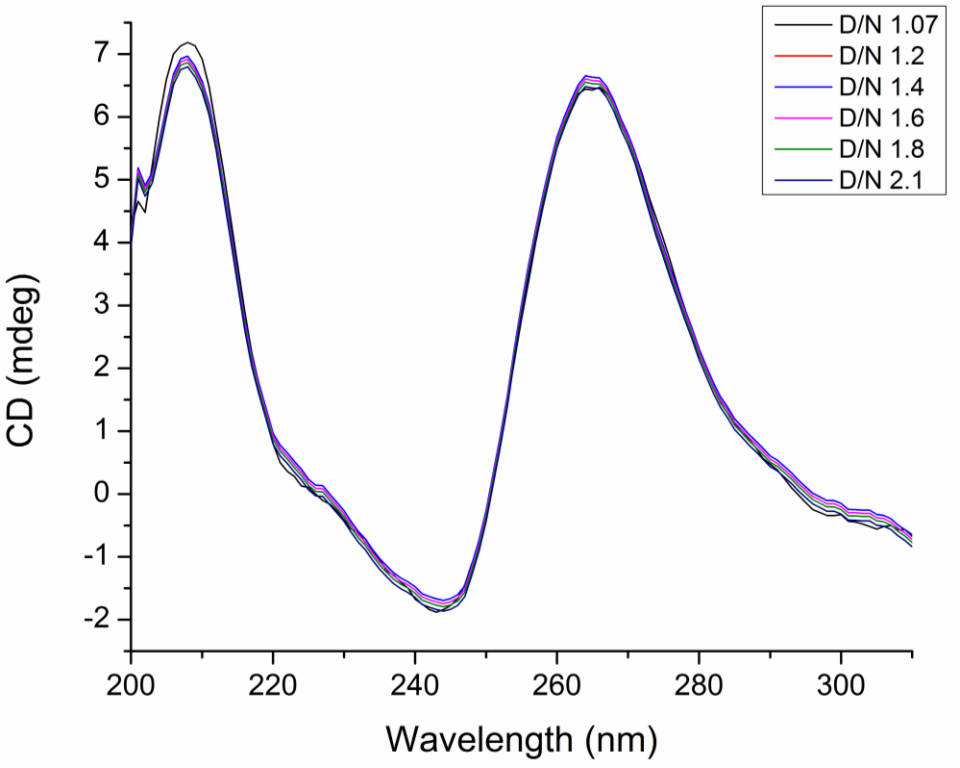

Figure 3.16(d) Expanded region Circular Dichroism (CD) spectra at varying D/N ratios (D/N 1.07-2.1).

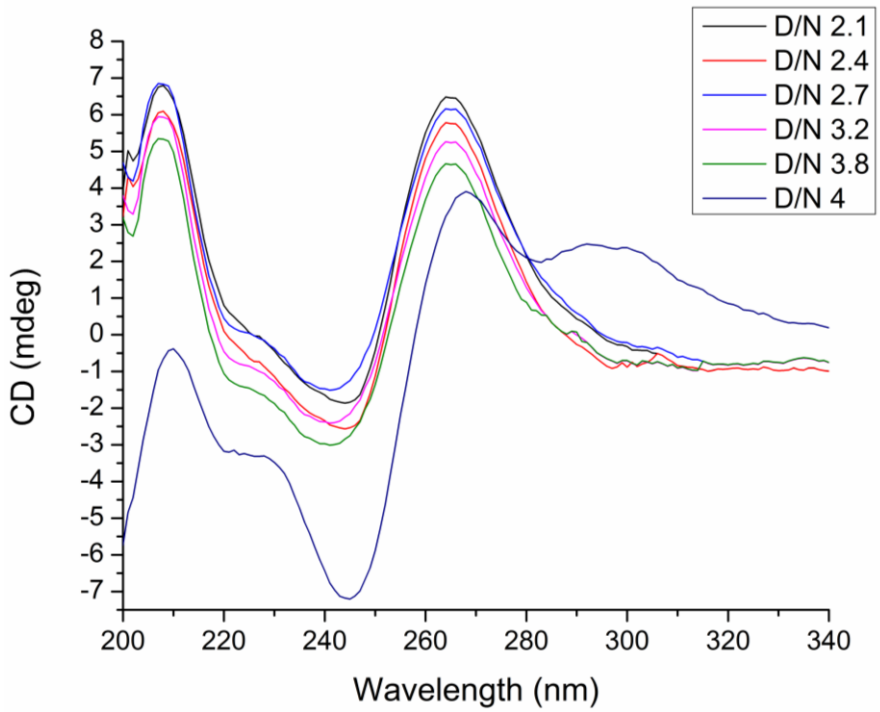

Figure 3.16(e) Expanded region Circular Dichroism (CD) spectra at varying D/N ratios (D/N 2.1-4.0).

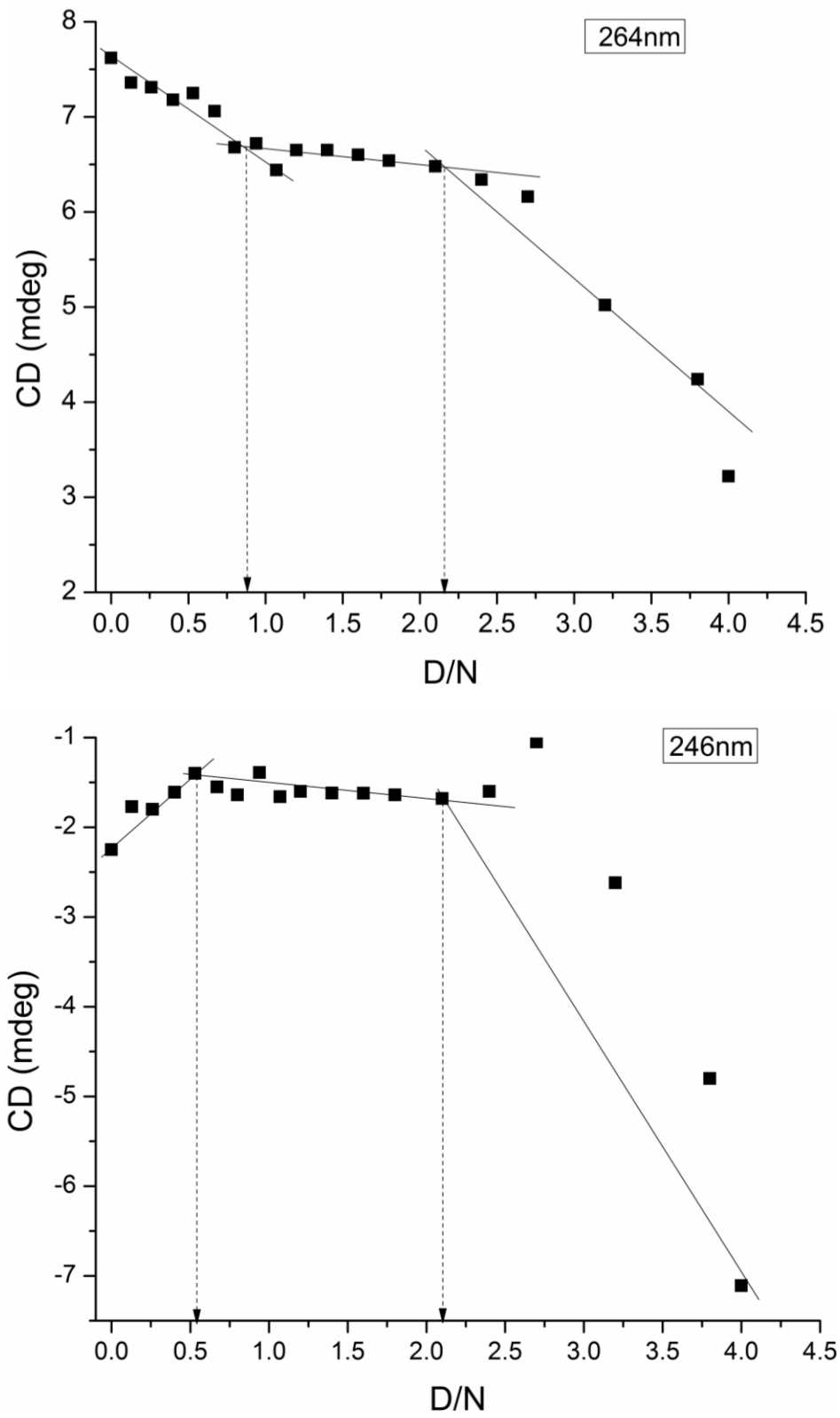

Figure 3.17 Plot of change in the circular dichroism (mdeg) versus varying D/N ratios for (a) positive CD band (264 nm) and (b) negative CD band (246 nm).

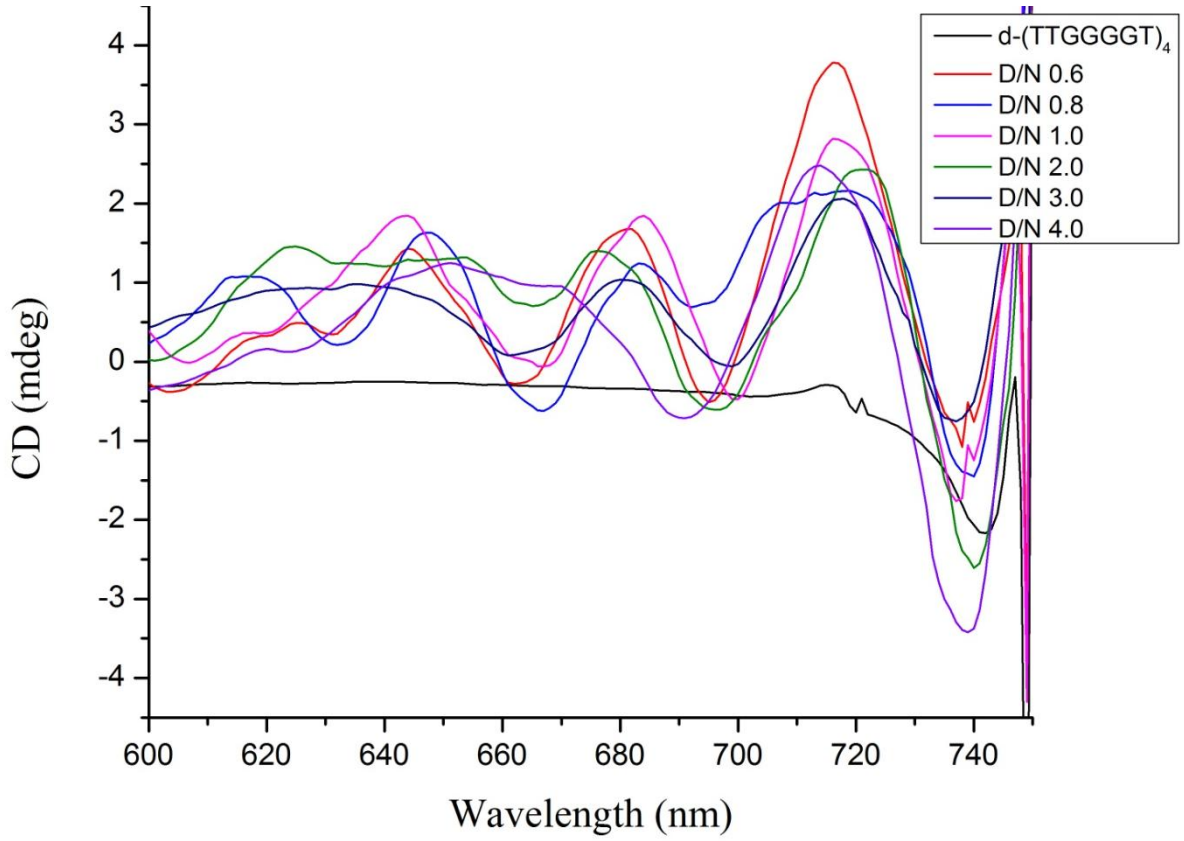

Figure 3.18 Circular dichroism (mdeg) spectra showing induced CD (ICD) band at varying D/N ratios of interaction of MTX with d-(TTGGGGT)$_4$ quadruplex DNA.

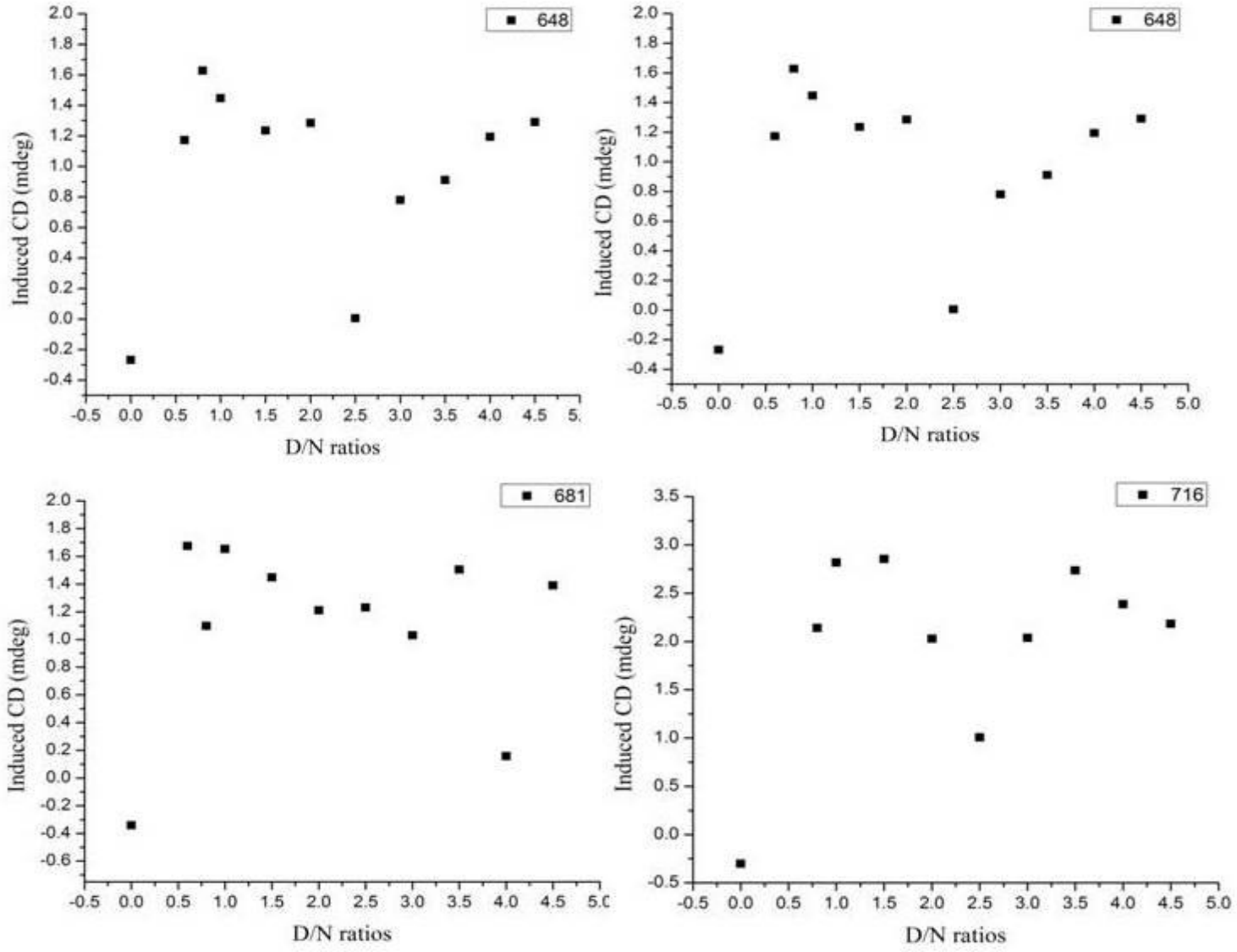

Figure 3.19 Plot of induced circular dichroism (ICD) upon binding of MTX to d-(TTGGGGT)$_4$ in mdeg at varying D/N ratios.

3.1.7 Surface Plasmon Resonance (SPR) studies

The interaction of MTX with d-(TTGGGGT)$_4$ was studied by means of Surface Plasmon resonance to monitor the molecular interaction in real time with the target d-(TTGGGGT)$_4$ immobilized on the sensor chip as detailed in Chapter 2,section 2.2.8.

The affinity plots along with kinetics of association and dissociation for two separate runs is shown in Figs. 3.20. The smooth lines is Figs. 3.21a,b are the best fit lines using a single site model. The dissociation constant K_D obtained is 9.654 x 10^{-5} M and 8.757 x 10^{-5} M with χ square 358.3 and 308.8, respectively. This gives affinity constant K_A as 1.037 x 10^4 M^{-1} and 1.142 x 10^4 M^{-1} with an average value of 1.086 x 10^4 M^{-1} from the response in steady state. The observed average response unit RU_{avg} in any steady state experiment in run 1 and 2, did not exceed the corresponding RU_{max} values of 1375 and 1174, respectively, which indicates that number of binding sites, *n*, does not exceed one.

The kinetic analysis of Figs. 3.20 a, b gives association (k_a) and dissociation (k_d) constants for run 1 and 2, which yielded two modes of binding. The affinity constant K_A for the faster mode of binding are 3.00 x 10^4 M^{-1} and 3.50 x 10^4 M^{-1}, respectively (Table 3.6). These values are in reasonably good agreement with those obtained from steady state analysis. The high ionic strength in these experiments minimizes the mass transfer effects. The observed very low affinity values of K_A = 0.190 and 0.216 M^{-1} do not appear to be related to binding but may be associated with a slow conformational change in MTX-DNA complex.

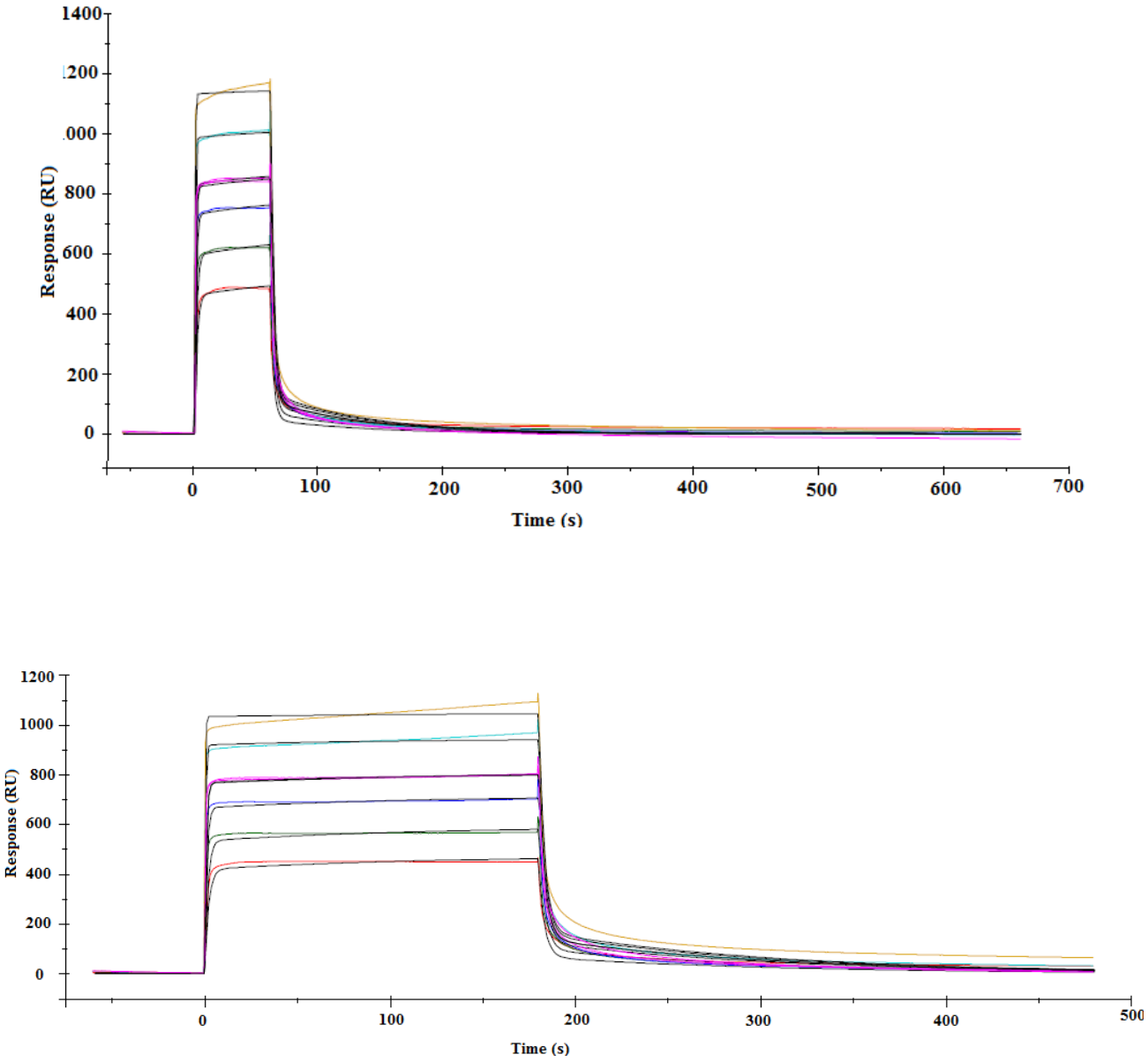

Figure 3.20 (a and b): SPR sensograms of interaction of MTX with d-(TTGGGGT)$_4$ at 298 K.

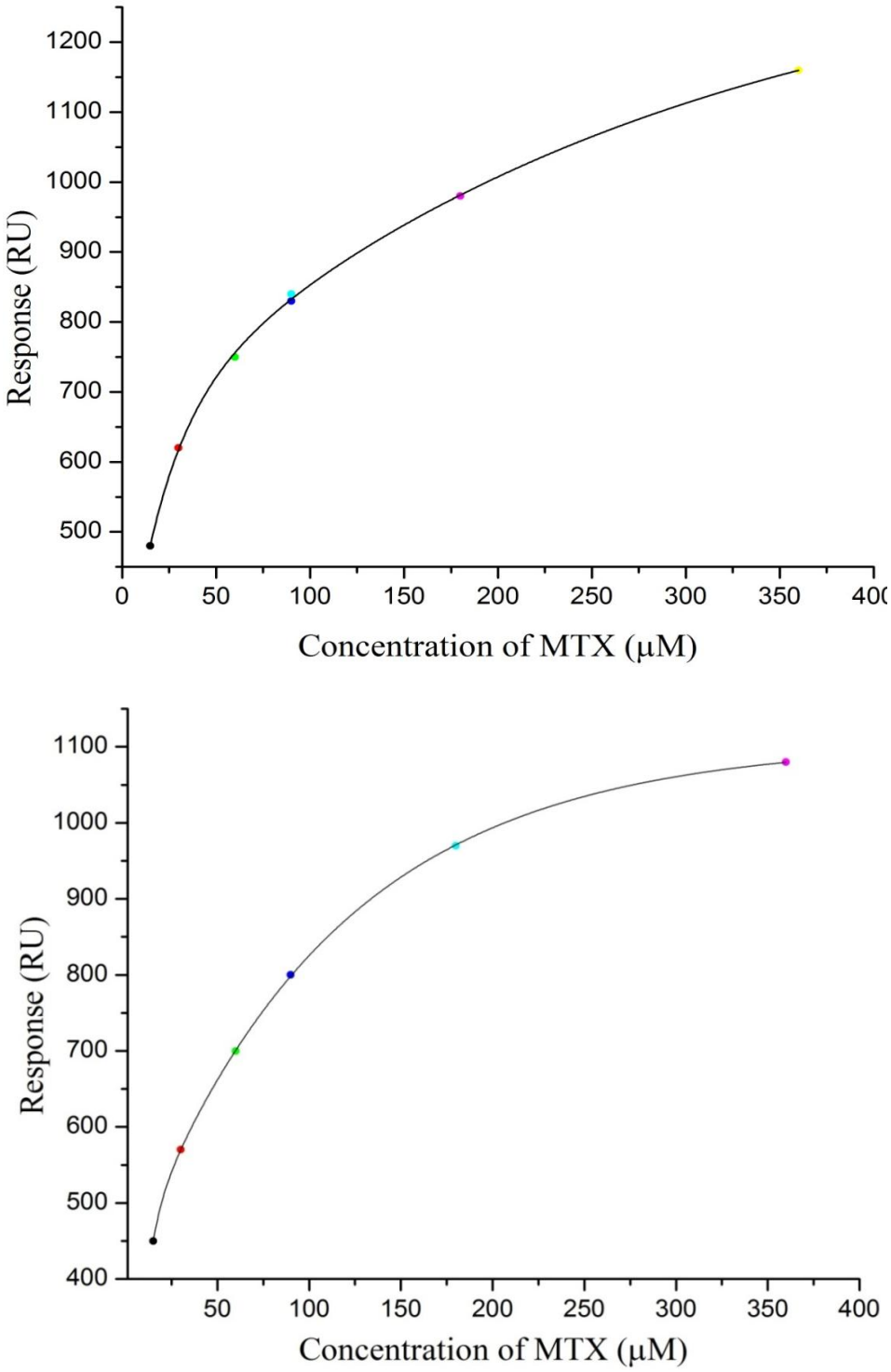

Figure 3.21(a and b): Binding plots using SPR data of interaction of MTX with d-(TTGGGGT)$_4$ at 298 K by fitting the steady state response curves into two state binding model.

Table 3.6 SPR run data with equilibrium binding constants for binding of MTX with d-$(TTGGGGT)_4$.

Experiment	Flow rate (µl/min)	RU_{max} (RU)	k_a ($M^{-1}\,s^{-1}$)	k_d (s^{-1})	K_D (M)	$K_A = K$ (M^{-1})	Chi^2 (RU^2)
Kinetics run 1	30	1375	1.185×10^4 2.498×10^{-3}	0.3947 0.01289	3.33×10^{-5} 5.160	3.00×10^4 0.190	171
Kinetics run 2	30	1174	1.134×10^4 1.715×10^{-3}	0.3236 0.00792	2.85×10^{-5} 4.620	3.50×10^4 0.216	354
Steady state run 1	30	1375	-	-	9.654×10^{-5}	1.037×10^4	358.3
Steady state run 2	30	1174	-	-	8.757×10^{-5}	1.142×10^4	308.8

3.1.8 TRAP assay

The dose dependent effect of mitoxantrone on the reverse transcriptase activity of the telomerase enzyme was investigated using two step Telomerase Repeat Amplification Protocol (TRAP) assay (Kim et al. 1994). The results obtained are shown in Fig. 3.22. Increasing concentration of MTX was tested in the range of 0.1 to 10 μM. Intense bands observed in the telomerase positive control lane indicates that cell extract from MCF-7 human cancer cell line has significant telomerase activity, and also infer that no PCR inhibitors (Taq polymerase) were present in the cell extract. Analysis of Fig. 3.22.a shows significant decrease in the intensity of the TRAP (6-base pair ladder) products after incubation with MTX in the concentration range of 1 to 5 μM. This reduced band intensity can be attributed to the inhibition of telomerase activity by MTX. The results clearly show the dose dependent inhibition of telomerase activity with IC50 value of ~2 μM. At highest MTX concentration (10 μM), ~ 90 % inhibition of the telomerase activity was observed. The IC50 values of the telomerase inhibition by MTX were also estimated by the fluorescence intensity measurements of the fluorescien and sulforhodamine amplifluor tag used in the primers of the TRAP assay reagent kit. Fig. 3.22b shows the $\Delta F_L/\Delta F_R$ values of the TRAP assay reactions, which clearly indicates that the increasing concentration of MTX results in decrease in the fluorescence intensity of the samples. The IC50 value for telomerase inhibition calculated from this method was found to be ~2 μM.

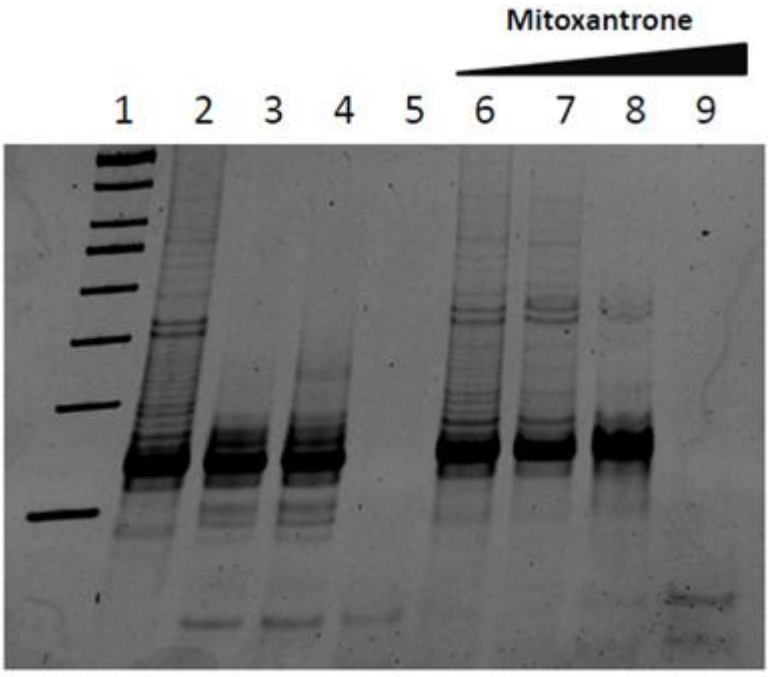

Lanes: 1- 50bp DNA ladder, 2- positive control, 3- negative control 4- heat inactivated, 5- Taq negative
6,7,8 & 9 - Mitoxantrone 0.01uM 0.1uM , 1uM and 10 uM

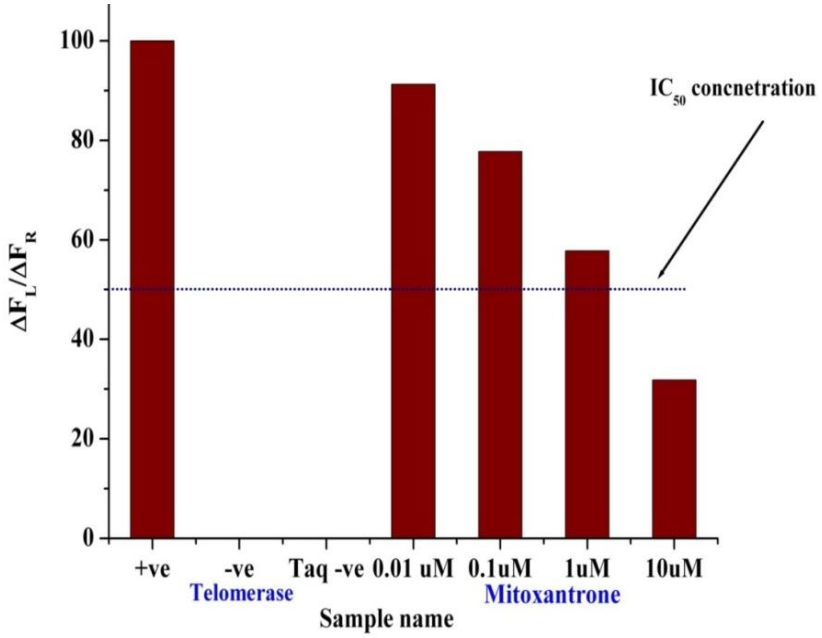

Figure 3.22 (a and b): TRAP assay of MTX: a) 10% polyacrylamide gel showing TRAP products, b) plot of $\Delta F_L/\Delta F_R$

3.2 Summary and Conclusion

The UV-vis studies shows the multiple mode of binding of MTX to d-(TTGGGGT)$_4$ quadruplex sequence. Both monomer and dimer peaks of MTX shows bathochromic shift with initial hypochromism till D/N ratio 2.0 and hyperchromism after this molar ratio. The Benesi - Hildebrand plot gives the binding constant K = 3.53 x 10^6 M^{-1} and 3.73 x 10^6 M^{-1} for D/N = 0.5 to 2.0 and D/N = 2.0 to 4.0, respectively. The plot of wavelength change versus D/N ratio does not show any change after D/N ratio of 4.0. The UV-vis thermal melting study gives the ΔT_m of ~ 25 K and the melting temperature of MTX bound d-(TTGGGGT)$_4$ increases till D/N 4.0 and saturates after this D/N ratio. The method of continuous variation studies also confirms the stoichiometric ratio of 4.0, as multiple inflection points were observed due to the formation of more than one MTX-d-(TTGGGGT)$_4$ complexes. The steady state and time resolved fluorescence studies shows that environment of MTX changes upon binding to quadruplex structure which is evidenced from the decreased fluorescence emission till D/N 2.0 with red shift. Increase in DNA molar ratio results in enhancement of emission. The binding constant of K = 6.6 x 10^5 M^{-1} and n = 0.9 for D/N ratio in the range 2.1- 4.0 and K = 5.4 x 10^5 $M^{-1}$and n = 1.8 for lower D/N values of 0.79 - 2.1 were obtained.

The binding of MTX to d-(TTGGGT)$_4$ doesnot change the structure of tetramolecular quadruplex till D/N 4.0. Both the positive and negative CD bands of quadruplex are intact and show very less change in intensity. After the D/N ratio 4.0, both the bands show red shift with drastic change in intensity, which may be attributed to aggregation of MTX around DNA structure. The plot of changes in CD of positive and negative bands of quadruplex versus D/N ratios shows inflection at D/N 2.0. Weak positive ICD bands were obtained at 625, 648 and 671 nm.

The two SPR runs give affinity constant of K_A as 1.037 x 10^4 M^{-1} and 1.142 x 10^4 M^{-1}, with an average value of 1.086 x 10^4 M^{-1}. Both runs show MTX binds with two distinct binding affinities, one is stronger and other is weaker (10 times weak). The binding affinity constants obtained by SPR and UV-Vis were in agreement with the change in T_m value obtained by thermal melting studies. Thus the results reported in present study prove that mitoxantrone binds to quadruplex with high selectivity and stabilizes the structure.

Chapter 4

Studies on interaction of anticancer drug mitoxantrone with tetramolecular parallel telomeric sequence d-$(TTGGGGT)_4$ by Nuclear Magnetic Resonance spectroscopy and restrained Molecular Dynamics simulations

The knowledge of stabilization of G-quadrulpex structure by small molecule ligands which leads to inhibition of telomerase enzyme activity is used as an effective strategy to develop anticancer drugs. Solution state NMR studies have been used to study interaction of small molecule ligands with various forms of G-quadruplex structure. In the present chapter, we investigate the mode of interaction of an important topoisomerase inhibitor, mitoxantrone (MTX) with tetramolecular parallel telomeric DNA sequence d-$(TTGGGGT)_4$. To understand the interaction between mitoxantrone and d-$(TTGGGGT)_4$ various one and two dimensional Nuclear Magnetic Resonance (NMR) spectroscopic experiments were done. Interproton distances obtained from two dimensional NMR techniques were used as distance restraints to obtain final energy minimized structure of mitoxantrone-d-$(TTGGGGT)_4$ complex. The present chapter contains the following experiments and their interpretation in analyzing the mitoxantrone-d-$(TTGGGGT)_4$ complex by using both one- and two-dimensional ^{1}H, ^{13}C and ^{31}P NMR experiments and restrained molecular dynamics simulations.

- 1D ^{1}H NMR titration of mitoxantrone-d-$(TTGGGGT)_4$ complex at various drug (D)/DNA quadruplex (N) ratios of 0.1, 0.25, 0.5, 0.75, 1.0, 1.25, 1.5, 1.75, 2.0, 2.5, 3.0, 3.5 and 4.0 at 298 K in 90% water and 10% D_2O.
- 1D NMR study as a function of temperature in the range 278-318 at D/N ratios 0.25, 0.5, 0.75, 1.0, 1.25, 1.5, 1.75 and 278-358 K at D/N ratio 2.0.
- 1D ^{31}P NMR titration studies of mitoxantrone-d-$(TTGGGGT)_4$ complex at various D/N ratios of 0.1, 0.25, 0.5, 0.75, 1.0, 1.25, 1.5, 1.75 and 2.0 at 298 K in 90% water and 10% D_2O
- 2D NOESY of alone d-$(TTGGGGT)_4$ and mitoxantrone-d-$(TTGGGGT)_4$ complex at D/N = 1.0, 1.5, 2.0 and 4.0 using mixing time τ_m =100, 200, 250 ms at 298 K in 90% H_2O and 10% D_2O.

- 2D COSY of alone d-(TTGGGGT)$_4$ and mitoxantrone-d-(TTGGGGT)$_4$ complex at 298 K for D/N 2.0 and 298K, 318 K for D/N 1.0 and 2.0.
- ^{1}H-^{13}C HSQC of alone mitoxantrone, alone d-(TTGGGGT)$_4$ and mitoxantrone--d-(TTGGGGT)$_4$ complex at D/N 2.0 at 298 K.
- Restrained molecular dynamics studies on the solution structure for the complex of mitoxantrone-d-(TTGGGGT)$_4$ complex in drug to DNA quadruplex ratio of 4:1 using inter-proton distances obtained from 2D NOESY as restraints.

4.1 Results and discussion

4.1.1 NMR study of drug mitoxantrone.

Assignment of mitoxantrone protons were done by using one dimensional ^{1}H and two dimensional ^{1}H-^{13}C HSQC and ^{1}H-^{1}H ROESY techniques. Analysis of proton spectra (Fig. 4.1) of mitoxantrone dissolved in 100 mM KCl containing phosphate buffered 90% H_2O and 10 % D_2O at 298 K, shows the presence of two resonances in the aromatic region, one resonance in the exchangeable proton region, five resonances in the aliphatic region. Mitoxantrone is a C_2-symmetry molecule, hence the aromatic protons 2H and 3H are expected to give a single resonance, and the same behavior/pattern is expected for aromatic protons 6 H and 7 H. The four methylene protons appear as triplets in the region between 3.2-4.0 ppm. The downfield resonating aromatic proton (6/7 H) was assigned straight forwardly as this proton gives distance correlation with 11CH_2 and 12CH_2 protons of the amino alkyl side chain resonating at 3.53 and 3.24 ppm, respectively. The upfield resonating (6.71 ppm) aromatic proton doesnot show any NOE correlation with aminoalkyl side chain methylene protons, hence was assigned to 2/3 H aromatic proton. Most downfield appearing resonance was assigned to the 1/4 OH proton, which is most de-shielded due to the fact that it attached to aromatic group and forms hydrogen bonding with carbonyl carbon (C=O) at C10 position. The exchangeable protons, i.e 12 NH and 14 OH were not observed due to exchange with solvent water molecules. The protons belong to adjacent methylene was identified by COSY correlations between themselves. The chemical shift assignment of MTX protons were unambiguous and matches with previously reported chemical shifts in the literature (*Davies, et al. 2001, Lown and Hanstock 1985; Dogra et al. 2014*). ^{1}H-^{13}C HSQC at 298 shows six ^{1}H-^{13}C single bond correlations were observed in MTX molecule (Fig. 4.2). The aromatic 6/7 and 2/3 ^{13}C resonances resonates around ~ 128 ppm, while four methylene ^{13}C resonances appear between ~ 40-60 ppm.

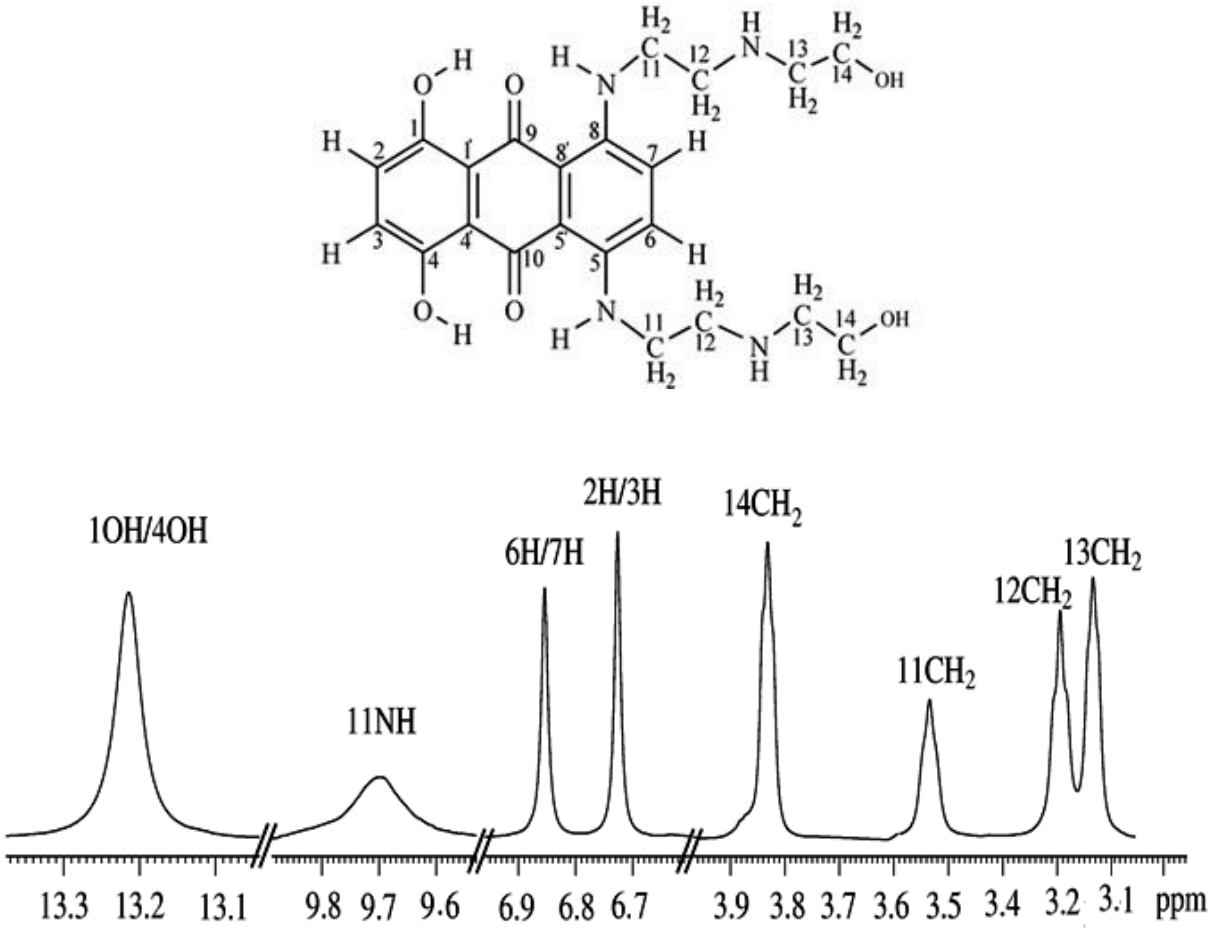

Figure 4.1: Molecular structure of mitoxantrone and ^{1}H spectrum of mitoxantrone in 100mM KCl containing phosphate buffered 90% H_2O and 10% D_2O at 298 K.

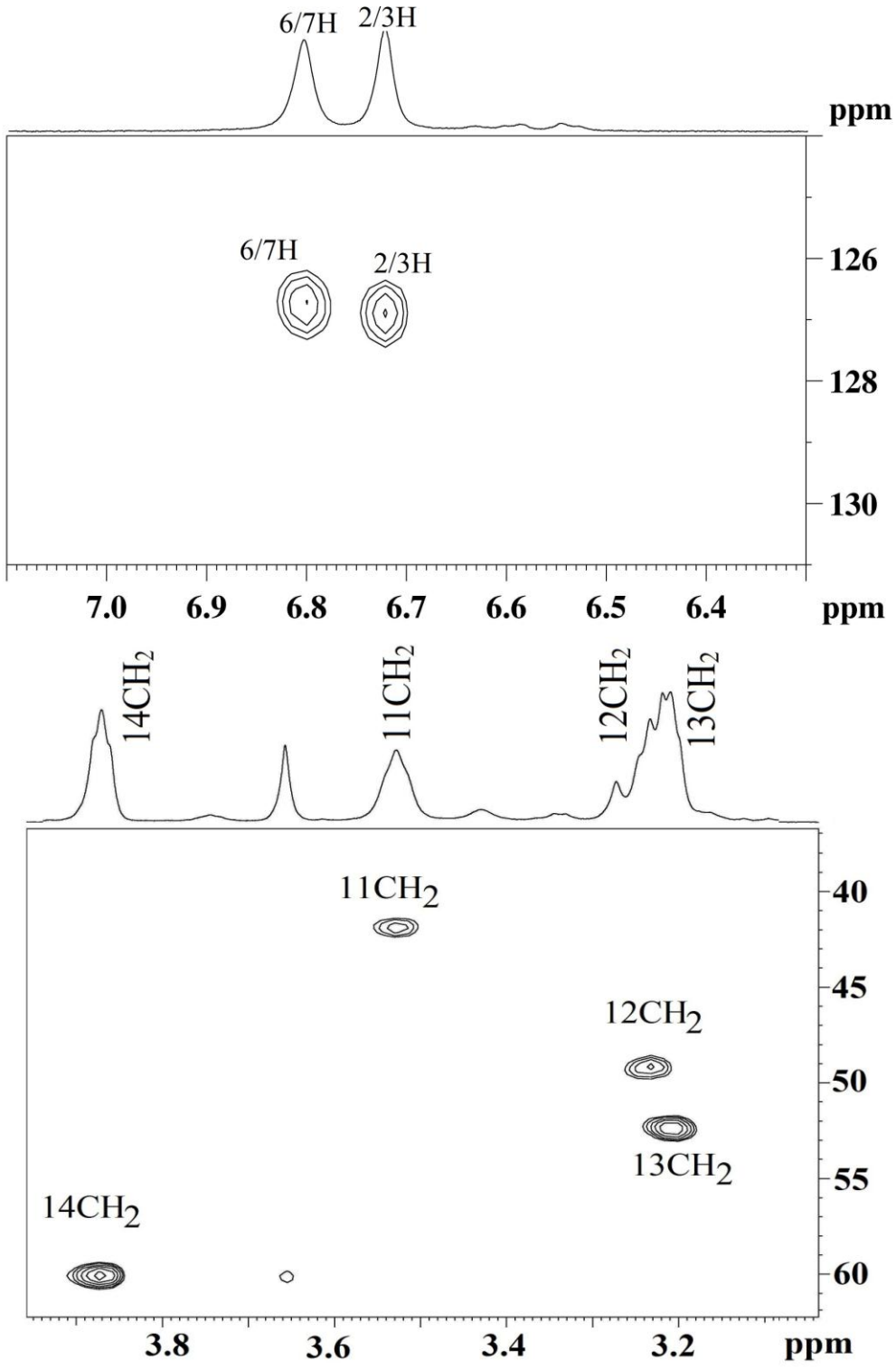

Figure 4.2: Expansion of ^{1}H-^{13}C HSQC spectrum of mitoxantrone in 90% H_2O and 10% D_2O at 298 K showing aromatic and amino-alkyl side chain correlations.

4.1.2 NMR studies of *Tetrahymena* telomeric DNA sequence d-(TTGGGGT)$_4$.

One dimensional 1H and two dimensional ^{1}H-^{1}H NOESY, ^{1}H-^{1}H COSY experiments were used to determine the structural conformation of d-(TTGGGGT)$_4$ DNA sequence. Proton NMR spectrum of d-(TTGGGGT)$_4$ at 100 mM KCl containing buffer in 10 % D_2O and 90 % H_2O at 298 K shows the four well resolved NH peaks resonating between 10.6 to 12 ppm region. This confirms the formation of single predominant stable structure by the TTGGGGT oligonucleotide sequence in present experimental conditions. These four NH resonances corresponds to the four guanines in the sequence d-(TTGGGGT)$_4$, that is G3:G4:G5:G6. The G3 imino proton resonates downfield of the spectrum followed by G4 and G5 imino resonances, whereas G6 imino proton resonates in the up-field region. This observation is consistent with the results of alone parallel tetramolecular structures formed by sequence d-(TTAGGGT)$_4$ and d-(TTGGGGT)$_4$ reported previously (*Gravathiotis et al. 2003; Wang and Patel, 1993*). The appearance of hydrogen bonded imino resonance in the region 10.6 to 12 ppm confirms the formation of Hoogsteen type hydrogen bonding between adjacent nucleotides. Hoogsteen type H-bonding, where gaunosine N-H protons hydrogen bond with nitrogen acceptors (N-H**O) results in the up-field shift of the imino resonances as compared to normal duplex Watson-Crick structures. Similar kind of upfield shift in the imino protons of guanine was also observed in the Wobble G-T pairs, in which guanine imino proton hydrogen bonds with the carbonyl group (*Patel et al. 1982*). Observance of only four NH resonances indicates the formation of tetramolecular quadruplex structure by the association of four identical strands of d-(TTGGGGT) and also confirms the C4 symmetry of the G-quartet structure formed (*Lu et al. 1992*). In C4 symmetric G-quartet structures, all the guanines are structurally equivalent, and present in an identical environment. The minor negligible resonances were also observed, which may be due to the presence of single stranded component, and is in slow equilibrium with the quadruplex structure.

The ^{1}H spectrum of d-(TTGGGGT)$_4$ recorded at 278 K exhibits the well resolved exchangeable imino and amino resonances. The imino proton resonances were sharp and are unaffected by increase in temperature, till 348 K. Analysis of Fig. 4.9 shows that two resonances which occupy

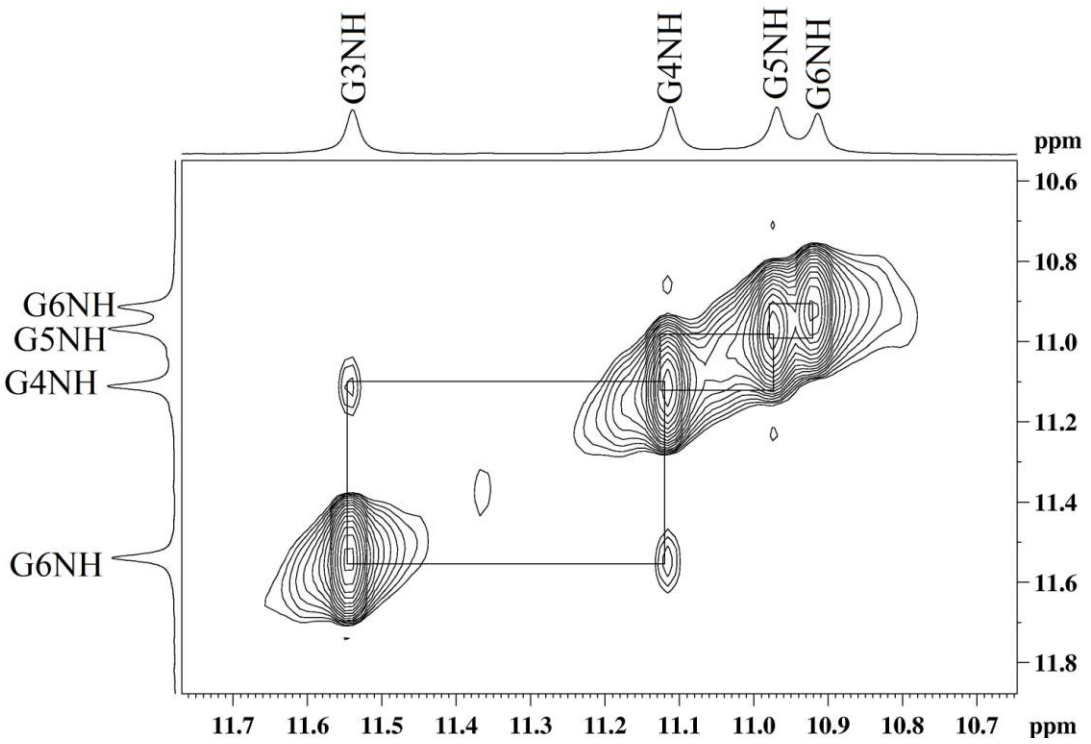

Fig 4.3 Expansion of 200 ms NOESY spectrum of d-(TTGGGGT)4 showing imino-imino correlations between successive G-quartets.

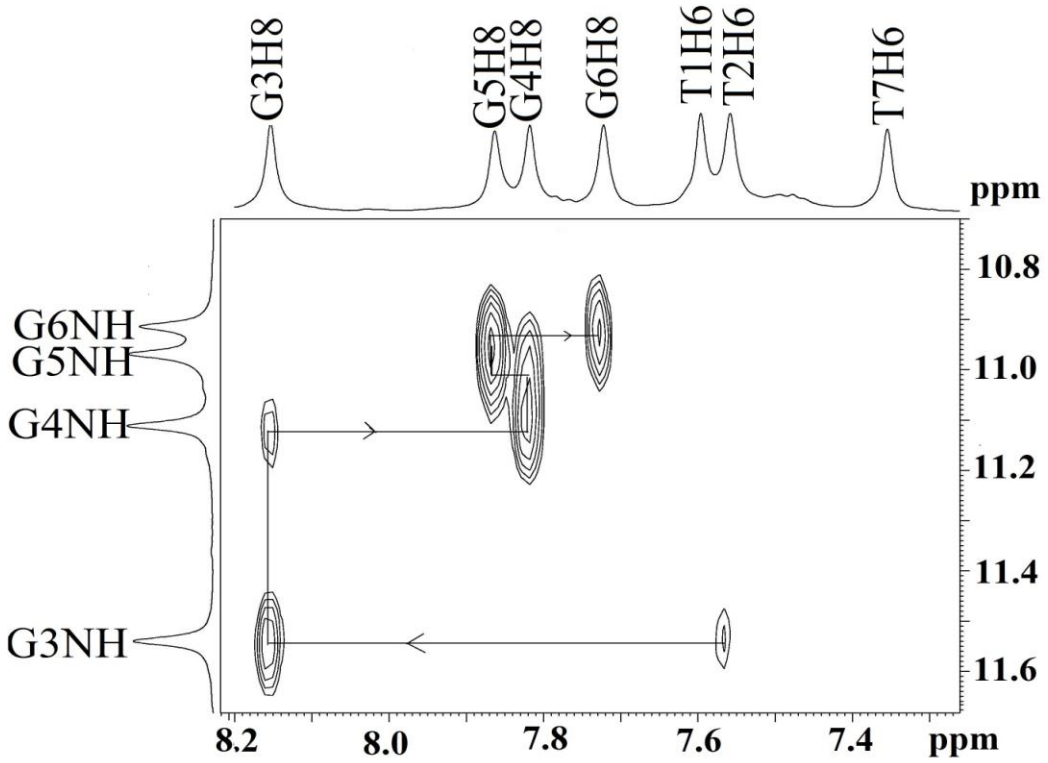

Figure 4.4: Expansion of 200 ms NOESY spectrum of d-(TTGGGGT)$_4$ at 298 K showing connectivities between aromatic H6/H8 with imino proton within a G-quartet plane and its 3'-flanking G-quartet imino proton.

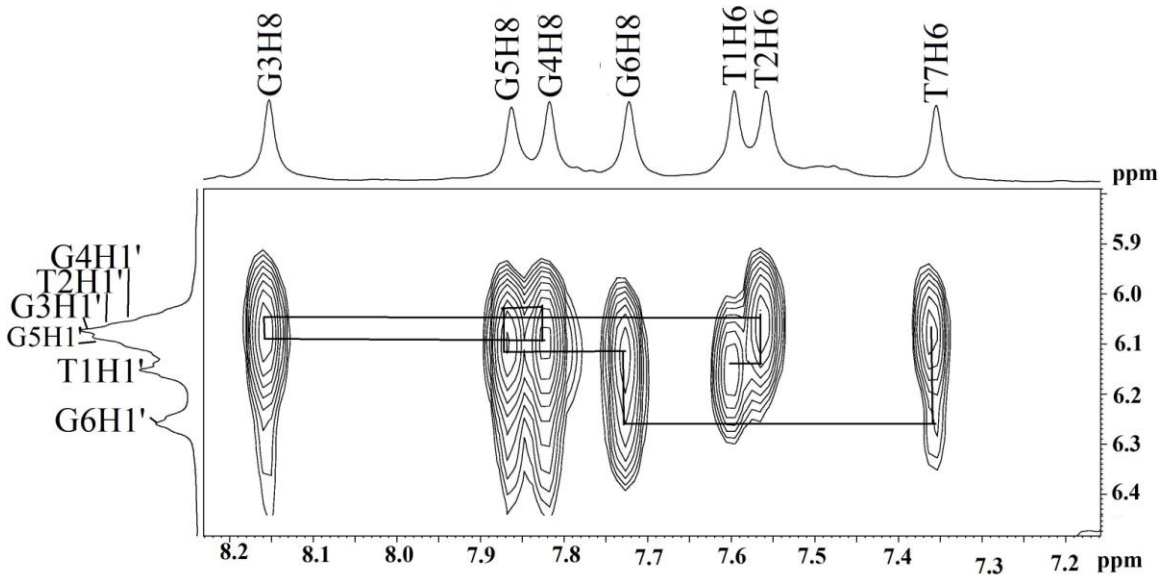

Figure 4.5: Expansion of 200 ms NOESY spectrum of d-(TTGGGGT)$_4$ at 298 K showing sequential connectivities between aromatic H6/H8 with sugar H1' protons.

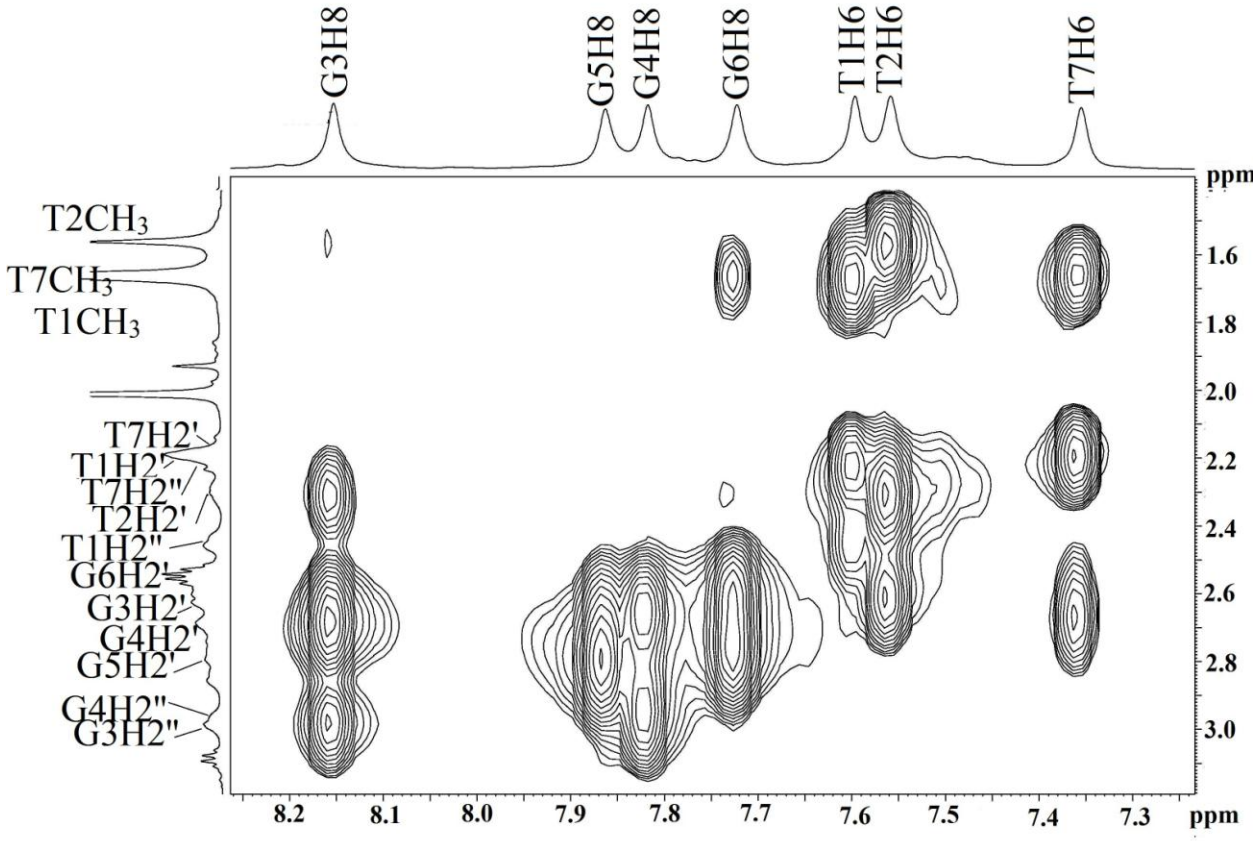

Figure 4.6: Expansion of 200 ms NOESY spectrum of d-(TTGGGGT)$_4$ at 298 K showing sequential connectivities between aromatic H6/H8 with sugar H2'/H2'' protons.

most up field and most downfield region among imino protons start to disappear upon increase in temperature. This may be attributed to the breakdown of G-quartet structure which results in the exchange of Hoogsteen H-bonded imino protons to exchange with solvent water molecules. Hence these two resonances were assigned as terminal guanines, either G6 or G3. The central G-quartet core is unperturbed at this temperature and hence shows stable imino signals at this temperature range. Appearance of sharp resonances for centrally located G4 and G5 imino protons clearly indicates that these protons are shielded from exchange with surrounding water molecules in NMR time scale.

Alignment of G-tetrad in a planar ring can be explained by monitoring NOEs between guanine imino protons with H8 proton of adjacent guanine (distance of ~ 4.2 Å). Due to the extensive stacking and alignment of four strands nearby to each other, guanine imino proton shows NOE with its own aromatic H8 proton and its 5' flanking base H8 proton. Hence T2H6 gives NOE correlation with G3NH, G3NH gives cross peak with G3H8, then G3NH gives correlation with G4NH and so on (Fig. 4.4). Due to the extensive stacking between G-quartet planes, protons which belongs to adjacent quartets show NOE connectivities between themselves (Fig. 4.3) The expanded NOESY plot (Fig. 4.5 and 4.6) of mixing time 200 ms at 298 K shows the correlation between aromatic base protons and sugar H1' protons. The presence of sequential connectivities between base H6/H8 to sugar H1'/H2'/H2" protons shows the right handed helical nature of quadruplex. Intensities of this sequential walk connectivities shows that all the bases are in anti conformation. The absence of NOE correlation between G6NH with G3H8 proton shows that d-(TTGGGGT) four strands are oriented parallel to each other.

The T1, T2 and T6 CH_3 resonances can be identified by observing NOE correlation between TCH_3 of n base with its own aromatic H6 proton and also with H8/H6 proton of n-1 base. Hence $T2CH_3$ gives correlation peak with its own H6 and T1H6 proton. Similarly, $T7CH_3$ gives NOE correlation with its own H6 and (n-1) G6H8 proton (Fig. 4.6).

The quadruplex structure is formed by parallel alignment of four d-(TTGGGGT) strands. The anti-parallel arrangement of strands can be ruled out as anti-parallel arrangement of any one or more d-(TTGGGGT) stands results in the appearance of NOEs between H8 and NH_2 protons of G3 and G6 residues (*Wang and Patel, 1992*).

4.1.3 Proton NMR studies on complex of mitoxantrone-d-$(TTGGGGT)_4$

Interaction of anticancer drug, mitoxantrone with *Tetrahymena* telomere sequence d-$(TTGGGGT)_4$ was studied by adding increasing concentration of MTX to parallel quadruplex solution to reach the desired D/N rations of 0.25, 0.5, 0.75, 1.0, 1.5, 2.0, 2.5, 3.0, 3.5 and 4.0. The resonance assignments of mitoxantrone-d-$(TTGGGGT)_4$ complex was done using the combination of one and two-dimensional NMR experiments like ^1H-^1H NOESY, ^1H-^1H COSY, ^1H-^1H TOCSY and ^1H-^{13}C HSQC.

Fig 4.7 (a-d) shows stacked expanded proton region of mitoxantrone-d-$(TTGGGGT)_4$ complex at various D/N ratios at 298K. On successive addition of mitoxantrone to d-$(TTGGGGT)_4$, new proton signals corresponding to the mitoxantrone protons starts to appear, which increase in intensity with increasing D/N ratios. With each successive addition of mitoxantrone, d-$(TTGGGGT)_4$ protons shows gradual shift in the position when compared to uncomplexed d-$(TTGGGGT)_4$ resonances (Table 4.1 and 4.2). The appearance of only four imino resonances in the Hoogsteen hydrogen bonded region clearly shows that C4 symmetry of quadruplex is not broken due to interaction with mitoxantrone. Absence of any extra bound and unbound resonances belonging to d-$(TTGGGGT)_4$ indicates binding is fast in NMR time scale. All four Hoogsteen hydrogen bonded imino resonances belonging to four steps of G-quartets, i.e G3NH, G4NH, G5NH and G6NH show progressive upfield shift upon complexation. G6NH shows maximum upfield shift of $\Delta\delta$ 0.26 ppm, followed by G3NH which shifts upfield by $\Delta\delta$ 0.17 ppm. G5NH and G4NH shift upfield by $\Delta\delta$ 0.16 and 0.15 ppm, respectively. Aromatic resonances of all bases show upfield shift except the T7H6, which shifts downfield by $\Delta\delta$ 0.13 ppm. Among methyl resonances, T7CH_3 resonance show downfield shift of $\Delta\delta$ 0.08 ppm, while other two CH_3 resonances belonging to T1 and T2 shifts upfield by $\Delta\delta$ 0.05 and 0.04 ppm, respectively.

Upon titration of MTX to d-$(TTGGGGT)_4$, G6NH and T7H6 resonances broaden out gradually and completely broadens at D/N 1.0, but further increase in MTX concentration to reach D/N 2.0 results in gradual sharpening of these two resonances. This indicates that G6pT7 step acts a binding site at this D/N ratio, as the concentration of ligand is low till D/N 1.0, this site is the high affinity binding site for MTX molecule. The magnitude of chemical shift variation is also more in T7H6 and G6NH protons, when compared to all other protons of d-$(TTGGGGT)_4$ till D/N 1.0.

Titration of MTX into d-(TTGGGGT)$_4$, results in appearance of new signals pertaining to MTX protons, which increase in intensity with increasing D/N ratios (Fig. 4.7 a-c). As the MTX is titrated into the quadruplex solution, at lower D/N ratio of 0.25 maximum amount of MTX is bound to DNA and hence correlates to the maximum upfield shift observed for MTX protons at this D/N ratio. The imino proton 11NH of MTX resonates in the amino bonded region of d-(TTGGGGT)$_4$ quadruplex DNA, but at 298 K these resonances broaden out due to exchange with solvent, this helps in easy identification of 11NH proton, which resonates at 9.70 ppm. The aromatic 6/7H signal of MTX resonates in the region upfield to quadruplex base H6/H8 resonances and downfield to sugar anomeric H1' resonances, but overlap with G6NH$_2^{nb}$ signal of quadruplex DNA. At temperatures above 298K, G6NH$_2^{nb}$ resonance broadens out due to exchange with solvent water, leaving behind sharp 6/7H signal of MTX at 6.80 ppm. The other aromatic resonance 2/3H overlaps with signals of sugar H1' region, which was identified by the use of two dimensional HSQC technique. Moreover at D/N ratio 2.0, this resonance shifts downfield at higher temperatures (> 328 K), which aids in identity of this signal, which resonates at 6.30 ppm.

The methylene protons of amino alkyl side chains show little upfield shift (Table 4.2). These protons resonate ~ 3.8–3.1 ppm, and this region of spectrum is devoid of any signals arising due to d-(TTGGGGT)$_4$ protons, except for T1H5'/H5" which overlaps with 14CH$_2$ proton. Hence methylene protons were easily identified form their increase in intensity upon titration. The 11CH$_2$ proton is considerably broader than other three CH$_2$ protons.

The observed change in chemical shift of uncomplexed and 4:1 d-(TTGGGGT)$_4$ complexed MTX protons at different D/N ratios were given in Table 4.2. At D/N ratio of 0.25, maximum numbers of MTX molecules were in bound state, which is reflected in the maximum upfield shift of MTX protons at this molar ratio. Increase in MTX concentration to reach higher D/N ratios till 4.0 results in the downfield shift of MTX protons. This may be attributed to the increase in concentration of unbound MTX molecules in the solution.

Throughout the titration experiments, a single set of d-(TTGGGGT)$_4$ and MTX protons were observed, which indicates that binding of MTX to d-(TTGGGGT)$_4$ is a fast process in NMR time scale.

Table 4.1: Chemical shift (ppm) of d-(TTGGGGT)$_4$ protons in uncomplexed state (δ^f) and that bound to drug (δ^b) at drug (D) to nucleic acid duplex (N) ratio D/N = 4.0 at 298 K. $\Delta\delta = \delta^b_{(D/N=2.0)} - \delta^f$. -ve $\Delta\delta$, +ve $\Delta\delta$ indicates upfield and downfield shift, respectively.

	T1			T2			G3			G4			G5		
	δ_b	δ_f	$\Delta\delta$	δ_b	δ_f	$\Delta\delta$	δ_b	δ_f	$\Delta\delta$	δ_b	δ_f	$\Delta\delta$	δ_b	δ_f	$\Delta\delta$
H8/H6	7.55	7.57	-0.02	7.53	7.54	-0.01	8.07	8.13	-0.06	7.72	7.80	-0.08	7.75	7.84	-0.09
H1'	6.17	6.13	0.04	6.00	6.05	-0.05	6.06	6.08	-0.02	6.04	6.06	-0.02	6.08	6.10	-0.02
H2'	2.21	2.21	0.0	2.28	2.30	-0.02	2.62	2.68	-0.06	2.63	2.62	0.01		2.74	
H2"	2.41	2.46	-0.05	2.58	2.62	-0.04	2.92	2.97	-0.05	2.89	2.94	-0.05			
H3'	4.72	4.74	-0.02	4.89	4.86	0.03	5.04	5.06	-0.02	5.00	5.05	-0.05	5.07	5.11	-0.04
H4'	4.30	4.32	-0.02	4.22	4.27	-0.05	4.41	4.43	-0.02		4.43		4.60	4.61	-0.01
H5'	3.74	3.79	-0.05	4.09	4.14	-0.05	4.20	4.25	-0.05	4.35	4.34	0.01	4.33	4.39	-0.06
H5"	3.71	3.75	-0.04	4.03	4.06	-0.03	4.10	4.09	0.01	4.26	4.24	0.02	4.26	4.33	-0.06
CH_3	1.59	1.65	-0.05	1.56	1.54	-0.04	-	-	-	-	-	-	-	-	-
$NH_2{}^b$	-	-	-	-	-	-	9.69	9.84	-0.15	9.12	9.25	-0.13	9.05	9.17	-0.12
$NH_2{}^{nb}$	-	-	-	-	-	-	6.18	6.24	-0.06	6.05	6.17	-0.12	6.06	6.23	-0.17
NH							11.36	11.51	-0.15	10.96	11.09	-0.13	10.81	10.95	-0.14

	G6			T7		
	δ_b	δ_f	$\Delta\delta$	δ_b	δ_f	$\Delta\delta$
H8/H6	7.70	7.70	0.0	7.48	7.33	0.15
H1'	6.22	6.24	-0.02	6.05	6.07	-0.02
H2'	2.54	2.53	0.01	2.19	2.14	0.05
H2"	2.77	2.76	0.01	2.26	2.23	0.03
H3'	5.03	4.97	0.06	4.52	4.51	0.01
H4'	4.56	4.56	0.0		4.46	
H5'	4.30	4.31	-0.01	4.26	4.24	0.02
H5"		4.23		4.07	4.05	0.02
CH_3	-	-		1.73	1.63	0.10
$NH_2{}^b$	7.45	7.45	0.0			
$NH_2{}^{nb}$	6.35	6.74	-0.			
NH	10.65	10.89	-0.24			

Table 4.2: Chemical shift (ppm) of d-(TTGGGGT)$_4$ protons in uncomplexed state (δ^f) and that bound to drug (δ^b) at drug (D) to nucleic acid duplex (N) ratio D/N = 2.0 at 298 K. $\Delta\delta = \delta^b_{(D/N=4.0)} - \delta^f$. -ve $\Delta\delta$, +ve $\Delta\delta$ indicates upfield and downfield shift, respectively.

	T1			T2			G3			G4			G5		
	δ_b	δ_f	$\Delta\delta$	δ_b	δ_f	$\Delta\delta$	δ_b	δ_f	$\Delta\delta$	δ_b	δ_f	$\Delta\delta$	δ_b	δ_f	$\Delta\delta$
H8/H6	7.55	7.57	-0.02	7.53	7.54	-0.01	8.03	8.13	-0.10	7.69	7.80	-0.11	7.71	7.84	-0.13
H1'	6.17	6.13	0.04	6.01	6.05	-0.04	6.06	6.08	-0.02	6.04	6.06	-0.02	6.08	6.10	-0.02
H2'	2.20	2.21	-0.01	2.28	2.30	-0.02	2.60	2.68	-0.08	2.58	2.62	-0.04		2.74	
H2"	2.39	2.46	-0.06	2.56	2.62	-0.04	2.90	2.97	-0.07	2.89	2.94	-0.06			
H3'	4.72	4.74	-0.02	4.89	4.86	0.03	5.00	5.06	-0.06	5.03	5.05	-0.02	5.05	5.11	-0.06
H4'	4.30	4.32	-0.02	4.22	4.27	-0.05	4.41	4.43	-0.02		4.43		4.60	4.61	-0.01
H5'	3.74	3.79	-0.05	4.09	4.14	-0.05	4.20	4.25	-0.05	4.35	4.34	0.01	4.33	4.39	-0.06
H5"	3.71	3.75	-0.04	4.03	4.06	-0.03	4.10	4.09	0.01	4.26	4.24	0.02	4.26	4.33	-0.06
CH_3	1.59	1.65	-0.05	1.56	1.54	-0.04	-	-	-	-	-	-	-	-	-
$NH_2{}^b$	-	-	-	-	-	-	9.51	9.84	-0.33	9.02	9.25	-0.13	9.00	9.17	-0.17
$NH_2{}^{nb}$	-	-	-	-	-	-	6.08	6.24	-0.16	6.06	6.17	-0.11	5.98	6.23	-0.25
NH							11.32	11.51	-0.17	10.94	11.09	-0.15	10.79	10.95	-0.16

	G6			T7		
	δ_b	δ_f	$\Delta\delta$	δ_b	δ_f	$\Delta\delta$
H8/H6	7.69	7.70	-0.01	7.46	7.33	0.13
H1'	6.20	6.24	-0.04	6.05	6.07	-0.02
H2'	2.55	2.53	0.01	2.07	2.14	-0.07
H2"	2.77	2.76	0.01	2.29	2.23	0.06
H3'	5.06	4.97	0.09	4.52	4.51	0.01
H4'	4.56	4.56	0.0		4.46	
H5'	4.30	4.31	-0.01	4.26	4.24	0.02
H5"		4.23		4.07	4.05	0.02
CH_3	-	-		1.71	1.63	0.08
$NH_2{}^b$	7.49	7.45	0.05			
$NH_2{}^{nb}$	6.76	6.74	0.02			
NH	10.63	10.89	-0.26			

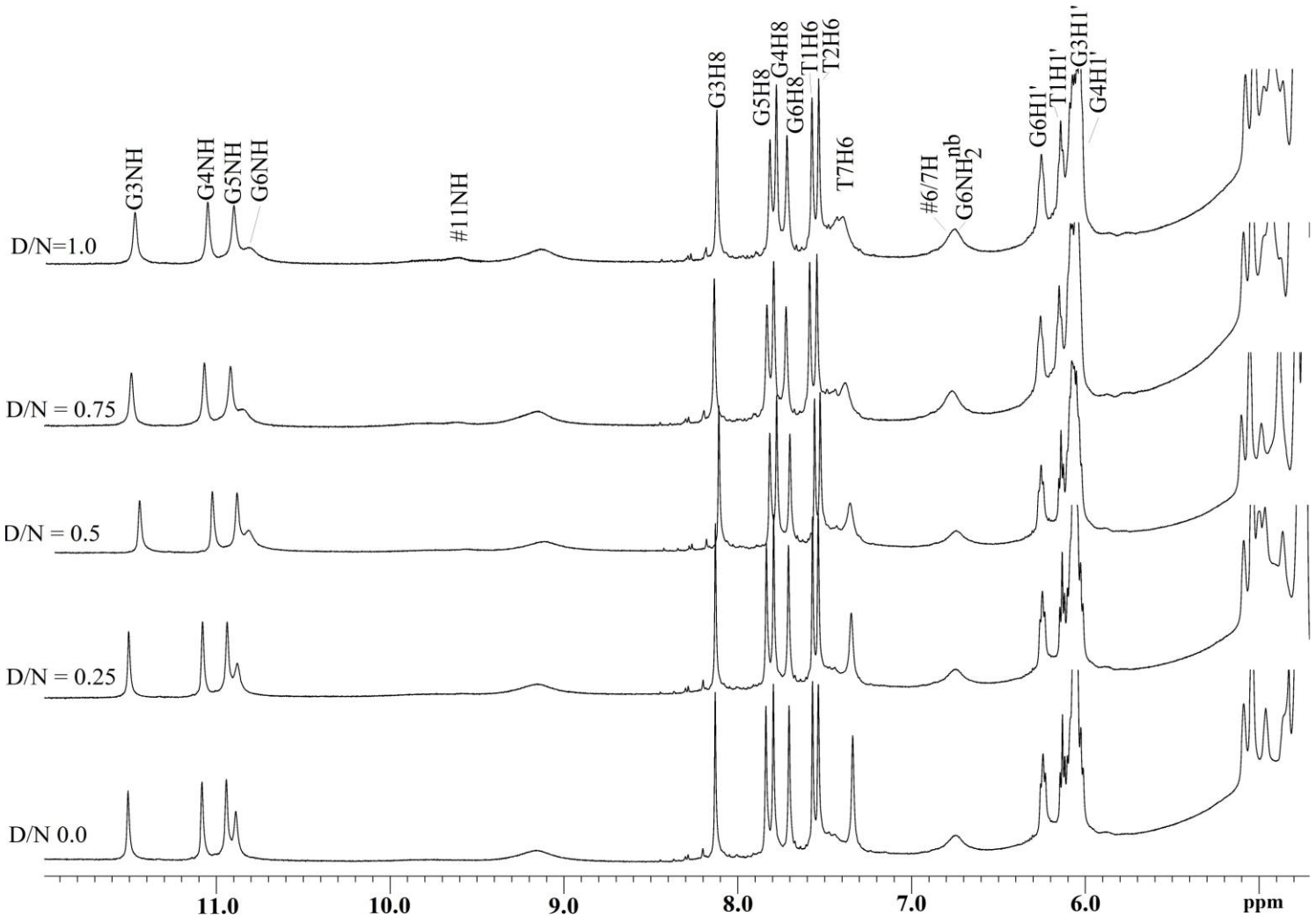

Figure 4.7: (a) Expansion of ^{1}H spectra of uncomplexed d-(TTGGGGT)$_4$ and MTX complexed d-(TTGGGGT)4 at D/N ratios 0.25, 0.5, 0.75 and 1.0 at 298 K.

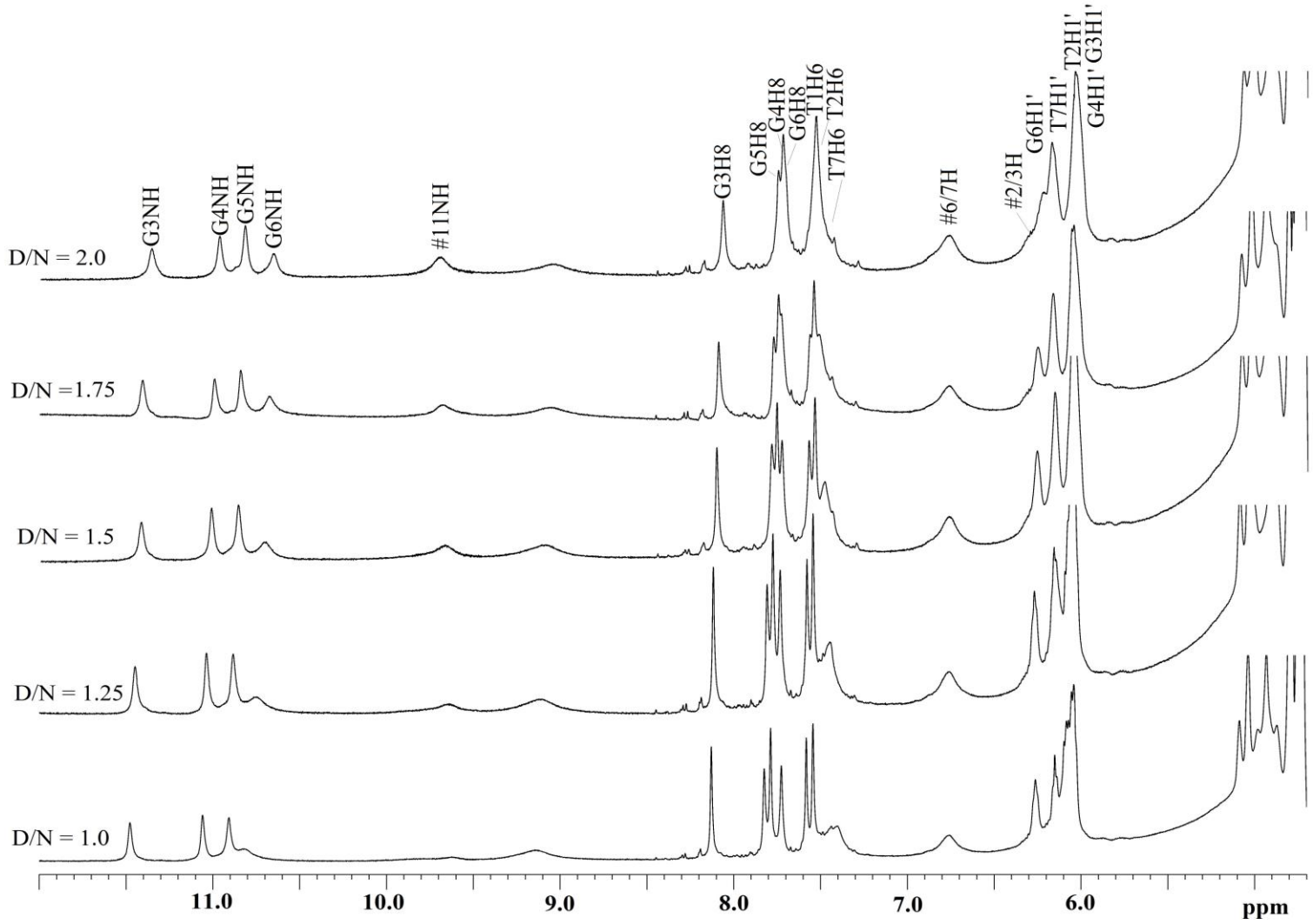

Figure 4.7: (b) Expansion of ^{1}H spectrum of MTX complexed d-(TTGGGGT)$_4$ at D/N ratios 1.0, 1.25, 1.5, 1.75 and 2.0 at 298 K

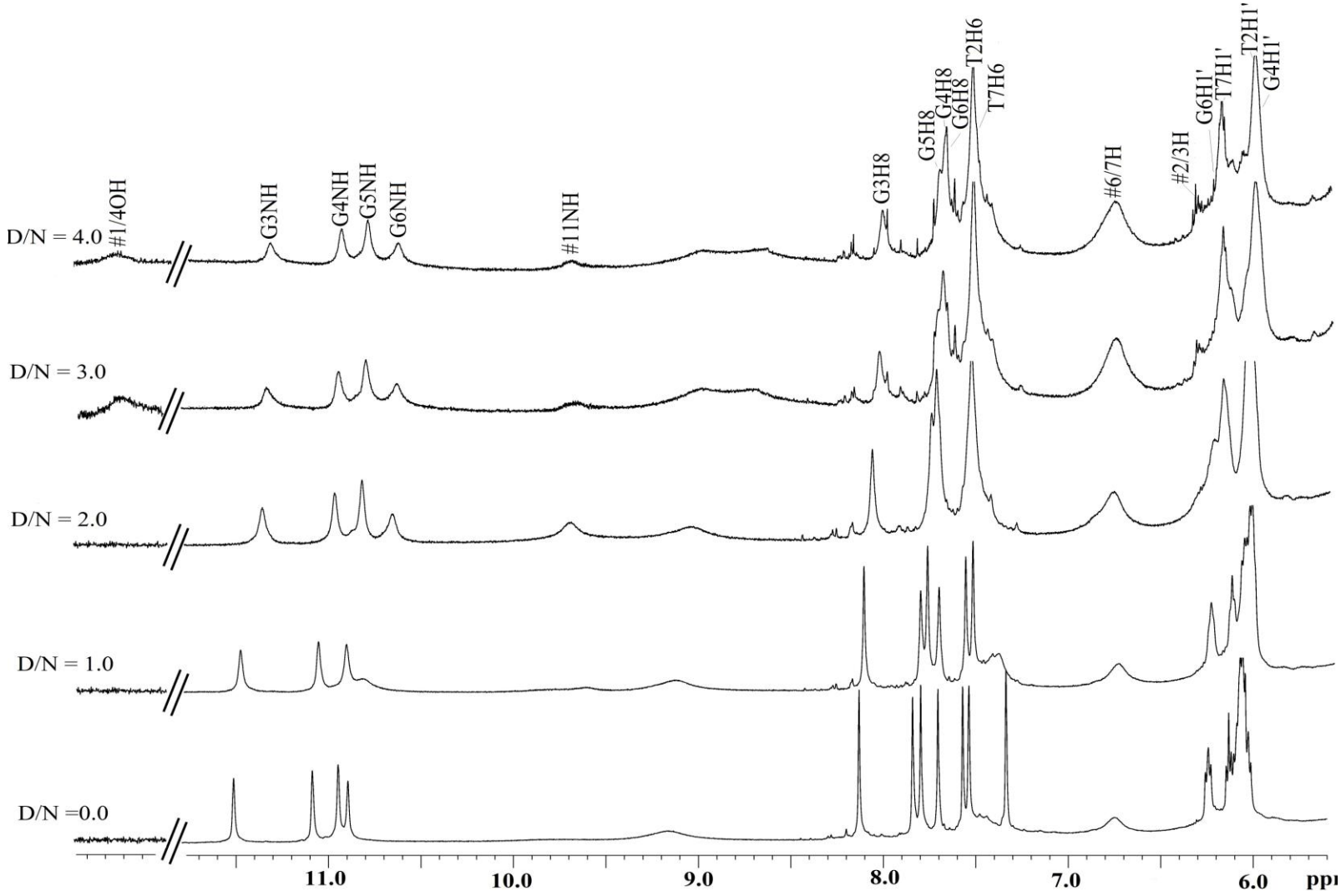

Figure 4.7: (c) Expansion of ^{1}H spectrum of uncomplexed d-(TTGGGGT)$_4$ and MTX complexed d-(TTGGGGT)4 at D/N ratios 1.0, 2.0, 3.0 and 4.0.

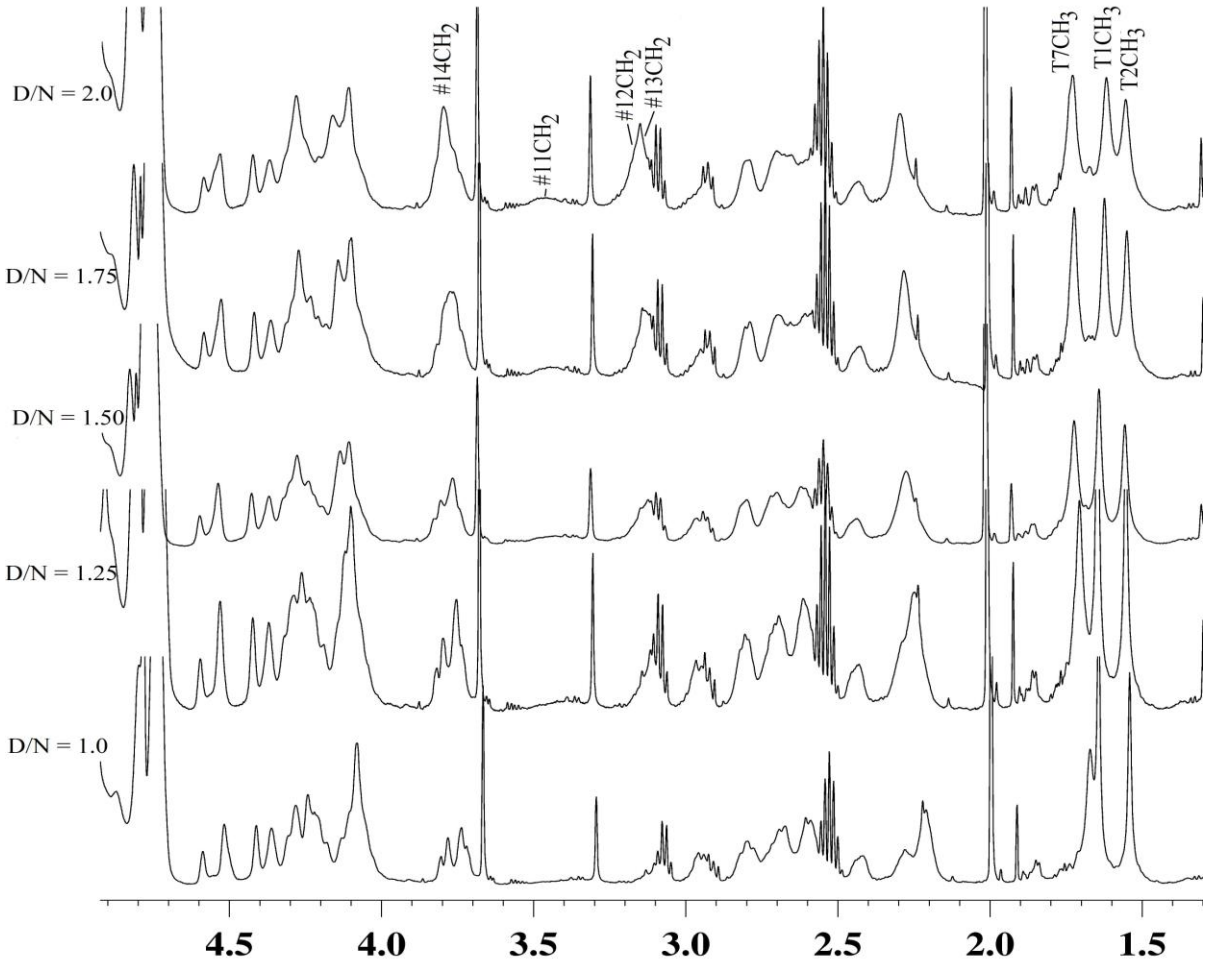

Figure 4.7: (d) Expansion of ^{1}H spectrum of MTX complexed d-(TTGGGGT)$_4$ at D/N ratios 1.0, 1.25, 1.5, 1.75 and 2.0 at 298 K showing alkyl amine side chain protons of MTX.

Table 4.2: Chemical shift (ppm) of MTX protons in uncomplexed (δ^f) and that bound (δ^b) to d-(TTGGGGT)$_4$ at drug (D) to Nucleic acid (N) ratio, D/N =4.0 at 298 K. $\Delta\delta = \delta^b_{(D/N=4)} - \delta^f_{(D/N=0.0)}$. --ve $\Delta\delta$, +ve $\Delta\delta$ indicates upfield and downfield shift, respectively.

Mitoxantrone Protons	δ^b	δ^f	$\Delta\delta = \delta^b - \delta^f$
11 NH	9.70	9.68	0.02
6/7 H	6.82	6.82	0.00
2/3 H	6.30	6.71	-0.41
11 CH_2	3.45	3.53	-0.08
12 CH_2	3.16	3.24	-0.08
13 CH_2	3.13	3.21	-0.07
14 CH_2	3.78	3.88	-0.10
1/4OH	12.77	13.23	-0.46

Table 4.4: Chemical shift (ppm) of nucleotide protons as a function of drug (D) to nucleic acid quadruplex (N) ratio, D/N, at 298 K. $\Delta\delta = \delta(D/N=4.0) - \delta(D/N=0.0)$. -ve $\Delta\delta$, +ve $\Delta\delta$ indicates upfield and downfield shift, respectively.

D/N	T1H1'	T2H1'	G3H1'	G4H1'	G5H1'	G6H1'	T7H1'	$T1CH_3$	$T2CH_3$	$T7CH_3$
0.0	6.13	6.05	6.08	6.06	6.10	6.24	6.07	1.65	1.54	1.63
0.25	6.13	6.03	6.07	6.06	6.10	6.24	6.07	1.65	1.54	1.64
0.5	6.14	6.03	6.065	6.06	6.10	6.25	6.07	1.65	1.54	1.65
0.75	6.15	6.03	6.065	6.06	6.10	6.26	6.06	1.65	1.54	1.66
1.0	6.15	6.02	6.06	6.05	6.10	6.26	6.06	1.64	1.54	1.67
1.25	6.15	6.02	6.06	6.05	6.09	6.27	6.06	1.63	1.535	1.69
1.5	6.16	6.02	6.06	6.05	6.09	6.26	6.05	1.62	1.535	1.70
1.75	6.16	6.01	6.06	6.04	6.09	6.25	6.05	1.61	1.53	1.71
2.0	6.17	6.00	6.06	6.04	6.08	6.22	6.05	1.60	1.53	1.71
2.5	6.17	6.00	6.06	6.04	6.08	6.21	6.05	1.60	1.55	1.73
3.0	6.17	6.01	6.06	6.04	6.08	6.21	6.05	1.59	1.56	1.73
3.5	6.17	6.01	6.06	6.04	6.08	6.20	6.05	1.59	1.56	1.73
4.0	6.17	6.01	6.06	6.04	6.08	6.20	6.05	1.59	1.56	1.73
$\Delta\delta$	0.04	-0.04	-0.02	-0.02	-0.02	-0.04	-0.02	-0.06	0.02	0.10

D/N ratios	T1H6	T2H6	G3H8	G4H8	G5H8	G6H8	T7H6	G3NH	G4NH	G5NH	G6NH
0.0	7.57	7.54	8.13	7.80	7.84	7.70	7.33	11.51	11.09	10.95	10.89
0.25	7.535	7.57	8.13	7.795	7.835	7.71	7.34	11.50	11.08	10.94	10.88
0.5	7.535	7.57	8.125	7.79	7.83	7.71	7.36	11.495	11.07	10.93	10.86
0.75	7.545	7.59	8.14	7.795	7.83	7.72	7.38	11.49	11.07	10.92	10.85
1.0	7.545	7.58	8.13	7.79	7.83	7.73	7.41	11.48	11.06	10.91	10.84
1.25	7.54	7.57	8.12	7.77	7.81	7.73	7.44	11.45	11.04	10.88	10.76
1.5	7.54	7.56	8.10	7.76	7.79	7.72	7.46	11.42	11.02	10.86	10.71
1.75	7.55	7.55	8.08	7.74	7.77	7.71	7.48	11.39	10.99	10.84	10.67
2.0	7.55	7.53	8.07	7.72	7.75	7.70	7.48	11.36	10.96	10.81	10.65
2.5	7.55	7.53	8.05	7.71	7.74	7.69	7.46	11.35	10.96	10.81	10.65
3.0	7.55	7.53	8.04	7.70	7.73	7.69	7.46	11.34	10.95	10.80	10.65
3.5	7.55	7.53	8.03	7.69	7.73	7.69	7.46	11.33	10.94	10.80	10.64
4.0	7.55	7.53	8.03	7.69	7.71	7.69	7.46	11.32	10.94	10.79	10.63
$\Delta\delta$	-0.02	-0.01	-0.10	-0.01	-0.13	-0.01	0.13	-0.17	-0.15	-0.16	-0.26

Table 4.5: Chemical shift (ppm) of mitoxantrone protons as a function of drug (D) to nucleic acid quadruplex (N) ratio, D/N, at 298 K. Also shown here is the change in chemical shift on binding, that is, $\Delta\delta1 = \delta_{(D/\ N=4.0)} - \delta_{(D/\ N=\ 0.0)}$. $\Delta\delta2 = \delta_{(D/\ N=0.25)} - \delta_{(D/\ N=\ 0.0)}$. $\Delta\delta3 = \delta_{(D/\ N=2.0)} - \delta_{(D/\ N=\ 0.0)}$. -ve $\Delta\delta$ indicates upfield shift, +ve $\Delta\delta$ indicates downfield shift.

D/N ratios	11NH	6/7H	2/3H	$11CH_2$	$12CH_2$	$13CH_2$	$14CH_2$	1/4OH
0.0	9.68	6.82	6.71	3.53	3.24	3.21	3.88	13.23
0.25	9.59	6.75	-	3.42	3.13	3.09	3.72	-
0.5	9.61	6.755	-	3.42	3.13	3.09	3.72	-
0.75	9.62	6.77	-	3.43	3.13	3.09	3.73	-
1.0	9.625	6.78	6.34	3.43	3.14	3.10	3.74	-
1.25	9.64	6.79	6.33	3.44	3.14	3.10	3.745	-
1.5	9.67	6.80	6.32	3.44	3.14	3.10	3.75	-
1.75	9.68	6.83	6.31	3.43	3.14	3.10	3.76	-
2.0	9.70	6.82	6.30	3.42	3.14	3.10	3.77	-
2.5	9.70	6.82	6.32	3.45	3.15	3.11	3.77	12.74
3.0	9.69	6.82	6.32	3.45	3.15	3.12	3.77	12.75
3.5	9.70	6.82	6.31	3.45	3.15	3.12	3.77	12.76
4.0	9.70	6.81	6.30	3.45	3.16	3.13	3.78	12.77
$\Delta\delta1$	**0.02**	**-0.01**	**-0.41**	**-0.08**	**-0.08**	**-0.08**	**-0.10**	**-0.46**
$\Delta\delta2$	**-0.09**	**-0.07**	**-**	**-0.11**	**-0.11**	**-0.14**	**-0.16**	**-**
$\Delta\delta3$	**0.02**	**0.00**	**-0.41**	**-0.11**	**-0.10**	**-0.11**	**-0.11**	**-**

4.1.4 Effect of temperature

Effect of temperature on mitoxantrone-d-$(TTGGGGT)_4$ complex were studied at temperature range of 278 K to 358 K at D/N 2.0. Fig 4.8 shows the effect of temperature on imino and aromatic protons of the mitoxantrone-d-$(TTGGGGT)_4$ complex. Table 4.5 shows the variation of chemical shifts at varying temperatures of both bound mitoxantrone and d-$(TTGGGGT)_4$. Increase in temperature from 278 K to 358 K results in the sharpening of the resonances of both mitoxantrone and d-$(TTGGGGT)_4$ protons. The imino and aromatic base protons shift progressively with increase in temperature. All four G-quartet imino protons i.e G3:G4:G5:G6NH which are upfield shifted upon complex formation, shifts more up-field with increase in temperature, this shows that rate of dissociation of MTX-d-$(TTGGGGT)_4$ complex is less even at higher temperatures. All the aromatic base protons (H6/H8) show progressive upfield shift upon increase in temperature from 278 to 358 K. The magnitude of upfield shift is more in T7H6, G3H8 and G6H8 protons when compared to T1H6, G4H8 and G5H8 protons.

Increase in temperature from 278 to 348 K results in downfield shift of 11NH and 2/3H MTX protons, while 6/7H, $11CH_2$ and $14CH_2$ peaks shift upfield. At temperatures below 298 K the aromatic 2/3H proton of MTX which resonates in the sugar H1' region of d-$(TTGGGGT)_4$ was difficult to identify in one dimensional ^1H spectrum, but at temperatures higher than 298 K this proton shifts downfield and appear as a separate resonance.

Temperature studies were used to study the thermal stabilization of d-$(TTGGGGT)_4$ structure upon complexation with MTX. Appearance of guanine imino protons in the Hoogsteen base pairing region is the characteristic of formation of quadruplex structure, and hence their disappearance at higher temperatures can be used to monitor the melting temperature (T_m) of these structures in the presence and absence of ligands. The ligands which stabilize the quadruplex structure upon binding will result in the increase in melting temperature of quadruplex structure when compared to its uncomplexed counterpart. Fig.4.9 shows the melting profile of imino protons of alone d-$(TTGGGGT)_4$ and its complex with MTX at molar equivalents of 2.0. The G3 and G6NH resonances start to disappear gradually with increasing temperature and completely vanishes at 328 K. But upon complexation these two imino resonances persists till 358 K. This shows the thermal stabilization of d-$(TTGGGGT)_4$ structure by about ~ 25 K. Hence this result clearly shows that MTX is interacting with d-$(TTGGGGT)_4$ quadruplex structure and stabilizing the quadruplex structure. The stabilization of both terminal G3 and G6NH resonances at higher temperature clearly shows that two molecules of MTX binds to quadruplex structure. This thermal stabilization by MTX was supported by independent thermal study experiments done by using absorption spectroscopy (section 3.2).

Table 4.5: Chemical shift (ppm) of d-(TTGGGGT)$_4$ protons in MTX –d-(TTGGGGT)$_4$ complex at D/N = 2.0 as a function of temperature. $\Delta\delta = \delta_{(363\ K)} - \delta_{(278\ K)}$. –

Tem	G3NH	G4NH	G5NH	G6NH	T1H6	T2H6	G3H8	G4H8	G5H8	G6H8	T7H6
278	11.36	11.04	10.81	10.68	7.64	7.64	8.17	7.74	7.74	7.71	7.64
283	11.36	10.99	10.81	10.68	7.60	7.60	8.17	7.74	7.74	7.71	7.60
288	11.36	10.97	10.81	10.67	7.59	7.59	8.11	7.74	7.70	7.705	7.55
293	11.36	10.96	10.82	10.66	7.54	7.54	8.09	7.73	7.70	7.705	7.50
298	11.36	10.97	10.83	10.65	7.54	7.53	8.07	7.73	7.75	7.70	7.51
303	11.36	10.97	10.83	10.65	7.53	7.53	8.05	7.725	7.75	7.70	7.51
308	11.37	10.98	10.84	10.64	7.53	7.53	8.033	7.73	7.74	7.69	7.49
313	11.37	10.99	10.85	10.63	7.53	7.53	8.01	7.73	7.73	7.685	7.46
318	11.37	10.99	10.86	10.62	7.53	7.55	8.00	7.735	7.725	7.68	7.44
323	11.36	11.01	10.87	10.62	7.54	7.55	7.97	7.74	7.715	7.64	7.41
328	11.35	11.01	10.86	10.61	7.54	7.55	7.97	7.74	7.705	7.63	7.40
333	11.35	11.00	10.86	10.61	7.54	7.55	7.96	7.74	7.71	7.63	7.41
338	11.34	11.01	10.86	10.60	7.54	7.55	7.96	7.74	7.70	7.63	7.40
343	11.34	11.01	10.86	10.59	7.54	7.55	7.96	7.74	7.70	7.62	7.39
348	11.33	11.01	10.86	10.59	7.54	7.55	7.95	7.74	7.70	7.61	7.39
353	11.32	11.01	10.86	10.58	7.54	7.55	7.95	7.74	7.69	7.60	7.39
358	11.31	11.00	10.86	10.58	7.55	7.55	7.94	7.74	7.69	7.59	7.38
363	11.30	11.00	10.85	10.57	7.55	7.55	7.93	7.74	7.69	7.58	7.38
Δ δ	**-0.06**	**-0.04**	**0.04**	**-0.09**	**-0.09**	**-0.09**	**-0.24**	**0.00**	**-0.05**	**-0.13**	**-0.26**

Table 4.6: Chemical shift (ppm) of MTX protons in MTX-d-(TTGGGGT)$_4$ complex at D/N = 2.0 as a function of temperature, $\Delta\delta = \delta_{(363\ K)} - \delta_{(288\ K)}$. -ve Δδ indicates upfield shift, +ve Δδ indicates downfield shift.

Temp (K)	11NH	6/7H	2/3H	11CH_2	12CH_2	13CH_2	14CH_2
288	9.70	-	6.29	-	-	-	-
293	9.70	-	6.29	3.47	3.13	3.12	3.78
298	9.695	6.78	6.305	3.45	3.13	3.12	3.78
303	9.67	6.78	6.31	3.43	3.13	3.12	3.78
308	9.65	6.77	6.32	3.41	3.12	3.11	3.77
313	9.62	6.75	6.33	3.39	3.12	3.10	3.76
318	9.60	6.73	6.33	3.37	3.12	3.12	3.75
323	-	6.72	6.34	3.37	3.13	3.12	3.76
328	-	6.72	6.34	3.36	3.13	3.12	3.76
333	-	6.72	6.34	3.36	3.13	3.12	3.76
338	-	6.72	6.34	3.36	3.13	3.12	3.76
343	9.51	6.71	6.34	3.36	3.13	3.12	3.76
348	9.51	6.71	6.34	3.36	3.13	3.12	3.76
353	9.51	6.71	6.34	3.36	3.13	3.12	3.76
358	9.51	6.71	6.34	3.36	3.13	3.12	3.76
363	9.51	6.71	6.34	3.36	3.13	3.12	3.76
Δ δ	**0.19**	**-0.07**	**0.05**	**-0.09**	**0.00**	**0.00**	**-0.02**

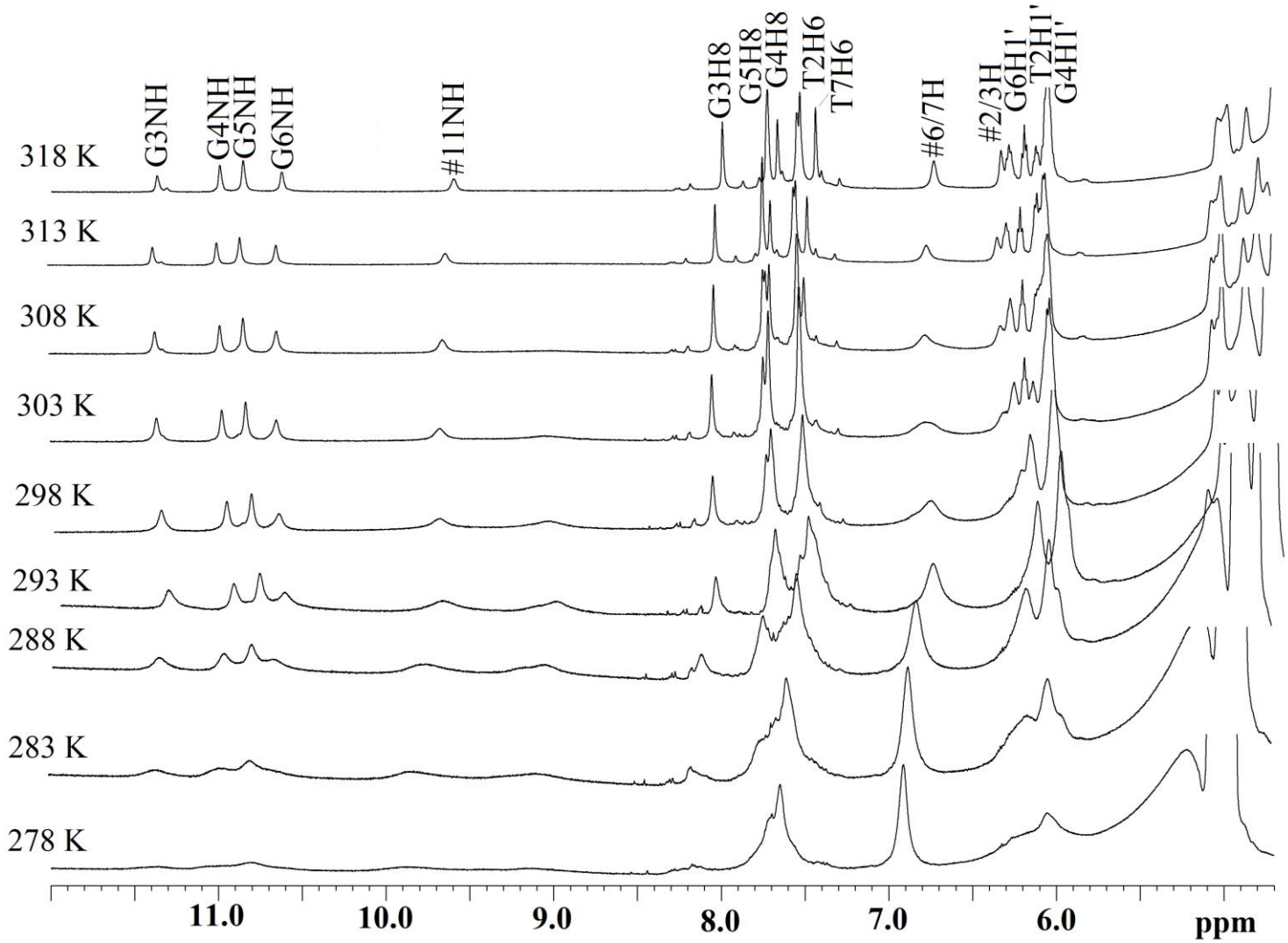

Figure 4.8: Stack of imino and aromatic region of 1H spectrum of MTX-d-(TTGGGGT)$_4$ complex versus different temperatures at D/N ratio 2.0.

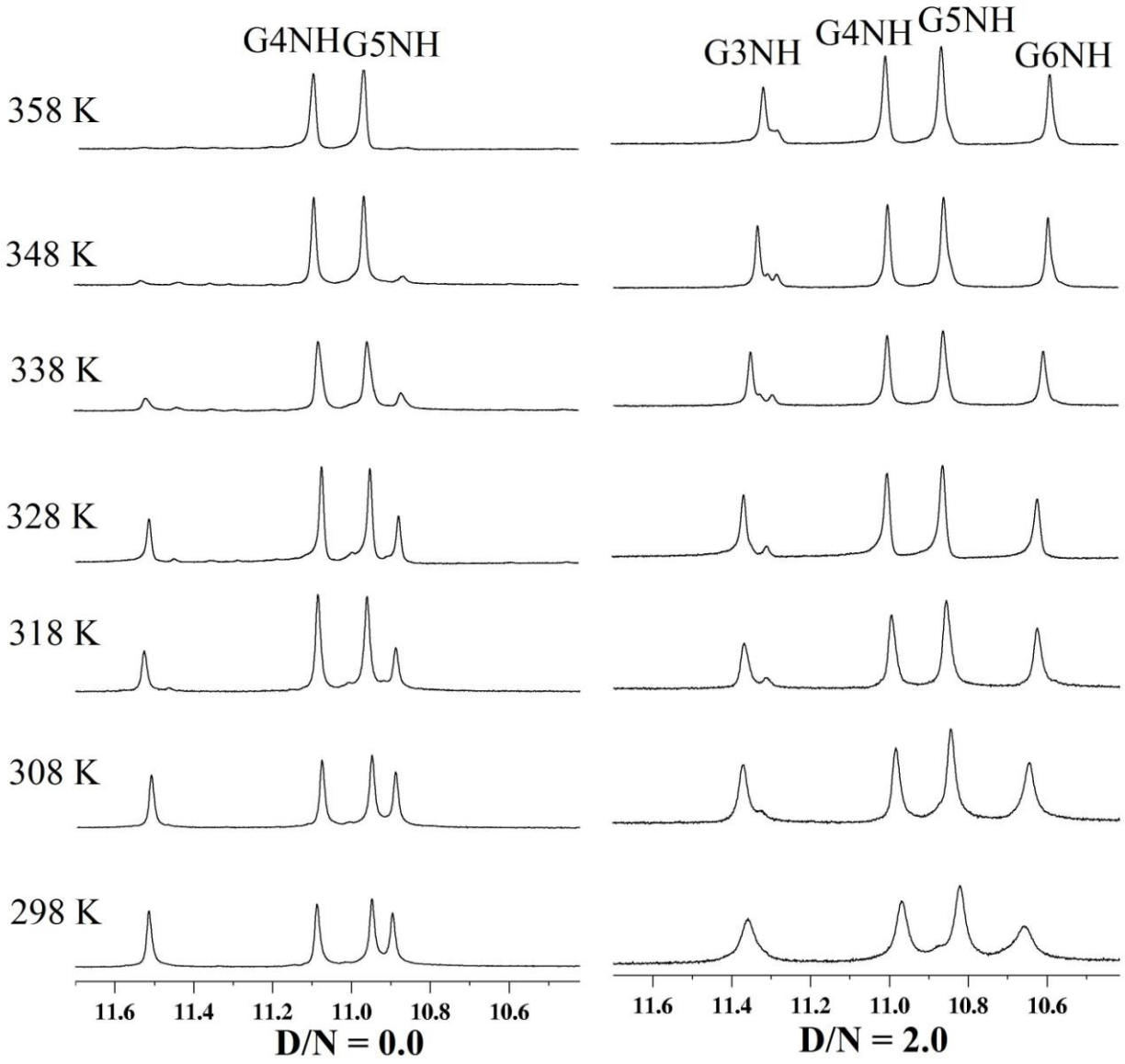

Figure 4.9: Expansion of imino region of ^{1}H spectrum of uncomplexed d-(TTGGGGT)$_4$ and 2:1 MTX complexed d-(TTGGGGT)$_4$ at various temperatures showing temperature stabilization of d-(TTGGGGT)$_4$ structure by MTX.

4.1.5 Phosphorous-31 NMR studies on complex of mitoxantrone-d-$(TTGGGGT)_4$

4.1.5.1 ^{31}P resonance assignment of alone d-$(TTGGGGT)_4$ quadruplex DNA.

Unambiguous assignment of backbone 31-phosphorous resonances of uncomplexed d-$(TTGGGGT)_4$ were done by using standard strategies of ^{1}H-^{31}P heteronuclear multiple bond correlation (HMBC) techniques . The ^{31}P signal belongs to n^{th} step shows strong correlation with three bond scalar coupled $(H3')_n$ and $(H5'/H5'')_{n+1}$ protons and a weak correlation with four bond scalar coupled $(H4')_n$ and $(H4')_{n+1}$ protons. The ^{31}P signals were denoted as d-(T1pT2pG3pG4pG5pG6pT7) for the six ^{31}P signals belongs to d-$(TTGGGGT)_4$ quadruplex sequence. The ^{31}P resonances were assigned using ^{1}H-^{31}P HMBC spectra of d-$(TTGGGGT)_4$ at 298 K (Fig. 4.10). The assignment of protons of d-$(TTGGGGT)_4$ at 298 K aids in the assignment of 31P resonances by providing the exact position of H3'/H4'/H5'/H5' signals. The terminal ^{31}P resonances of T1pT2 and G6pT7 resonates at - 0.437 and - 0.712 ppm, respectively. The remaining four signals belong to T2pG3, G3pG4, G4pG5 and G5pG6 resonates at - 0.619, - 0.861, - 0.733 and -0.831 ppm, respectively. As TTGGGGT sequence forms tetramolecular parallel quadruplex structure, with C4 symmetry, we observe six phosphorous signals for the quadruplex structure. The observed ^{31}P chemical shift range between - 0.43 ppm to - 0.861 ppm, clearly indicates that quadruplex adopts right handed helical geometry.

4.1.5.2 Phosphorous-31 NMR of mitoxantrone-d-$(TTGGGGT)_4$ quadruplex DNA.

Effect of complex formation on ^{31}P resonances of d-$(TTGGGGT)_4$ quadruplex DNA were monitored by acquiring ^{31}P spectra as a function of different drug to nucleotide ratios and temperature . Fig4.11 (a-b) shows the effect of addition of MTX as a function of D/N ratios (0.25, 0.5, 0.75, 1, 1.25, 1.5 1.75 and 2.0). Upon addition of MTX, no extra resonance develops in the down-field of up-field region of the existing ^{31}P resonances. Only six ^{31}P signals were observed even after the addition of two mol equivalent of MTX to quadruplex DNA. This confirms the quadruplex DNA doesn't open up to accommodate the MTX molecule and quadruplex structure along with its C4 symmetry was maintained even at this D/N ratio. Addition of MTX results in the broadening of ^{31}P signals of d-$(TTGGGGT)_4$ at higher D/N ratios.

Titration of MTX to d-$(TTGGGGT)_4$ (D/N =2.0) results in upfiled shift of G3pG4, G4pG5 and G5pG6 ^{31}P signals, while T1pT2, T2pG3 and G6pT7 ^{31}P signals shift downfield. G5pG6 ^{31}P signal

shows maximum upfield shift of Δδ 0.146 ppm, while G3pG4 and G4pG5 signal shifts upfield by Δδ 0.089 and 0.006 ppm, respectively. The shift for G4pG5 being centrally located ^{31}P signal was minimum. G6pT7 resonance shows maximum downfield shift of Δδ 0.125 ppm, followed by terminal T1pT2, which shifts by Δδ 0.053 ppm, while T2pG3 step ^{31}P signal shifts downfield by Δδ 0.021 ppm (Table 4.7). The change in chemical shifts of ^{31}P signals clearly shows that G5pG6 and GpT7 step is involved in interaction with MTX.

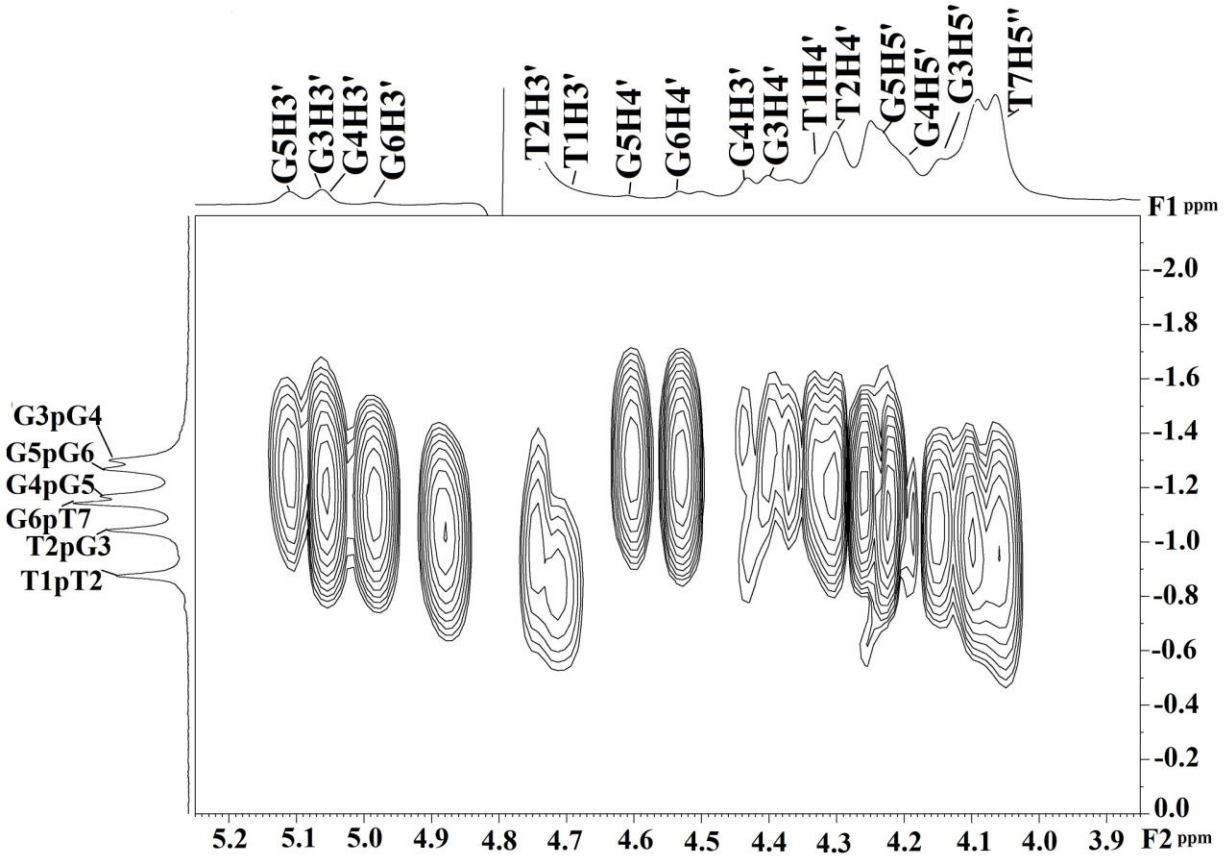

Figure 4.10: Two dimensional ^{1}H-^{31}P Hetero Multiple Bond Correlation (HMBC) spectra of d-(TTGGGGT)$_4$ at 298 K, showing correlation between ^{1}H (*F2*) and ^{31}P (*F1*).

Literature reports are not available on changes in ^{31}P signals of tetramolecular quadruplex DNA upon ligand binding. As this sequence adopts right handed geometry we compare our results with available right handed DNA data. Absence of large downfield shift in ^{31}P signals (> 1.5 ppm) shows that MTX doesnot intercalate into the d-(TTGGGGT)$_4$ quadruplex structure. As intercalation of drug chromophore results in the opening of base quartet pair at intercalation site from initial ~ 3.2 Å in tetramolecular d-(TTGGGGT)$_4$ quadruplex to more than 6Å. This result in

the changes in backbone torsional angles α = O3'-P-O5'-C5' and ζ = C3'- O3'-P-O5' which affects the phopshodiester backbone and results in unwinding of DNA quadruplex helix. Variations in the backbone O-P-O angle results in shifts in the position of attached ^{31}P signals. Intercalation of ligand to DNA results in the opening up of base pair and hence large changes in the backbone angle associated with O-P-O bond. This variation results in the large down-field shift of ^{31}P signals by > 1.5 ppm (*Gorenstein et al., 1992, Patel et al., 1974, Searle et al., 1988, Mazzini et al., 1998*). Whereas the external binding of ligand results in the minor changes in backbone torsional angles of associated O-P-O bond, hence results in the downfield shift in the range of 0 to 0.5 ppm (Favier et al., 2001, Mazzini et al., 2003). The observed changes in ^{31}P signals were consistent with the external binding of MTX to d-(TTGGGGT)$_4$ quadruplex structure.

The MTX-d-(TTGGGGT)$_4$ complex at D/N ratio 2.0 was also studied as a function of temperature. The stack of ^{31}P signals at different temperatures (278 -308 K) shows that terminal step ^{31}P signals of T1pT2, T2pG3 and G6pT7 shows large shift in position upon increase in temperature, whereas the central core ^{31}P signals of G3pG4, G4pG5 and G5pG6 doesnot shift much (Fig 4.12).

Table 4.7: ^{31}P Chemical shift (ppm) of uncomplexed d-(TTGGGGT)$_4$ and MTX – d-(TTGGGGT)$_4$ complex at various D/N ratios. Δδ = δ (D/N=2.0) - δ (D/N=0.0). -ve Δδ, +ve Δδ indicates upfield and downfield shift, respectively.

D/N	T1pT2	T2pG3	G3pG4	G4pG5	G5pG6	G6pT7
0	-0.437	-0.619	-0.861	-0.733	-0.831	-0.712
0.25	-0.434	-0.638	-0.869	-0.737	-0.852	-0.718
0.5	-0.428	-0.634	-0.869	-0.737	-0.858	-0.702
0.75	-0.428	-0.634	-0.869	-0.737	-0.858	-0.702
1.0	-0.424	-0.634	-0.871	-0.737	-0.871	-0.692
1.25	-0.414	-0.634	-0.876	-0.737	-0.888	-0.677
1.5	-0.339	-0.628	-0.877	-0.740	-0.906	-0.640
1.75	-0.388	-0.616	-0.911	-0.739	-0.954	-0.598
2.0	-0.384	-0.598	-0.950	-0.739	-0.977	-0.587
Δδ	**0.053**	**0.021**	**-0.089**	**-0.006**	**-0.146**	**0.125**

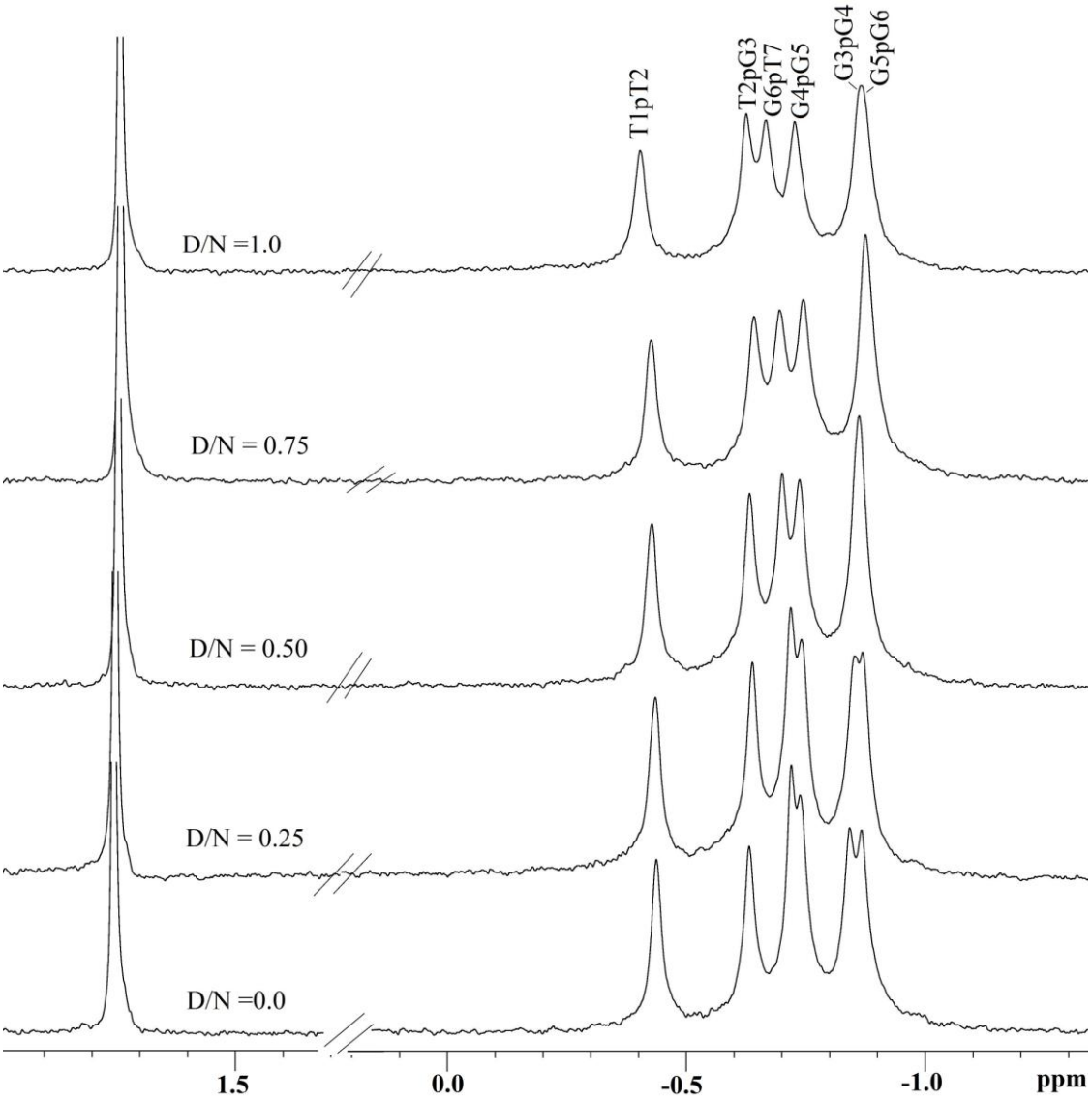

Figure 4.11: (a) Expansion of ^{31}P spectrum of uncomplexed d-(TTGGGGT)$_4$ and MTX complexed d-(TTGGGGT)4 at D/N ratios 0.25, 0.5, 0.75 and 1.0 at 298 K..

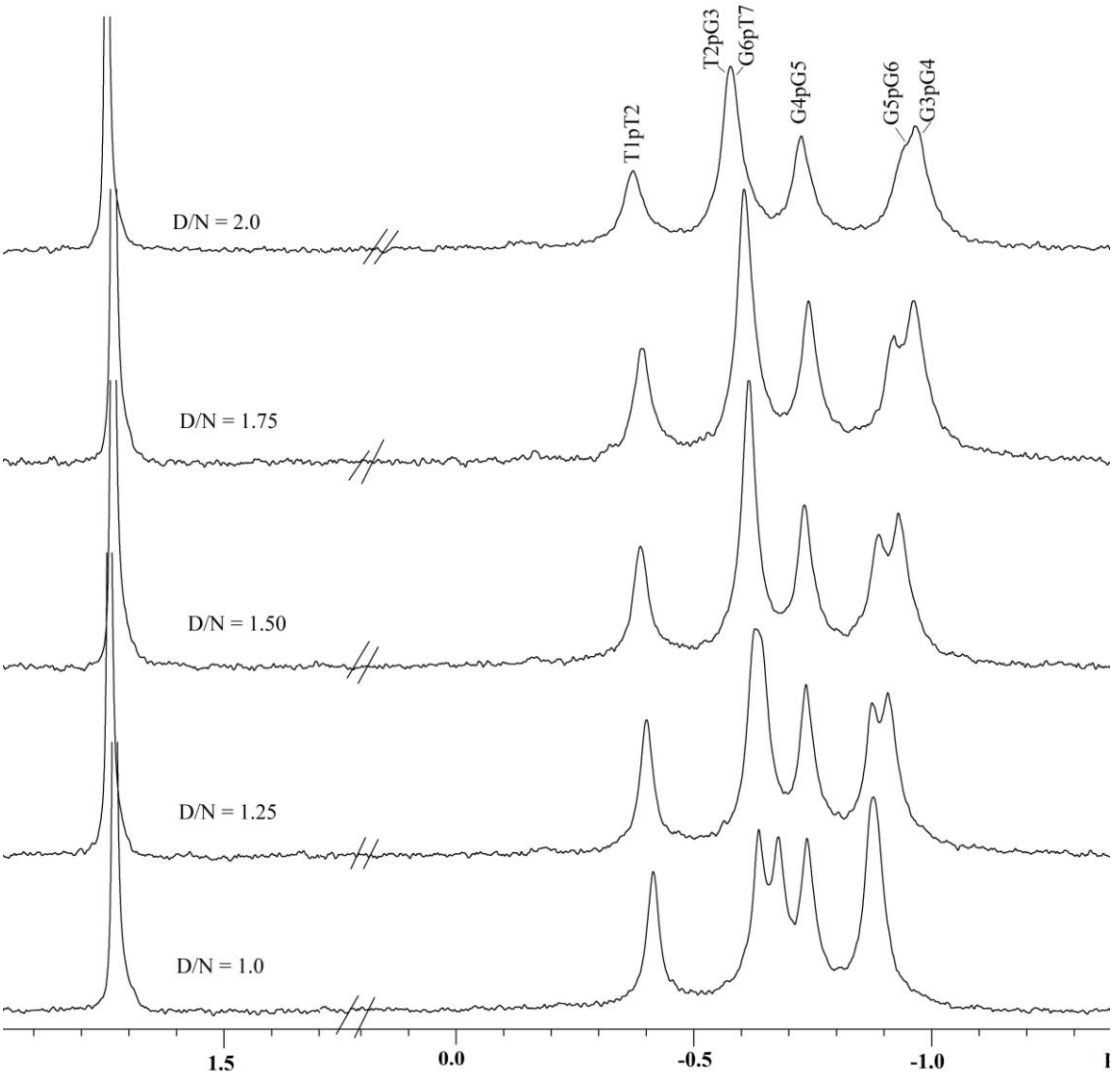

Figure 4.11: (b) Expansion of ^{31}P spectrum of MTX complexed d-(TTGGGGT)$_4$ at D/N ratios 1.0, 1.25, 1.5, 1.75 and 2.0 at 298 K.

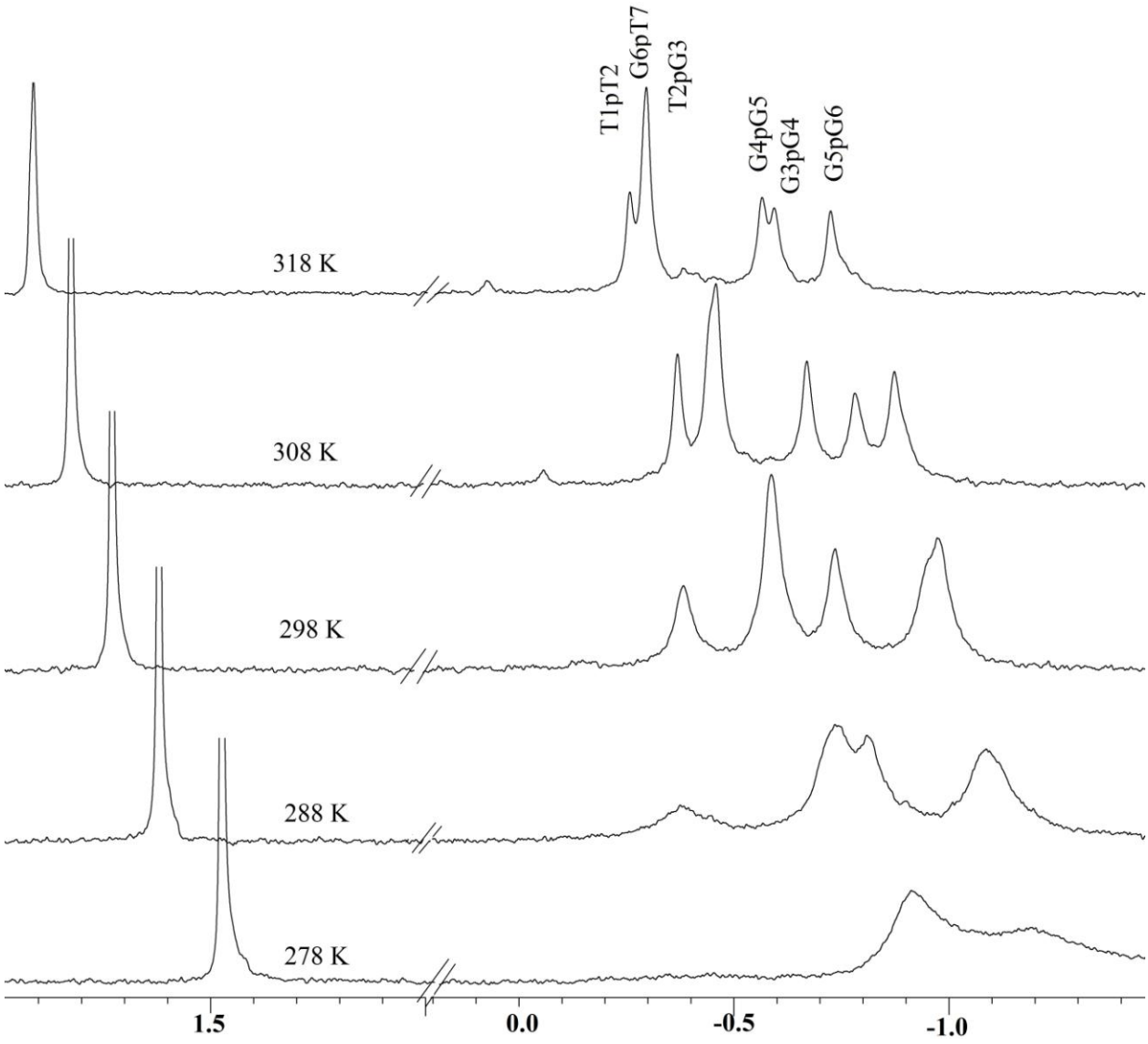

Figure 4.12: Expansion of ^{31}P spectrum of MTX complexed d-(TTGGGGT)$_4$ at D/N 2.0 as a function of temperature.

4.1.6 Resonance assignment of MTX-d-(TTGGGGT)$_4$ complex.

Two dimensional ^{1}H-^{1}H NOESY, ^{1}H-^{1}H COSY and ^{1}H-^{13}C HSQC techniques were used to unambiguously assign resonances of MTX-d-(TTGGGGT)$_4$ complex at D/N 1.0, 2.0 and 4.0 at 298 K. The NOESY experiments at different mixing time (τ_m) of 100, 200 and 250 ms were used to analyze the interaction of MTX with d-(TTGGGGT)$_4$. The resonances were assigned using the strategies used to assign the uncomplexed d-(TTGGGGT)$_4$ and MTX protons as mentioned in the section 4.1.2. The NOESY expansion of aromatic base and sugar H1' protons region, all

correlations between base H8/H6 proton with its sugar H1' proton and sequential inter base H8/H6 proton with its 3' end (n+1) sugar H1'/H2'/H2" protons were present. The NOESY spectra of MTX-d-$(TTGGGGT)_4$ complex at D/N 4.0 shows overlap of G3:G4:G5:G6 H8 resonances, hence it was difficult to identify the sequential connectivities involving them. But these signals appear less overlapped at D/N 2.0 and hence used for sequential assignment. Moreover the appearance of signature NOE correlations between GNH with its own GH8 and its 5' flanking (n-1) H8/H6 protons for e.g. G3NH gives NOEs with its own G3H8 and 5' flanking T2H6 protons similar NOE correlations were observed for all G4, G5 and G6 quartet protons. This clearly confirms that G-quadruplex structure is intact and does not open up to accommodate MTX molecules. NOESY spectra shows existence of single set of resonances for both MTX and d-$(TTGGGGT)_4$, which clearly indicates that quadurplex maintains C4 symmetry upon binding with MTX. Presence of NOE connectivities between successive G-quartet NH protons shows that G-quartets did not open up upon binding thus excluding the possibility of intercalation of MTX (Fig.4.13).

The monitoring of titration data helps in identifying the chemical shift position of MTX protons, as resonance of these protons grow in intensity with each increasing D/N ratio. The utilization of ^{1}H-^{13}C natural abundance HSQC experiment to assign MTX proton helps in the fact that, the aromatic ^{13}C resonances of MTX molecule resonate between ~122-124 ppm while that of quadruplex, having heterocyclic aromatic ring resonances resonates between ~132 -140 ppm. This region is downfield to MTX aromatic region and hence the resonances show correlation peaks in ^{1}H-^{13}C HSQC experiment is attributed to the aromatic protons of MTX molecule (Fig. 4.14 and 4.15).

The methylene protons were assigned by using ^{1}H-^{1}H COSY and NOESY experiments, as $11CH_2$ and $13CH_2$ protons gives COSY correlation with $12CH_2$ and $14CH_2$ protons, respectively. The expansion of NOESY region at D/N 2.0 shows NOE connectivities between 6/7H aromatic proton (δ = 6.80 ppm) with $11CH_2$ (δ =3.45 ppm) and $12CH_2$ (δ = 3.16 ppm) protons, which is expected, as these protons are proximity to each other in space. Similarly $11CH_2$ and $13CH_2$ protons give NOE connectivities with $12CH_2$ and $14CH_2$ protons, respectively.

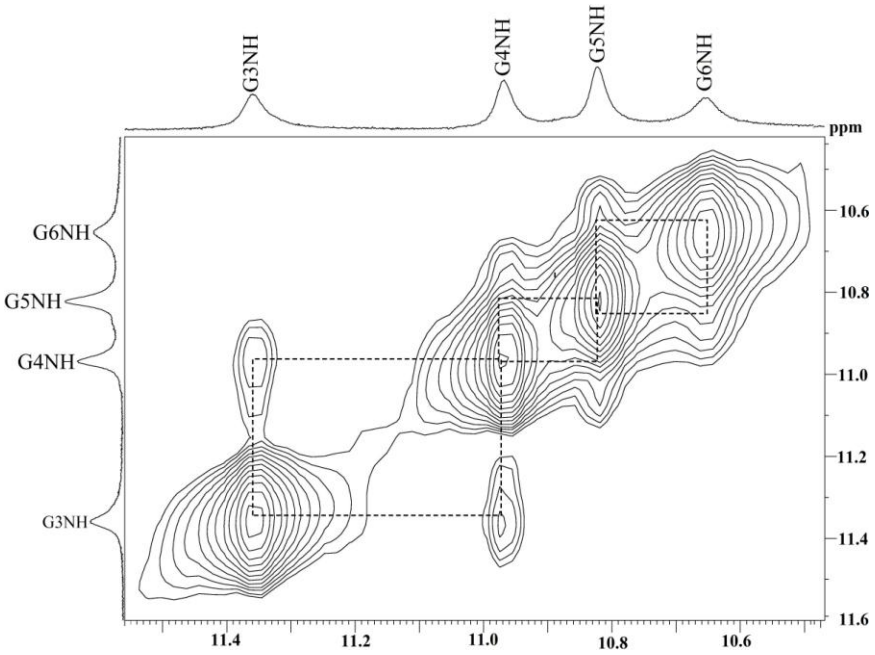

Figure 4.13: Expansion of the NOESY spectra of 2:1 MTX-d-(TTGGGGT)$_4$ complex at 298 K showing NH-NH connectivity between adjacent imino protons.

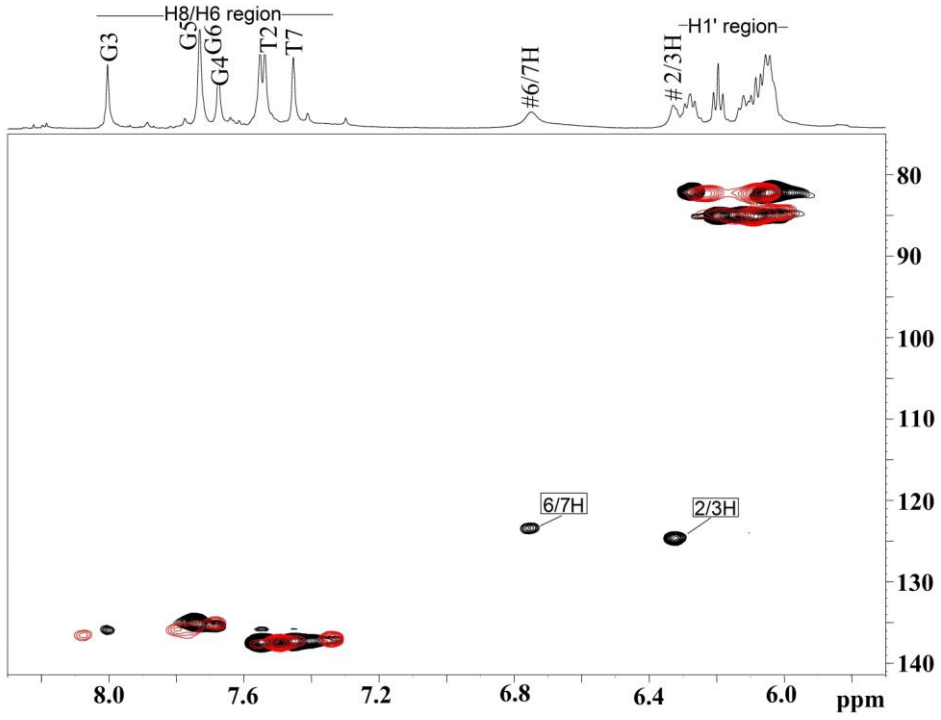

Figure 4.14: Overlap of region of ^{1}H-^{13}C HSQC spectrum of 2:1 MTX-d-(TTGGGGT)$_4$ complex (black) upon uncomplexed d-(TTGGGGT)$_4$ (red) at 298 K showing MTX aromatic 6/7H and 2/3H protons with their corresponding ^{13}C correlations.

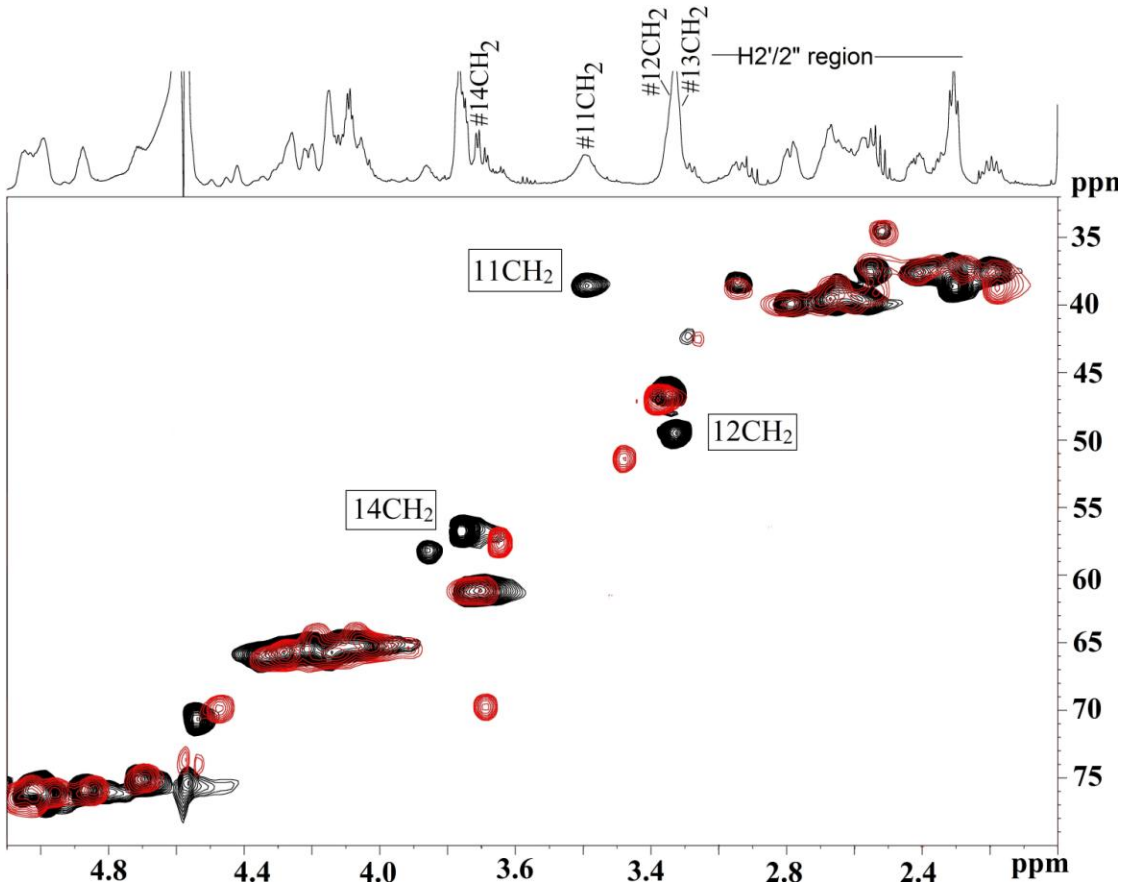

Figure 4.15: Overlap of region of ^{1}H-^{13}C HSQC spectrum of 2:1 MTX-d-(TTGGGGT)$_4$ complex (black) upon uncomplexed d-(TTGGGGT)$_4$ (red) at 298 K showing MTX side chain 11CH$_2$, 12CH$_2$, 13CH$_2$ and 14CH$_2$ protons with their corresponding ^{13}C correlation.

Table 4.10: Intra molecular connectivities of MTX molecule and inter molecular connectivities between MTX-MTX head-to-tail dimer observed in the 4:1 MTX-d-$(TTGGGGT)_4$ complex from 298 K (s = strong, m = medium, w = weak, ww = very weak, o = overlap)

Sl. no	MTX Intramolecular peaks	NOE volume intensity	NOE distance (Å)	rMD distance (Å)
1	11NH-6/7 H	s	2.8	2.75
2	11NH-11CH_2	s	2.9	2.9
3	11NH-12CH_2	s	3.5	3.6
4	6/7H-11CH_2	s	3.0	3.0
5	6/7H-12CH_2	s	3.5	3.4
6	11CH2-12CH_2	s	2.8	2.7
7	11CH2-13CH_2	o	o	4.4
8	13CH2-14CH_2	s	3.0	2.9
9	1/4OH-2/3H	s	3.2	3.2
MTX-MTX head-to-tail dimer peaks				
	MTX Intermolecular peaks			
1	11NH-2/3H	m	4.0	3.8
2	6/7H-2/3H	ww	4.5	4.2
3	2/3H-11CH_2	m	3.8	3.4
4	2/3H-12CH_2	s	3.2 (overlap)	3.4
5	2/3H-14CH_2	ww	4.8	4.9
6	1/4OH-11CH_2	ww	4.4	4.4
7	1/4OH-12CH_2	w	4.0	3.9

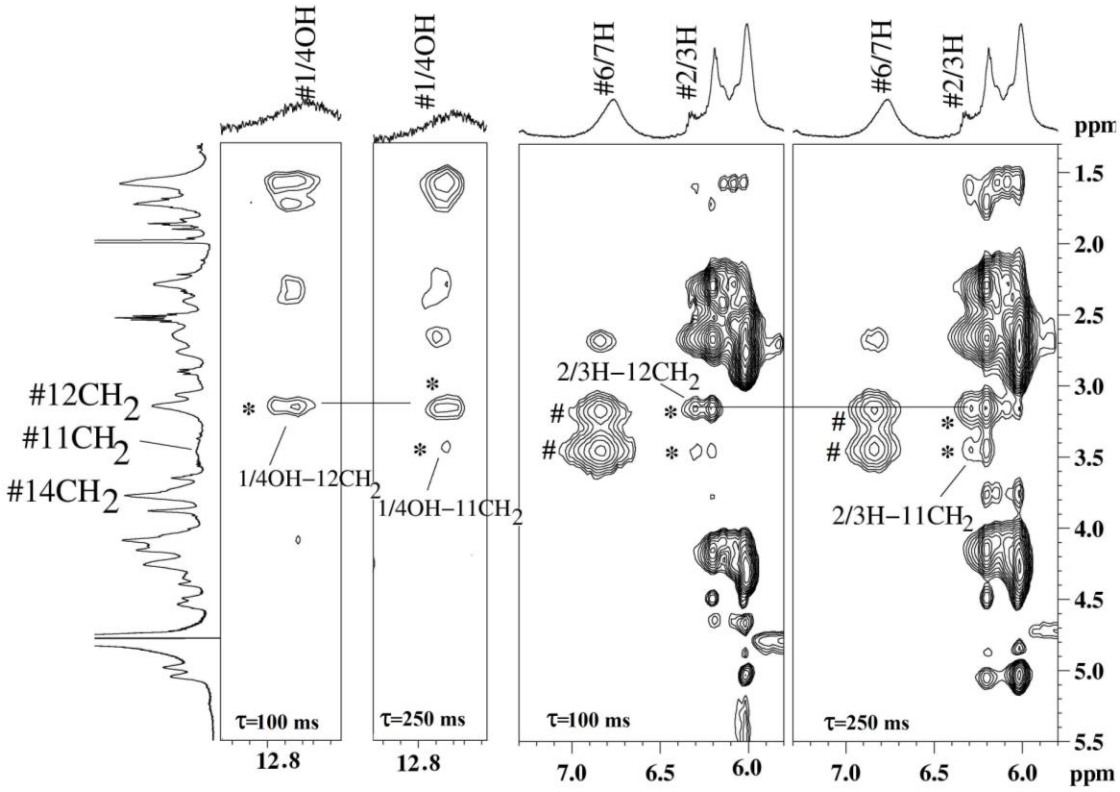

Figure 4.16: Expansion of region of NOESY spectra at different mixing times (τ_m=100 and 250 ms) showing MTX intermolecular peaks (MTX-MTX dimer peaks labeled as *) and MTX intramolecular peaks (monomer peaks labeled as #) in MTX-d-(TTGGGGT)$_4$ complex D/N = 4.0 at 298 K.

The NOESY spectra of MTX-d-(TTGGGGT)$_4$ complex at D/N ratios 1.0, 2.0 and 4.0 show NOEs between aromatic 2/H proton with side chain 11CH_2 and 12CH_2 protons. This NOE correlation is not expected within a single MTX molecule, as the distance of aromatic A ring 2/3H proton with aminoalkyl side chain 11CH_2 and 12CH_2 protons is greater than 5Å (approx distance). Hence we assume that observed NOEs were due to intermolecular magnetization transfer and between two MTX molecules present in close proximity, may be as a dimer. We observed the NOEs between 2/3H with 11CH_2 and 12CH_2 in a medium range till D/N 2.0. The 1/4 OH proton which was not observed till D/N 2.0 starts to appear after this molar ratio. The 1/4 OH proton gives NOE correlation with 2/3H proton at D/N ratio of 4.0. The analysis of intermolecular NOEs (Table 4.10) suggests that two molecules of MTX are arranged in head-to-tail fashion to bind to the d-(TTGGGGT)$_4$ quadruplex molecule.

The NOEs between aromatic 2/3H protons and alkyl amine side chain $11CH_2$ and $12CH_2$ protons were also observed in NOESY experiments done at lower mixing time of τ_m of 100 ms (Fig. 4.16). Hence this rules out the possibility of spin diffusion phenomenon for the appearance of dimer NOE peaks.

The association of two MTX molecules to form a head-to-tail dimer has been reported earlier (*Davies et al., 2001*) in studies of MTX and its hetero-association with caffeine molecule. They showed that MTX forms head-to-tail dimer and interacts with caffeine molecule. The similar arrangement of ligands head to tail dimer formation was observed in binding of Distamycin-A (Dist-A) to the tetramolecular parallel G-quadruplex structure formed by d-$(TGGGGT)_4$ sequence. In this study two distamycin molecules arranged in a head-to-tail dimer and binds to the opposite grooves of d-$(TGGGGT)_4$ quadruplex DNA, thereby preserving its C4 symmetry (*Randazzo et al. 2001; Martino et al. 2007*).

The appearance of single set of signals for MTX protons during the whole course of titration experiments suggests that association of MTX-MTX dimer molecules and interaction of MTX with d-$(TTGGGGT)_4$ quadruplex DNA is in a fast exchange process in NMR time scale.

The NOESY (τ_m = 200ms) expansion of MTX- d-$(TTGGGGT)_4$ complex D/N 2.0 at 298 K (Fig.4.17) show NOE correlations (intermolecular contacts) between MTX and d-$(TTGGGGT)_4$ protons (labeled as #). The spectra of MTX-d-$(TTGGGGT)_4$ complex at D/N ratio 2.0 shows intermolecular NOEs between MTX and d-$(TTGGGGT)_4$ protons. Both aromatic (6/7H and 2/3H) and alkylamino side chain ($11CH_2$, $12CH_2$, $13CH_2$ and $14CH_2$) protons show NOEs with the G-quadruplex protons. The maximum NOEs were observed with the alkyl amino side chain protons $12CH_2$ and $11CH_2$ with d-$(TTGGGGT)_4$. Due to the overlapping with G6H1' resonance, intermolecular contacts of 2/3H proton of MTX with quadruplex DNA could not be assigned properly. Similarly intermolecular contacts of $13CH_2$ proton with quadruplex DNA couldn't be assigned as it overlaps with $12CH_2$ resonance.

The NOESY (τ_m = 200ms) expansion of MTX- d-$(TTGGGGT)_4$ complex D/N 4.0 at 298 K shows all the NOE correlations (intermolecular contacts) between MTX and d-$(TTGGGGT)_4$ protons which exists previously in D/N 2.0 apart from this due to the development of 1/4 OH resonance, new NOE connectivities were visible between 1/4OH and $11CH_2$ and $12CH_2$ protons of MTX, which again reinforces the head to tail dimer formation by MTX (Fig.4.19).

Total 38 intermolecular NOE contacts were observed between MTX and d-(TTGGGGT)$_4$ quadruplex protons. The intermolecular NOEs were separated into two groups, one set of NOEs between MTX and T1pT2pG3 step protons and second set of NOEs between MTX and G6pT7 step protons. Majority of the NOEs (25 out of 38 NOEs) were observed between MTX dimer with protons of T1pT2pG3 residues. Analysis of observed NOEs, clearly shows that d-(TTGGGGT)$_4$ has two binding sites for MTX molecules. No NOESY cross peaks were observed between MTX protons and central G4 and G5 quartet protons. The observed strong and medium NOEs of MTX protons were with protons present in the groove region of d-(TTGGGGT)$_4$ quadruplex DNA.

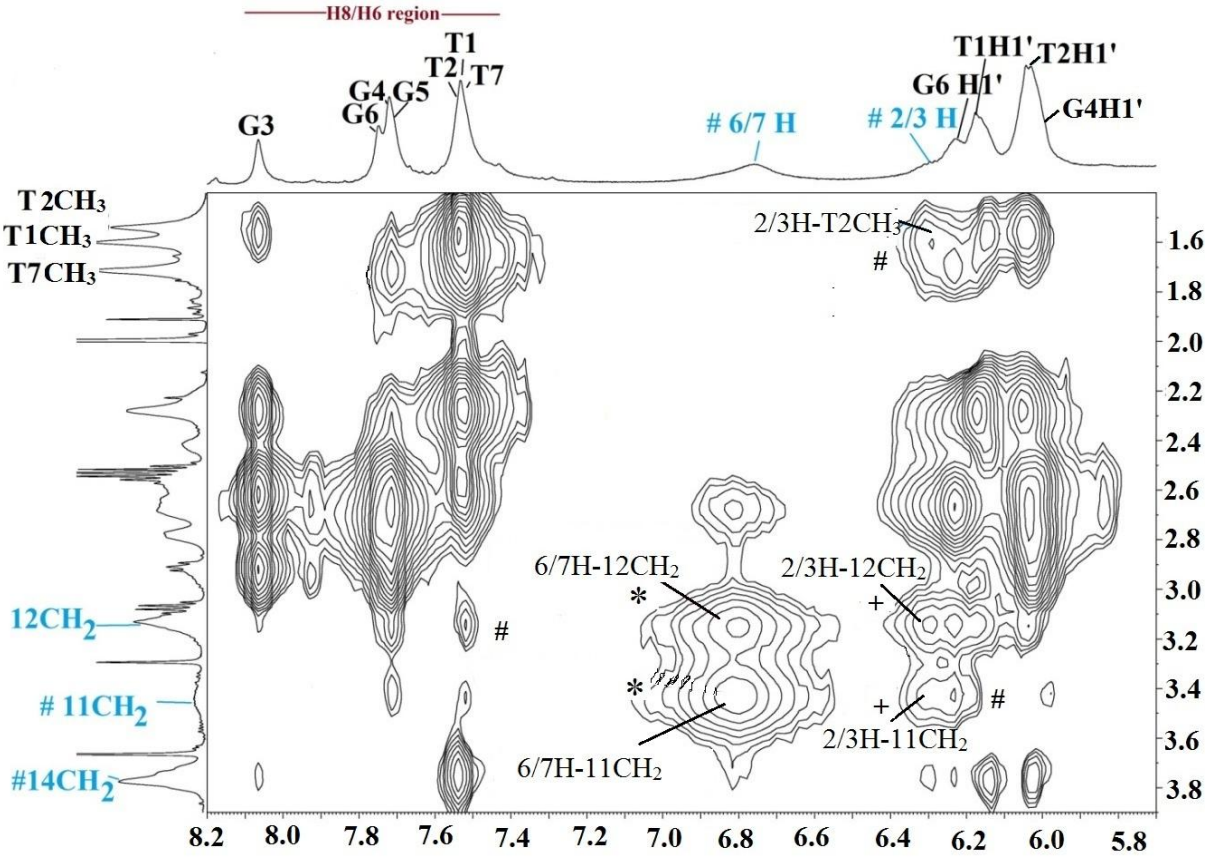

Figure 4.17: Expansion of 200ms NOESY spectrum of 2:1 MTX-d-(TTGGGGT)$_4$ complex at 298 K showing intermolecular contacts between MTX and d-(TTGGGGT)4 protons (denoted as #) , intramolecular contacts between MTX protons (denoted as *) and MTX-MTX dimer contacts (denotes as +).

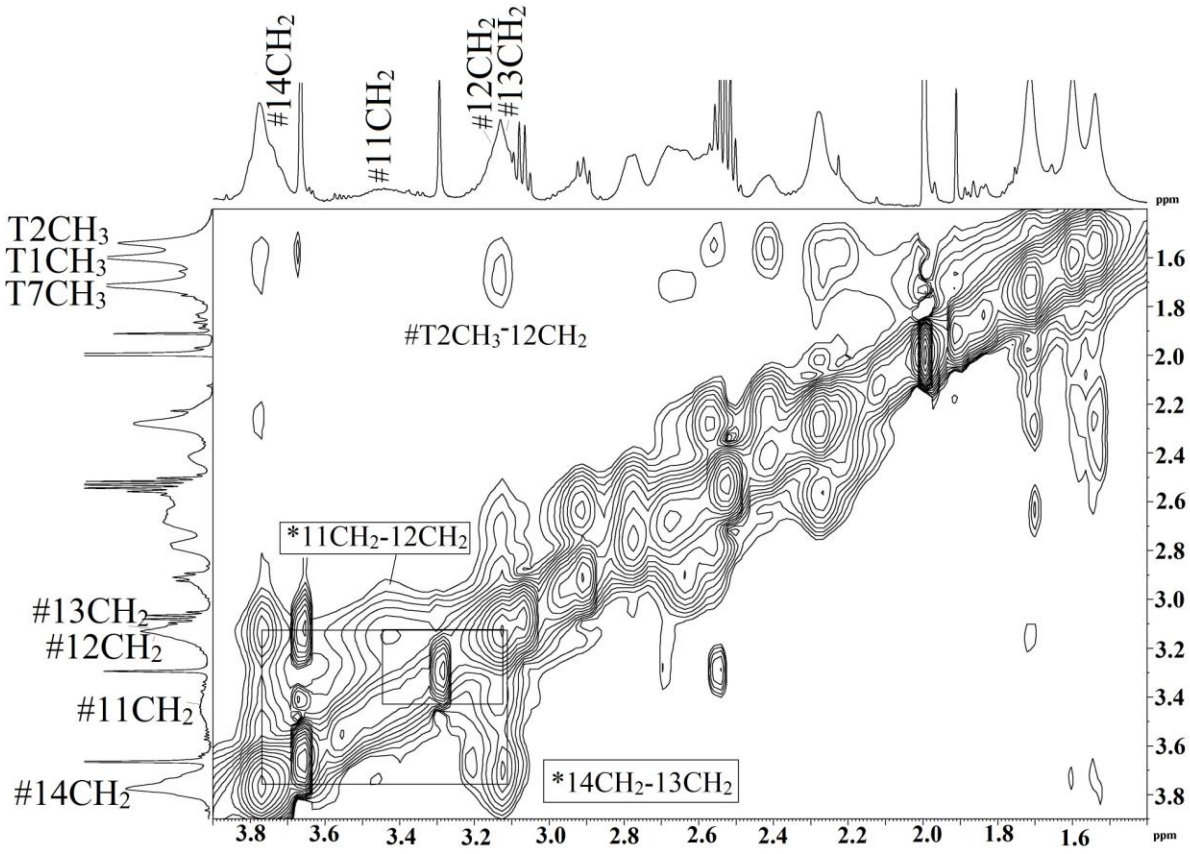

Figure 4.18 Expansion of 200ms NOESY spectrum of 2:1 MTX-d-$(TTGGGGT)_4$ complex at 298 K showing intermolecular contacts between MTX and d-(TTGGGGT)4 protons (denoted as #) , intramolecular contacts between MTX protons (denoted as *) and MTX-MTX dimer contacts (denotes as +).

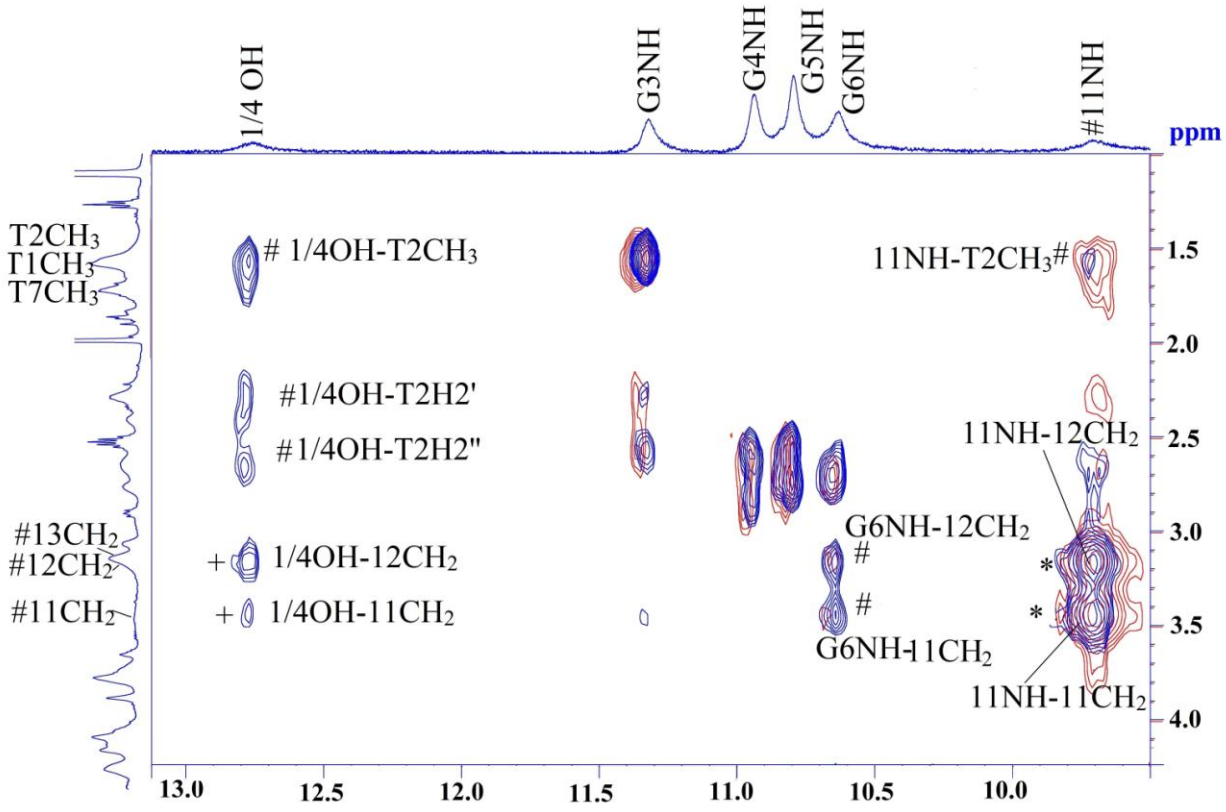

Figure 4.19 Overlap of region of 200ms NOESY spectrum of 2:1 (red) and 4:1 (blue) MTX-d-(TTGGGGT)$_4$ complex at 298 K showing intermolecular contacts between MTX protons and d-(TTGGGGT)4 protons (denoted as #) , intramolecular contacts between MTX protons (denoted as *) and MTX-MTX dimer contacts (denotes as +).

The observed intermolecular contacts (I peaks) were listed in Table. 4.10 with distances obtained from integration of NOE volume. The interproton distances present were divided into weak, medium and strong based on the intensity of the cross peaks. All the observed NOE cross peaks were in the range of medium to weak. These intermolecular contacts provide the direct insight into the possible orientation of MTX head-to-tail dimer molecules in the binding site.

The presence of base H8/H6 - sugar H1'/H2'/H2" sequential connectivities and guanine imino-imino (GNH) NOE connectivities between successive G-quartet planes (G3:G4:G5:G6) in the NOESY spectrum of 2:1 and 4:1 MTX complexed d-(TTGGGGT)$_4$ excludes intercalative mode of binding by MTX. The absence of extra bound resonances in the downfield region (> 1.5 ppm) of phosphorous-31 spectrum also supports this conclusion. GNH protons show upfield shift of $\Delta\delta_{max}$ ~ 0.26 ppm for G6NH, which is intermediate between well known G-quadruplex end stackers like

RHPS4 ($\Delta\delta_{max}$ = 0.45 ppm) and groove binders like distamycin-A and its derivatives ($\Delta\delta_{max}$ = 0.18 ppm) (*Gavathiotis et al. 2003; Martino et al. 2007; Cosconati et al. 2010*). Distamycin and its derivatives interact with tetramolecular quadruplex structure via a groove binding mode.

Solution NMR studies of interaction of MTX with any form of G-quadruplex DNA has not been reported in literature. Due to its importance as an anticancer agent, numerous solution NMR studies have been reported with duplex DNA (*Lown and Hanstock, 1985; Kotovych et al. 1986*) as well as RNA (*Zheng et al. 2009*). But none of these results provide any model that MTX binds to DNA as a dimer molecule, although it is known to form head-to-tail dimer with other aromatic molecules like caffeine (*Davies et al. 2001*). In solution condition MTX known to exist between the fast equilibrium with monomer and dimer form and dimer concentration tend to dominate at higher molar concentrations (> 10 μM). Although NMR experiments require high molar (mM) concentration of MTX, due to its high affinity with DNA bases, it shows intercalation/stacking mode of interaction with its aliphatic side chains protruding into the groove region making electrostatic interaction and hence stabilizing the binding event. Therefore in our studies, four molecules of MTX binds as a two head-to-tail dimers to d-$(TTGGGGT)_4$ structure. The presence of head-to-tail dimer NOEs at lower molar ratio of 1.0, and also their persistence in lower mixing time NOEs of 100ms clearly shows that MTX binds to d-$(TTGGGGT)_4$ quadruplex structure as a head-to-tail dimer, rather than drug dimerization in solution.

Table 4.10: Intermolecular Peaks between mitoxantrone and d-$(TTGGGGT)_4$ complex D/N = 4.0 at 298 K , ww = very weak, w = weak, m = medium, s = strong, ss= very strong.

Sl No	MTX	d-$(TTGGGGT)_4$	DN 4.0 (298K)		Distance (Å)
			250ms	**100ms**	
I1	11NH	T2CH_3	m	m	3.5
I2	11NH	T2H6	m	m	3.6
I3	11NH	T1H1'	w	w	4.0
I4	6/7 H	T2CH_3	m	m	3.6
I5	6/7 H	T2H2"	s	s	3.0
I6	2/3H	T2CH_3	m	m	3.5
I7	2/3H	T2H6	ww	-	
I8	2/3H	T2H2"	w	w	4.0
I9	11CH_2	T2CH_3	m	m	3.5
I10	11CH_2	T1H1'	w	w	4.0
I11	11CH_2	T2H6	ww	-	4.8
I12	11CH_2	G6NH	w	w	3.9
I13	12CH_2	T1H1'	m	m	3.4
I14	12CH_2	T2H6	m	m	3.2
I15	12CH_2	T7CH_3	s	s	2.9
I16	12CH_2	T2H1'	w	w	4.2
I17	12CH_2	T2H5'	w	w	4.3
I18	12CH_2	G6NH	ww	-	4.8
I19	11NH	T2H2'	w	w	4.1
I20	11NH	T2H2"	w	w	4.1
I21	14CH_2	G3H8	w	w	4.2
I22	11NH	G3NH	w	w	4.6
I23	12CH_2	G6H1'	m	m	3.4
I24	14CH_2	G6H1'	w	-	5.0
I25	14CH_2	T7H6	m	m	3.1
I26	12CH_2	G6H8	w	w	4.5
I27	11CH_2	G6H8	w	w	4.6
I28	6/7 H	G6H2"	s	s	3.0
I29	14CH_2	T1CH_3	s	s	3.2
I30	11CH_2	G6H1'	m	m	3.6
I31	14CH_2	T2H2'	w	w	4.5
I32	12CH_2	G6H2"	m	m	3.6
I33	11CH_2	G6H2"	m	m	3.6
I34	6/7 H	G6H5"	ww	-	4.8
I35	1/4 OH	T2CH_3	m		3.6
I36	1/4 OH	T2H2'	w		4.2
I37	1/4 OH	T2H2"	w		4.2
I38	1/4 OH	T2H6	w		4.1

4.1.7 Restrained Molecular Dynamics studies

The distance restraints obtained from MTX-MTX intermolecular and intra molecular contacts from NOESY (τ_m = 200ms) of 4:1 complex at 298 K were used to build the initial MTX-MTX head-to-tail dimer. Total of 9 intra molecular MTX distances were used and 7 intermolecular distances between two MTX-MTX molecules were used to build the MTX-MTX head-to-tail dimer model. After the addition of restraints, the head-to-tail dimer was energy minimized for 1000 steps using CVFF1 force field. The final energy minimized MTX-MTX dimer model (Fig.4.20 and 4.21) was used as ligand to build final structure.

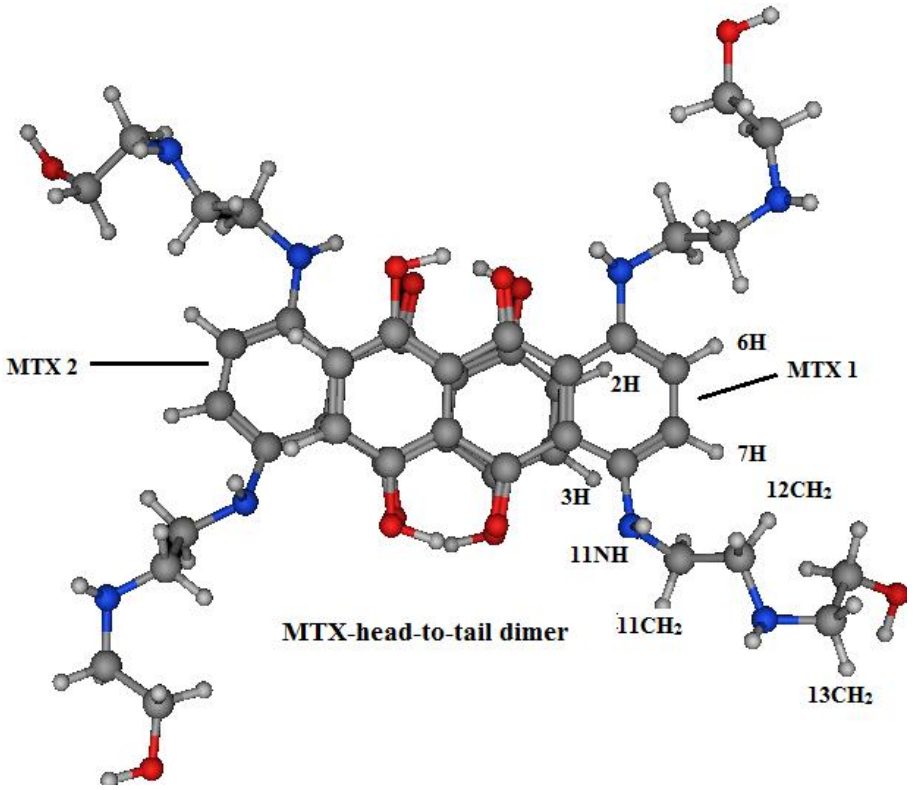

Figure 4.20: Top view of head-to-tail mitoxantrone dimer after rMD simulation using constraints from 4:1 ratio MTX-d-(TTGGGGT)$_4$ complex NOESY experiment (200 ms) at 298 K.

To obtain final structure of MTX-d(TTGGGGT)$_4$ complex distance restraints obtained from 4:1 complex NOESY (τ_m = 200 ms) at 298 K were used. A total of 280 experimental restraints including inter and intramolecular MTX-MTX, intermolecular MTX-d(TTGGGGT)$_4$, and intramolecular d-(TTGGGGT)$_4$ restraints were used to build the final model. The different types of

restraints used before energy minimization and simulated annealing were given in Table 4.11. To maintain the planarity of G-quartets during simulation planar constraints were used in the each G-quartet steps. The MTX-MTX head-to-tail dimer was placed near the binding sites such that all the inter molecular restraints between MTX dimer and d-$(TTGGGGT)_4$ were satisfied. After the addition of restraints, the energy minimized for 1000 steps using CVFF1 force field, and dynamics simulations were performed using steepest descent protocol.

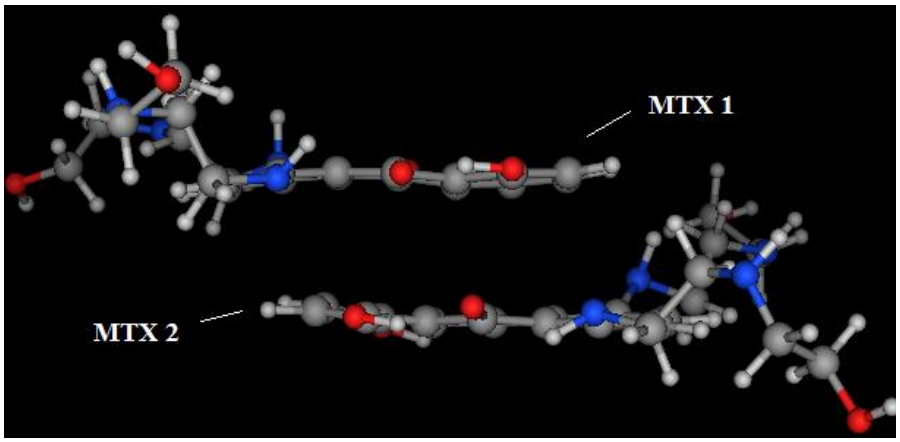

Figure 4.21: Side view of head-to-tail mitoxantrone dimer after rMD simulation using constraints from 4:1 ratio MTX-d-$(TTGGGGT)_4$ complex NOESY experiment (200 ms) at 298 K.

After the complete restrained energy simulation run, the model with minimum energy was selected and analyzed for energy terms during the course of dynamics. Table 4.11 shows the energy terms for the initial and final model of MTX-d-$(TTGGGGT)_4$ complex after 25 ns equilibration. The total potential energy of the final complex/model is 3070 kcal mol^{-1} which is significantly lower than corresponding initial structure. The electrostatic energy contribution which explains the interaction between side chain methylene and imino protons of MTX molecule with d-$(TTGGGGT)_4$ protons was -866.8 kcal mol^{-1}. The forcing potential of the final structure, which indicates contribution from potential energy because of violations of experimental restraints, exhibits a decrease from 518.4 to 200.4 kcal mol^{-1} after restrained energy minimization and restrained molecular dynamics simulation run. The final summary of experimental restraints and statistical analysis of ensemble of final structures generated by restrained molecular dynamics (rMD) was shown in Table.4.11.

Table 4.11: Structural data and energy terms of the final MTX-d-$(TTGGGGT)_4$ complex.

Experimental Restraints	
Intramolecular	
MTX-MTX intra-molecular	9
Quadruplex-Quadruplex	240
Intermolecular	
MTX-MTX inter-molecular (Head-to-tail dimer)	7
MTX-quadruplex	25
CVFF energy (kcal mol^{-1}) of the minimized structures	
Total	3070
Torsional	433.2
Electrostatic	-866.8
Restraint	200.4
Average rmsd	0.52Å
Restraint Violations	
Distance (>0.5Å)	14

The final MTX-d-$(TTGGGGT)_4$ structure after rMD simulations (Fig.4.22 and Fig. 4.23) shows four MTX molecules as a dimer of two each interacting at the T1pT2 step and G6pT7 step of quadruplex DNA. Close analysis of final model shows the interaction between MTX dimer and d-$(TTGGGGT)_4$ was stabilized by π-π aromatic interaction between anthraquinone aromatic rings and with amino-alkyl side chains forming H-bonds with guanine G6pT7 step, providing additional stabilization with complex. The oxygen atom of 1/4 OH of MTX side chain forms H-bond with H2' of T2 sugar proton. The amino alkyl side chain occupies the groove of G-quadruplex near G6pT7 step, which may be due to the flexible nature of MTX side chain.

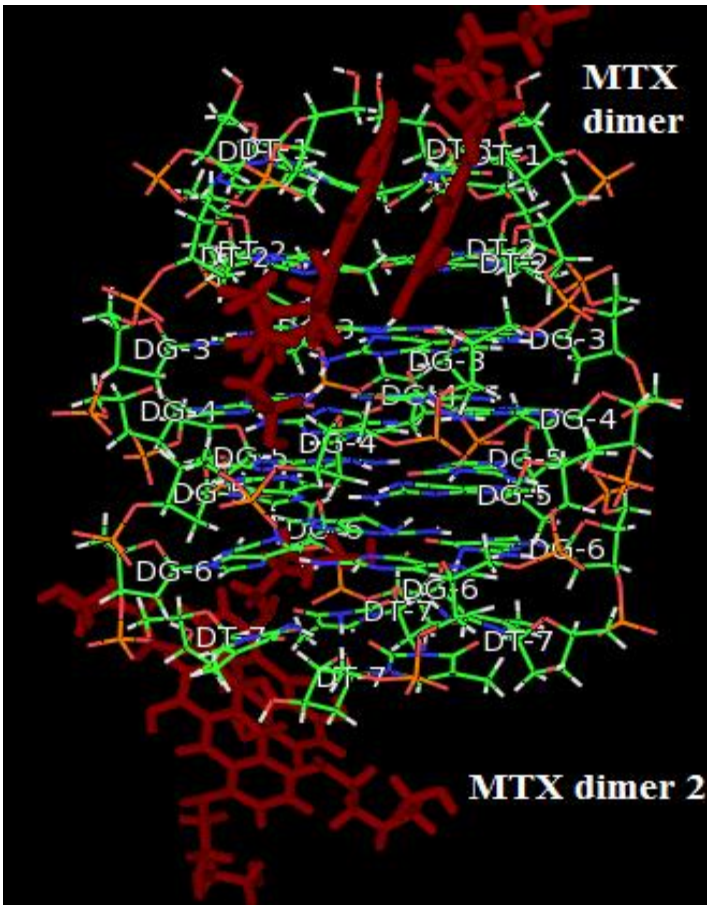

Figure 4.22: Side view of final complex of MTX with d-(TTGGGGT)$_4$ after rMD simulations using constraints from 4:1 ratio MTX-d-(TTGGGGT)$_4$ complex NOESY experiment (200 ms) at 298 K.

The rMD results clearly shows that binding of MTX-d-(TTGGGGT)$_4$ via with mitoxantrone as a head-to-tail dimer interacting in two different sites one dimer at T1pT2pG3 step and another MTX dimer at G6pT7 step and amino-alkyl side chains occupying the groove region of quadruplex DNA.

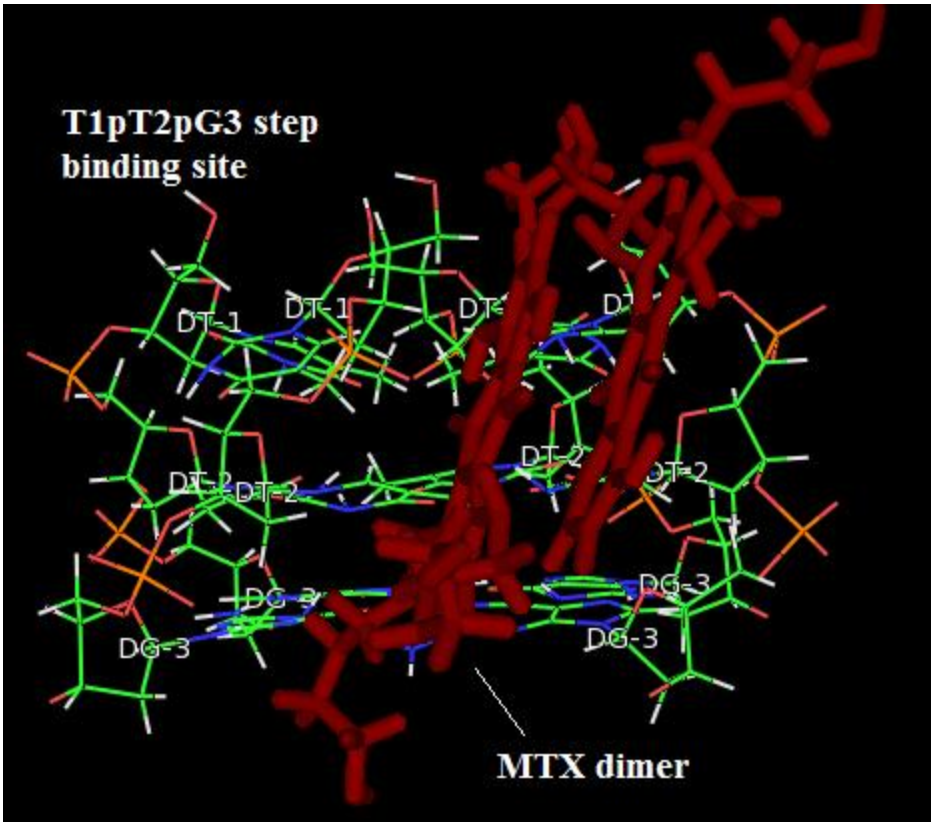

Figure 4.23: Side view of head-to-tail mitoxantrone dimer binding to T1pT2pG3 step after rMD simulation using constraints from 4:1 ratio MTX-d-(TTGGGGT)$_4$ complex NOESY experiment (200 ms) at 298 K.

4.2 Summary and Conclusions

The mitoxantrone (MTX) shows usual characteristic ^{1}H and ^{13}C chemical shifts as reported earlier in the literature (*Davies et al. 2001;Zheng et al. 2009; Dogra et al. 2014*), the minor variations was due to the high salt concentration (100 mM KCl) used in the present study. The amino alkyl side chains shows characteristic splitting behavior.

The G3:G4:G5:G6 imino protons resonante in the Hoogsteen hydrogen bonding region of 12-10.5 ppm, along with characteristic connectivities in 200 ms NOESY spectra at 298 K confirms the formation of G-quadruplex structure. The sequential connectivities between aromatic H8/H6 protons with sugar H1'/H2'/H2" protons confirms that d-(TTGGGGT)$_4$ adopts a right handed

backbone geometry. Presence of only single set of resonances confirms that molecule adopts C4 symmetry upon quadruplex formation.

Initial addition of MTX to d-(TTGGGGT)$_4$ results in the upfield shift of aromatic protons of MTX. The presence of single set of resonances for d-(TTGGGGT)$_4$ at all D/N ratios till 4.0 suggests that quadruplex structure maintains its C4 symmetry. The G6NH, T7H6, T7CH$_3$ protons of d-(TTGGGGT)$_4$ shows broadening of resonances till D/N ratio 1.0, and addition of MTX to reach higher molar ratio D/N 2.0 results in the sharpening of these resonances. The complex formation results in the upfield shift of imino resonances corresponding to all four G-quartet steps i.e. G3:G4:G5:G6. The G6NH shows maximum upfiled shift of 0.26 ppm, which is comparable with the well known G-quadruplex binders like RHPS4, TMPyP4. The structure of the quadruplex is intact upon complex formation with MTX. The presence of imino-imino NOE correlation between successive G-quartet steps, and sequential connectivities between aromatic H6/H8 with sugar H1'/H2'/H2" protons confirms that MTX does not intercalate between G-quartets.

The terminal G-quartet imino protons (G3 and G6) in uncomplexed d-(TTGGGGT)$_4$ disappears at 328 K, whereas in the presence of 2 mol equivalent of MTX these two imino proton signals persists till 353 K. This ΔT_m by ~ 25 K proves the stabilization of quadruplex structure by d-(TTGGGGT)$_4$ structure. This imino proton melting temperature was independently confirmed by melting studies using UV-vis studies, which shows ΔT_m of ~ 24 K in complex D/N 4.0. ^{31}P resonances doesnot show any significant shift upon complex formation and no extra signal was observed in the downfield region of the spectra. No correlation peaks were observed in ^{31}P-^{31}P NOESY exchange experiment which confirms that MTX doesnot intercalates between any of the G-quartet steps.

Presence of NOE connectivities between 2/3H proton of MTX and 11CH$_2$ and 12 CH$_2$ protons confirms the formation of MTX-MTX head-to-tail dimer. These correlations present even at lower mixing time NOESY experiments of 100 ms. Seven MTX-MTX dimer NOE connectivities, and nine MTX intra molecular connectivities were observed and aids in the restrained molecular simulations (rMD). The MTX protons show NOEs with protons of G6pT7 and T1pT2 step and 38 inter molecular NOE connectivities were observed between MTX dimer and d-(TTGGGGT)$_4$ of D/N 4.0 at 298 K. The final model of MTX bound to d-(TTGGGGT)$_4$ after rMD simulations confirms that MTX dimer binds to d-(TTGGGGT)$_4$ quadruplex structure at G6pT7 step with alkyl

amine side chains in the groove region while the second dimer binds externally to T1pT2 step in the groove region.

The results obtained in this chapter supports extensively that well known anti-cancer drug MTX interacts with d-$(TTGGGGT)_4$ quadruplex structure and stabilizes it. These results augment well with the results obtained in Chapter 3, and hence clearly prove that MTX effectively binds and stabilizes G-quadruplex structure inhibiting the activity of telomerase enzyme, a well known tumor marker.

Chapter 5

Studies on interaction of the flavonoid quercetin with tetramolecular parallel *Tetrahymena* telomeric sequence d-(TTGGGGT)$_4$ by Nuclear Magnetic Resonance Spectroscopy and restrained Molecular Dynamics simulations

Quercetin, a well known antioxidant, due to its aromatic structure along with its hydroxyl groups binds to biomolecules efficiently. To investigate mode of interaction of quercetin with tetramolecular parallel telomeric DNA sequence d-(TTGGGGT)$_4$ data was obtained from both one and two dimensional Nuclear Magnetic Resonance (NMR) spectroscopic experiments. Interproton distances obtained from two dimensional NMR techniques were used as distance restraints to obtain final energy minimized structure of quercetin-d-(TTGGGGT)$_4$ complex. The present chapter contains results obtained the following experiments and their interpretation in analyzing the quercetin--d-(TTGGGGT)$_4$ complex by using both one- and two-dimensional ^{1}H, ^{13}C and ^{31}P NMR experiments and restrained molecular dynamics simulations.

- 1D ^{1}H and ^{13}C NMR and 2D ^{1}H-^{1}H ROESY, TOCSY, COSY study of quercetin at 298 K in DMSO-*d6*.
- 1D ^{1}H NMR titration studies of quercetin-d-(TTGGGGT)$_4$ complex at various drug (D)/ quadruplex (N) ratios of 0.25, 0.5, 0.75, 1.0 and 2.0 at 278, 283 and 298 K in 90% water and 10% D_2O.
- 1D NMR study as a function of temperature in the range 278-353 K at D/N = 2.0.
- 31P 1D NMR study as a function of D/N 0.25, 0.5, 0.75, 1.0 and as a function of temperature at D/N 1.0.
- 2D NOESY at D/N = 1.0, using mixing time τ_m = 200, 250 ms at 278 and 298 K and D/N 2.0, τ_m = 200 at 298 K in 90% H_2O and 10% D_2O.
- ^{1}H-^{13}C HSQC spectrum of quercetin- d-(TTGGGGT)$_4$ complex of D/N 2.0 at 298K.
- Restrained molecular dynamics studies on the solution structure for the complex of quercetin with d-(TTGGGGT)$_4$ at drug to DNA quadruplex ratio of 2:1 using inter-proton distances obtained from 2D NOESY as restraints.

5.1 Results and Discussion

5.1.1 NMR studies of quercetin

Complete unambiguous assignment of all proton and carbon resonances of quercetin were done using standard NMR techniques of one dimensional ^{1}H, ^{13}C and two dimensional ^{1}H-^{13}C HSQC, ^{1}H-^{13}C HMBC, ^{1}H-^{1}H ROESY, ^{1}H-^{1}H TOCSY, ^{1}H-^{1}H COSY techniques. Analysis of the proton NMR spectrum of quercetin (Fig 5.1b) shows ten resonances which are classified into aromatic and hydroxyl ring protons. The aromatic protons are directly attached to the benzene nucleus and experience more ring current effect and hence appear up-field to the hydroxyl protons which are attached to electron with drawing oxygen atom. The five aromatic proton resonances show characteristic splitting patterns (Table 5.1).

The appearance of doublet of a doublet peak at 7.4 ppm was assigned to the H6', which shows the presence of both *ortho* (*J*=1-2 *Hz*) and *meta* (*J*=8-9 *Hz*) coupled protons in flavonoid nucleus. The resonance at 7.4 ppm shows a doublet due to the presence of H5' meta proton (*J*=8.6 *Hz*) further which splits another time to give characteristic doublet of a doublet appearance, this second splitting is attributed to the presence of *ortho* proton at H2' in ring B. The other aromatic protons H2, H8 and H2' show *ortho* effect (*J*=2.5 *Hz*) and appear as weak doublets. Protons H8 and H6 are attached to ring A.

Due to the electronegative character of oxygen atom the hydroxyl bonded H atoms resonate downfield to the aromatic group of protons. All these resonances appear as singlets and show no correlation to the carbon resonances in two dimensional ^{1}H-^{13}C HSQC (Fig 5. 2) experiments. But heteronuclear ^{1}H-^{13}C HMBC experiments reveal the long range coupling of OH signals to the nearby coupled carbon atoms, thus helping in unambiguous assignment of OH protons. The most downfield shifted proton was assigned as H5, attached to carbon-5 of ring A, which forms a hydrogen bond with the 4-keto group of C ring. This hydrogen bonding is stable and plays an important role in the structural properties of flavonoid quercetin. Analysis of the Fig. 5.1(a) shows that OH5, OH7, OH3 resonances are sharp when compared to OH4' and OH3', which are broad in NMR time scale. This observation is explained on the basis that OH5, OH7 and OH3 forms intramolecular hydrogen bonding and thus the proton exchange slowly with the surrounding solvent molecules.

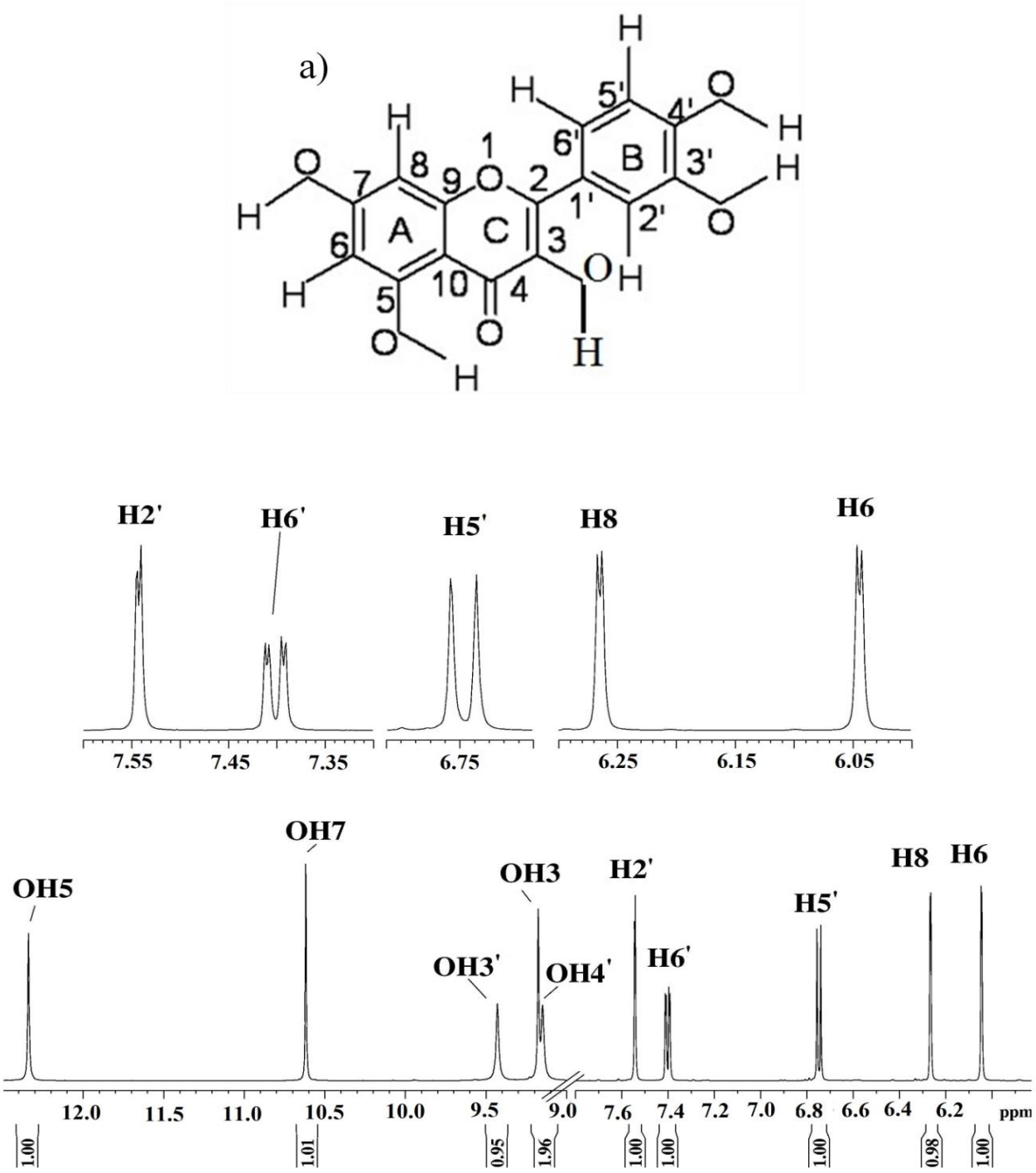

Figure 5.1: (a) Chemical structure of quercetin and (b) proton one dimensional ^{1}H spectrum at 298 K in DMSO-d_6.

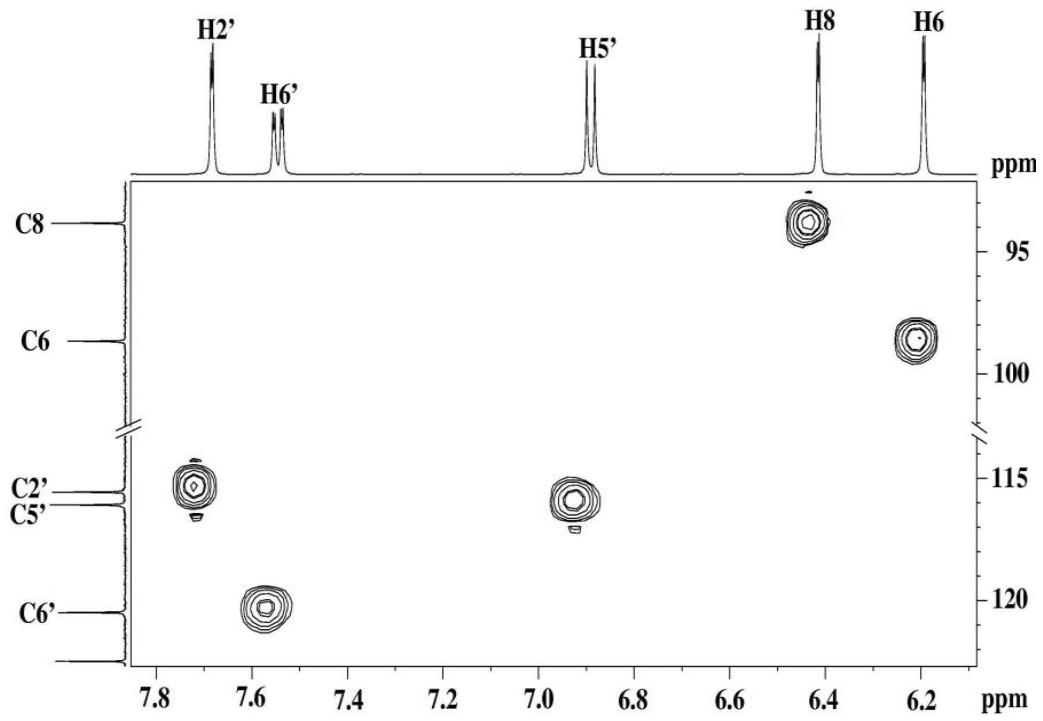

Figure 5.2: Expansion of region of ^{1}H-^{13}C HSQC spectra of quercetin showing single bond correlation between ^{1}H and ^{13}C resonances at 298 K in DMSO-d_6.

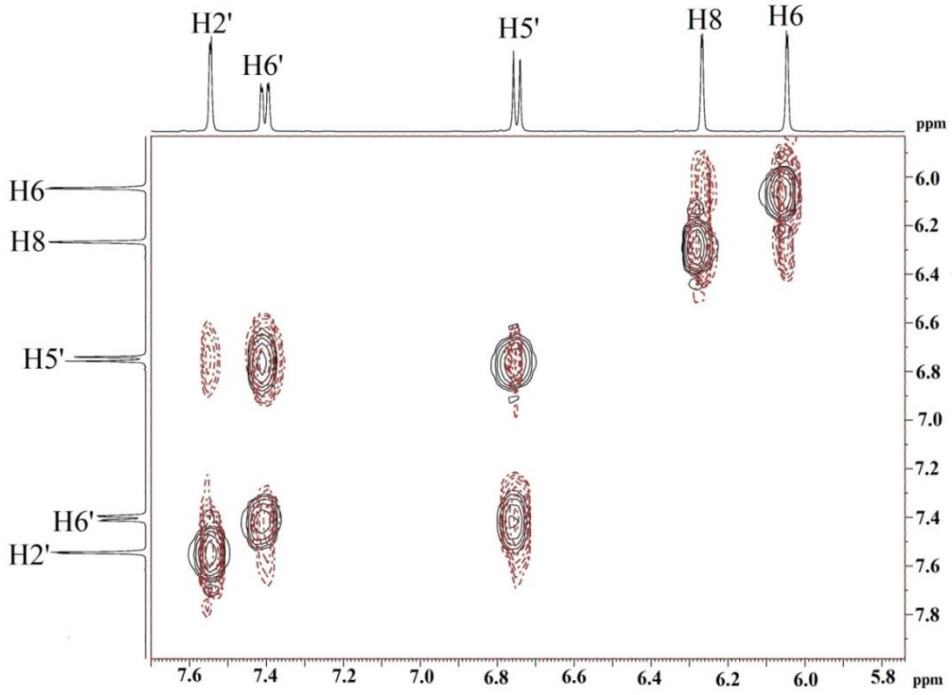

Figure 5.3: Overlap of expansion of TOCSY (dotted lines) and COSY (black lines) spectra of quercetin showing aromatic protons at 298 K in DMSO-d_6.

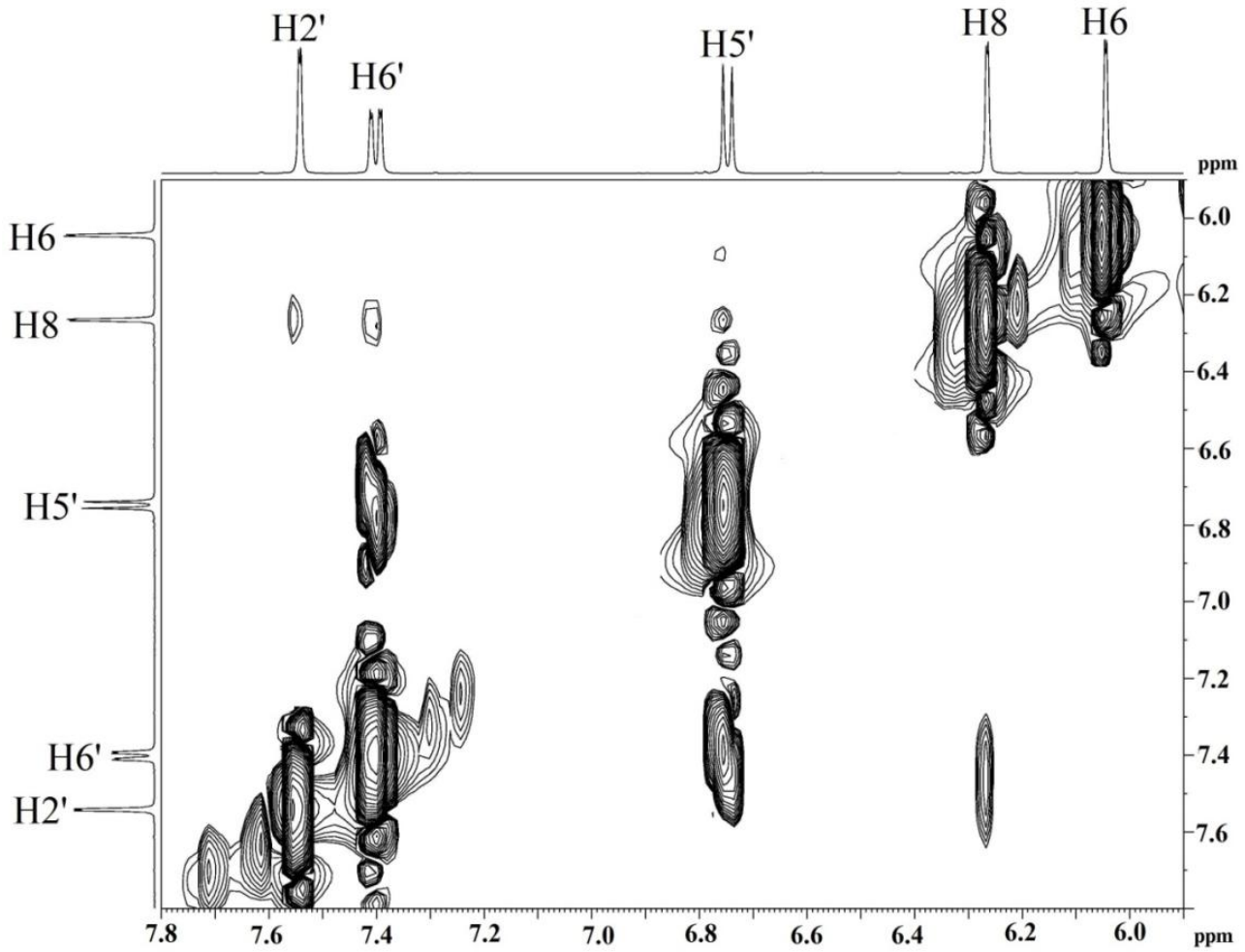

Figure 5.4: (a) Expansion of region of 250 ms ROESY spectrum of quercetin showing aromatic protons at 298 K in DMSO-d_6.

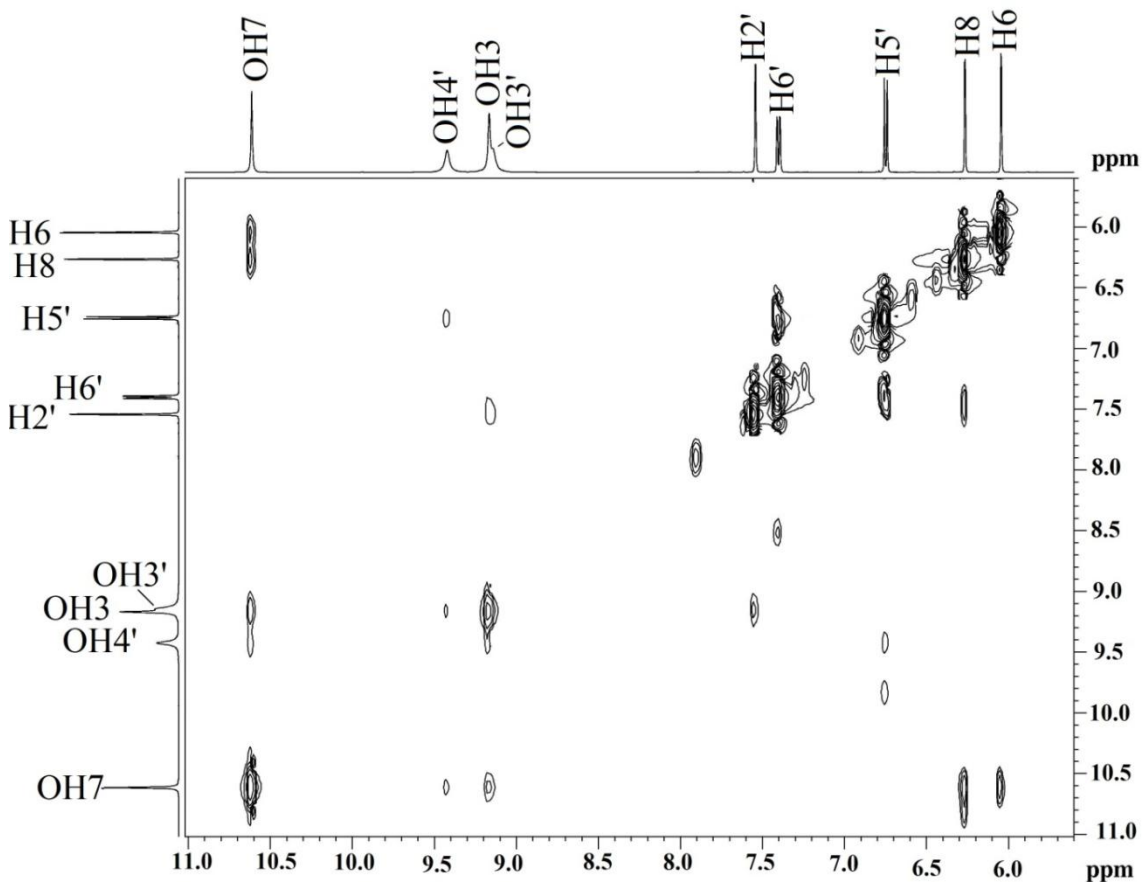

Figure 5.4: (b) Expansion of region of 250 ms ROESY spectrum of quercetin at 298 K in DMSO-d_6.

Table 5.1: Chemical shift of quercetin protons in DMSO-d_6 (6.14 mM) and compared with reported chemical shifts in literature and observed J-couplings between quercetin protons in the present study.

Quercetin proton	Present work δ (ppm)	J coupling (*Hz*)	Nickavar et. al (2011) δ (ppm)	Lee et. al (2008) δ (ppm)	Fathiazad et. al (2006) δ (ppm)	Spencer et.al (2003) δ (ppm)
H2’	7.54	2.16 (d,H6')	7.65	7.67	7.69	7.71
H5’	6.74	8.61 (d,H6')	6.88	6.88	6.90	6.92
H6’	7.40	8.52 (dd,H5') 1.89 (d,H2')	7.53	7.54	7.56	7.56
H6	6.04	1.89 (d, H8)	6.15	6.18	6.20	-
H8	6.26	1.86 (d, H8)	6.39	6.40	6.42	-
OH3	9.17	s		9.34	9.63	9.34
OH5	12.33	s		12.48	12.52	12.51
OH7	10.61	s		10.76	10.82	10.81
OH3’	9.15	s		9.34	9.35	9.39
OH4’	9.42	s		9.57	9.41	9.62

Table 5.2: Proton chemical shifts of quercetin and observed one bond ^{1}H-^{13}C correlations along with multiple bonds ^{1}H-^{13}C correlations.

Quercetin protons	Chemical shifts (ppm)	C-H correlation in HSQC	C-H multiple bond correlation in HMBC (bond coupling)
H2'	7.54	C2'	C3'(^{2}J), C4'(^{3}J), C6'(^{3}J),
H5'	6.74	C5'	C4'(^{2}J), C3'(^{3}J), C6'(^{2}J),
H6'	7.40	C6'	C5'(^{2}J), C2' (^{3}J)
H6	6.04	C6	C7(2J), C8(3J), C5(2J), C10(^{3}J)
H8	6.26	C8	C6(^{3}J), C7(^{2}J), C9(^{2}J),
OH3	9.17	C3	C3(^{2}J), C2(^{3}J), C4(^{3}J)
OH5	12.33	C5	C5(^{2}J), C6 (^{3}J), C7(^{4}J), C10(^{3}J)
OH7	10.61	C7	C6 (^{3}J), C8 (3*J*)
OH3'	9.15	C3'	C3' (^{2}J), C2' (^{3}J), C4'(^{3}J)
OH4'	9.42	C4'	C4'(^{2}J), C5'(^{3}J),C3'(^{3}J)

Table 5.3: Table showing observed ROESY, COSY and TOCSY correlations between quercetin protons in the present study and integral volume, distance obtained from integral volume and distance obtained after rMD simulations from ROESY.

	ROESY correlations (298K 200ms)	Distance from ROESY (Å)	Integral volume	Distance from rMD (Å)	COSY correlations	TOCSY correlations
1	H5'-H6'	2.45	35139008	2.36	H5'-H6'	H5'-H6' (ring A)
2	H2'-H6'	-		4.43		H2'-H6' (ring A)
3	H8-H2'	3.18	7264091	3.90		H2'-H5' (ring A)
4	H8-H6’	3.62	3300473	4.22		H8-H6 (ring B)
5	H8-OH7	3.08	8574962	3.11		
6	H6-OH7	3.15	7500107	2.80		
7	H2'-OH3	Overlap				
8	H6'-OH3	4.23	1293968	3.53		
9	H5'-OH4'	3.16	7467841	2.98		
10	H2'-OH3'	3.56	3868653	3.27		

As carbons atoms are shielded from the outer environment, chemical shift of the carbons were largely determined by the electron density at that particular carbon atom. Thus the carbon resonating at the lowest field was attributed to the carbonyl at position 4, followed by hydroxylated aromatic carbons.

Fig. 5.3 shows the ^{1}H-^{1}H TOCSY and ^{1}H-^{1}H COSY overlap of quercetin aromatic region which helps in the identification of spin systems present in the molecule. The most de-shielded aromatic proton H2' shows a weak TOSCY correlation with both H6' and H5' protons. The meta-coupled protons H5' and H6' shows a very intense peak, which is expected for a three bond coupled protons. The most shielded aromatic proton H6 gives a weak TOCSY correlation with H8 proton. This confirms the presence of aromatic protons attached to two separate spin systems (ring A and B). H2', H5', H6' protons are attached to aromatic ring A and H6 and H8 protons to another aromatic ring B. Rings A and B are separated by the heterocyclic ring C. The presence of meta coupled proton was also confirmed by the presence of intense cross peak between H6' and H5' in the magnitude mode ^{1}H-^{1}H COSY spectra (Fig. 5.3)

^{1}H-^{1}H ROESY experiment was used to obtain the three dimensional conformation of quercetin molecule. Fig 5.4 a and 5.4 b shows the 250 ms ROESY spectra of quercetin at 298 K in dMSO-d_6. Meta coupled protons H5'-H6' shows a strong cross peak, apart from this scalar coupled protons, other correlations were also observed for H8 with H2', OH7 with H8 and H6, OH3 with H6', OH4' with H5', OH3' with H2' protons. These cross peak volumes were integrated to get distance and used in the energy minimization and restrained molecular dynamics to get final minimized structure. Table 5.3 shows the ROESY cross peaks, distance obtained from ROESY experiment and distances after energy minimization of quercetin molecule using rMD simulations. Structural feature can be explained on the basis that, due to the presence of 3-OH group quercetin molecule possess planarity. The C3-C2-C1'-C2' torsional angle between A,C-ring and B-ring determines this planarity and varies between 0 Å to 1.2 Å (*Kim et al. 2006*).

5.1.2 NMR studies of *Tetrahymena* telomeric DNA sequence d-(TTGGGGT)$_4$

The formation of tetramolecular parallel quadruplex structure by sequence d-(TTGGGGT)$_4$ was studied by using both one and two dimensional NMR experiments. The resonance assignments of the uncomplexed d-(TTGGGGT)$_4$ has been made by following the standard strategies of Wang and Patel (*Wang and Patel, 1994*) and as discussed in detail in Chapter 4 (section 4.1.2). The appearance of four resonances in the Hoogsteen base pairing region confirms the formation of a single predominant structure with C4 symmetry. Formation of G-quartet structure by TTGGGGT sequence was confirmed by monitoring NOEs between imino and H8 protons of adjacent gaunosine residues in a G-tetrad (Fig. 5.5). The right handed helical nature of d-(TTGGGGT)$_4$

quadurplex DNA was established by monitoring the NOEs from the base protons to its 5' flanking sugar H1', H2'/H2" and H3' protons (Fig. 5.6). The chemical shift positions and parallel tetramolecular structure formed by sequence the d-(TTGGGGT)$_4$ has been previously reported (*Wang and Patel, 1994*). The chemical shift position of all four NH, six H6/H8 and sugar protons does not show any major variation, but none of the thymine imino protons were observed which may be due to the fast exchange with solvent. The terminal T1, T2 and T7 step protons have more freedom to interact with solvent and hence are more mobile, therefore their chemical shift positions may vary depending upon experimental conditions. The complete assignment of chemical shift positions for uncomplexed d-(TTGGGGT)$_4$ done at 298 K were given in Table 5.4.

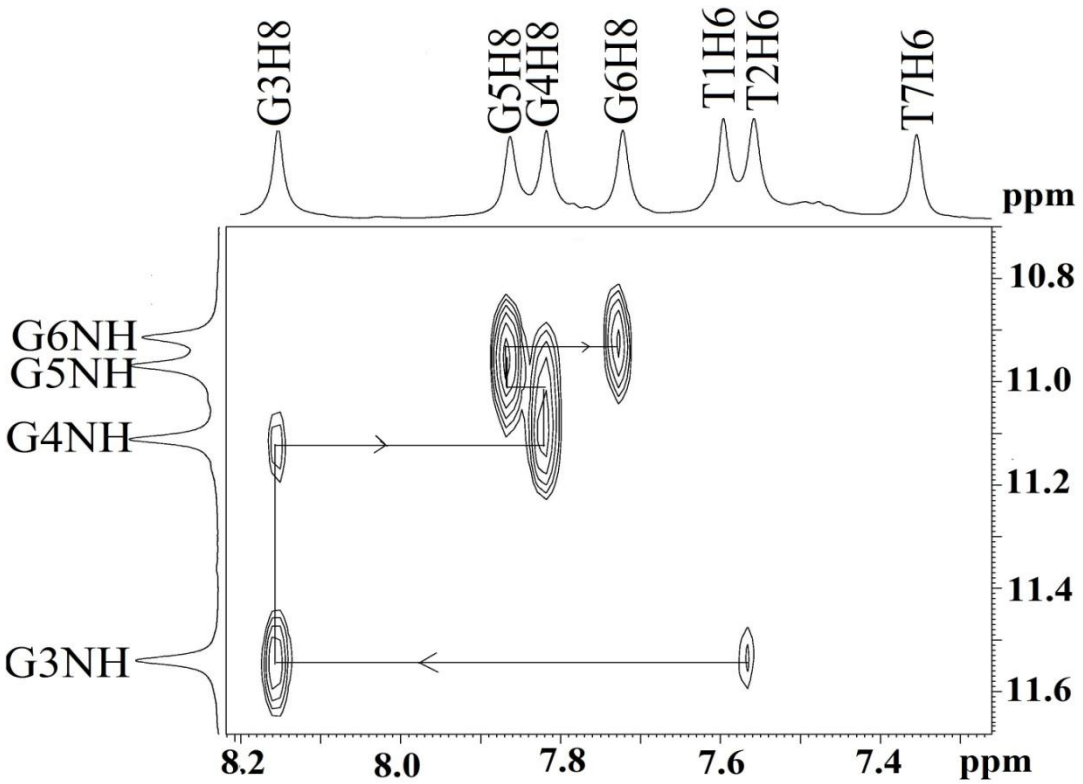

Figure 5.5: Expansion of NOESY region of uncomplexed d-(TTGGGGT)$_4$ at 298 K, showing the connectives within a G-quartet plane and between two G-quartets.

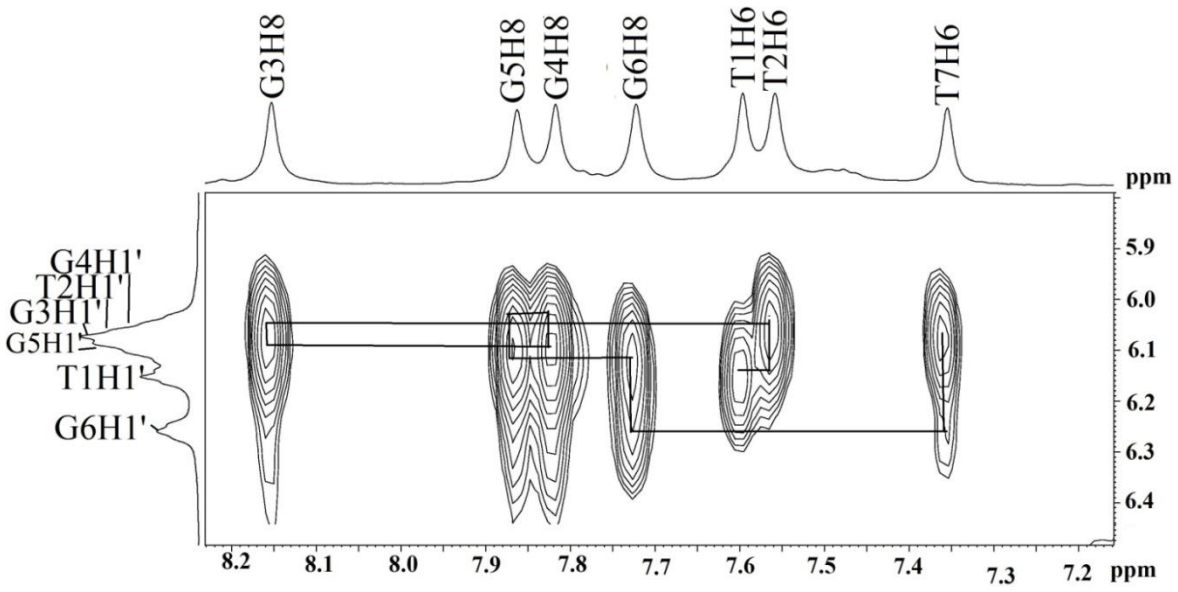

Figure 5.6: Expansion of NOESY region of uncomplexed d-(TTGGGGT)$_4$ at 298 K, showing the sequential connectivities between aromatic H8/H6 with sugar H1' protons.

5.1.3 Proton NMR studies on complex of quercetin-d-(TTGGGGT)$_4$

To examine the binding interaction of bioflavonoid, quercetin with telomere sequence d-(TTGGGGT)$_4$ increasing concentration of quercetin was added to parallel quadruplex solution to reach the desired D/N rations of 0.25, 0.5, 0.75, 1.0 and 2.0. The complete spectral assignment of quercetin complexed with d-(TTGGGGT)$_4$ is done on the basis of two dimensional NMR experiments. Fig 5.7 (a) shows the stack of expanded imino and aromatic proton region of quercetin-d-(TTGGGGT)$_4$ complex at various D/N ratios at 298 K. The appearance of only four imino resonances clearly shows that C4 symmetry of quadruplex is not broken due to interaction with quercetin. The absence of any extra bound and unbound resonances belonging to d-(TTGGGGT)$_4$, indicates that binding of quercetin is in fast regime in NMR time scale. No significant changes were observed in chemical shift position of d-(TTGGGGT)$_4$ resonances upon complex formation.

On addition of quercetin to d-(TTGGGGT)$_4$, new flavonoid proton signals appear in the aromatic region of the spectrum, which increase in intensity with increasing D/N ratios. Only aromatic protons of quercetin molecule appeared and all of these protons show upfield shift upon complex formation. The observed change in chemical shift of uncomplexed and 2:1 complexed quercetin protons are shown in Table 5.5. The H6 and H8 protons of ring A shows maximum upfield shift of

Δδ 0.56 ppm, followed by H2' proton which shifts upfield by Δδ 0.50 ppm, H6' and H5' protons shift upfield by Δδ 0.49 and 0.44 ppm, respectively. None of the five OH protons of quercetin were observed upon complex formation, which may be due to the solvent effect.

Table 5.4 shows the chemical shift of uncomplexed and 2:1 quercetin complexed d-$(TTGGGGT)_4$ quadruplex protons at 298 K. Upon complex formation imino resonances of all four quartet steps i.e. G3:G4:G5:G6 show upfield shift. The G6NH shows the maximum upfield shift of Δδ 0.14 ppm, G3 NH shifts upfield by Δδ 0.13 ppm, which is followed by G5 and G4NH, which shifts by Δδ 0.11 and 0.09 ppm, respectively. The base H8/H6 resonances show less change in chemical shift upon complex formation except for the T7H6 resonance which shifts downfield by Δδ 0.16 ppm. All other resonances show little change in chemical shift position.

The observation of only one set of proton resonance for ligand and quadruplex DNA with little line broadening suggests that exchange rate between ligand with DNA is fast on the NMR time scale.

5.1.4 Effect of temperature:

Effect of temperature on quercetin-d-$(TTGGGGT)_4$ complex was studied at temperature range of 278 K to 348 K at D/N 2.0. Fig 5.9 (a) shows the effect of temperature on imino and aromatic protons of the quercetin-d-$(TTGGGGT)_4$ complex. The chemical shift changes at varying temperatures of both bound quercetin and d-$(TTGGGGT)_4$ protons are shown in Table 5.9-5.11. Increase in temperature from 278 to 348 K results in the sharpening of the resonances of both quercetin and d-$(TTGGGGT)_4$ protons. The imino and aromatic base protons shift progressively with increase in temperature. Quercetin protons grow in intensity and shift downfield on increase in temperature from 278 to 348 K. At temperatures below 308 K the aromatic H5' proton of quercetin which resonates in the sugar H1'region of d-$(TTGGGGT)_4$ was difficult to identify in 1D spectrum, but at temperatures higher than 308 K this proton shifts downfield and appear as a separate resonance. At temperature 318 K and above, quercetin H6' and H5' protons show their characteristic scalar splitting due to ^3J coupling.

Temperature studies were used to study the thermal stabilization of d-$(TTGGGGT)_4$ structure upon complexation with quercetin. Appearance of guanine imino protons in the Hoogsteen base pairing region is the characteristic of formation of quadruplex structure, and hence their disappearance at higher temperatures can be used to monitor the melting temperature (T_m) of these structures in the

presence and absence of ligands. The ligands which stabilize the quadruplex structure upon binding will result in the increase in thermal melting temperature of quadruplex structure when compared to its uncomplexed counterpart. Fig.5.10 shows the melting profile of imino protons of alone d-$(TTGGGGT)_4$ and its complex with quercetin at molar equivalents of 2.0. The G3 and G6NH resonances start to disappear gradually with increasing temperature and completely vanishes at 348 K. But upon complexation these two imino resonances persists till 353 K. This shows the thermal stabilization of d-$(TTGGGGT)_4$ structure by about 5 K. Hence this result clearly shows that quercetin is interacting with d-$(TTGGGGT)_4$ quadruplex structure and stabilizing the quadruplex structure.

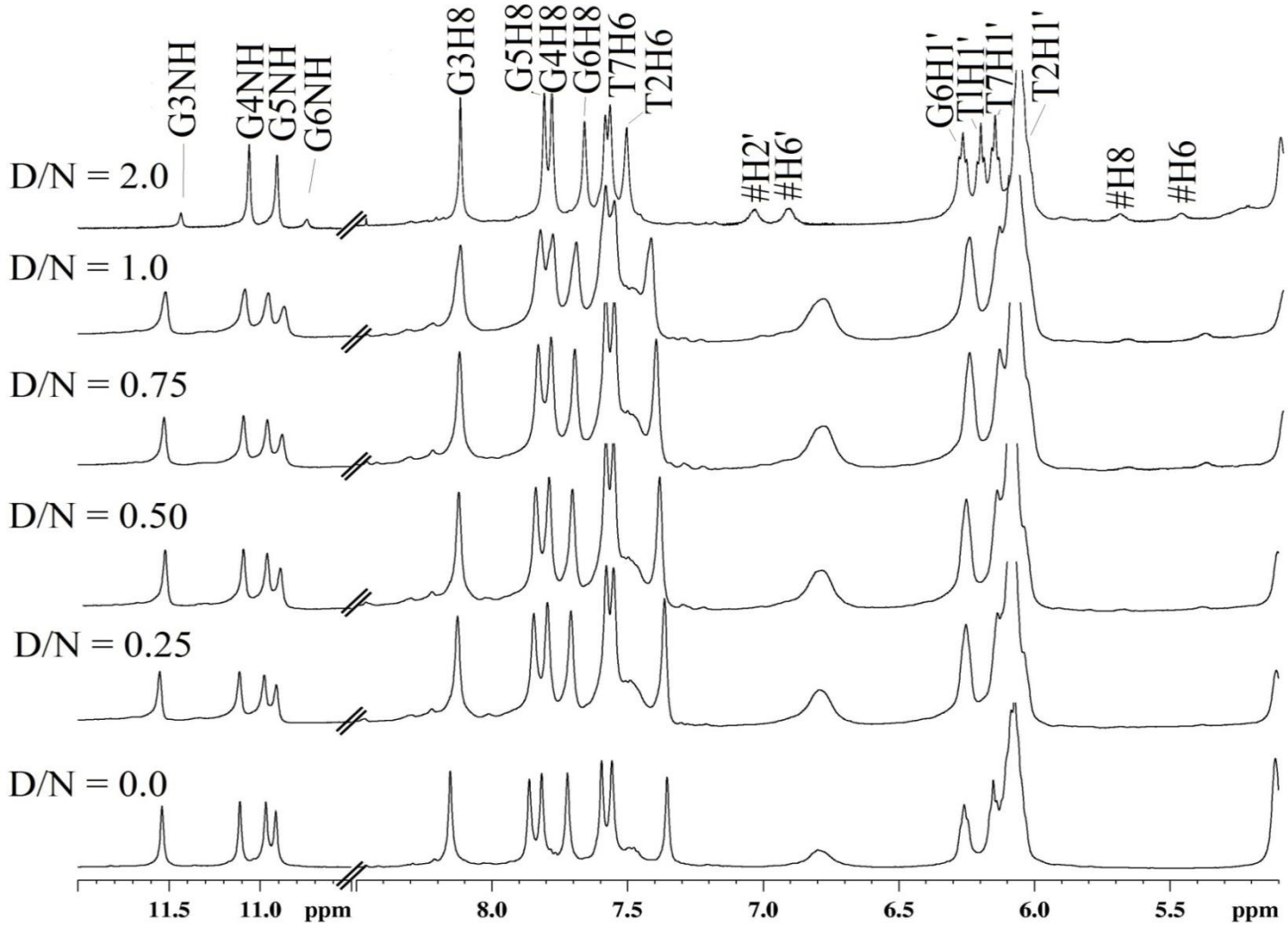

Figure 5. 7: (a) Proton spectrum of uncomplexed d-(TTGGGGT)$_4$ and quercetin complexed d-(TTGGGGT)$_4$ as a function of quercetin (D)/quadruplex (N) ratio at 298 K.

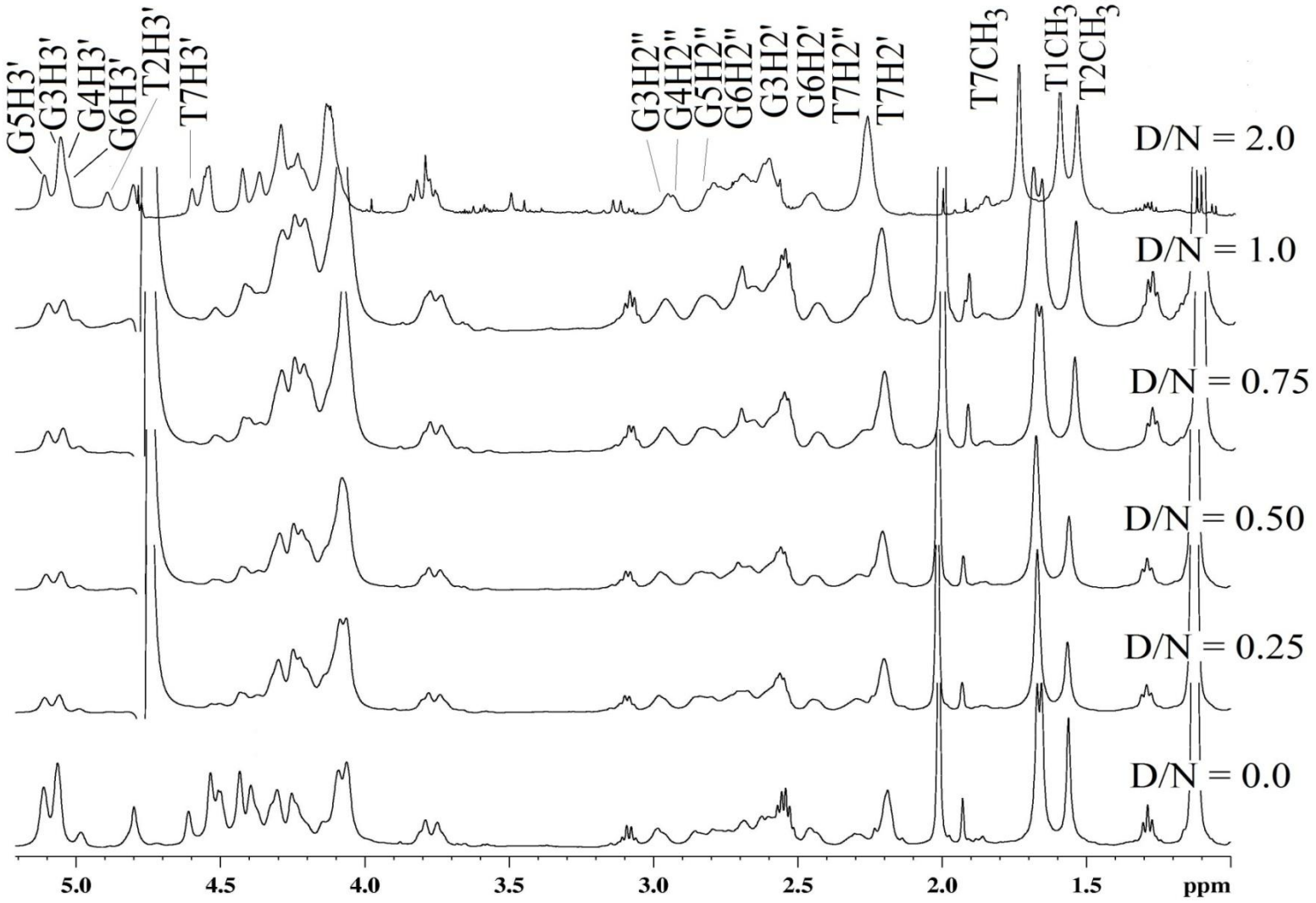

Figure 5. 7: (b) Proton spectrum of uncomplexed d-(TTGGGGT)$_4$ and quercetin complexed d-(TTGGGGT)$_4$ as a function of quercetin (D)/quadruplex (N) ratio at 298 K.

Table 5. 4: Chemical shift δ (ppm) of d-(TTGGGGT)$_4$ protons in uncomplexed state (δ^f) and bound to quercetin (δ^b) at quercetin (D) to nucleic acid quadruplex (N) ratio D/N = 2.0 at 298 K. $\Delta\delta = \delta^b_{(D/N=2.0)} - \delta^f$. -ve Δδ indicates upfield shift, +ve Δδ indicates downfield shift.

	T1			T2			G3			G4			G5		
	δ^b	δ^f	Δδ	δ^b	δ^f	Δδ	δ^b	δ^f	Δδ	δ^b	δ^f	Δδ	δ^b	δ^f	Δδ
H8/H6	7.58	7.59	-0.01	7.57	7.56	+0.01	8.11	8.15	-0.04	7.78	7.82	-0.04	7.81	7.86	-0.05
H1'	6.21	6.15	+0.06	6.03	6.05	-0.02	6.09	6.08	+0.01	6.05	6.06	-0.01	6.07	6.10	-0.03
H2'	2.20	2.21	-0.01	2.27	2.30	-0.03	2.64	2.68	-0.04	2.58	2.62	-0.04	2.69	2.74	-0.05
H2"	2.49	2.46	+0.03	2.58	2.62	-0.04	2.96	2.97	-0.01	2.88	2.94	-0.06	2.79	2.81	-0.02
H3'	4.83	4.74	+0.07	4.90	4.86	+0.04	5.05	5.06	-0.01	5.03	5.05	-0.02	5.11	5.11	0.00
H4'	4.28	4.32	-0.04	4.29	4.27	+0.02	4.36	4.43	-0.07		4.43			4.61	
H5'	3.81	3.79	+0.02	4.12	4.14	-0.04	4.17	4.25	-0.08	4.33	4.34	-0.01	4.35	4.39	-0.04
H5"	3.77	3.75	+0.02	4.08	4.06	+0.02		4.09		4.25	4.24	+0.01	4.31	4.33	-0.02
CH_3	1.60	1.67	-0.06	1.55	1.56	-0.01	-	-	-	-	-	-	-	-	-
$NH_2{}^b$	-	-	-	-	-	-	9.81	9.84	-0.03	9.18	9.25	-0.07	9.08	9.17	-0.09
$NH_2{}^{nb}$	-	-	-	-	-	-	6.23	6.24	-0.01	6.06	6.17	-0.11	6.09	6.23	-0.14
NH							11.41	11.54	-0.13	11.02	11.11	-0.09	10.86	10.97	-0.11

	G6			T7		
	δ^b	δ^f	Δδ	δ^b	δ^f	Δδ
H8/H6	7.66	7.72	-0.06	7.51	7.35	+0.16
H1'	6.28	6.26	+0.02	6.15	6.07	+0.08
H2'	2.50	2.53	-0.03	2.19	2.14	+0.05
H2"	2.71	2.76	-0.05	2.30	2.23	+0.07
H3'	5.04	4.97	+0.07	4.55	4.51	+0.04
H4'	4.52	4.56	-0.04	4.49	4.46	+0.03
H5'	4.29	4.31	-0.02	4.16	4.24	-0.08
H5"	4.19	4.23	-0.04	4.07	4.05	+0.02
CH_3	-	-	-	1.71	1.66	+0.06
$NH_2{}^b$						
$NH_2{}^{nb}$						
NH	10.67	10.91	-0.14			

Table 5.5: Chemical shift δ (ppm) of free (δ_f) and bound quercetin (δ_b) protons in quercetin-d-$(TTGGGGT)_4$ complex D/N 2.0 at 298 K. $\Delta\delta = \delta_{b\ (D/N=2.0)} - \delta_{f\ (D/N=0.0)}$. +ve Δδ downfield shift and -ve Δδ upfield shift.

Quercetin protons	Quercetin in DMSO-d_6, 298 K (δf)	Quercetin in complex D/N 2.0 (δb)	$\Delta\delta = \delta_b - \delta_f$
H2'	7.54	7.04	-0.50
H5'	6.74	6.30	-0.44
H6'	7.40	6.91	-0.49
H6	6.04	5.48	-0.56
H8	6.26	5.70	-0.56
OH3	9.17	-	-
OH5	12.33	-	-
OH7	10.61	-	-
OH3'	9.15	-	-
OH4'	9.42	-	-

Table 5.6: Chemical shift (ppm) of quadruplex protons in d-$(TTGGGGT)_4$-quercetin complex as a function of D/N 298K. $\Delta\delta = \delta_{b\ (D/N=2.0)} - \delta_{f\ (D/N=0.0)}$. +ve Δδ downfield shift and -ve Δδ upfield shift.

	G3NH	G4NH	G5NH	G6NH	$T1CH_3$	$T2CH_3$	$T7CH_3$
0.0	11.54	11.11	10.97	10.91	1.67	1.56	1.66
0.25	11.55	11.11	10.97	10.91	1.67	1.56	1.67
0.5	11.54	11.10	10.98	10.89	1.67	1.56	1.67
0.75	11.53	11.09	10.96	10.89	1.67	1.56	1.69
1.0	11.53	11.09	10.96	10.89	1.67	1.57	1.69
2.0	11.41	11.02	10.86	10.69	1.60	1.55	1.74
Δδ	**-0.13**	**-0.09**	**-0.11**	**-0.22**	**-0.07**	**-0.01**	**+0.08**

Table 5.7: Chemical shift (ppm) of quadruplex protons in d-(TTGGGGT)4-quercetin complex as a function of D/N 298K. $\Delta\delta = \delta_{b\ (D/N=2.0)} - \delta_{f\ (D/N=0.0)}$. +ve Δδ downfield shift and -ve Δδ upfield shift.

	T1H6	T2H6	G3H8	G4H8	G5H8	G6H8	T7H6
0.0	7.59	7.56	8.15	7.82	7.86	7.72	7.35
0.25	7.58	7.55	8.13	7.80	7.84	7.71	7.36
0.5	7.58	7.55	8.12	7.79	7.84	7.70	7.38
0.75	7.59	7.55	8.12	7.78	7.83	7.70	7.40
1.0	7.59	7.55	8.12	7.78	7.83	7.70	7.40
2.0	7.58	7.57	8.11	7.78	7.81	7.66	7.51
Δδ	**-0.01**	**+0.01**	**-0.04**	**-0.04**	**-0.05**	**-0.06**	**+0.16**

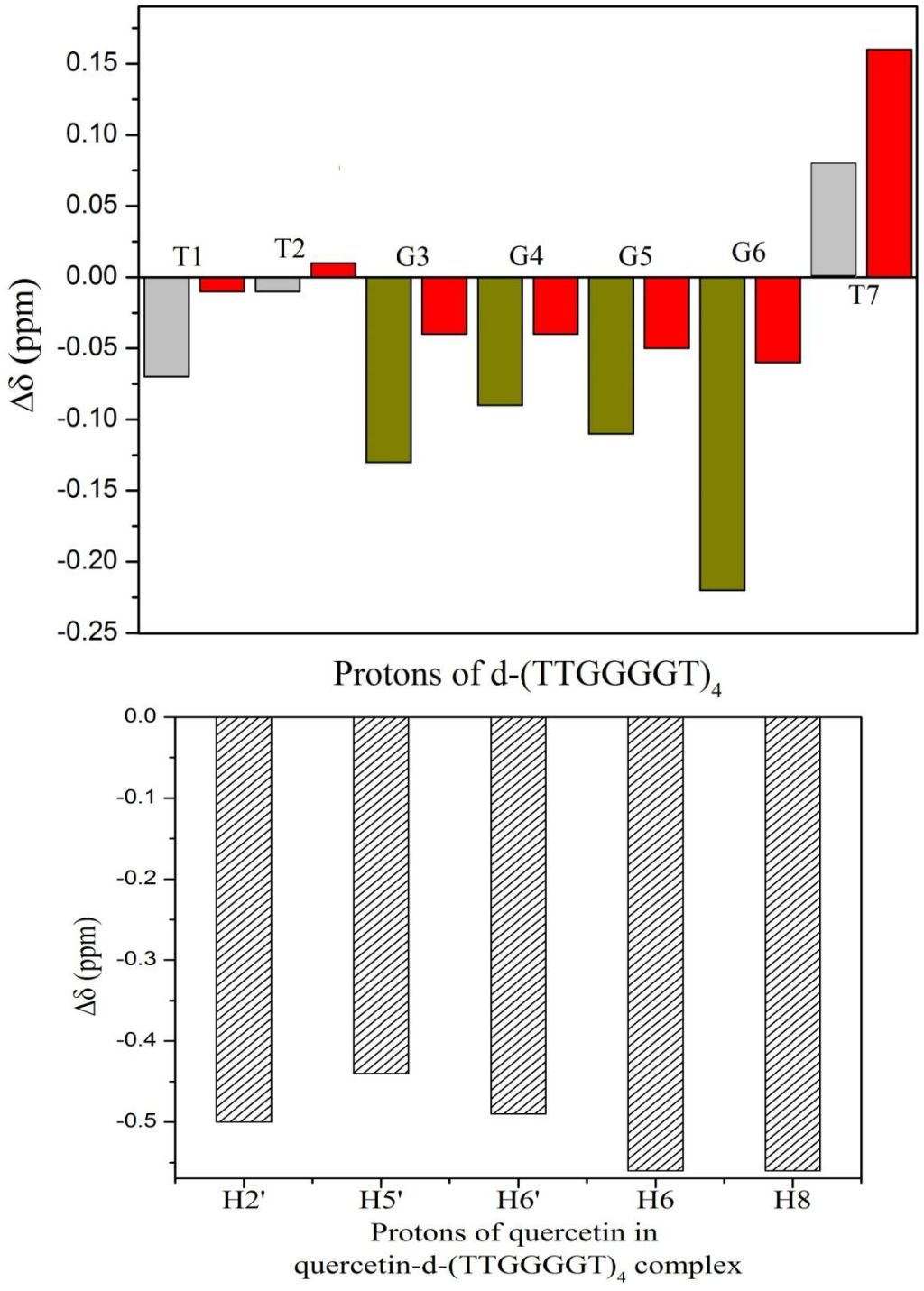

Figure 5.8: Changes in chemical shift position ($\Delta\delta = \delta_{2.0}-\delta_{0.0}$) of d-(TTGGGGT)4 protons and quercetin protons upon complexation (Grey = methyl, dark yellow = guanine imino, red = aromatic H6/H8 protons, unfilled dashes = quercetin protons).

Table 5.8 ^{1}H chemical shift (ppm) of quercetin protons in d-$(TTGGGGT)_4$-quercetin complex as a function of D/N ratio at 298K. $\Delta\delta = \delta_{b\ (D/N\ 2.0)} - \delta_{f\ (D/N\ 0.0)}$. +ve $\Delta\delta$ downfield shift and -ve $\Delta\delta$ upfield shift.

	Quercetin protons				
D/N	H2'	H5'	H6'	H6	H8
0.0	7.54	6.74	7.40	6.04	6.26
0.25	-	-	-	5.38	5.68
0.5	7.00	-	6.94	5.38	5.68
0.75	7.01	-	6.94	5.38	5.68
1.0	7.01	-	6.94	5.39	5.68
2.0	7.04	6.30	6.91	5.48	5.70
$\Delta\delta$	**-0.50**	**-0.44**	**-0.49**	**-0.46**	**-0.56**

Table 5.9 ^{1}H chemical shift (ppm) of quadruplex protons in d-$(TTGGGGT)_4$-quercetin complex as a function of temperature at D/N 2.0. $\Delta\delta = \delta_{b\ (353\ K)} - \delta_{f\ (278\ K)}$. +ve $\Delta\delta$ downfield shift and -ve $\Delta\delta$ upfield shift.

	G3NH	G4NH	G5NH	G6NH	$T1CH_3$	$T2CH_3$	$T7CH_3$
278	11.45	11.07	10.84	10.67	1.67	1.55	1.70
283	11.43	11.05	10.85	10.69	1.63	1.55	1.71
298	11.41	11.02	10.86	10.69	1.60	1.55	1.74
303	11.415	11.02	10.87	10.69	1.61	1.55	1.76
308	11.44	11.07	10.87	10.71	1.61	1.55	1.77
313	11.45	11.03	10.89	10.71	1.63	1.56	1.77
318	11.45	11.03	10.89	10.70	1.64	1.57	1.77
323	11.46	11.04	10.90	10.70	1.65	1.58	1.78
328	11.46	11.045	10.90	10.69	1.67	1.59	1.79
333	11.47	11.05	10.90	10.69	1.68	1.61	1.79
338	11.48	11.06	10.91	10.68	1.69	1.62	1.80
343	11.48	11.06	10.91	10.68	1.70	1.64	1.80
348	11.48	11.07	10.91	10.68	1.71	1.66	1.80
353	11.48	11.07	10.92	10.68	1.72	1.67	1.81
$\Delta\delta$	**+0.03**	**0.00**	**+0.08**	**+0.01**	**+0.05**	**+0.12**	**+0.11**

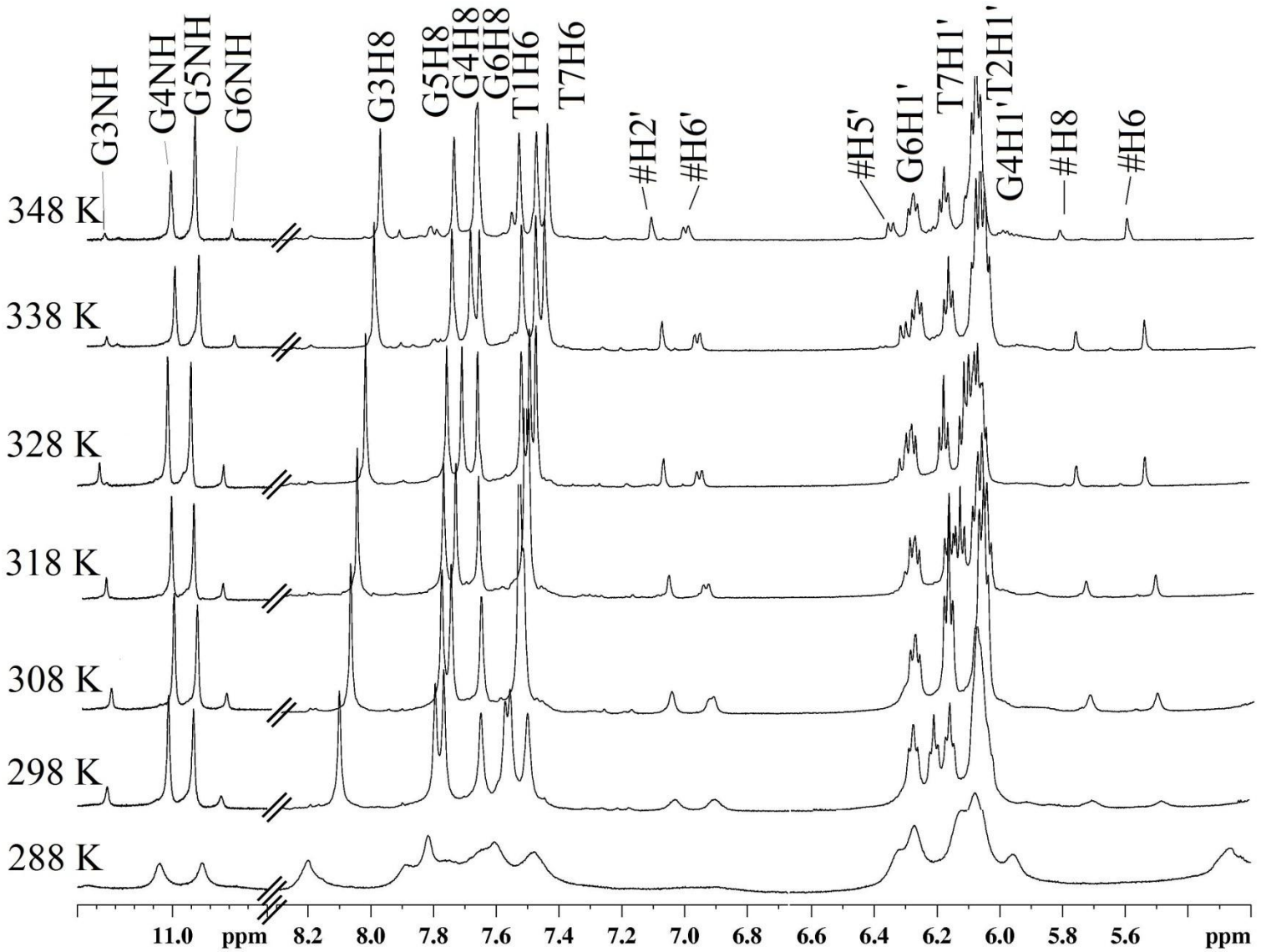

Figure 5.9: (a) Proton spectrum of quercetin complexed d-(TTGGGGT)$_4$ at D/N 2.0 as a function of temperature.

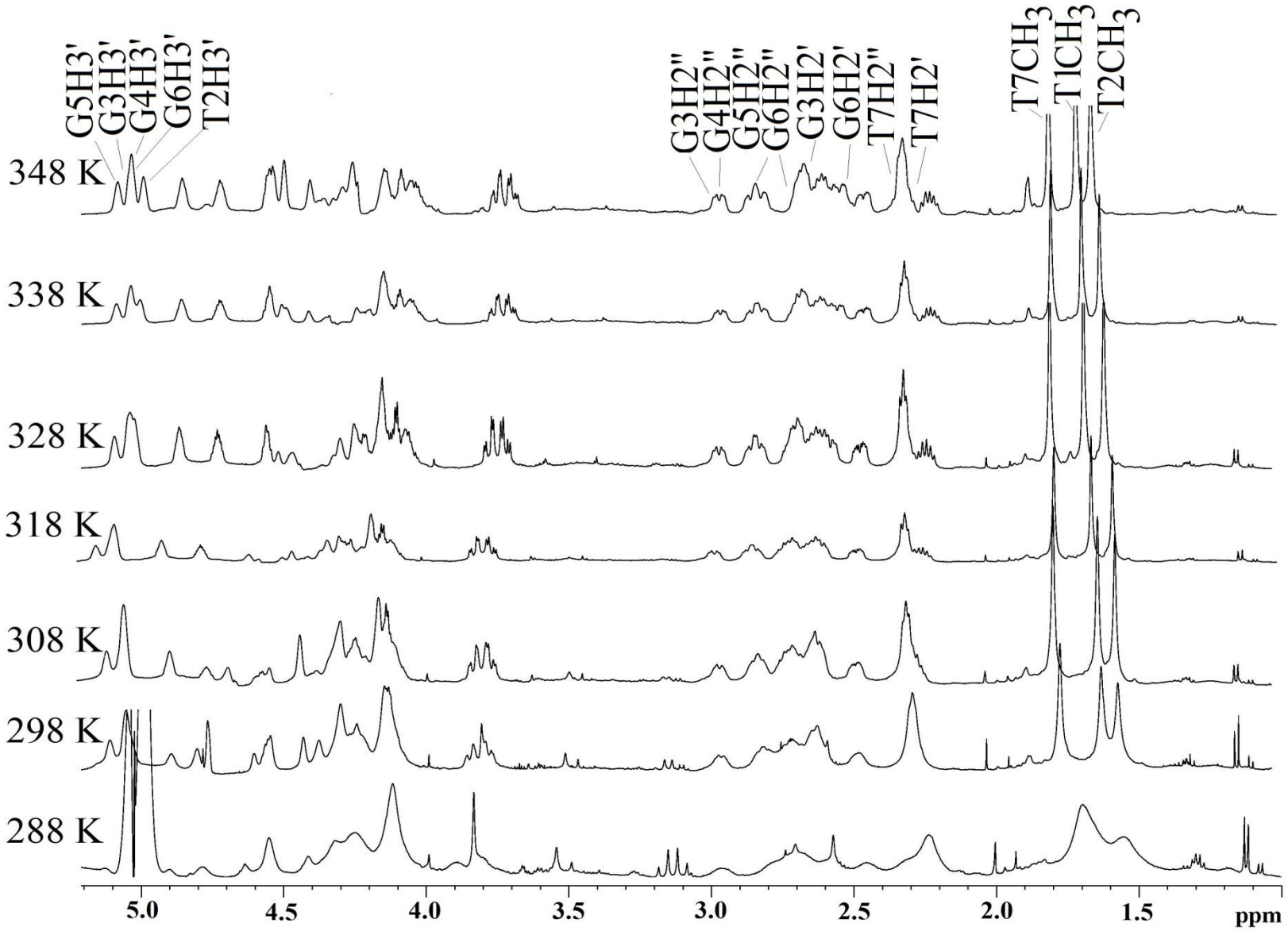

Figure 5.9: (b) Proton spectrum of quercetin complexed d-(TTGGGGT)$_4$ at D/N 2.0 as a function of temperature.

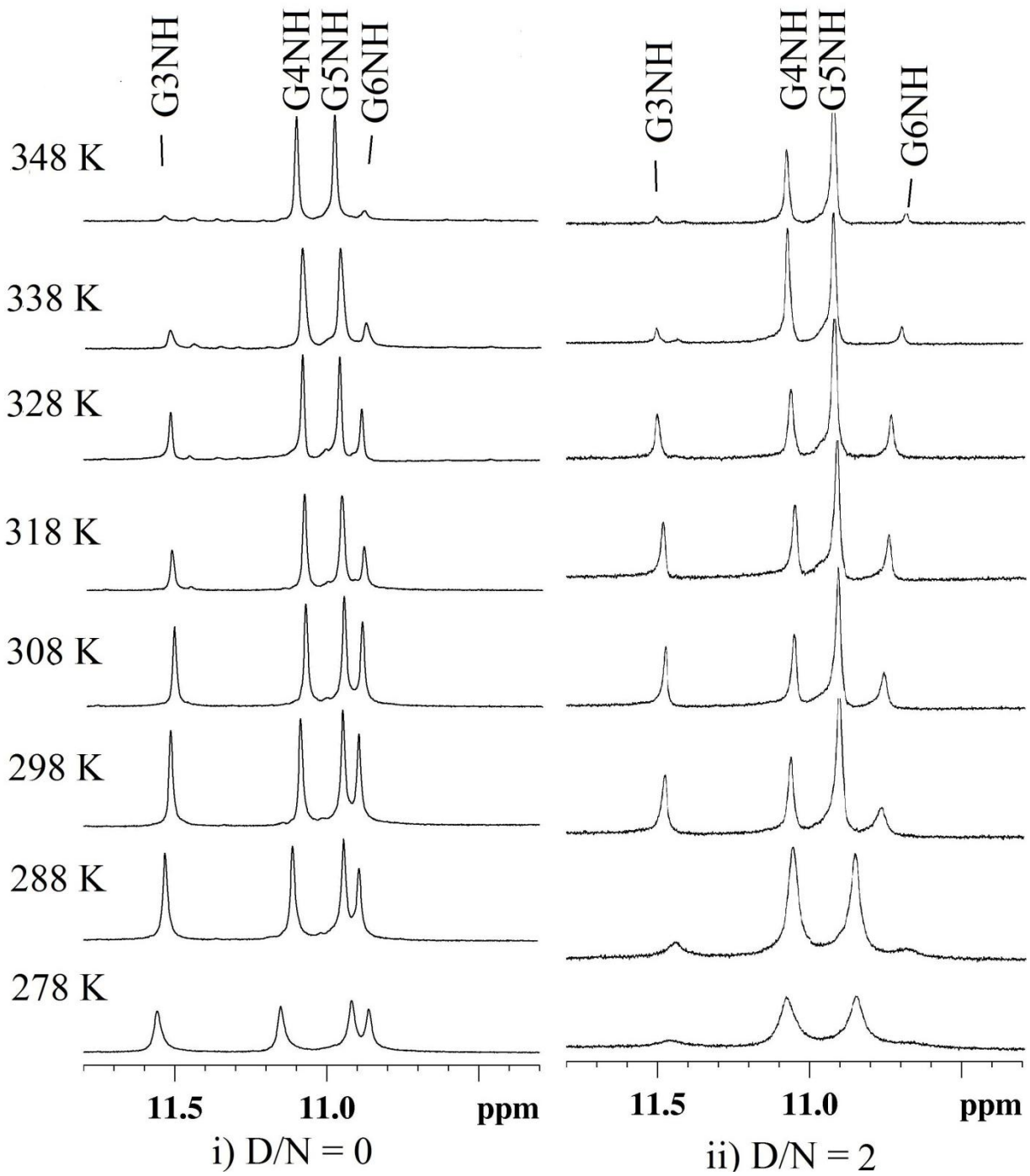

Figure 5.10: Imino melting: Region of Imino protons of uncomplexed d-(TTGGGGT)$_4$ and 2:1 quercetin complexed d-(TTGGGGT)$_4$ at different temperatures.

Table 5.10 ^{1}H chemical shift δ (ppm) of quadruplex protons in d-(TTGGGGT)$_4$-quercetin complex as a function of temperature at D/N 2.0. $\Delta\delta = \delta_{b\ (353\ K)} - \delta_{f\ (278\ K)}$. +ve Δδ downfield shift and -ve Δδ upfield shift.

	T1H6	T2H6	G3H8	G4H8	G5H8	G6H8	T7H6
278	7.64	7.60	8.20	7.81	7.89	7.67	7.48
283	7.66	7.60	8.18	7.81	7.86	7.69	7.49
298	7.58	7.57	8.11	7.78	7.81	7.66	7.51
303	7.56	7.56	8.09	7.77	7.80	7.66	7.52
308	7.54	7.54	8.08	7.76	7.79	7.66	7.53
313	7.52	7.53	8.07	7.75	7.79	7.67	7.53
318	7.51	7.52	8.06	7.74	7.78	7.67	7.52
323	7.50	7.51	8.04	7.73	7.77	7.67	7.53
328	7.48	7.505	8.03	7.72	7.77	7.67	7.53
333	7.47	7.50	8.02	7.71	7.76	7.67	7.53
338	7.46	7.49	8.00	7.70	7.76	7.67	7.54
343	7.45	7.49	7.99	7.69	7.75	7.67	7.54
348	7.45	48	7.98	7.68	7.75	7.67	7.54
353	7.48	7.44	7.97	7.67	7.74	7.67	7.54
Δδ	**-0.16**	**-0.16**	**-0.23**	**-0.14**	**-0.15**	**0.00**	**+0.06**

Table 5.11 ^{1}H chemical shift of quercetin protons in d-(TTGGGGT)$_4$-quercetin complex at D/N 2.0 as a function of temperature. $\Delta\delta = \delta_{b\ (353\ K)} - \delta_{f\ (283\ K)}$. +ve Δδ downfield shift and -ve Δδ upfield shift.

	Quercetin protons				
Temp (K)	H2'	H5'	H6'	H6	H8
278	-	-	-	-	-
283	7.00	-	6.89	-	-
298	7.04	6.30	6.91	5.48	5.70
303	7.05	6.30	6.92	5.50	5.72
308	7.06	6.30	6.93	5.51	5.72
313	7.06	6.30	6.94	5.51	5.73
318	7.07	6.31	6.95	5.51	5.73
323	7.07	6.31	6.96	5.52	5.74
328	7.08	6.31	6.96	5.53	5.75
333	7.08	6.32	6.97	5.55	5.77
338	7.08	6.33	6.98	5.56	5.78
343	7.11	6.34	7.00	5.59	5.8
348	7.12	6.37	7.01	5.60	5.89
353	7.14	6.38	7.03	5.63	5.84
Δδ	**+0.14**	**+0.08**	**+0.14**	**+0.15**	**+0.14**

5.1.5 Phosphorous-31 NMR studies on complex of quercetin-d-(TTGGGGT)$_4$

5.1.5.1 Phosphorous-31 NMR of alone d-(TTGGGGT)$_4$ quadruplex DNA.

Unambiguous assignment of backbone 31-phosphorous resonances of uncomplexed d-(TTGGGGT)$_4$ were done by using standard strategies of ^{1}H-^{31}P heteronuclear multiple bond correlation (HMBC) techniques. The ^{31}P signal which belongs to nth step shows strong correlation with three bond scalar coupled (H3')$_n$ and (H5'/H5")$_{n+1}$ protons and a weak correlation with four bond scalar coupled (H4')$_n$ and (H4')$_{n+1}$ protons. The ^{31}P signals were named as d-(T1pT2pG3pG4pG5pG6pT7) for the six ^{31}P signals of d-(TTGGGGT)$_4$ quadruplex sequence. The 31P resonances were assigned using ^{1}H-^{31}P HMBC spectra of d-(TTGGGGT)$_4$ at 298 K. The assignment of protons of d-(TTGGGGT)$_4$ at 298 K aids in the assignment of 31P resonances by providing the exact position of H3'/H4'/H5'/H5' signals. The terminal ^{31}P resonances of T1pT2 and G6pT7 resonates at -0.437 and -0.712 ppm, respectively. The remaining four signals of T2pG3, G3pG4, G4pG5 and G5pG6 resonates at -0.619, -0.861, -0.733 and -0.831 ppm, respectively. As TTGGGGT sequence forms tetramolecular parallel quadruplex structure, with C4 symmetry, we observe six phosphorous signals for the quadruplex structure. The observed ^{31}P chemical shift range between -0.43 ppm to -0.861 ppm, clearly indicates that the quadruplex adopts right handed helical geometry.

5.1.5.2 Phosphorous-31 NMR of quercetin- d-(TTGGGGT)$_4$ quadruplex DNA.

Behavior of ^{31}P resonances has been monitored as a function of D/N ratios and as function of temperature at D/N 1.0. Fig 5.11 shows the stack of ^{31}P resonances at D/N 0, 0.25, 0.5, 0.75 and 1.0 at 298 K and changes in chemical shift position upon complex formation were mentioned in Table 5.12. Successive addition of quercetin shows the line broadening of all six ^{31}P resonances of d-(TTGGGGT)$_4$, there is no significant chemical shift change observed for any resonances. Downfield shift is observed for resonances of T1pT2, G3pG4, G4pG5 and G6pT7 step, while T2pG3 and G5pG6 step ^{31}P resonances show upfield shift. Resonance of G6pT7 step shows maximum downfield shift of $\Delta\delta$ 0.037 ppm, followed by G4pG5 and T1pT2 ^{31}P resonance, which shows shift of 0.036 and 0.027 ppm, respectively. G5pG6 step ^{31}P resonance show upfield shift by 0.017 ppm. There is no appearance of any extra resonance in the downfield region of the spectrum

upon addition of quercetin till D/N 1.0. ^{31}P resonance shifts downfield by 1.5-2 ppm if a ligand is intercalating into the nucleic acid (Searle et al., 1988, Mazzini et la., 1998). This may be due to the opening of base pair to accommodate the ligand, which results in changing the backbone torsional angle α = O3'-P-O5'-C5' and ζ = C3'- O3'-P-O5' (*Gorenstein et al. 1992; Patel et al. 1974*).

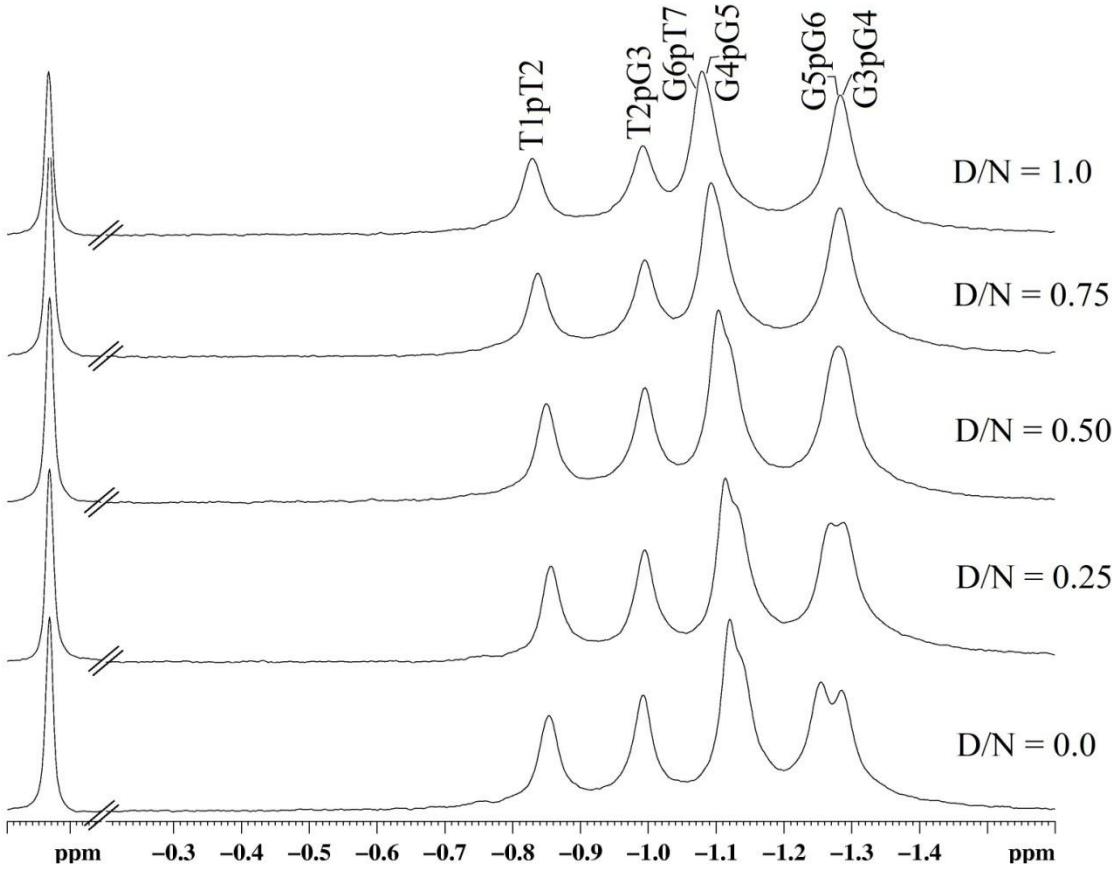

Figure 5.11: Proton decoupled ^{31}P NMR spectra of d-(TTGGGGT)$_4$ in uncomplexed state and complexed with mitoxantrone with increasing quercetin (D) to quadruplex (N) ratio, at 298 K.

There is no data in the literature available for changes in ^{31}P resonance positions with the interaction of ligands with quadruplex DNA. But due to its B-DNA right handed nature, the tetramolecular quadruplex sequence d-(TTGGGGT)$_4$ is expected to show similar behavior as B-DNA after interaction with different class of ligands. The observed chemical shift changes and

absence of any extra resonance in the downfield region upon complexation clearly indicates that quercetin binds to the d-(TTGGGGT)$_4$ quadruplex by external binding mode.

Table 5.12: ^{31}P chemical shift of d-(TTGGGGT)$_4$ protons in d-(TTGGGGT)$_4$-quercetin complex at 298 K as function of D/N. $\Delta\delta = \delta_{b\ (D/N\ 1.0)} - \delta_{f\ (D/N\ 0.0)}$. +ve $\Delta\delta$ downfield shift and -ve $\Delta\delta$ upfield shift.

	^{31}P resonances of d-(TTGGGGT)$_4$					
D/N	T1pT2	T2pG3	G3pG4	G4pG5	G5pG6	G6pT7
0.0	-0.856	-0.991	-1.290	-1.131	-1.261	-1.116
0.25	-0.854	-0.992	-1.288	-1.129	-1.265	-1.112
0.5	-0.850	-0.992	-1.284	-1.121	-1.279	-1.102
0.75	-0.834	-0.992	-1.282	-1.098	-1.279	-1.091
1.0	-0.829	-0.992	-1.281	-1.095	-1.278	-1.079
$\Delta\delta$	**+0.027**	**-0.001**	**+0.009**	**+0.036**	**-0.017**	**+0.037**

Table 5.13: ^{31}P chemical shift of d-(TTGGGGT)$_4$ protons in d-(TTGGGGT)$_4$-quercetin complex D/N 1.0 vs temperature. $\Delta\delta = \delta_{b\ (303\ K)} - \delta_{f\ (278\ K)}$. +ve $\Delta\delta$ downfield shift and -ve $\Delta\delta$ upfield shift.

	^{31}P resonances of d-(TTGGGGT)$_4$					
Temp (K)	T1pT2	T2pG3	G3pG4	G4pG5	G5pG6	G6pT7
278	-1.071	-1.539	-1.755	-1.628	-1.721	-1.539
283	-0.98	-1.361	-1.586	-1.431	-1.565	-1.359
288	-0.916	-1.287	-1.518	-1.378	-1.461	-1.289
293	-0.837	-1.069	-1.344	-1.172	-1.314	-1.136
298	-0.829	-0.992	-1.280	-1.095	-1.278	-1.079
303	-0.812	-0.926	-1.230	-1.054	-1.234	-1.018
$\Delta\delta$	**+0.259**	**+0.613**	**+0.525**	**+0.574**	**+0.487**	**+0.521**

5.1.6 Resonance assignment of quercetin-d-(TTGGGGT)$_4$ complex.

Unambiguous assignment of resonances in 2:1 complex of quercetin-d-(TTGGGGT)$_4$ at 298 K, were done by using various one dimensional and two dimensional experiments like ^{1}H-^{1}H NOESY, ^{1}H-^{1}H COSY and ^{1}H-^{13}C HSQC experiments. The resonances were assigned using strategies mentioned in the section 5.1.2. Fig.5.16 shows the NOESY expansion of aromatic base and sugar H1" protons region, all the correlations between intra base H8/H6 protons with its sugar H1' proton and sequential inter base sugar H8 proton with its 3' end (n+1) base H8/H6 proton were present. Similarly all the sequential correlations between aromatic H8/H6 protons with sugar H2'/H2" protons were present (Fig. 5.17). This shows that d-(TTGGGGT)$_4$ structure doesnot open up to

accommodate quercetin, hence ruling out the possibility of intercalation. The possibility of quercetin intercalating into the any one of the guanine quartet can be ruled out by observation of NOE cross peak between imino resonances of the two successive G-quartet steps. G3NH shows NOE correlation with G4NH, similarly G4NH and G5NH protons show correlation with its 3' flanking G5NH and G6NH protons, respectively (Fig.5.14).

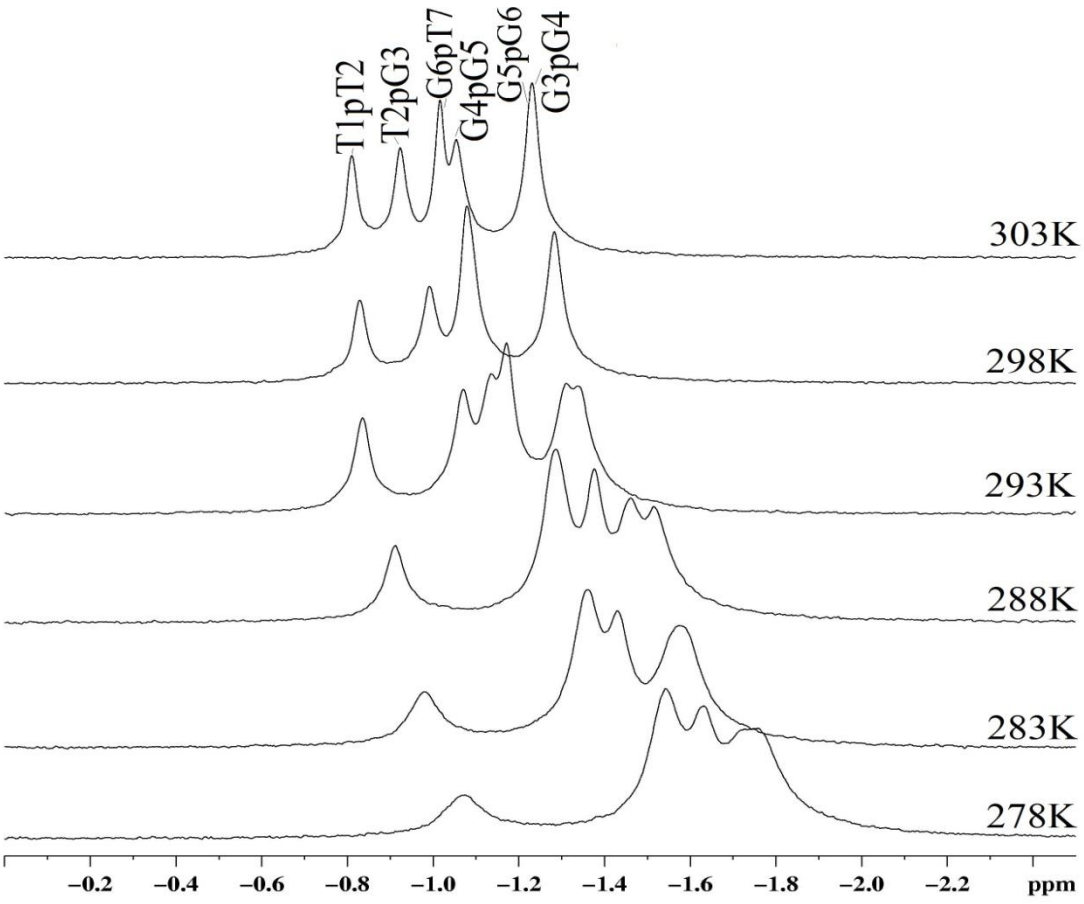

Figure 5.12: Proton decoupled ^{31}P NMR spectra of d-(TTGGGGT)$_4$ complexed with quercetin at quercetin (D) to quadruplex DNA (N) ratio 1.0 as a function of temperature (K).

Once the quadruplex protons were assigned, quercetin resonances were assigned using the correlations present in ^{1}H-^{1}H NOESY and ^{1}H-^{13}C HSQC experiments of complex at D/N 2.0. The monitoring of titration data helps in the identifying the quercetin protons, as resonances of quercetin grow with each increasing DN ratio. The utilization of ^{1}H-^{13}C HSQC experiment to assign quercetin proton helps in the fact that, the aromatic ^{13}C resonances of quercetin molecule resonates in the region between ~ 125 - 90 ppm, while that of quadruplex bases contains aromatic

heterocyclic ring in which ^{13}C resonances resonates between ~ 130 - 140 ppm and the quadruplex sugar 13C resonances appear upfield to ~ 90 ppm. Hence the five ^{1}H and ^{13}C single bond correlations appears between ~ 94-123 ppm in the complex ^{1}H-^{13}C HSQC spectrum belongs to five aromatic protons of quercetin molecule (Fig.5.13 and Table. 5.14).

Table 5.14: HSQC correlation (single bond correlation) of quercetin ^{1}H-^{13}C resonances observed in complex at D/N 2.0 298 K.

Protons	Proton chemical shifts of uncomplexed quercetin in DMSO-*d6* (ppm)	Proton chemical shifts in complex D/N 2.0 (ppm)	C-H correlation in HSQC	Carbon chemical shifts in alone in DMSO-*d6* (ppm)	Carbon chemical shifts in complex D/N 2.0 (ppm)
H2'	7.54	7.04	C2'	115.5	116.75
H5'	6.74	6.30	C5'	116.08	117.42
H6'	7.40	6.91	C6'	120.48	122.91
H6	6.04	5.48	C6	98.66	100.28
H8	6.26	5.70	C8	93.8	95.14

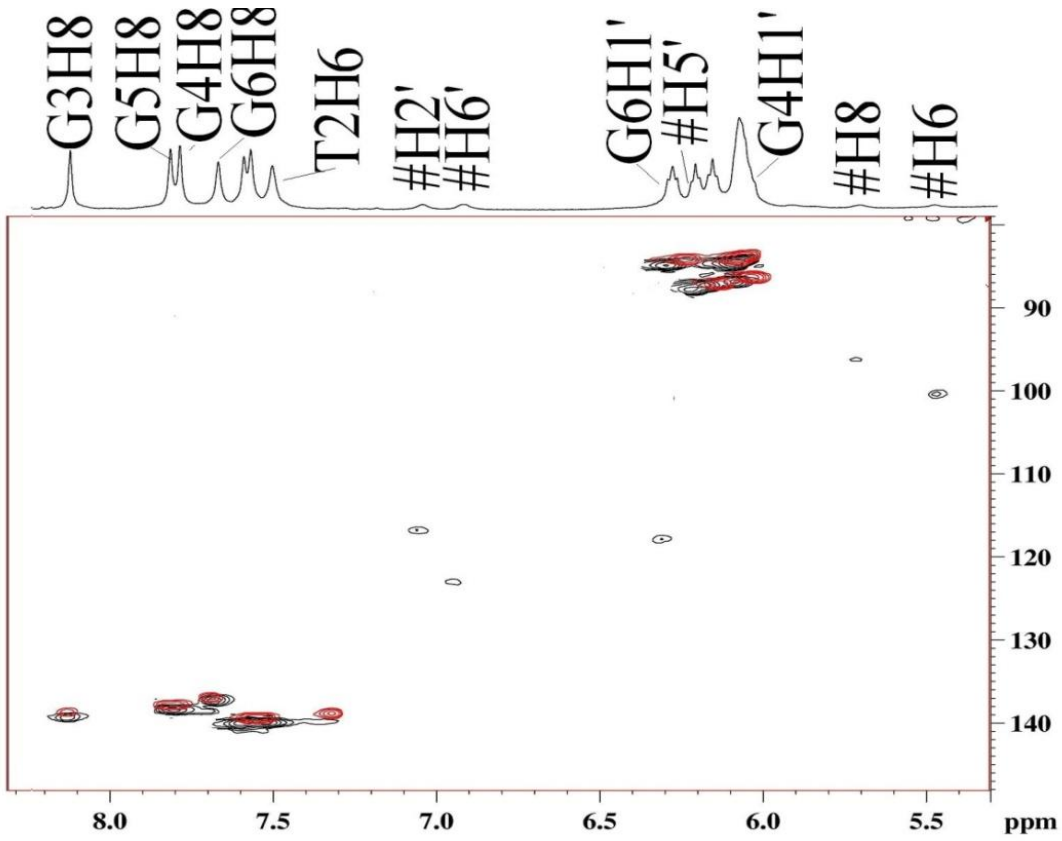

Figure 5.13: Overlap of region of ^{1}H-^{13}C HSQC spectrum of 2:1 quercetin-d-(TTGGGGT)$_4$ complex (black) upon uncomplexed d-(TTGGGGT)$_4$ (red) at 298 K showing quercetin aromatic H2', H6', H5', H8 and H6 protons with their corresponding ^{13}C correlations.

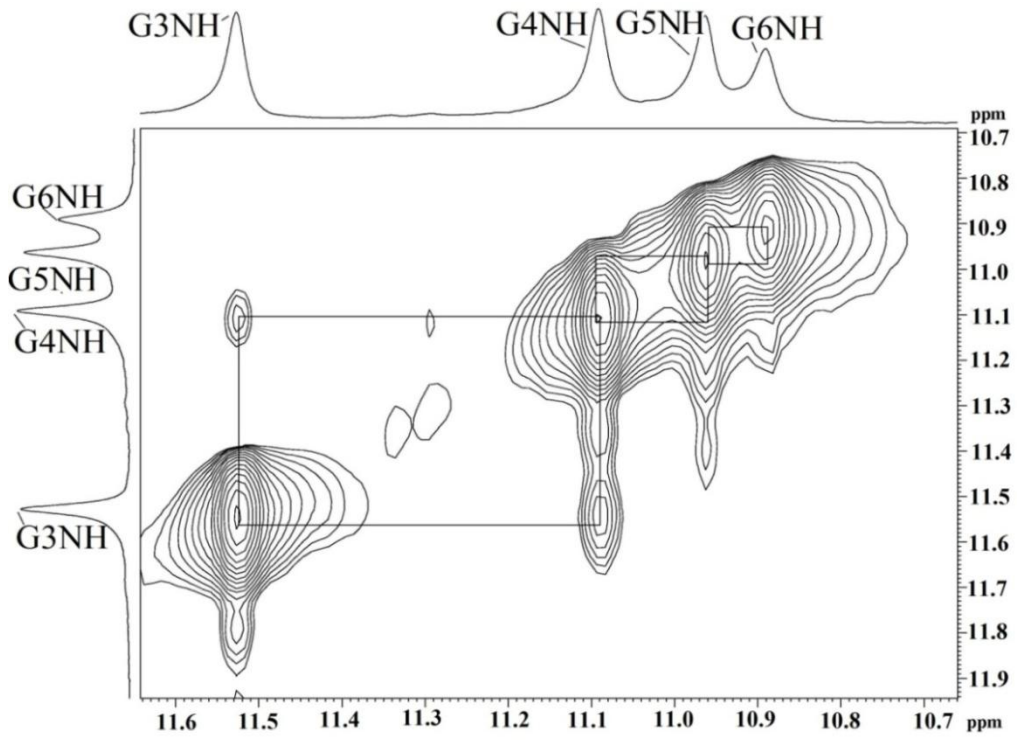

Figure 5.14: NOESY expansion (τ_m =200 ms) of d-(TTGGGGT)4-quercetin complex, D/N 1.0 showing GNH-GNH correlation at 298 K.

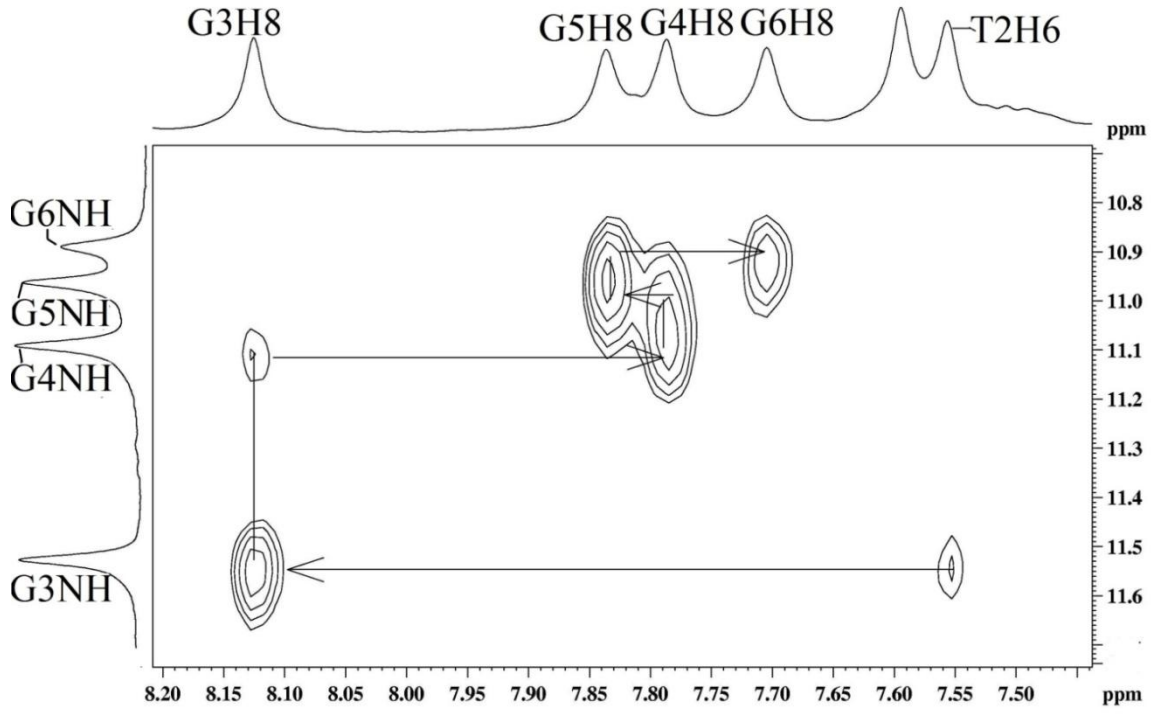

Figure 5.15: NOESY expansion (τ_m =200 ms) of d-(TTGGGGT)$_4$-quercetin complex, D/N 1.0 showing connectivities involved in the G-quartet formation and connectivities between successive G-tetrads at 298 K.

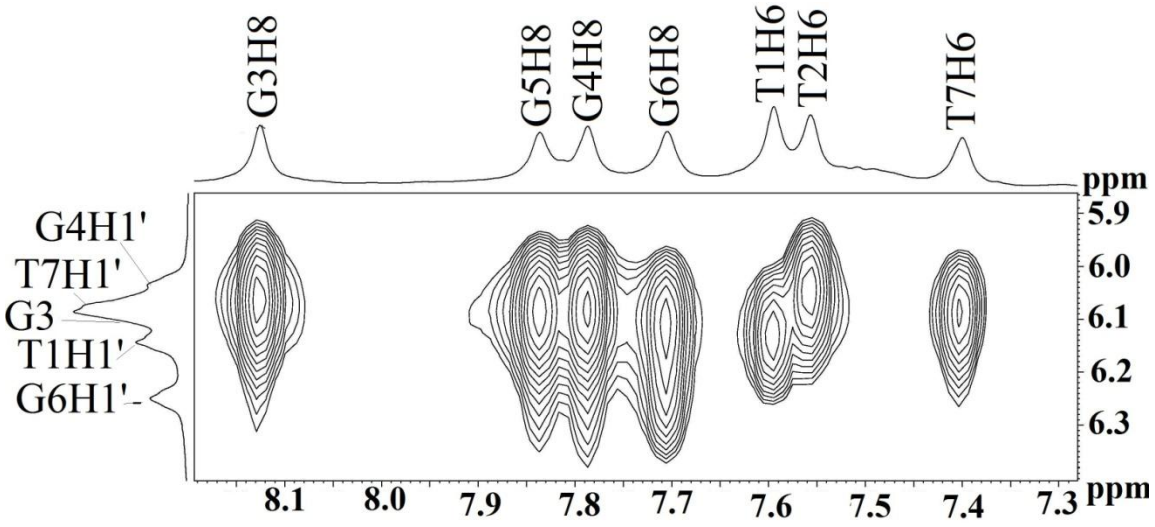

Figure 5.16: NOESY expansion (τ_m =200 ms) of d-(TTGGGGT)$_4$-quercetin complex, D/N 1.0 showing sequential connectivities between aromatic H8/H6 protons with sugar H1' protons.

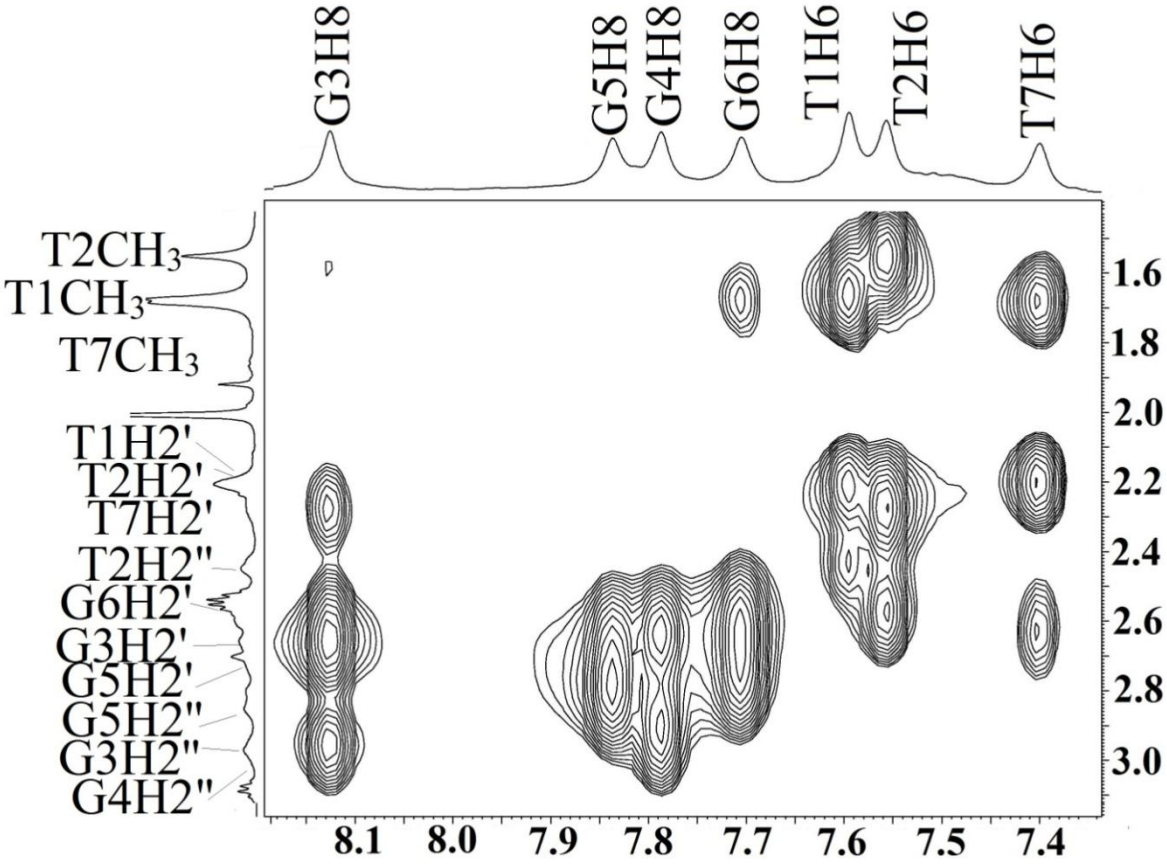

Figure 5.17: NOESY expansion (τ_m =200 ms) of d-(TTGGGGT)$_4$-quercetin complex, D/N 1.0 showing sequential connectivities between aromatic H8/H6 protons with sugar H2'/H2'' protons.

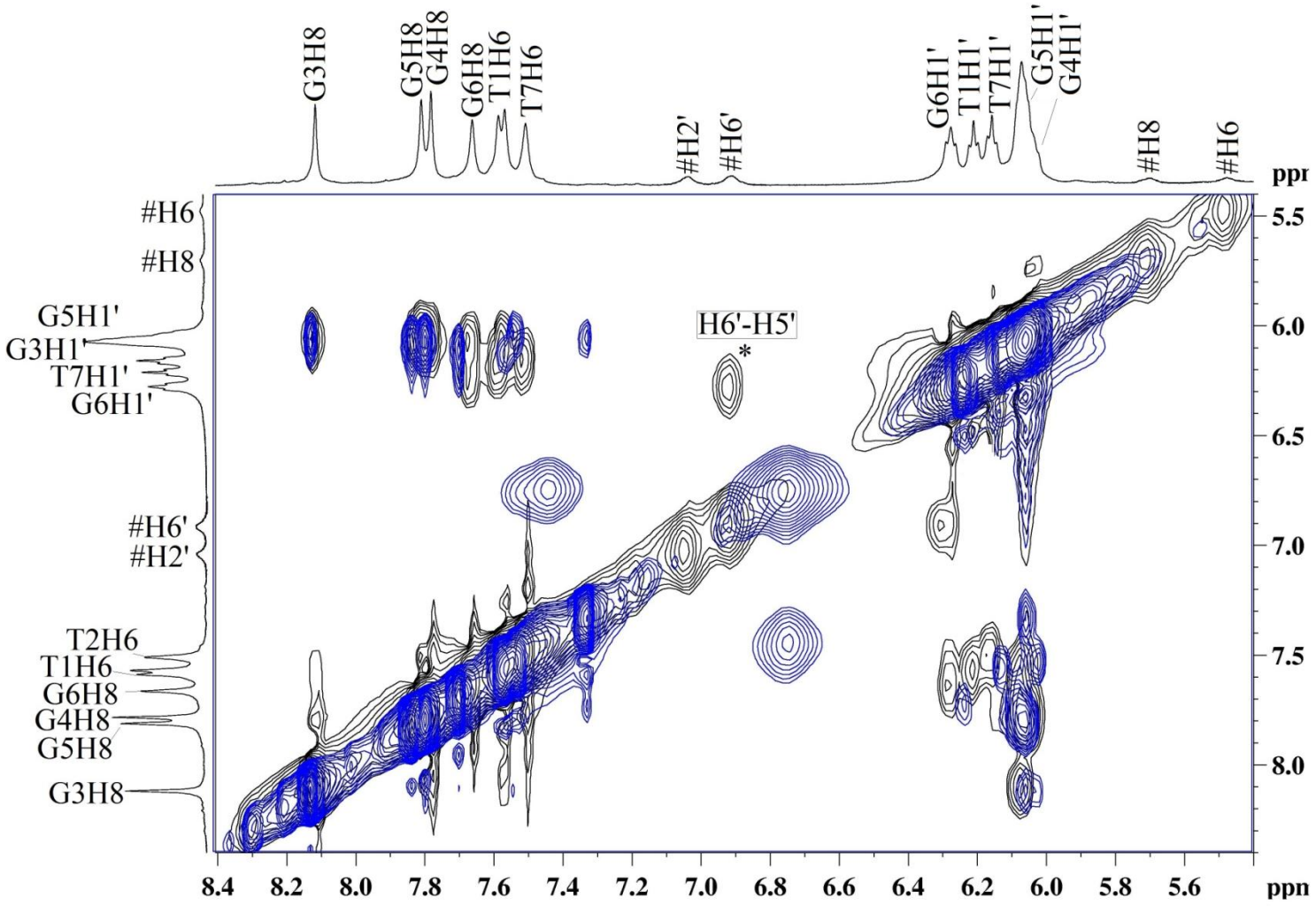

Figure 5.18: NOESY overlap of expansion (τ_m=200 ms) of uncomplexed d-(TTGGGGT)$_4$ and 2:1 quercetin complexed d-(TTGGGGT)4 showing intermolecular contact between quercetin H5'-H6' protons.

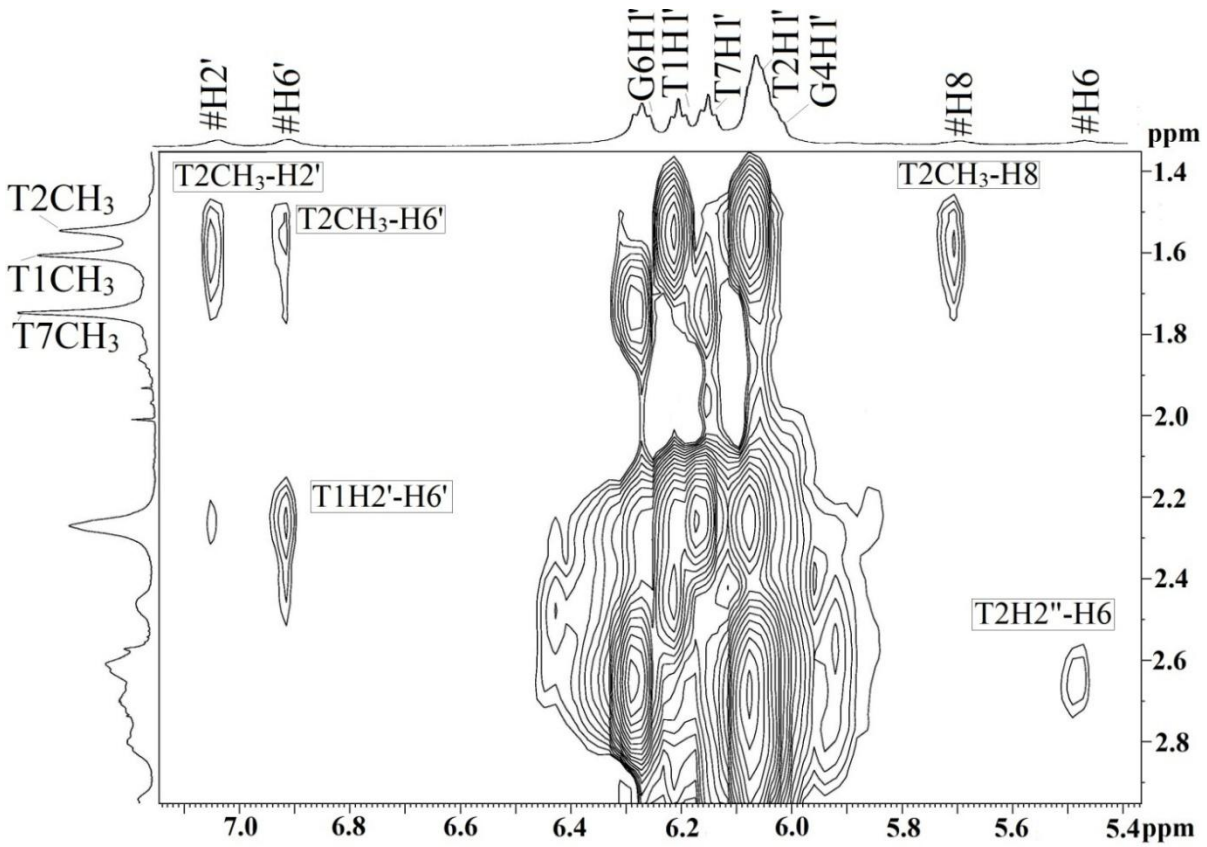

Figure 5.19: NOESY expansion (τ_m =200 ms) of d-(TTGGGGT)$_4$-quercetin complex, D/N 2.0 at 298 K showing quercetin-d(TTGGGGT)$_4$ intermolecular (I) connectivities.

Table 5.15: Intramolecular NOE contacts within the quercetin molecule in quercetin- d-(TTGGGGT)$_4$ complex at D/N = 2.0 at 298 K.

NOE Contacts	Intensity	Distance from NOE (Å)	Distance from rMD (Å)
H5'-H6'	s	2.5	2.47
H5'-H2'	m	4.9	5.0
H2'-H8	w	4.2	4.1
H6'-H8	w	4.6	4.5

The NOESY overlap of expansion of uncomplexed d-(TTGGGGT)$_4$ and quercetin-d-(TTGGGGT)$_4$ at 298 K (Fig.5.18) shows NOE correlation between aromatic H6' and H5' protons of quercetin molecule, as these two protons are scalar (^3J) coupled (distance of ~ 2.44 Å). This

results in very strong NOE correlation peak between them, which can be easily identified. Hence this aids in assignment of aromatic H5' proton of quercetin B ring. This can be further confirmed by ^{1}H-^{13}CHSQC experiments.

The NOESY spectra of quercetin-d-$(TTGGGGT)_4$ complex at D/N ratio 1.0 doesnot show any intermolecular contacts between quercetin and d-$(TTGGGGT)_4$ protons. But increase in quercetin concentration to reach molar equivalent ratio (D/N 2.0) of 2.0 shows the development of new NOE correlations between quercetin and d-$(TTGGGGT)_4$ protons.

The NOESY expansion of quercetin- d-$(TTGGGGT)_4$ complex of D/N 2.0 at 298 K (Fig.5.19) shows NOE correlations (intermolecular contacts) between quercetin and d-$(TTGGGGT)_4$ protons (labeled as #). Total 15 intermolecular NOE contacts were observed between quercetin and d-$(TTGGGGT)_4$ quadruplex protons. The maximum number of NOEs were observed between protons of quercetin B ring with quadruplex protons. Due to the overlapping with G6H1' proton resonance, intermolecular contacts of H5' proton and quadruplex DNA could not be assigned properly. The NOE cross peaks were observed between the aromatic protons of quercetin with T1 and T2 step methyl and sugar H2'/H2" protons. The aromatic A ring H6 proton gives medium intensity NOE correlation with G3H2' proton. Absence of NOE correlations between quercetin and G3pG4, G4pG5, G5pG6 and G6pT7 step protons of the quadruplex DNA clearly suggest that, quercetin molecule is interacting with T1pT2 step.

The observed intermolecular contacts (I peaks), distances obtained from integration of NOE volume are listed in Table 5.16. The interproton distances present were separated into weak (w), medium (m) and strong (s) based on the intensity of NOE cross peaks. All the observed intermolecular NOEs between quercetin and d-$(TTGGGGT)_4$ cross peaks were in the range of medium to weak. These intermolecular contacts provide the direct insight into the possible orientation of quercetin molecule in the binding site. Out of the observed 14 intermolecular contacts, 11 contacts belong to T2 residue with quadruplex. Quercetin H6' and H8 protons shows medium range NOE contacts with quadruplex T2H2' and $T2CH_3$ protons, respectively. The $T1CH_3$, $T2CH_3$ and T2H2'/H2" protons occupy the groove region of the d-$(TTGGGGT)_4$ quadruplex structure, the observed NOEs between quercetin and d-$(TTGGGGT)_4$ indicates the possibility of quercetin binding to the groove region of quadruplex.

Table 5.16: Intermolecular NOE contacts between quercetin and d(TTGGGGT)$_4$ in quercetin-d(TTGGGGT)$_4$ complex (τ_m = 200 ms) at D/N = 2.0 at 298 K.

Sl No	Intermolecular NOEs	Intensity	Distance from NOE (Å)	Distance from rMD model (Å)
I1	H2'- T1CH$_3$	w	4.4	4.3
I2	H2'- T2CH$_3$	w	4.0	3.8
I3	H2'- T2H2'	w	4.5	3.6
I4	H2'- T2H2"	w	4.6	4.8
I5	H6'- T1CH$_3$	w	4.3	4.1
I6	H6'- T2CH$_3$	w	4.1	4.0
I7	H6'- T2H2'	m	3.5	3.5
I8	H6'- T1H2"	w	4.1	4.0
I9	H6- T2H2"	w	3.8	3.7
I10	H6- T2H2'	w	4.0	3.9
I11	H6- G3H2'	w	4.0	4.05
I12	H8- T1CH$_3$	w	4.0	4.1
I13	H8- T2CH$_3$	m	3.4	3.6
I14	H8- T2H2'	w	4.0	3.9

All the obtained NOEs The observed chemical shift changes of d-(TTGGGGT)$_4$ protons upon complex formation (Table.5.16) contradicts the observed NOEs between quercetin and d-(TTGGGGT)$_4$ protons. Generally, chemical shift perturbation of protons is more in the ligand binding site, as binding affects the chemical and electronic property of interacting protons. Whereas, in our study, protons of G6pT7 step shows more chemical shift variation when compared with the protons of the other steps. While none of the observed intermolecular quercetin-d-(TTGGGGT)$_4$ NOE contacts belong to this step.

The presence of base H8/H6 - sugar H1' /H2'/H2" sequential connectivities and guanine imino-imino (GNH) NOE connectivities between successive G-quartet planes (G3:G4:G5:G6) in the NOESY spectrum of 2:1 quercetin complexed d-(TTGGGGT)$_4$ excludes intercalative mode of binding by quercetin. The absence of extra bound resonances in the downfield region (> 1.5 ppm) of ^{31}P spectrum also supports this conclusion. More over GNH protons does not show any large

upfield shift ($\Delta\delta_{max} \approx 0.14$ ppm) as reported for well known quadruplex end stackers like TMPyP4 ($\Delta\delta_{max} = 0.21$ ppm) (*Mita et al. 2006*) and RHPS4 ($\Delta\delta_{max} = 0.45$ ppm) (*Gavathiotis et al. 2003*). Magnitude of chemical shift change observed in quadruplex protons upon quercetin binding is also very less. The chemical shift changes of G-imino protons in our studies ($\Delta\delta_{max} = 0.14$ ppm upfield shift) is comparable to that of the changes observed in-that of G-imino protons of d-(TGGGGT)4-distamycin-A complex ($\Delta\delta_{max} = 0.18$ ppm upfield shift) (*Martino et al. 2007*) and also in d-(TGGGGT)4-distamycin analogue/derivative complex ($\Delta\delta_{max} = 0.15$ ppm upfield shift) (*Cosconati et al. 2010*). Distamycin and its derivatives interact with tetramolecular quadruplex structure via a groove binding mode. These results shows that quercetin molecule interacts with quadruplex structure via external binding mode like groove binding.

Studies suggest that quercetin molecule interacts with double stranded nucleic acids via intercalative mode of binding (*Solimani, 1996*). But all these reports explain the binding behavior on the basis of UV-Vis, fluorescence spectroscopic changes upon binding and enzymatic assays, until date no high resolution NMR or X-ray structures have been reported for quercetin complexed nucleic acids. Quercetin was also shown to interact with tetramolecular human quadruplex DNA via end-stacking or groove binding mode depending upon the structure of quadruplex DNA (*Sun et al., 2006*). The one dimensional NMR studies of quercetin interaction with quadruplex shows upfield shift of guanine NH protons by 0.1 ppm. But these reports provide shifts in resonance due to quercetin-quadruplex interaction. The changes in chemical shift position upon ligand binding in drug-DNA interaction studies helps in predicting the binding type and binding site rather than elucidation of exact structure adopted upon interaction and numerous energy terms associated with binding. Therefore our study provides the valuable information on intermolecular interactions between quercetin and quadruplex structure, which helps in determining the exact binding mode for quercetin biding to tetramolecular G-quadruplex DNA sequence d-$(TTGGGGT)_4$.

5.1.7 Restrained Molecular dynamics

To obtain the distances NOE peaks at mixing time of 200ms in quercetin-d-$(TTGGGGT)_4$ complex, D/N 2.0 at 298 K was used. The NOE peaks were integrated using SPARKY software (*Goddard. T. D and Kneller. D. G, University of California, San Francisco*) and distances obtained were calculated using the methodology given in section 2.14. The distance between aromatic H5'-H6' protons of quercetin (2.44 Å) was use as a standard reference distance to calculate the

distances. Distances obtained by above mentioned step can be cross verified using the distance of T7CH_3-H6 (2.99 Å).

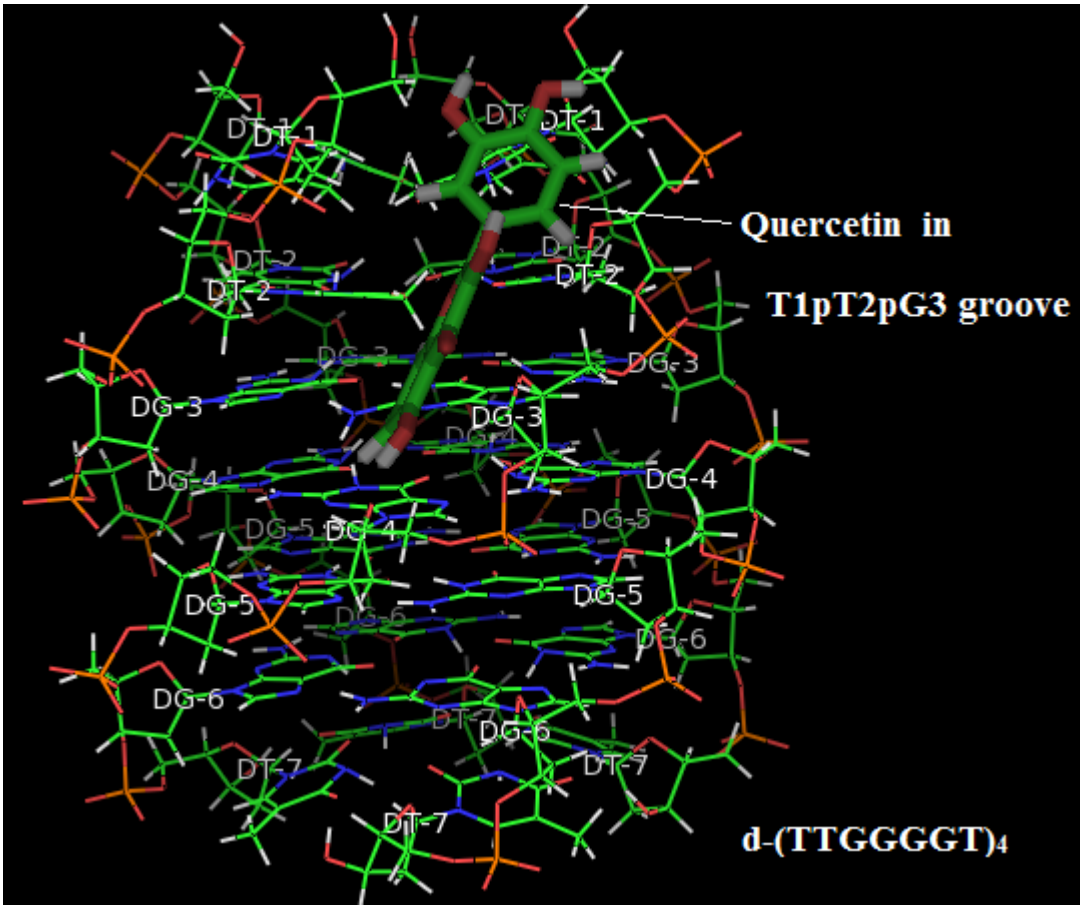

Figure 5.20: Model of final complex of quercetin with d-(TTGGGGT)$_4$ after rMD simulations using constraints from 2:1 ratio quercetin-d-(TTGGGGT)$_4$ complex NOESY experiment (200 ms) at 298 K.

The inter and intra molecular distances obtained in quercetin- d-(TTGGGGT)$_4$ complex were classified into three categories, namely i) intermolecular distances between quercetin and d-(TTGGGGT)$_4$ protons, ii) intra molecular distances obtained between protons of quercetin molecule and iii) intra molecular distances between protons of d-(TTGGGGT)$_4$. Based on this, obtained NOE restraints were classified into quadruplex-quercetin constraints, quercetin-quercetin constraints and quadruplex-quadruplex constraints. These distances were used as NOE restraints to build a structure using restrained molecular dynamics simulation protocol. The PDB ID for tetramolecular quadruplex d-(TTGGGGT)$_4$ 139D (Wang and Patel, 1994) was used for building

quadruplex structures. The potentials of the atoms were changed to suit the potential setup of CVFF force field provided by INSIGHT II. Initial quercetin structure was built using the builder module of INSIGHT II, version 2005 (Accelyrs Inc., San Diego, California) on Silicon Graphics Fuel (SGI) workstation and energy minimized using biopolymer module. The distances obtained from 200 ms NOESY spectra of quercetin-d-$(TTGGGGT)_4$ complex at 298 K were used as quercetin intramolecular restraints. The energy minimized structures were used as starting templates to build a final model.

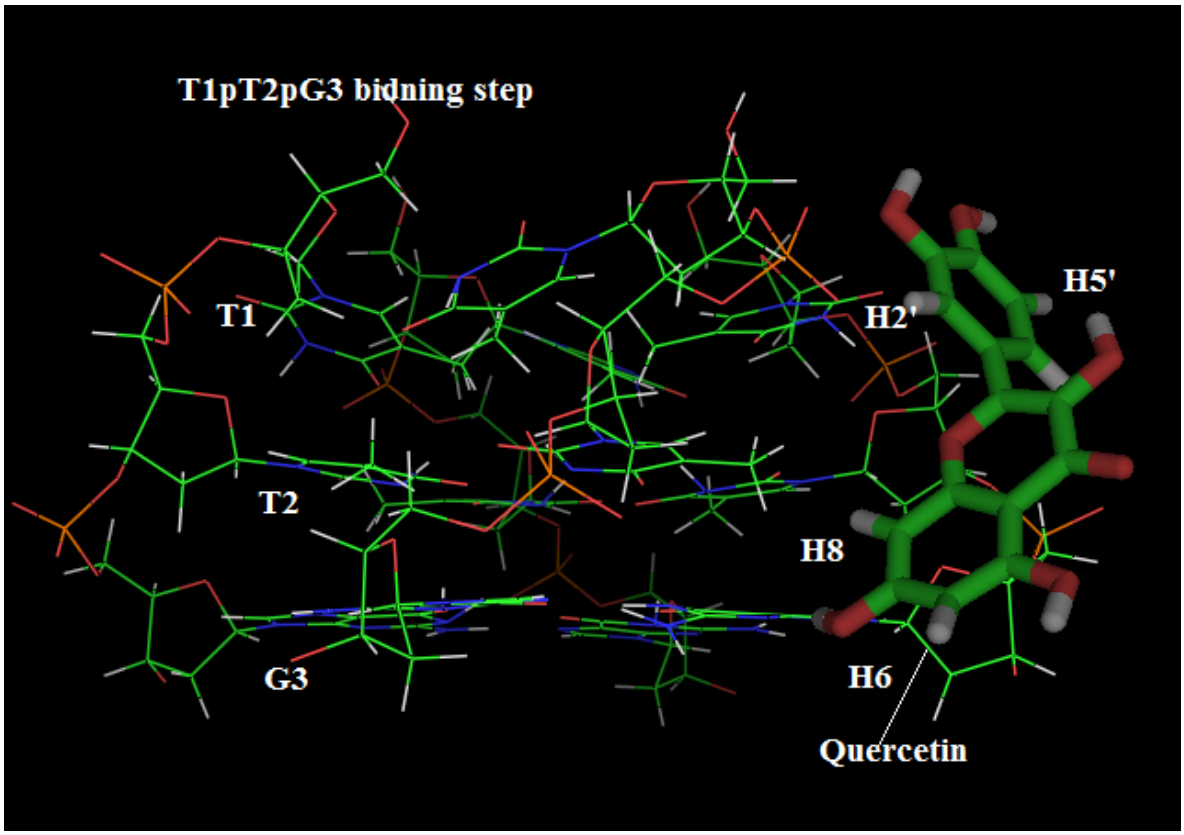

Figure 5.21: Model of final complex of quercetin with d-$(TTGGGGT)_4$ after rMD simulations using constraints showing groove binding of quercetin to T1pT2pG3 step of quadruplex.

The quercetin molecule was placed in the groove region of the quadruplex DNA such that all constraints between quercetin and d-$(TTGGGGT)_4$ were met satisfactorily. Once the quercetin molecule is placed in the binding site, i.e groove region of T1pT2 step, the quercetin-quadruplex, intramolecular quercetin-quercetin and quadruplex-quadruplex NOE restraints were incorporated using generic distance option of the Discover module with a force constant of 25, 15, 10 Kcal mol^{-1} $Å^{-2}$ for strong, medium and weak interactions, respectively. Apart from NOEs obtained from our

studies planar constraints between guanines in G-quartet planes were used in order to stabilize the repulsion due to centrally located four oxygen atoms of a G-quartet.

Table 5.11: Structural data and energy terms of the final quercetin-d-$(TTGGGGT)_4$ complex.

Experimental Restraints	
Intramolecular	
Quercetin-Quercetin	4
Quadruplex-Quadruplex	240
Intermolecular	
Quercetin-quadruplex	14
CVFF energy (kcal mol^{-1}) of the minimized structures	
Total	184.6
Torsional	3361.1
Electrostatic	-155.4
Restraint	101.6
Average rmsd	0.21Å
Restraint Violations	
Distance (>0.5Å)	8

Analysis of the final structure shows that the quercetin molecule occupies the groove region of d-$(TTGGGGT)_4$ quadruplex near 5'-end T1pT2pG3 step. The quercetin binds to quadruplex such that its aromatic protons H6' and H8 were close to T2 sugar ring and CH_3 group (Fig. 5.20 and Fig 5.21). The tetramolecular quadruplex structure formed by d-$(TTGGGGT)_4$ sequence has more ordered 5'-terminal T1pT2 residues when compared to tetramolecular structure formed by human single repeat telomeric sequence d-$(TTAGGGT)_4$ (*Gavathiotis et al. 2003*). Hence binding of quercetin to the groove region of d-$(TTGGGGT)_4$ is energetically favorable. Moreover stacking interaction of quercetin is not energetically favorable, as aromatic surface of quercetin molecule is small when compared to the aromatic surface of other well known quadruplex end stackers like PIPER (*Fedoroff et al. 1998*), TMPyP4 (*Mita et al. 2006*), RHPS4 (*Gavathiotis et al. 2003*). The obtained ΔT_m value of ~ 5 K from imino proton melting studies also supports the external groove binding rather than end stacking binding mode, which results in larger ΔTm value of ~15 K (*Ferreira et al. 2013*). Therefore based on the detailed one and two-dimensional NMR experiments, we are proposing that quercetin binds to the tetramolecular G-quadruplex structure by external groove binding mode and stabilizes the structure.

5.2 TRAP assay

PCR based two steps telomeric repeat amplification protocol (TRAP) assay (*Kim et al. 1994, Wright et al. 1995*) was used to assess the level of telomerase inhibition by quercetin molecule. After the telomerase elongation step, the ligand was added prior to that of PCR elongation. This effectively reduces the ligand inhibiting the telomerase or polymerase enzyme. The modified protocol helps in ligand interacting with G-quartet structures formed prior to PCR step. Telomerase extract from MCF-7 cell lines were selected as it has more telomerase activity than available cancer cell types, and has been well documented in literature (*Ramachandran et al. 2002, Herbert et al. 2006*). The detailed protocol was given in section 2.9. The quercetin concentration in the range of 0.1 μM to 100 μM was used to check the telomerase inhibition activity.

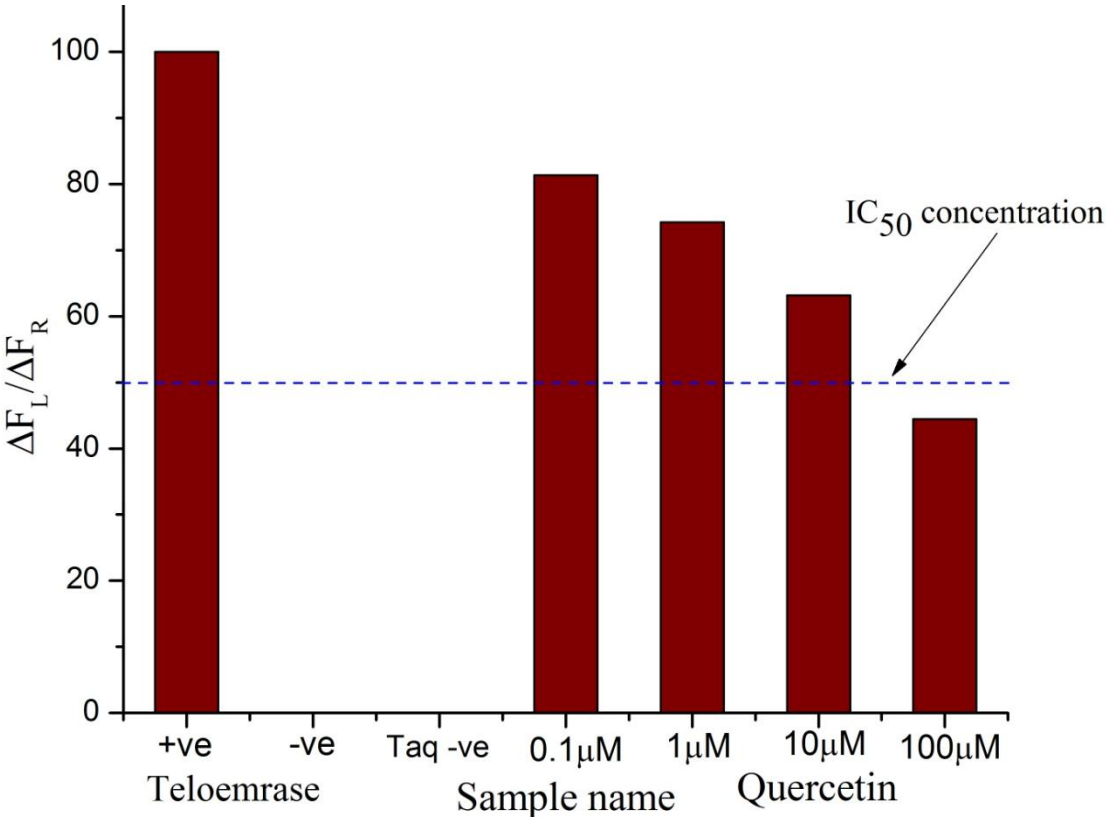

Figure 5.23: TRAP assay of quercetin, showing $\Delta F_L/\Delta F_R$ values from fluorescence based assay.

The assay procedure utilizes the fluorescent tags of fluorescein and sluphorhodamine for the final detection of telomerase activity. The $\Delta F_L/\Delta F_R$ value of untreated telomerase positive cells were

used as positive control and the vales of sample without telomerase used as negative control. Quercetin in the concentration range of 0.1 μM to 100 μM was used.

Analysis of the results (Fig 5.23) shows that quercetin at concentration of 10 μM shows 30 % inhibition of telomerase activity, but at 100 μM concentrations it shows 60 % inhibition. Hence the effective IC_{50} value of quercetin is about ~ 45 μM. Quercetin and other flavonoids are shown to have anti-cancer properties. Even though quercetin inhibits several processes in cancer development and progression its effect on telomerase activity has not been reported in literature. Menichincheri and Co-workers reported the telomerase inhibition activity of tetra-hydroxy flavones and its derivatives (*Menichincheri et al. 2004*), but penta-hydroxy flavonol, i.e. quercetin is having prominent position among flavonoids due to its benefits as anti-oxidative and anti-cancer agent. Our structural and cell based assay results shows effective inhibition of telomerase through G-quadruplex stabilization by quercetin. Therefore stabilization of G-quadurplex acts as one of the important mechanism, through which quercetin exerts its anti-tumor activity.

5.3 Summary and Conclusion

Quercetin is an important flavonoid representative, as it shows numerous health benefits like antioxidant activity, anti-inflammatory effect, cardio-vascular protection, anti-tumor activity, anti-allergic activity, anti-bacterial, anti-viral, anti-helminthes activity. Its anti-cancer activity is mainly attributed to its topoisomerase I poisoning activity, but it also shows binding and stabilization of G-quadruplex structure. Hence it can be effectively used to inhibit the activity of telomerase enzyme, an important cancer marker. In this chapter we studied the interaction of quercetin of with tetra molecular parallel G-quadruplex structure formed by d-$(TTGGGGT)_4$ using various one and two dimensional NMR studies.

Presence of four proton resonances in Hoogsteen base pairing region shows that given sequence forms Hoogsteen hydrogen bonded structure. The presence of NOEs between G3NH and G3H8 and also G3H8 with G4NH, and so on shows that square planar arrangement of Hoogsteen bonded G-quartets. Presence of H8/H6-H1' and H8/H6-H2'/H2" sequential connectivities shows that structure adopts right handed geometry with all guanines in *anti*- conformation.

Addition of two mol equivalents to quercetin to d-$(TTGGGGT)_4$ quadruplex DNA results in development of new intermolecular and intra molecular NOEs between quercetin and quercetin-d-

$(TTGGGGT)_4$ protons. Total of 15 inter molecular NOE peaks were observed between quercetin and d-$(TTGGGGT)_4$ protons, most of which with the TCH_3, TH2' and TH2" forms the groove region of quadruplex. Further absence of inter molecular NOEs between quercetin and any G step protons, and presence of GNH-GNH NOE correlation and all sequential connectivities proves that G-quartet doesnot open up. Hence discarding the intercalation mode of binding by quercetin to d-$(TTGGGGT)_4$ quadruplex structure. Moreover the final energy minimized structure shows quercetin binds to the T1pT2pG3 step groove region of d-$(TTGGGGT)_4$ quadruplex structure.

Binding of quercetin results in stabilization of d-$(TTGGGGT)_4$ quadruplex structure. This can be proved by Hoogsteen hydrogen bonded G-tetrad imino proton melting studies using NH line shapes. Dissociation of G-quartets at higher temperature results in the exchange of GNH proton with solvent water and hence decreased intensity of these protons. Uncomplexed d-$(TTGGGGT)_4$ shows melting temperature of (T_m) of 348 K and addition two mol equivalents of quercetin results in the increase in meting temperature to 353 K. Hence ΔT_m of 5 K suggests that quercetin molecule stabilizes the G-quadurplex structure.

Finally the TRAP assay results showed that quercetin inhibits telomerase activity at effective IC50 valve of ~ 45 μM. Hence our solution NMR studies show quercetin interacts with tetramolecular G-quadruplex structure by groove binding at T1pT2pG3 step and cell based assay results shows effective inhibition of telomerase through G-quadruplex stabilization by quercetin. Therefore stabilization of G-quadurplex acts as one of the important mechanism, through which quercetin may exert its anti-tumor activity.

Chapter 6

Studies on interaction of flavonoid glycoside rutin with tetramolecular parallel telomeric sequence d-$(TTGGGGT)_4$ by Nuclear Magnetic Resonance spectroscopy and restrained Molecular Dynamics simulations

The knowledge of stabilization of G-quadruplex structure in telomere regions, leads to the inhibition of telomerase enzyme activity. This strategy could potentially be used to develop effective anti-cancer agents. In the present chapter, we investigate the mode of interaction of an important flavonoid glycoside, rutin with tetramolecular parallel telomeric DNA sequence d-$(TTGGGGT)_4$. To elucidate the mode of binding various one and two dimensional Nuclear Magnetic Resonance (NMR) spectroscopic experiments were done. Inter-proton distances obtained from two dimensional NMR techniques were used as distance restraints to obtain final energy minimized structure of rutin-d-$(TTGGGGT)_4$ complex. The present chapter contains the following experiments and their interpretation in analyzing the rutin-d-$(TTGGGGT)_4$ complex by using both one and two-dimensional ^1H, ^{13}C and ^{31}P NMR experiments and restrained molecular dynamics simulations.

- 1D ^1H and ^{13}C NMR and 2D ^1H-^1H ROESY, TOCSY, COSY and ^1H-^{13}C HSQC study of rutin at 298 Kin DMSO-d_6.
- 1D ^1H NMR titration studies of rutin-d-$(TTGGGGT)_4$ complex at various drug (D)/DNA quadruplex (N) ratios of 0.25, 0.5, 0.75, 1.0 and 2.0 at 278, 283 and 298 K in 90% water and 10% D_2O.
- 1D NMR study as a function of temperature in the range 278-353 K at D/N = 2.0.
- ^{31}P 1D NMR study as a function of D/N 0.25, 0.5, 0.75, 1.0 and as a function of temperature at D/N 1.0.
- 2D NOESY at D/N = 1.0, using mixing time τ_m = 200, 250 ms at 278 and 298 K and at D/N 2.0, τ_m = 200 at 298 K in 90% H_2O and 10% D_2O.
- ^1H-^{13}C HSQC spectrum of rutin- d-$(TTGGGGT)_4$ complex D/N 2.0 at 298K.

• Restrained molecular dynamics studies on the solution structure for the complex of rutin with d-$(TTGGGGT)_4$ in drug to DNA quadruplex ratio of 2:1 using inter-proton distances obtained from 200 ms NOESY experiment.

6.1 Results and Discussion

6.1.1 NMR studies of rutin

Unambiguous assignment of all proton and carbon resonances of rutin molecule were done by using various NMR techniques like one dimensional proton, 13-C, DEPT, JMOD and two dimensional ^{1}H-^{13}C HSQC, ^{1}H-^{13}C HMBC, ^{1}H-^{1}H TOCSY, ^{1}H-^{1}H COSY, ^{1}H-^{1}H ROESY. As rutin is a flavonol glycoside with different protons, for the assignment of NMR resonances the protons of rutin were designated as follows the ring A of flavonol ring were labeled without any primes (H6, H8, OH5 and OH7), aromatic ring B protons with single prime (H2', H5', H6' and OH3', OH4'), the glucose sugar ring protons with two primes (H1", H2", H3", H4", H5" and H6") and rahmnose sugar ring protons with three primes (H1'", H2'", H3'", H4'", H5'" and H6'") (Fig. 6.1a).

Analysis of the proton NMR spectrum of rutin at 298 K shows signals with characteristic splitting patterns (Fig 6a and Table 6.1), which can be further divided into two groups, flavone and sugar protons. Protons which are directly attached to the flavone, quercetin backbone resonate in the aromatic region and OH protons attached to this backbone resonate further downfield. The most downfield shifted resonance was assigned to the OH5 attached to the C5 atom, which forms a strong H-bond with C4=O keto group. The inability to exchange its proton with neighboring solvent owing to the strong H-bonding contributes to the appearance of sharp resonance of OH5. The remaining three OH groups, namely OH7, OH4' and OH3' appear at δH of 10.83, 9.67 and 9.16 ppm, respectively. These resonances were rather broad, which may be due to the absence of H-bonding and due to exchange with solvent protons.

The aromatic region of the proton spectra shows appearance of five resonances with characteristic splitting patterns. The protons H6' (δH 7.54, *dd*, ^{3}J = 8.4 Hz, ^{4}J=1.8 Hz) and H5' (δ 6.85, d, J = 8.4 Hz) shows characteristic *ortho* coupling effect, with a splitting of 8-9 Hz. Moreover, the doublet peak of H6' proton shows weak meta coupling of 1.8 Hz due to the presence of H2' proton (δ 7.53, dd, ^{4}J=1.8 Hz).

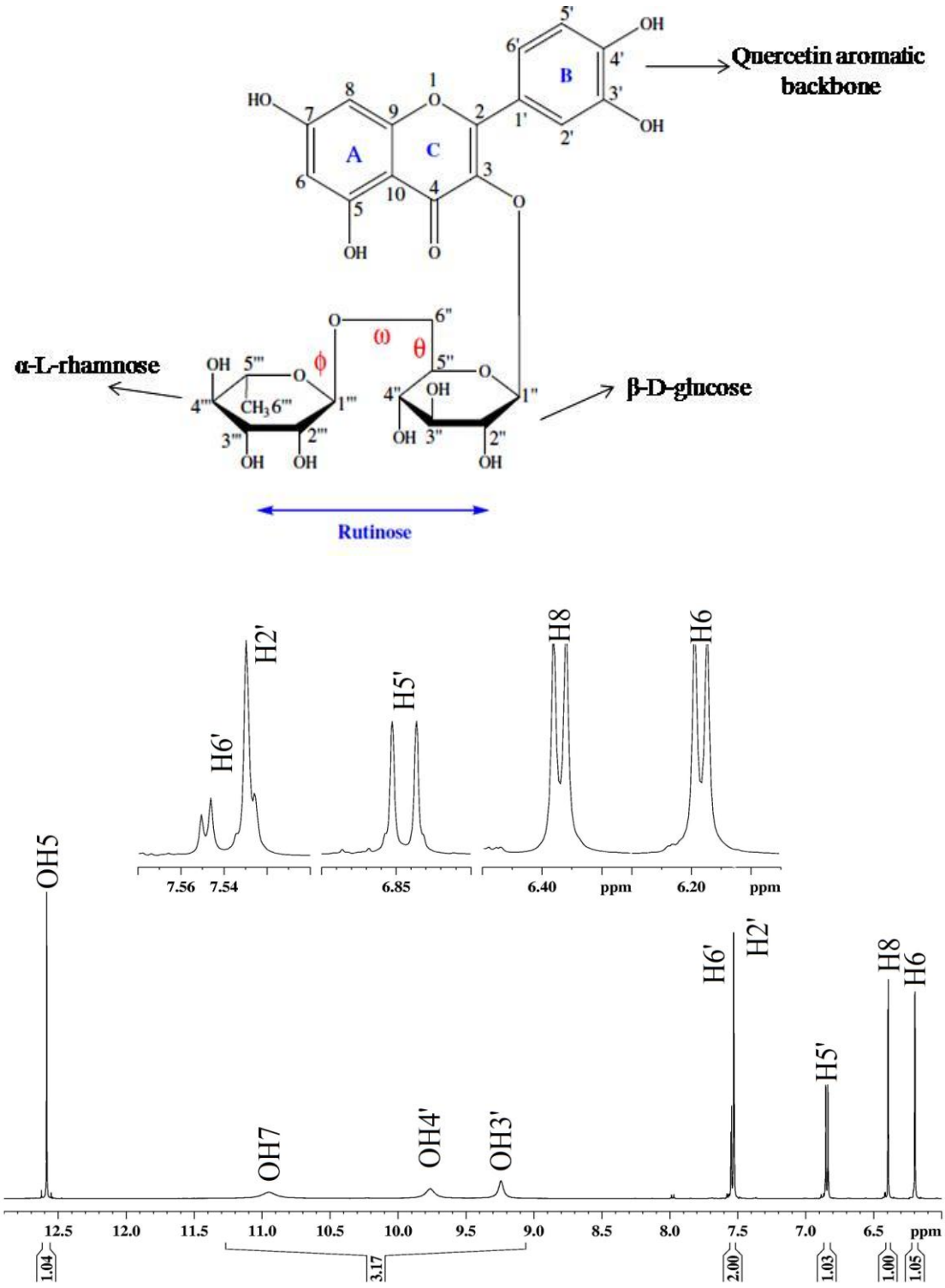

Figure 6.1: (a) Chemical structure of rutin and (b) proton one dimensional ^{1}H spectrum at 298 K in DMSO-d_6 showing aromatic and hydroxyl protons of rutin.

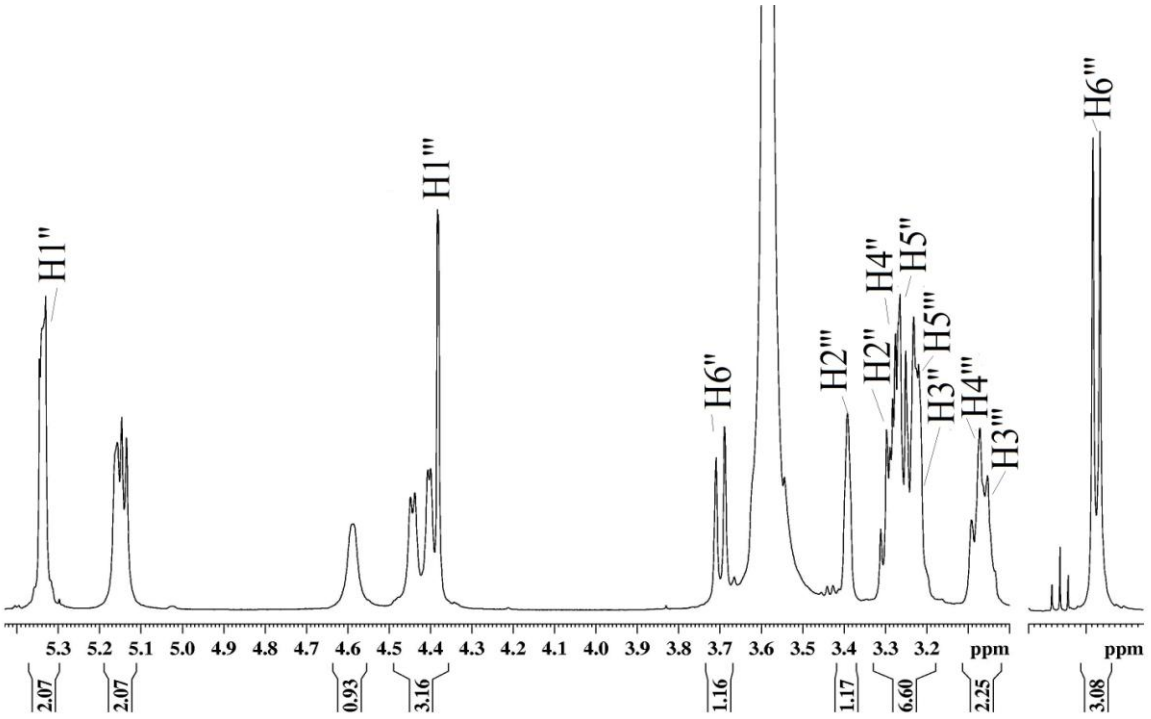

Figure 6.1: (c) proton one dimensional ^{1}H spectrum at 298 K in DMSO-d_6 showing glycosidic protons of sugar and rahmnose residues.

The H8 (δ 6.39, d, J = 1.9 Hz) and H6 (δ 6.19, d, J =1.9 Hz) protons attached to ring A resonates upfield, and show characteristic *meta* coupling effect.

The protons attached to the two sugar moieties resonate in the higher field region of the spectra, due to more shielding effect; they appear between δH of ~ 5.5 to 0.8 ppm. The most up-field shifted proton was assigned to the methyl resonance (H6''') (δ 0.98, d, J = 6.17 *Hz*) of rahmnose sugar which splits into doublet due to the presence of ^{3}J coupled proton H5''' (δ, d, J = 6.17 *Hz*). Similar case arises for the methylene protons (H6") (δ 3.70, d, J = 10.76 *Hz*) of glucose residue which splits into doublet due to the presence of H5" (δ, d, J = 6.17 *Hz*) protons. The remaining coupling constants which belong to sugar protons cannot be measured accurately due to the presence of overlapping signals.

Table 6.1: Chemical shifts of rutin protons in DMSO-d_6 and compared with reported chemical shifts in literature and observed J-couplings between rutin protons in the present study.

Rutin protons	Present work 298 K DMSO-*d6*	J coupling (*Hz*)	El-Sawai and Saleem 2010	Fatemeh Fathiazad *et al.* 2006	Ghisai. M *et al.* 2010 d6-DMSO	José G. Napolitano *et al.* 2012
H2'	7.53			7.55	7.53	7.53
H5'	6.84	8.21	6.85	6.86	6.84	6.84
H6'	7.54	2.27 8.25	7.56	7.56	7.54	7.54
H6	6.19	2.11	6.20	6.21	6.19	6.19
H8	6.38	2.30	6.39	6.40	6.38	6.38
OH5	12.65	-		12.62		12.60
OH7	10.95	-		10.86		10.83
OH3'	9.24	-		9.21		
OH4'	9.77	-		9.71		
H1"	5.34	7.27	5.33	5.35	5.33	5.34
H2"	3.23				3.25	3.22
H3"	3.17				3.19	3.20
H4"	3.42				3.41	3.05
H5"	3.29				3.28	3.24
H6"	3.70	10.3			3.70	3.70
H1"'	4.38		4.37	5.12	4.38	4.37
H2"'	3.42				3.26	3.38
H3"'	3.09				3.07	3.27
H4"'	3.06				3.06	3.07
H5"'	3.28				3.16	3.26
H6"'	0.99	6.33	1.11	1.00	1.0	0.99

All other remaining resonances including anomeric H1' and H1" protons were assigned using the combination of HSQC, HMBC, TOCSY and COSY techniques. The ^{13}C spectrum of rutin molecule shows 27 ^{13}C signals. DEPT and JMOD experiments were used to distinguish and identify the resonances of primary, secondary, tertiary and quaternary carbons. The^{13}C signals resonate in two distinct frequency regions, i.e the carbons of the 15 membered flavonol backbone and two anomeric carbons C1" and C1"' resonate in the downfield region between ~ 180 to 115 ppm and the remaining carbons which belong to glucose and rahmnose sugar resonate in region between ~ 105-65 ppm, except the C6"' resonance of rahmnose sugar. The methyl resonance (C6"'), of rahmnose sugar moiety resonate in the upfield region δC ~ 18.2 ppm.

Table 6.2: ROESY, COSY and TOCSY correlations observed for rutin in at 298 K, along with distances calculated from

ROESY correlations (298K 200ms)	Distance (Å)	Distance from rMD (Å)	COSY correlations	TOCSY correlations
H5'-H6'	2.45	2.48	H5'-H6' (^3J)	H5'-H6' (ring A)
H2'-H6'	-	4.9	H2'-H6'(^4J)	H2'-H6' (ring A)
H8-H2'	3.28	3.3		H2'-H5' (ring A)
H8-H6'	3.62	3.7		H8-H6 (ring B)
H6'-H1"	3.4	3.4		
H2'-H1'"	o			
H5'-H5"	3.8	3.8		
H6'-H5"	2.9	2.9		
H6"-H5"	2.8	2.9		
H6"-H3"	4.1	4.1		
H5"-H3"	3.8	3.8		
H4"-H3"	3.6	3.5		
H6'"-H4'"	3.0	3.1		
H6'"-H5'"	2.9	3.0		

Table 6.3: ^{1}H-^{13}C HSQC (single bond) experiment showing chemical shifts of ^{13}C atoms attached to rutin protons

Rutin protons	^{1}H chemical shift (δ) at 298 K	C-H correlation in HSQC (ppm)	^{13}C chemical shift (ppm)
H2'	7.53	C2'	116.6
H5'	6.84	C5'	115.6
H6'	7.54	C6'	122.0
H6	6.19	C6	99.0
H8	6.38	C8	94.88
H1"	5.34	C1"	101.6
H2"	3.23	C2"	76.3
H3"	3.17	C3"	70.4
H4"	3.42	C4"	72.2
H5"	3.29	C5"	76.7
H6"	3.70	C6"	67.44
H1'"	4.38	C1'"	101.2
H2'"	3.42	C2'"	70.7
H3'"	3.09	C3'"	70.9
H4'"	3.06	C4'"	74.4
H5'"	3.28	C5'"	68.7
H6'"	0.99	C6'"	18.2

The assignment of ^{1}H resonances were also aided by COSY and TOCSY experiments (Fig. 6.5 and 6.6), the TOCSY spectra at 298 K (Fig 6.6) shows presence of four different spin systems. The H6' proton gives a strong TOCSY correlation with H5' proton, as these protons are ^{3}J coupled. Both H5' and H6' protons show a weak TOCSY correlation with H2' proton. Due to the overlapping of H6' and H2' proton resonances, cross correlation between these two protons was not distinguishable. Hence H2', H5' and H6' protons attached to single spin system was assigned as phenyl ring B of flavonol nucleus.

Fig. 6.7 shows the COSY and TOCSY overlap of aromatic region of rutin molecule. The H6' (red colored) proton (δ 7.54 ppm) shows a COSY correlation with H5' proton (δ 6.84 ppm), which also shows a strong TOCSY correlation. The H5' and H6' protons show a weak TOCSY correlation with H2' proton (δ 7.53 ppm). Hence this spin system is attributed to B ring of rutin molecule, which has two ^{3}J coupled protons (H5' and H6') and one ^{4}J coupled proton (H2' with H6') system. The H8 proton (δ 6.38 ppm) resonates in the upfield region of A-ring's H5' resonance and shows weak TOCSY correlation with H6 proton (δ 6.19 ppm). These two protons were attributed to aromatic protons of ring A, i.e. H6 and H8, which are ^{4}J coupled and hence doesnot show any COSY correlation between them. As the two aromatic A and B ring protons were separated by electronegative oxygen atom and doesnot show any through bond TOCSY correlations. Similarly these two aromatic rings containing flavonol backbone was separated from rutinose sugar moiety by glycosidic bond (-O-C). Hence no TOCSY correlation can be observed between aromatic ring protons and sugar ring protons.

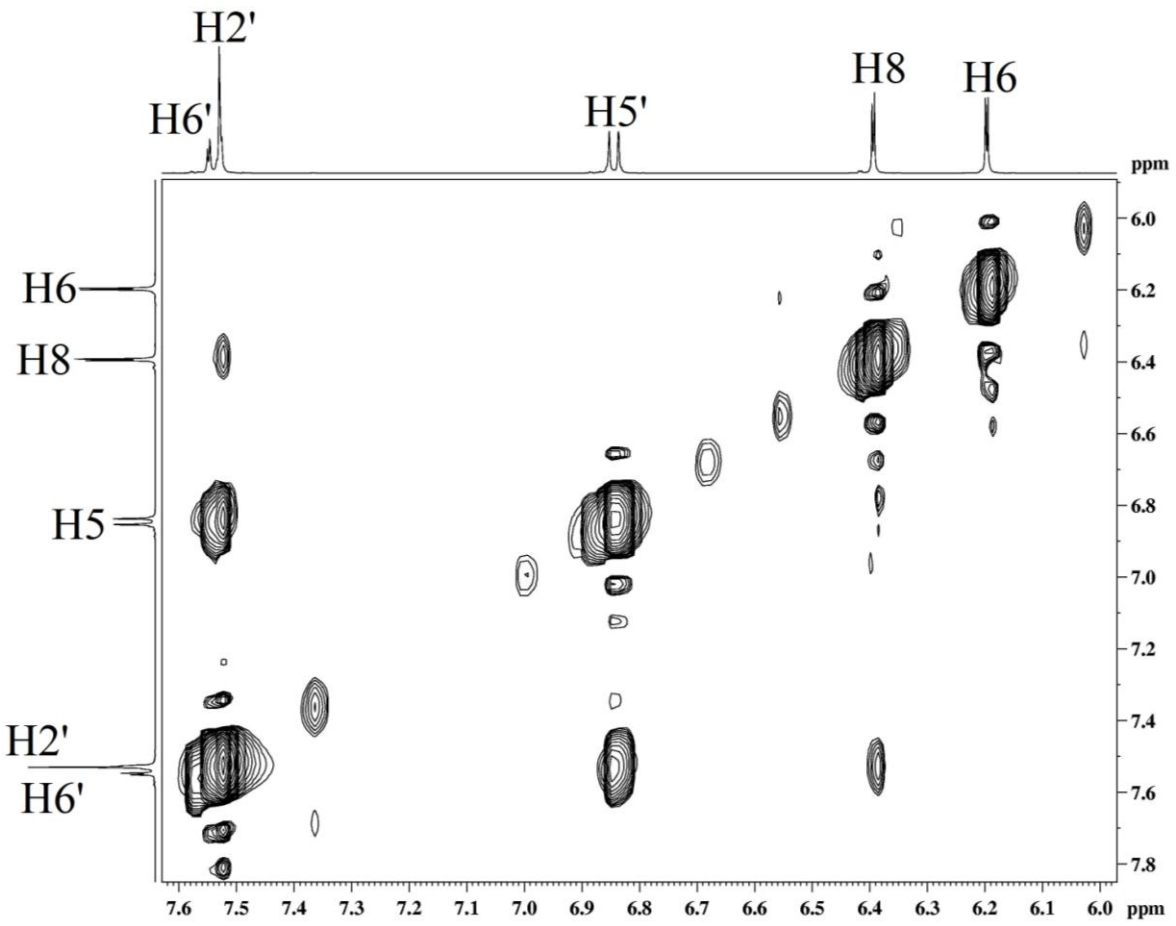

Figure 6.3: Expanded region of ROESY spectrum at 298 K showing aromatic proton region of rutin.

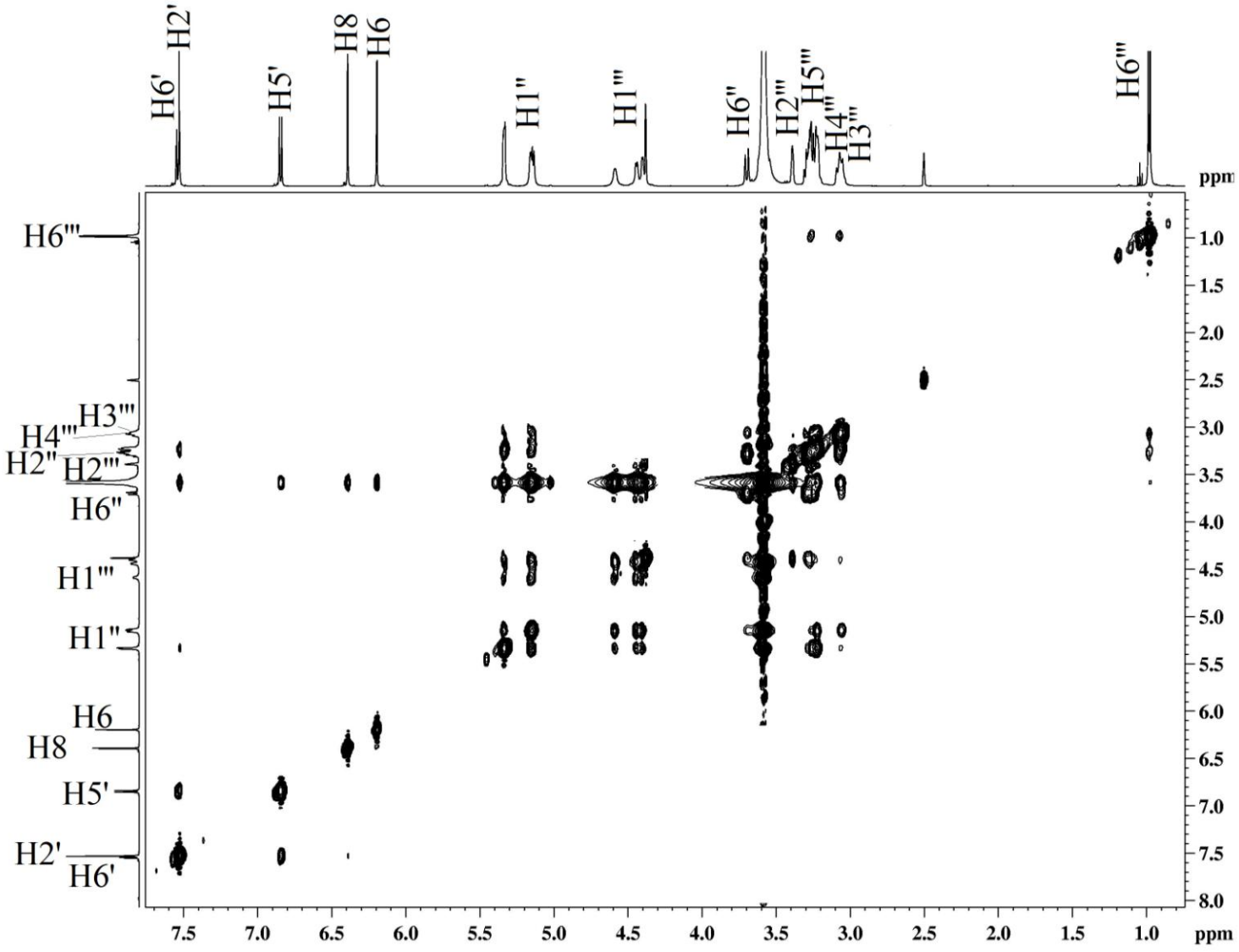

Figure 6.4: Expanded region of ROESY spectrum at 298 K showing aromatic, glucose and rahmnose sugar region of rutin.

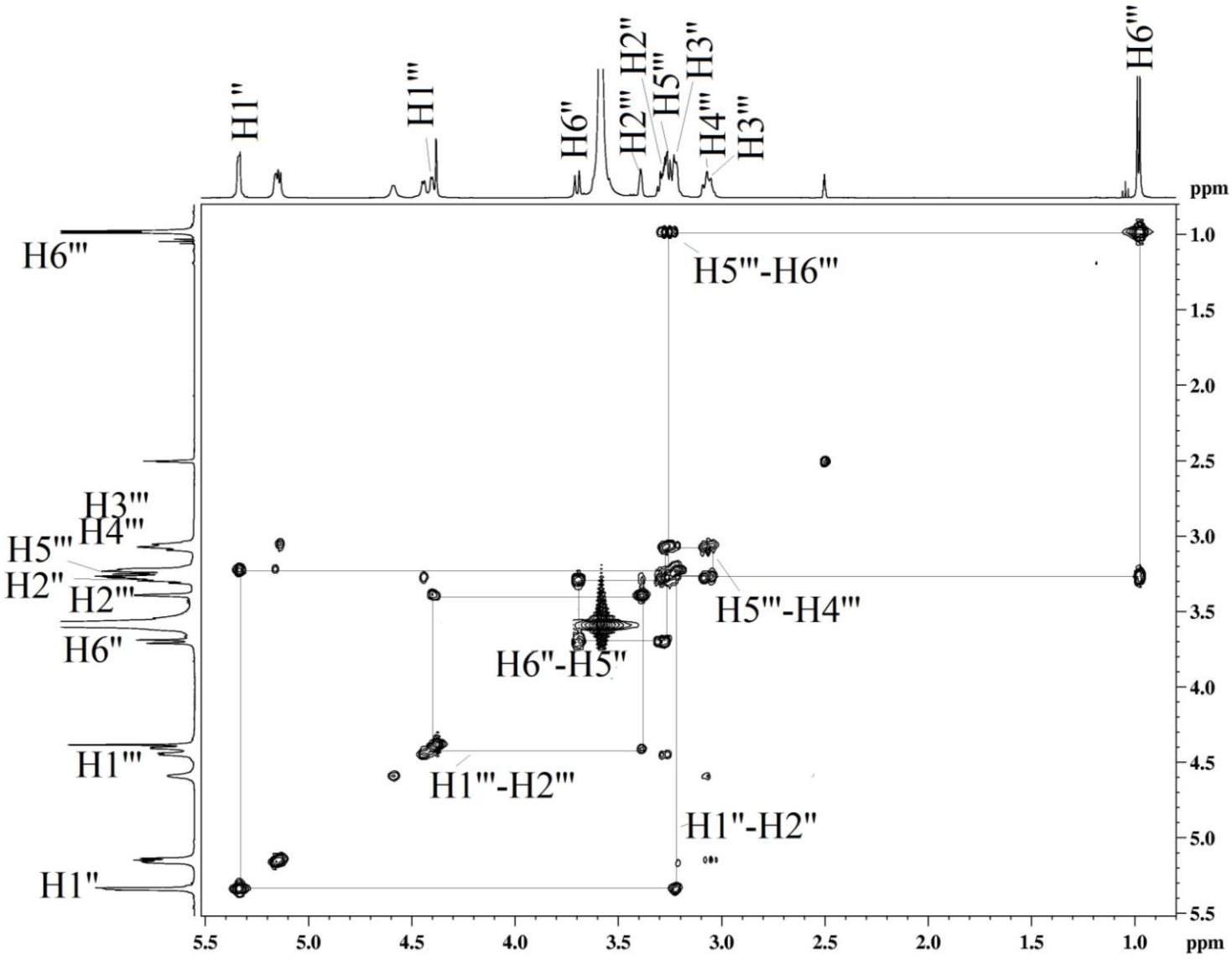

Figure 6.5: Expanded region of COSY spectrum at 298 K showing glucose and rahmnose sugar protons of rutin.

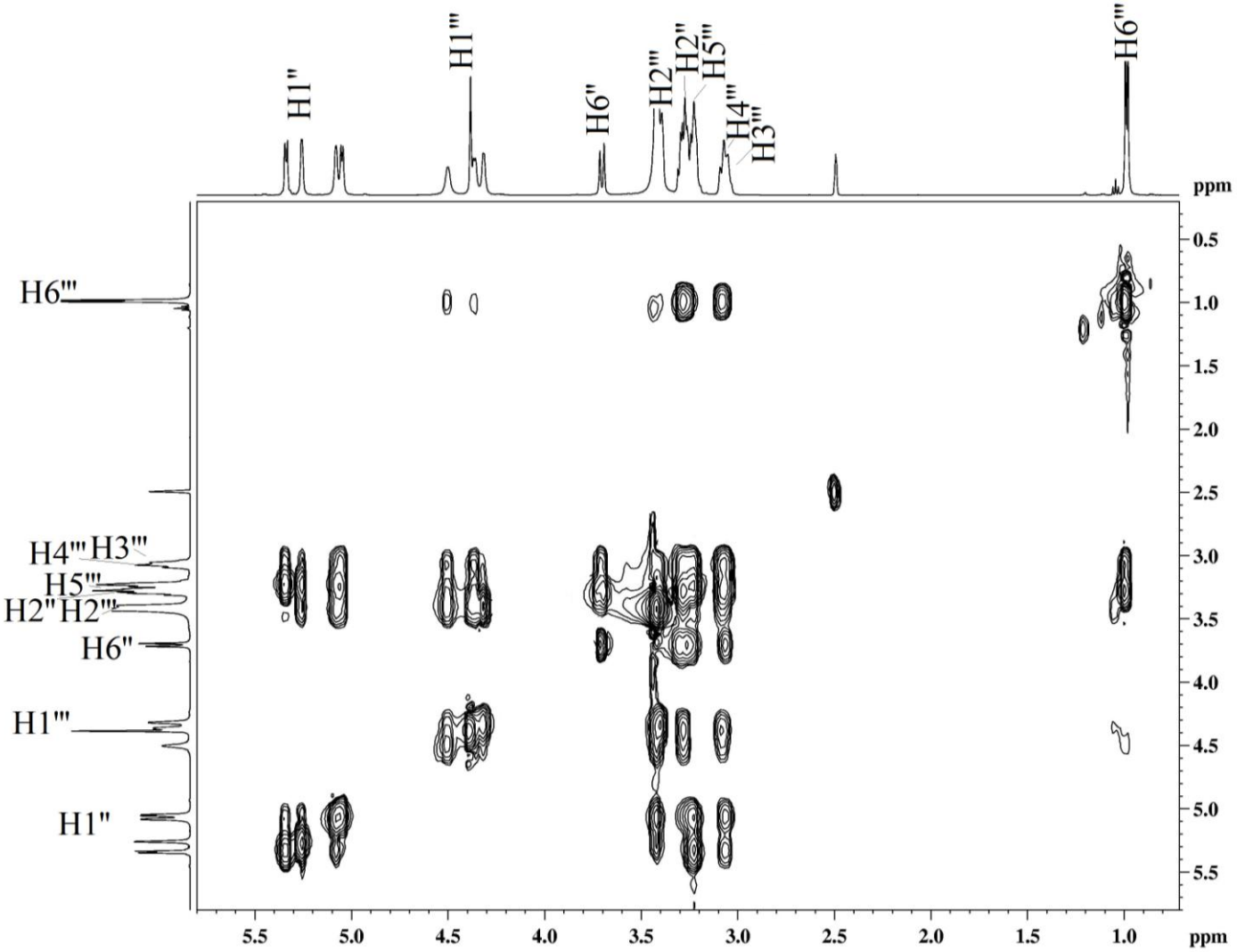

Figure 6.6: Expanded region of TOCSY spectrum at 298 K showing glucose and rahmnose sugar protons of rutin.

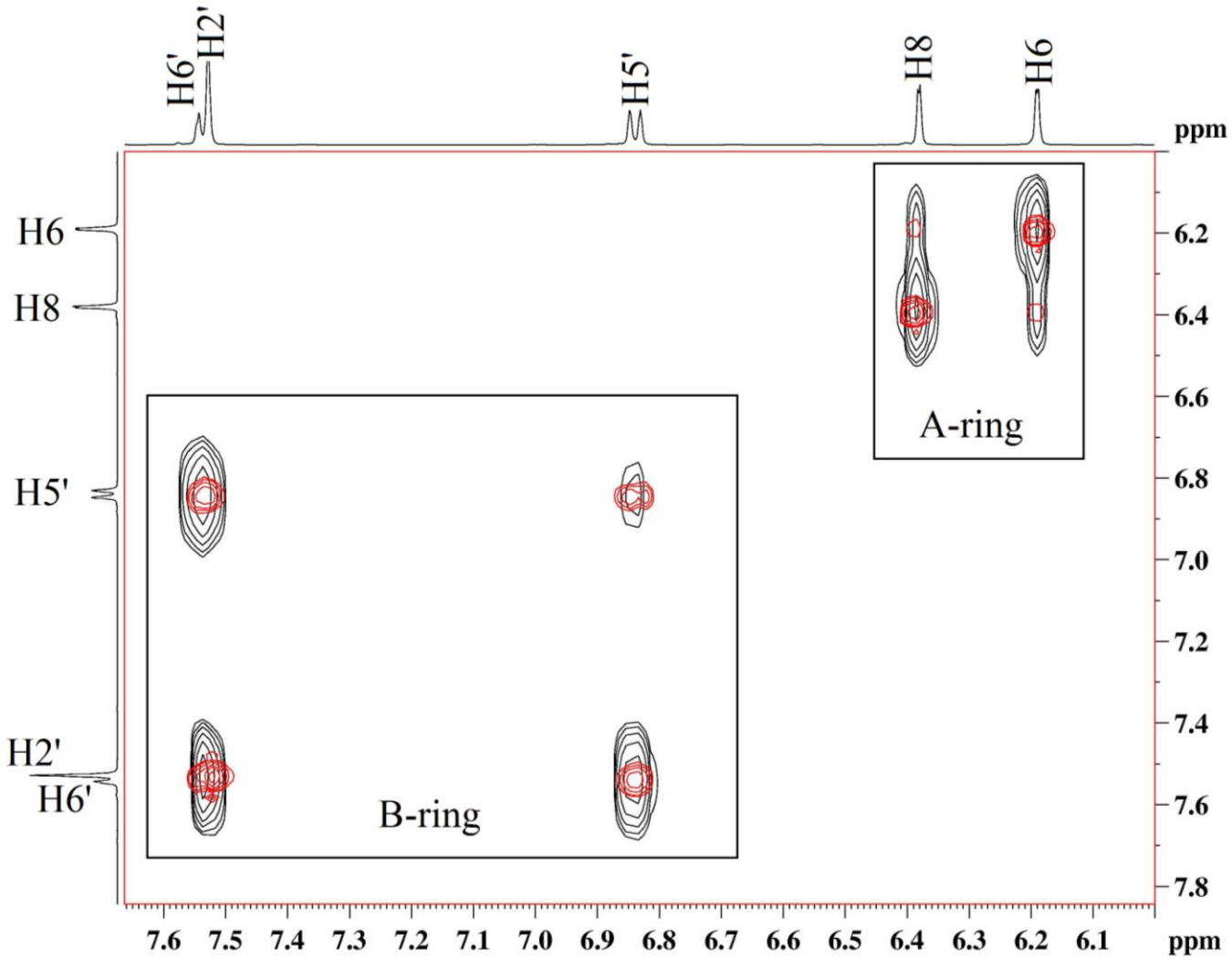

Figure 6.7: Expanded region of TOCSY (black) and COSY (red) overlap of rutin aromatic protons region at 298 K.

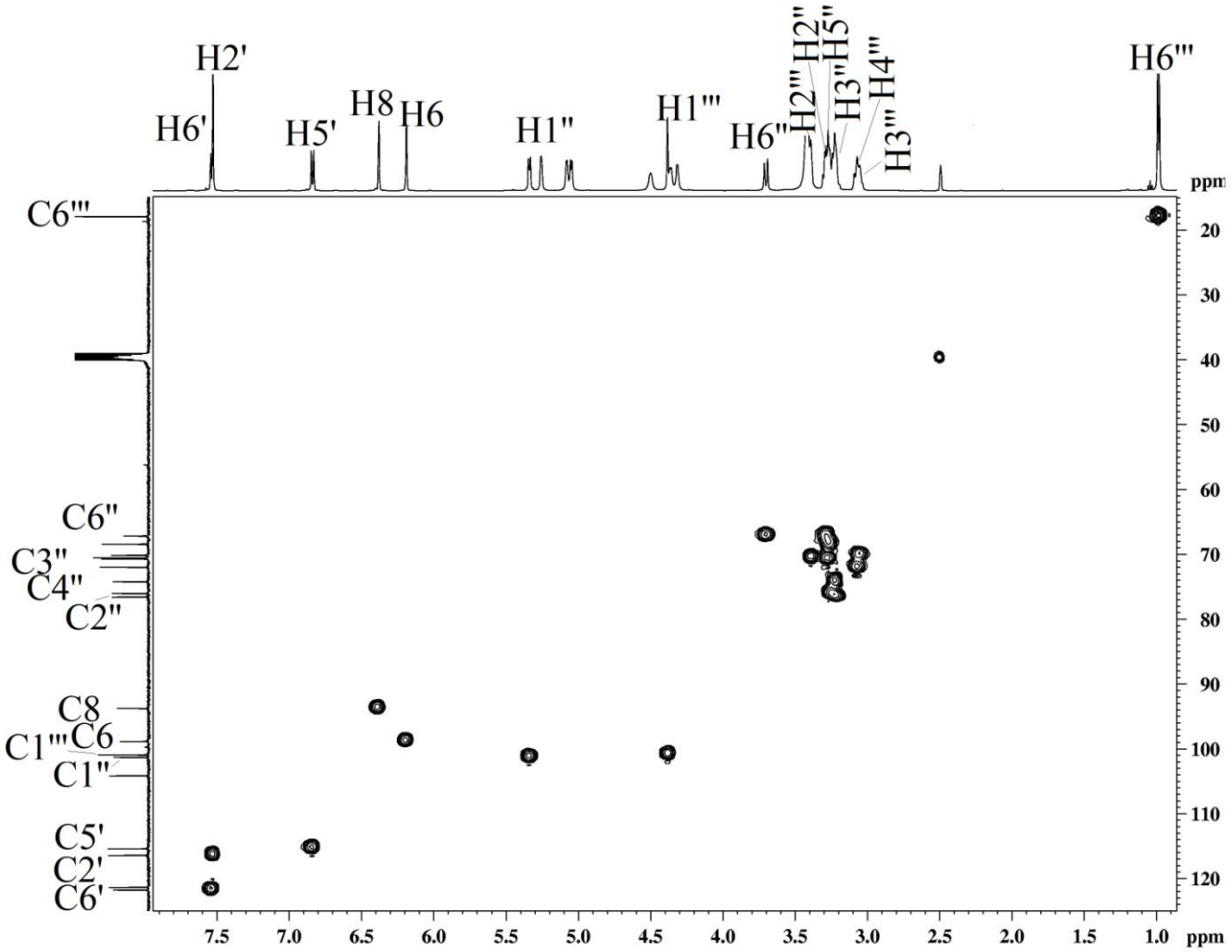

Figure 6.8: Expanded region of ^{1}H-^{13}C spectrum at 298 K showing ^{1}H and ^{13}C single bond correlations of rutin.

.

The rutinose sugar ring protons were identified by a combination of TOCSY, COSY, HSQC and HMBC experiments. As rutinose sugar is made up of α-glucose attached to β-D-rahmnose moieties, these two sugar rings show distinct TOCSY correlations. As these two sugars were separated between themselves by a glycosidic bond, no TOCSY correlation was observed between them. Due to the electropositive character rahmnose protons were upfield shifted when compared to glucose protons in the spectrum at 298 K. The most upfield resonating proton resonance of H6''' shows a strong TOCSY correlation with H5''' proton, medium correlation with H4''' proton and rather weak correlations with H3''', H2''' protons.

The H1'' proton of glucose sugar resonates in the most downfield region (δ 5.34 ppm) among rutinose sugar ring protons due to its proximity to aromatic flavonol nucleus. This proton shows the TOCSY correlation with H2'', H3'', H4'', H5'' and H6''' protons.

To identify the proton attached to particular carbon atom, heteronuclear ^{1}H-^{13}C HSQC experiment was used. Fig 6.8 shows the expansion of HSQC spectrum, the appearance of seventeen H-C correlations confirm the existence of seventeen protons directly attached to carbon. The downfield shifted 15 carbon resonances were assigned to the flavonol backbone (quercetin) and remaining twelve resonances were assigned to the rutinose sugar moieties glucose and rahmnose.

Rutin is a biologically important flavonoid glycoside, with its sugar moiety plays an important role in the bioavailability across the epithelium in human colon. Determination of conformation of rutin helps in understanding the mechanism of action of this flavonol glycoside. Rutin adopts a unique conformation in various solvent conditions due to the presence of three rotatable bonds (*Gihasi et al. 2011*).

6.1.2 NMR studies of *Tetrahymena* telomeric DNA sequence d-(TTGGGGT)$_4$

The formation of tetramolecular parallel quadruplex structure by sequence d-(TTGGGGT)$_4$ was studied by using both one dimensional and two dimensional NMR experiments. The resonance assignments of the uncomplexed d-(TTGGGGT)$_4$ was made by following the standard strategies of Wang and Patel, (Wang and Patel., 1994) and as explained in Chapter 4, section 4.1.2. The presence of four proton resonances in the Hoogsteen hydrogen bonding region confirms the formation of single predominant species of quadruplex by d-(TTGGGGT) sequence and quadurplex has C4 symmetry. The presence of characteristic NOE connectivities between aromatic H8 protons of a quartet plane with its own and with 3' flanking GNH

proton clearly shows the quartet arrangement and alignment of G-tetrads. The presence of sequential connectivities between base H6/H8 to sugar H1'/H2'/H2" protons shows the right handed helical nature of quadruplex (Fig, 6.9-11).

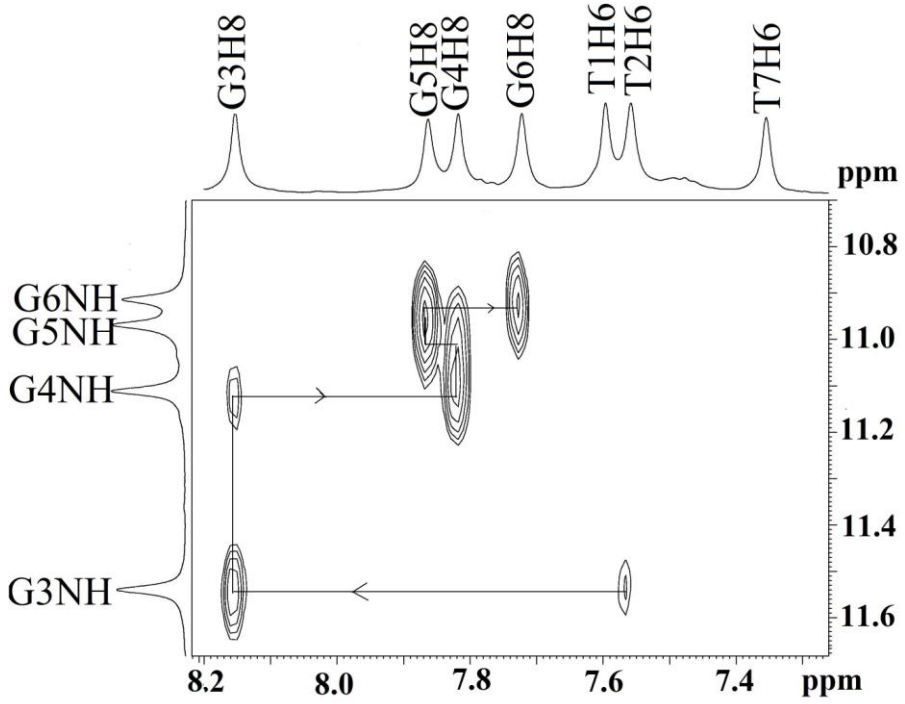

Figure 6.9: Expansion of 200 ms NOESY spectrum of d-(TTGGGGT)$_4$ at 298 K showing sequential connectivities within a G-quartet protons.

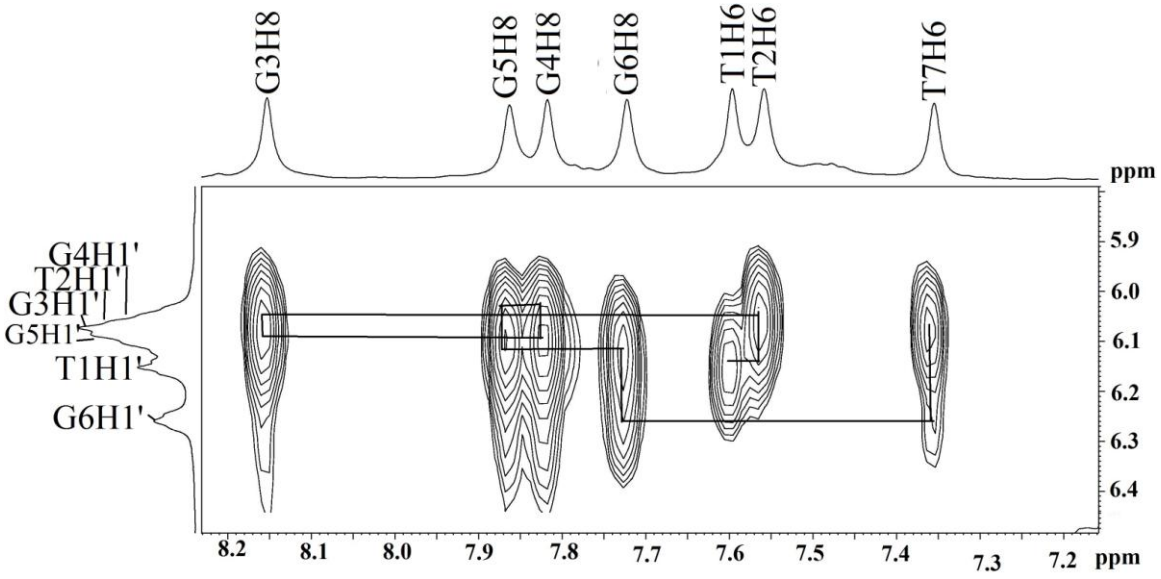

Figure 6.10: Expansion of 200 ms NOESY spectrum of d-(TTGGGGT)$_4$ at 298 K showing sequential connectivities between aromatic H6/H8 with sugar H1' protons.

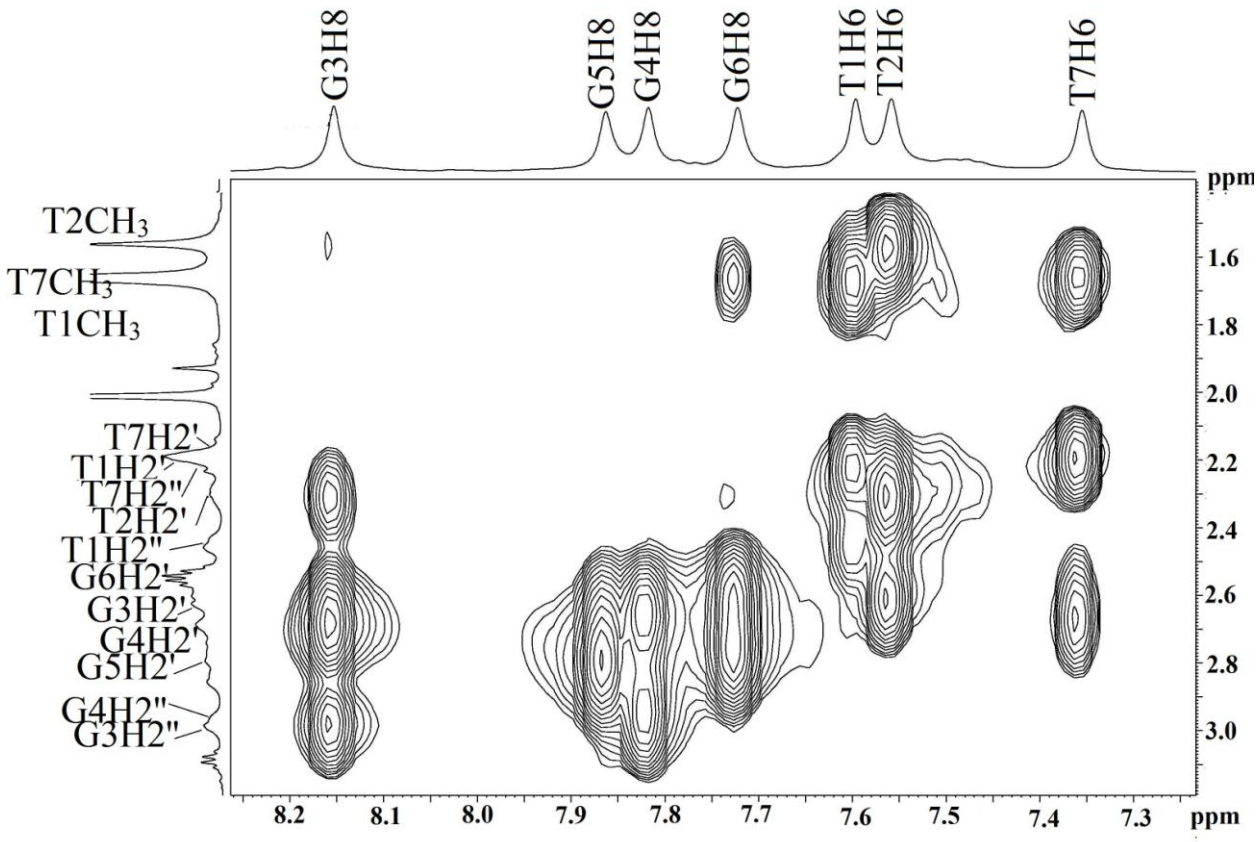

Figure 6.11: Expansion of 200 ms NOESY spectrum of d-(TTGGGGT)$_4$ at 298 K showing sequential connectivities between aromatic H6/H8 with sugar H2'/H2'' protons.

6.1.3 Proton NMR studies on complex of rutin-d-(TTGGGGT)$_4$

Interaction of flavonoid glycoside, rutin with *Tetrahymena* telomere sequence d-(TTGGGGT)$_4$ was studied by adding increasing concentration of rutin to parallel quadruplex solution to reach the D/N ratios of 0.25, 0.5, 0.75, 1.0 and 2.0. The resonance assignments of rutin-d-(TTGGGGT)$_4$ complex were done using the combination of one and two-dimensional NMR experiments like ^{1}H-^{1}H NOESY, ^{1}H-^{1}H COSY, ^{1}H-^{1}H TOCSY and ^{1}H-^{13}C HSQC.

Fig 6.12 and 6.13 shows expanded imino and aromatic proton region of rutin-d-(TTGGGGT)$_4$ complex at various D/N ratios at 298 K. On addition of rutin to d-(TTGGGGT)$_4$, new proton signals corresponding to the rutin protons appear in the spectrum, which increase in intensity with increasing D/N ratios. With each successive addition of rutin, d-(TTGGGGT)$_4$ protons shows gradual shift in the position when compared to uncomplexed d-(TTGGGGT)$_4$ resonances

(Table.6.4). All four Hoogsteen hydrogen bonded imino resonances belonging to four steps of G-quartets, i.e G3NH, G4NH, G5NH and G6NH show progressive upfield shift upon complexation. G6NH shows maximum upfield shift of Δδ 0.24 ppm, followed by G5NH which shifts upfield by Δδ 0.11 ppm. G3NH and G4NH shift upfield by Δδ 0.09 and Δδ 0.06 ppm, respectively. Aromatic base protons show very little shift in resonance position upon complexation, except for T7H6 proton, which shifts downfield by Δδ 0.32 ppm. T7CH_3 resonance shows downfield shift of Δδ 0.22 ppm, while other two CH_3 resonances belonging to T1 and T2 show very little shift compared to their uncomplexed position. The sugar protons doesnot show much shift upon binding of rutin. Upon complexation d-$(TTGGGGT)_4$ resonances show little line broadening effect.

The appearance of only four imino resonances clearly shows that C4 symmetry of quadruplex is not broken due to interaction with quercetin. Fig.6. 12 shows absence of any extra bound and unbound resonances belonging to d-$(TTGGGGT)_4$, which indicates binding is fast in NMR time scale. The upfield shift of G6 step protons coupled with the downfield shift of T7 step protons shows that rutin molecule is interacting with G6pT7 step of the quadruplex DNA.

Titration of rutin into d-$(TTGGGGT)_4$, results in appearance of new proton signals belonging to rutin, which increase in intensity with increasing D/N ratios. All five aromatic protons belonging to ring A and B shows upfield shift in position when compared to uncomplexed rutin. The magnitude of chemical shift change is less in glycosidic protons attached to glucose and rahmnose moieties when compared with the aromatic protons (Table.6.5). The aromatic H8 and H6 protons of ring A shows maximum upfield shift of Δδ 0.79 and Δδ 0.67 ppm, followed by H5' proton of ring B which shifts upfield by Δδ 0.56 ppm. Other two aromatic protons of B ring H6' and H2' protons shift upfield by Δδ 0.25 and Δδ 0.43 ppm, respectively. None of the five OH protons of flavone nucleus were observed upon complex formation, which may be due to the solvent effect. The sugar protons show very little change in chemical shift except for H6''' proton, which shifts upfield by Δδ 0.16 ppm. The anomeric proton H1'' shows upfield shift of ~ 1.01 ppm. This large chemical shift change may be explained by the fact that, the resonance position of the anomeric H1'' and H1''' protons of both the sugar rings were sensitive to changes in glycosidic torsional angle. Hence their chemical shifts were sensitive to any subtle changes in these torsion angle due to complexation with d-$(TTGGGGT)_4$.

Table 6. 4: Chemical shift (ppm) of d-$(TTGGGGT)_4$ protons in uncomplexed state (δ^f) and bound to rutin (δ^b) at rutin (D) to nucleic acid quadruplex (N) ratio D/N = 2.0 at 298 K. $\Delta\delta = \delta^b_{(D/N=2.0)} - \delta^f_{(D/N=0.0)}$. -ve $\Delta\delta$ indicates upfield shift, +ve $\Delta\delta$ indicates downfield shift.

DNA protons	T1			T2			G3			G4			G5		
	δ^b	δ^f	$\Delta\delta$	δ^b	δ^f	$\Delta\delta$	δ^b	δ^f	$\Delta\delta$	δ^b	δ^f	$\Delta\delta$	δ^b	δ^f	$\Delta\delta$
H8/H6	7.67	7.59	0.08	7.57	7.56	0.01	8.14	8.15	-0.01	7.78	7.82	-0.04	7.83	7.86	-0.03
H1'	6.27	6.15	0.12	6.08	6.05	0.03	6.10	6.08	0.02	6.03	6.06	-0.03	6.09	6.10	-0.01
H2'	2.28	2.21	0.07	2.28	2.30	-0.02	2.69	2.68	0.01	2.62	2.62	0.00	2.66	2.74	-0.08
H2"	2.44	2.46	-0.02	2.64	2.62	0.02	2.97	2.97	0.00	2.83	2.94	-0.11	2.83	2.81	0.02
H3'	4.70	4.74	-0.04	4.92	4.86	0.04	5.08	5.06	0.02	5.07	5.05	0.02	5.12	5.11	0.01
H4'	4.20	4.06	0.14	4.23	4.27	-0.04		4.43		4.42	4.43	-0.02	4.60	4.61	-0.01
H5'	3.83	3.79	0.04	4.14	4.14	0.00		4.25		4.27	4.34	-0.07	4.31	4.39	-0.08
H5"	3.74	3.75	-0.01	4.05	4.06	-0.01		4.09		4.34	4.24	0.10	4.29	4.33	-0.04
CH_3	1.69	1.67	0.02	1.55	1.56	-0.01									
$NH_2{}^b$	-						9.83	9.84	-0.01	9.21	9.25	-0.04	9.12	9.17	-0.05
$NH_2{}^{nb}$	-						6.20	6.24	-0.04	6.15	6.17	-0.02	6.19	6.23	-0.05
NH							11.45	11.54	-0.09	11.05	11.11	-0.06	10.86	10.97	-0.11

DNA protons	G6			T7		
	δ^b	δ^f	$\Delta\delta$	δ^b	δ^f	$\Delta\delta$
H8/H6	7.72	7.72	0.00	7.66	7.35	0.31
H1'	6.30	6.26	0.04	6.25	6.07	0.18
H2'	2.58	2.53	0.05	2.25	2.14	0.11
H2"	2.70	2.76	-0.06	2.32	2.23	0.09
H3'	5.07	4.97	0.10	4.56	4.51	0.04
H4'	4.55	4.56	-0.01	4.23	4.46	-0.23
H5'	4.29	4.31	-0.02	4.16	4.24	-0.08
H5"	4.21	4.23	-0.02	4.04	4.05	-0.01
CH_3				1.88	1.66	0.22
$NH_2{}^b$						
$NH_2{}^{nb}$						
NH	10.67	10.91	-0.24			

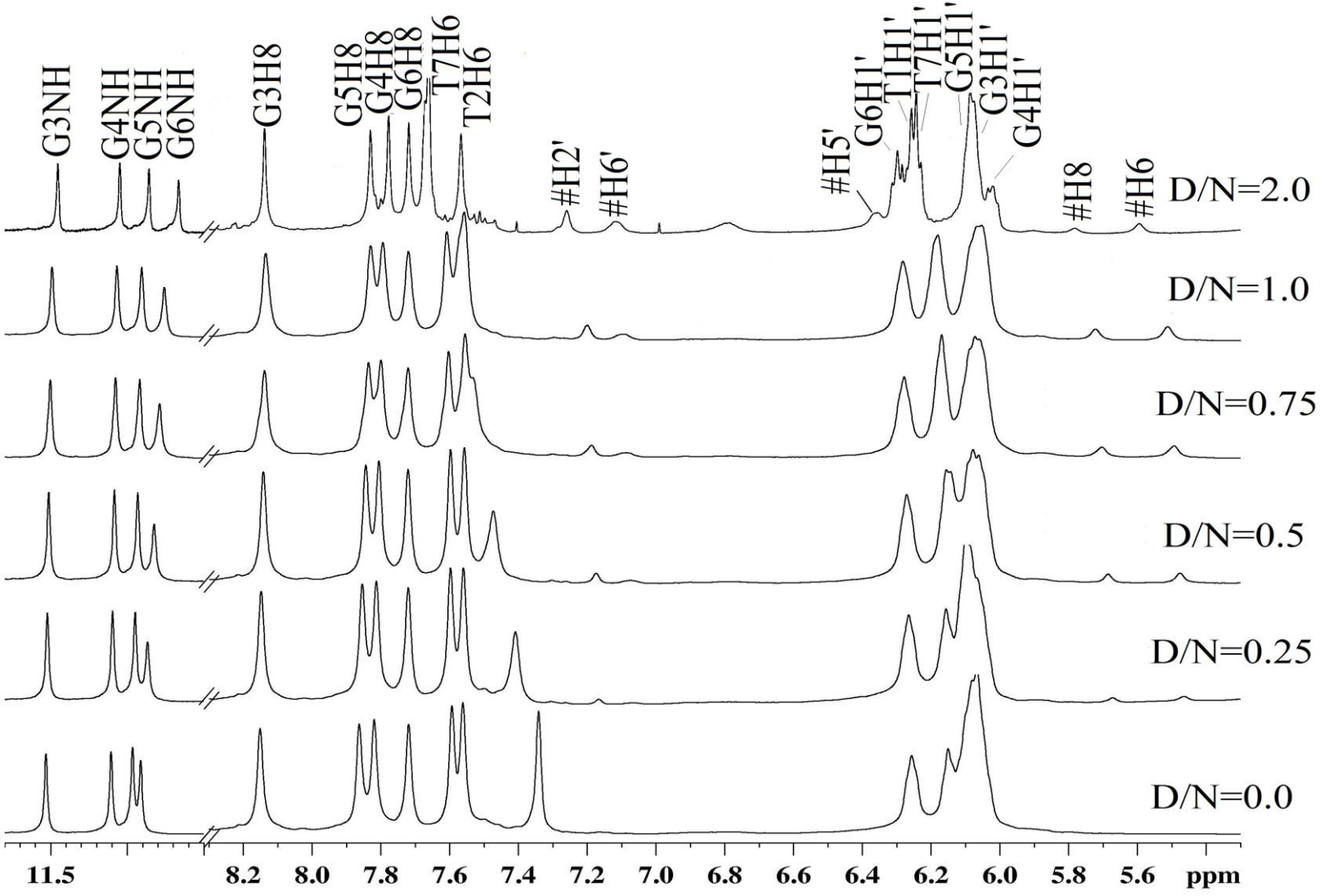

Figure 6.12: Expansion of ^{1}H spectrum of uncomplexed d-(TTGGGGT)$_4$ and rutin complexed d-(TTGGGGT)4 at D/N ratios 0.25, 0.5, 0.75 , 1.0 and 2.0 at 298 K (Rutin protons marked as #).

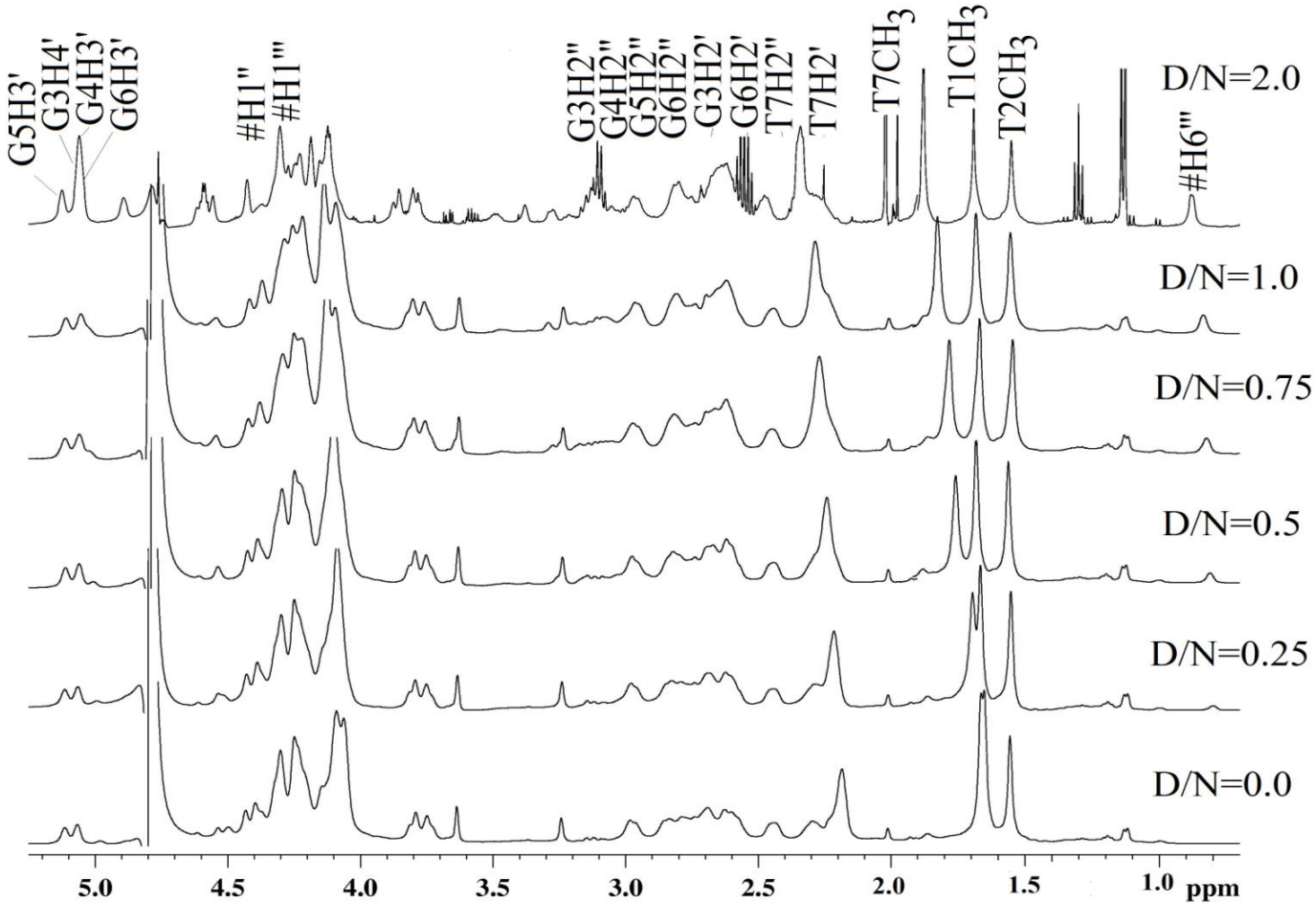

Figure 6.13: Expansion of ^{1}H spectrum of uncomplexed d-(TTGGGGT)$_4$ and rutin complexed d-(TTGGGGT)4 at D/N ratios 0.25, 0.5, 0.75 , 1.0 and 2.0 at 298 K (Rutin protons marker as #).

Table 6.5: Chemical shift (ppm) of free (δ_f) and bound rutin (δ_b) protons in rutin-d-$(TTGGGGT)_4$ complex D/N 2.0 at 298 K. $\Delta\delta = \delta_{b\ (D/N=2.0)} - \delta_{f\ (D/N=0.0)}$. +ve Δδ downfield shift and -ve Δδ upfield shift.

Rutin protons	Rutin protons in DMSO-d_6 δ_f	Rutin protons in complex D/N 2.0 δ_b	$\Delta\delta = \delta_b - \delta_f$
H2'	7.53	7.26	-0.27
H5'	6.84	6.36	-0.48
H6'	7.54	7.12	-0.42
H6	6.19	5.60	-0.59
H8	6.38	5.79	-0.59
OH5	12.65	-	-
OH7	10.95	-	-
OH3'	9.24	-	-
OH4'	9.77	-	-
H1"	5.34	4.33	-1.01
H2"	3.23	3.21	-0.02
H3"	3.17	3.05	-0.12
H4"	3.42	2.94	-0.48
H5"	3.29	3.14	-0.15
H6"	3.70	3.88	0.18
H1"'	4.38	4.28	-0.10
H2"'	3.42	3.37	-0.05
H3"'	3.09	3.15	0.06
H4"'	3.06	3.10	0.04
H5"'	3.28	3.27	-0.01
H6"'	0.99	0.83	-0.16

Table 6.6: ^1H chemical shift (ppm) quadruplex protons of d-$(TTGGGGT)_4$-rutin complex vs D/N 298K. $\Delta\delta = \delta_{b\ (D/N=2.0)} - \delta_{f\ (D/N=0.0)}$. +ve Δδ downfield shift and -ve Δδ upfield shift.

	G3NH	G4NH	G5NH	G6NH	$T1CH_3$	$T2CH_3$	$T7CH_3$
0.0	11.54	11.11	10.97	10.91	1.65	1.55	1.66
0.25	11.52	11.097	10.95	10.87	1.66	1.55	1.69
0.5	11.51	11.09	10.94	10.83	1.67	1.55	1.74
0.75	11.50	11.08	10.92	10.79	1.67	1.54	1.78
1.0	11.49	11.07	10.91	10.76	1.67	1.54	1.81
2.0	11.45	11.05	10.86	10.67	1.67	1.55	1.88
Δδ	-0.09	-0.06	-0.11	-0.24	0.02	0.00	0.22

Table 6.7 ^{1}H chemical shift δ (ppm) of quadruplex protons in d-(TTGGGGT)$_4$-rutin complex vs D/N 298K. $\Delta\delta = \delta_{b\ (D/N=2.0)} - \delta_{f\ (D/N=0.0)}$. +ve Δδ downfield shift and -ve Δδ upfield shift.

	T1H6	T2H6	G3H8	G4H8	G5H8	G6H8	T7H6
0.0	7.59	7.56	8.15	7.82	7.86	7.72	7.34
0.25	7.60	7.56	8.15	7.81	7.85	7.72	7.41
0.5	7.60	7.56	8.14	7.80	7.84	7.72	7.47
0.75	7.60	7.56	8.14	7.80	7.84	7.72	7.53
1.0	7.61	7.56	8.14	7.81	7.83	7.72	7.57
2.0	7.67	7.57	8.14	7.78	7.83	7.72	7.66
Δδ	0.08	0.01	-0.01	-0.04	-0.03	0.00	0.32

Table 6.8 ^{1}H chemical shift of rutin protons in d-(TTGGGGT)$_4$-rutin complex vs D/N at 298 K. $\Delta\delta = \delta b_{\ (D/N\ 2.0)} - \delta f_{\ (D/N\ 0.0)}$. +ve Δδ downfield shift and -ve Δδ upfield shift.

	H2’	H5’	H6’	H6	H8	H6'''
0.0	7.53	6.84	7.54	6.19	6.38	0.99
0.25	7.17	-	7.06	5.47	5.67	0.80
0.5	7.18	-	7.07	5.48	5.69	0.81
0.75	7.19	-	7.09	5.49	5.71	0.83
1.0	7.20	6.28	7.10	5.51	5.72	0.84
2.0	7.26	6.36	7.12	5.60	5.79	0.86
Δδ	-0.27	-0.48	-0.42	-0.59	-0.59	-0.13

The observed change in chemical shift of uncomplexed and 2:1 d-(TTGGGGT)$_4$ complexed rutin protons at different D/N ratios were given in Table 6.8. At D/N ratio of 0.25 all the rutin molecules were in bound state, which is reflected in the maximum upfield shift of rutin aromatic protons in that molar ratio. Increase in rutin concentration to reach higher D/N ratios till 2.0 results in the downfield shift of rutin aromatic protons. This may be attributed to the increase in concentration of unbound rutin in the solution. No separate bound and unbound resonances were observed at any D/N ratios in our study, hence chemical shift position of bound ligand proton may arise from the weighted average of the species in bound and unbound form (*Williamson, 2013*)

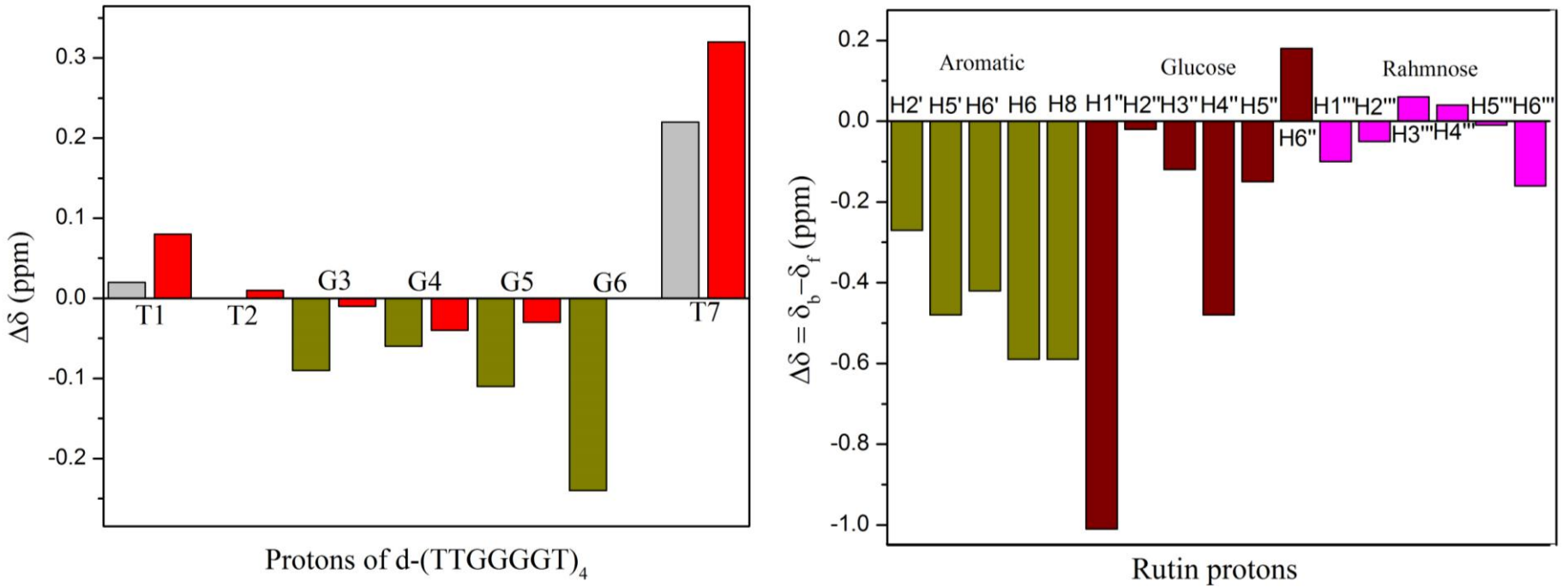

Figure 6.14: Chemical shift differences ($\Delta\delta = \delta_{2.0} - \delta_{0.0}$) of d-$(TTGGGGT)_4$ and rutin protons in D/N 2.0 complex at 298 K (for quadruplex protons- methyl (grey), aromatic (red), imino (dark green) and for rutin protons aromatic (dark green), glucose moiety (wine), rahmnose(magenta).

6.1.4 Effect of temperature

Effect of temperature on quercetin-d-$(TTGGGGT)_4$ complex were studied at temperature range of 278 K to 348 K at D/N 2.0. Fig 6.15 and 6.16 shows the effect of temperature on imino and aromatic protons of the rutin-d-$(TTGGGGT)_4$ complex. Table 6.9 and 6.11 shows the variation of chemical shifts at varying temperatures of both bound rutin and d-$(TTGGGGT)_4$. Increase in temperature from 278 to 348K results in the sharpening of the resonances of both rutin and d-$(TTGGGGT)_4$ protons. The imino and aromatic base protons shift progressively with increase in temperature (Table.6.9 and 6.10). All four guanine imino protons i.e G3:G4:G5:G6NH which are upfield shifted upon complex formation, shifts downfield with increase in temperature, this may be due to the high rate of dissociation of rutin-d-$(TTGGGGT)_4$ complex at this temperature. The aromatic base protons (H6/H8) show progressive upfield shift upon increase in temperature from 278 to 348K. The magnitude of upfield shift is more in T1H6, T2H6, G3H8, G4H8 and G5H8 protons when compared to G6H8 andT7H6 protons. This may be explained on the basis that, rutin binds to d-$(TTGGGGT)_4$ quadurplex at G6pT7 step and hence stabilizing protons involved in binding interaction in this step.

Increase in temperature from 278 to 348 K results in downfield shift of rutin protons. At temperatures below 308 K the aromatic H5' proton of rutin which overlaps with the sugar H1' region of d-$(TTGGGGT)_4$ was difficult to identify in 1D spectrum, but at temperatures higher than 308 K this proton shifts downfield and appear as a separate resonance. At temperature 318K and above, rutin H6' and H5' protons show their characteristic scalar splitting due to ^3J coupling.

Temperature studies were used to study the thermal stabilization of d-$(TTGGGGT)_4$ structure upon complexation with rutin. Appearance of guanine imino protons in the Hoogsteen base pairing region is the characteristic of formation of quadruplex structure, and hence their disappearance at higher temperatures can be used to monitor the melting temperature (T_m) of these structures in the presence and absence of ligands. The ligands which stabilize the quadruplex structure upon binding will result in the increase in melting temperature of quadruplex structure when compared to the uncomplexed structure. Fig. shows the melting profile of imino protons of uncomplexed d-$(TTGGGGT)_4$ and its complex with quercetin at molar equivalents of 2.0 (D/N = 2.0). In uncomplexed structure, the G3 and G6NH resonances start to disappear gradually with increasing temperature after 308 K and completely vanish at 338 K. But upon complexation signals of these

two imino resonances persist till 353 K (data shown till 348 K). This shows the thermal stabilization of d-(TTGGGGT)$_4$ structure upon complexation by rutin by about 15 K. Careful analysis of Fig. 6.17 shows that at 348 K, the intensity of G6 imino proton signal is more when compared to G3NH proton signal. As in uncomplexed structure it was expected that imino resonances i.e. G3NH and G6NH belongs to terminal G-quartets G3 and G6, open up simultaneously with increase in temperature. But ligand binding near any one of these terminal G-quartets results in the stabilization of the imino resonances of that particular G-quartet. Hence it can be assumed that rutin binds to the terminal G6pT7 step. This can also be supported by chemical shift perturbation data of protons belonging to G6pT7 step, which shows large change in chemical shift position when compared to other step protons. These above results clearly establishes that flavonoid rutinoside stabilizes the d-(TTGGGGT)$_4$ quadruplex structure.

Table 6.9: ^{1}H chemical shift δ (ppm) of quadruplex protons in d-(TTGGGGT)$_4$-rutin complex as a function of temperature at D/N 2.0. $\Delta\delta = \delta b_{(353\ K)} - \delta f_{(278\ K)}$. +ve Δδ downfield shift and -ve Δδ upfield shift.

	G3NH	G4NH	G5NH	G6NH	T1CH$_3$	T2CH$_3$	T7CH$_3$
278	11.48	11.10	10.82	10.63	1.76	1.56	1.84
283	11.48	11.08	10.84	10.65	1.73	1.55	1.84
288	11.47	11.07	10.85	10.65	1.71	1.55	1.85
293	11.47	11.06	10.86	10.67	1.70	1.55	1.86
298	11.47	11.05	10.87	10.68	1.69	1.55	1.87
303	11.47	11.05	10.88	10.69	1.68	1.56	1.87
308	11.47	11.05	10.88	10.69	1.68	1.56	1.87
313	11.48	11.05	10.89	10.70	1.68	1.57	1.87
318	11.49	11.05	10.90	10.70	1.68	1.58	1.88
323	11.50	11.06	10.90	10.70	1.69	1.59	1.88
328	11.51	11.06	10.91	10.70	1.69	1.60	1.88
333	11.51	11.07	10.91	10.70	1.70	1.61	1.87
338	11.52	11.08	10.92	10.71	1.71	1.62	1.87
343	11.53	11.08	10.93	10.71	1.71	1.64	1.87
348	11.54	11.09	10.94	10.71	1.72	1.65	1.87
353	11.54	11.10	10.95	10.71	1.72	1.66	1.87
Δδ	0.06	0.00	0.13	0.08	-0.04	0.06	0.03

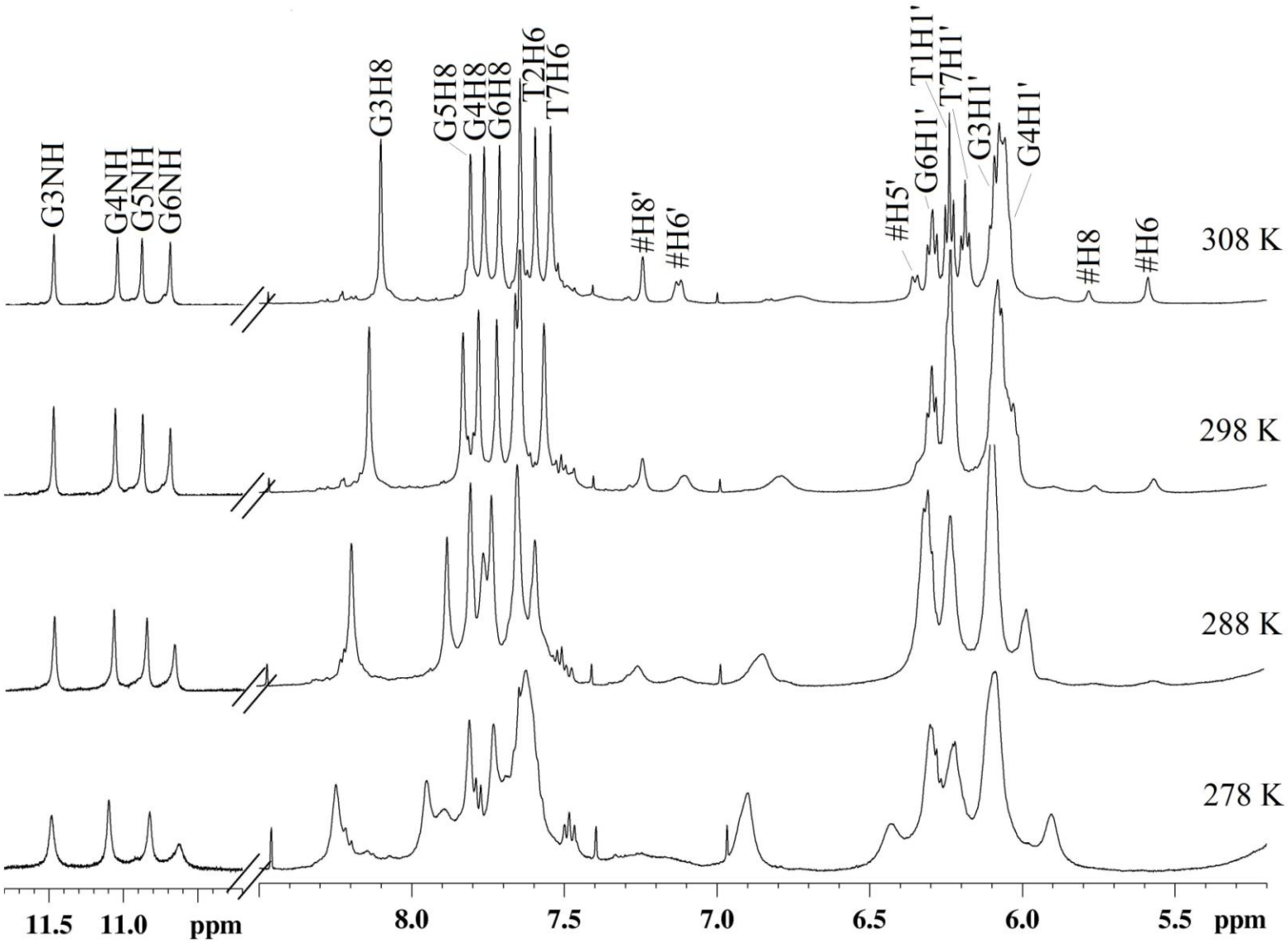

Figure 6.15 Overlap of ^{1}H spectra of rutin complexed d-(TTGGGGT)$_4$ at D/N ratio 2.0 versus temperature range of 278-308 K (Rutin protons marked as #).

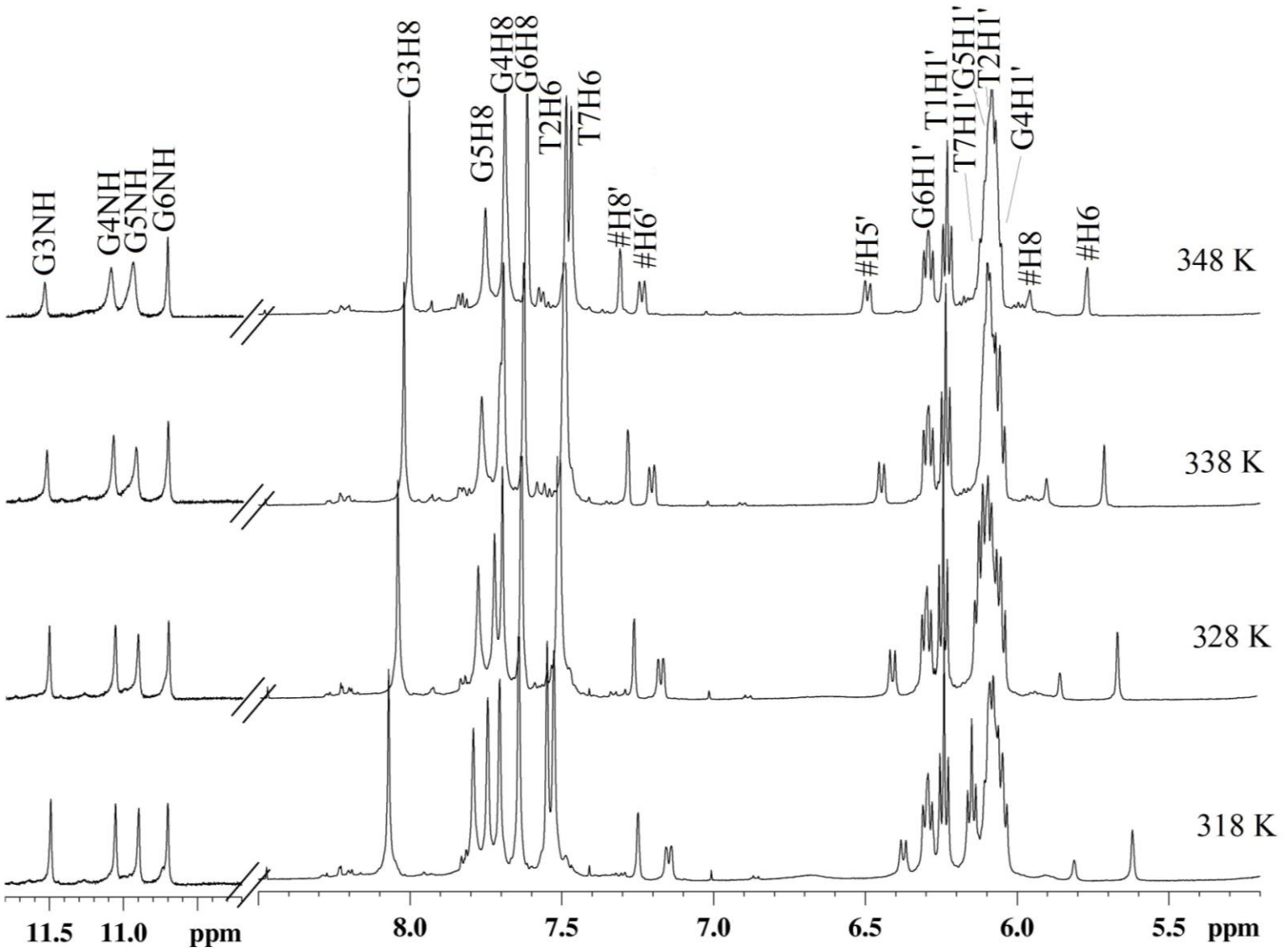

Fig 6.16 Overlap of ^{1}H spectra of rutin complexed d-(TTGGGGT)$_4$ at D/N ratio 2.0 versus temperature range of 318-348 K (Rutin protons marked as #).

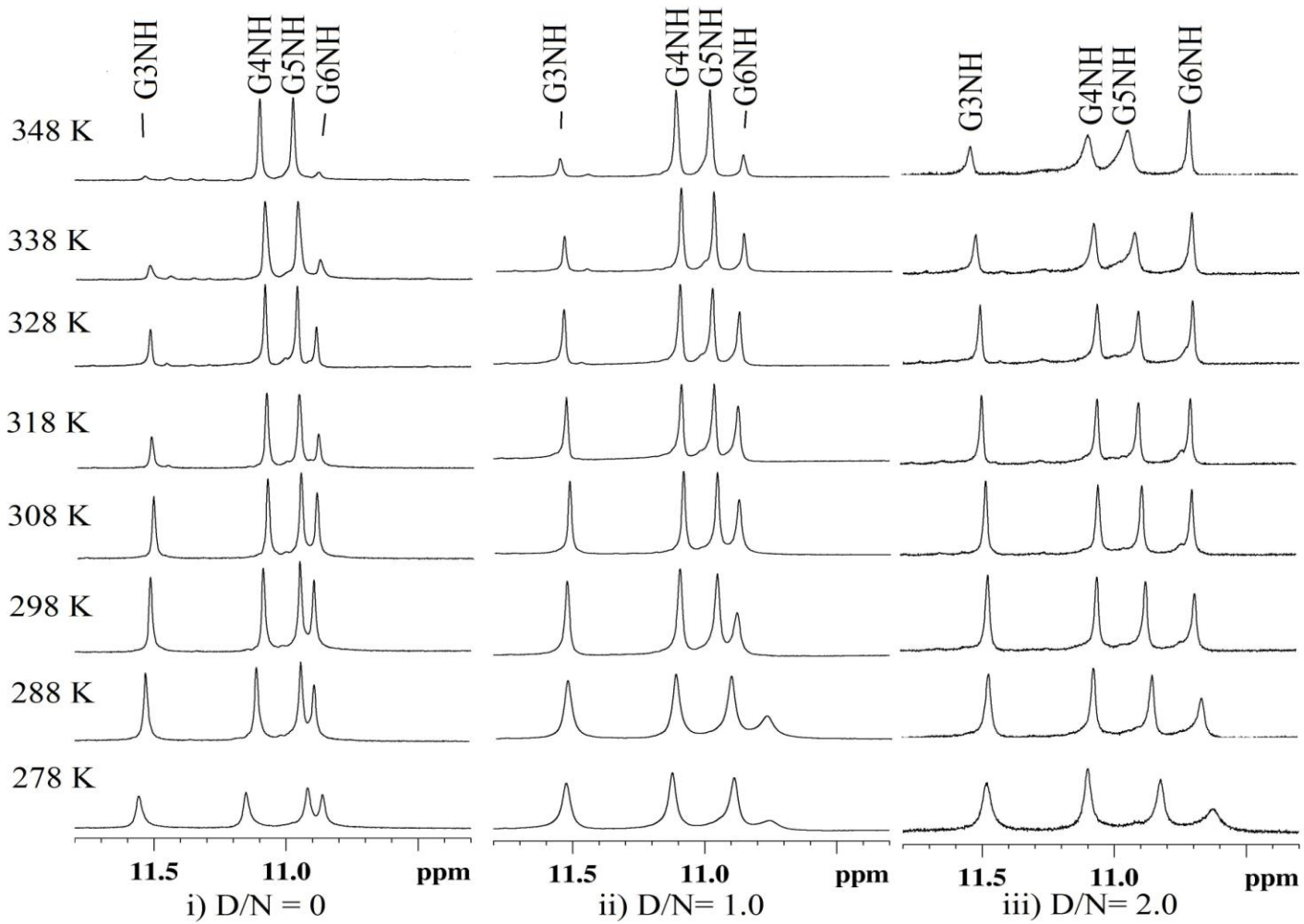

Figure 6.17: Stack of G-quartet NH protons melting profiles studied over a temperature range of 278 K- 348 K i) uncomplexed d-$(TTGGGGT)_4$, ii) rutin-d-$(TTGGGGT)_4$ at D/N 1.0 , iii) rutin-d-$(TTGGGGT)_4$ at D/N 2.0.

Table 6.10: ^{1}H chemical shift δ (ppm) of quadruplex protons in d-(TTGGGGT)$_4$-rutin complex as a function of temperature at D/N 2.0. $\Delta\delta = \delta b_{(353\ K)} - \delta f_{(278\ K)}$. +ve Δδ downfield shift and –ve Δδ upfield shift.

	T1H6	T2H6	G3H8	G4H8	G5H8	G6H8	T7H6
278	7.78	7.62	8.25	7.81	7.95	7.73	7.63
283	7.78	7.59	8.22	7.80	7.91	7.73	7.64
288	7.76	7.59	8.19	7.80	7.87	7.73	7.65
293	7.70	7.58	8.16	7.79	7.85	7.72	7.65
298	7.66	7.57	8.14	7.78	7.83	7.72	7.65
303	7.62	7.56	8.12	7.77	7.82	7.71	7.65
308	7.59	7.55	8.10	7.76	7.81	7.71	7.65
313	7.57	7.54	8.08	7.75	7.80	7.71	7.64
318	7.55	7.53	8.07	7.74	7.79	7.70	7.64
323	7.53	7.52	8.06	7.73	7.78	7.70	7.64
328	7.51	7.51	8.04	7.72	7.78	7.70	7.63
333	7.50	7.50	8.03	7.71	7.77	7.69	7.63
338	7.49	7.49	8.02	7.70	7.76	7.69	7.63
343	7.48	7.49	8.00	7.69	7.76	7.69	7.62
348	7.47	7.48	8.00	7.68	7.75	7.69	7.61
353	7.46	7.48	7.99	7.67	7.74	7.68	7.61
Δδ	-0.32	-0.14	-0.26	-0.14	-0.21	-0.05	-0.02

Table 6.11: ^{1}H chemical shift of rutin protons in d-(TTGGGGT)$_4$-rutin complex at D/N 2.0 vs temperature. $\Delta\delta = \delta b_{(353\ K)} - \delta f_{(278\ K)}$. +ve Δδ downfield shift and -ve Δδ upfield shift.

	H2'	H5'	H6'	H6	H8	H6'''
278	7.25	-	7.16	-	-	0.90
283	7.25	-	7.14	-	-	0.88
288	7.25	-	7.11	5.57	5.75	0.87
293	7.25	-	7.11	5.57	5.75	0.87
298	7.24	6.34	7.11	5.57	5.76	0.86
303	7.24	6.34	7.11	5.58	5.77	0.86
308	7.24	6.35	7.13	5.59	5.78	0.86
313	7.24	6.36	7.14	5.60	5.79	0.86
318	7.25	6.37	7.15	5.62	5.81	0.86
323	7.25	6.39	7.16	5.64	5.83	0.86
328	7.26	6.40	7.17	5.66	5.85	0.86
333	7.27	6.42	7.19	5.69	5.88	0.86
338	7.28	6.45	7.20	5.72	5.90	0.87
343	7.29	6.47	7.22	5.74	5.93	0.87
348	7.31	6.49	7.24	5.77	5.96	0.88
353	7.32	6.52	7.25	5.80	5.99	0.89
Δδ	0.07	0.18	0.09	0.23	0.24	-0.01

6.1.5 Phosphorous-31 NMR studies on complex of rutin-d-$(TTGGGGT)_4$

6.1.5.1 ^{31}P resonance assignment of alone d-$(TTGGGGT)_4$ quadruplex DNA.

Unambiguous assignment of backbone 31-phosphorous resonances of uncomplexed d-$(TTGGGGT)_4$ were done by using standard strategies of ^{1}H-^{31}P heteronuclear multiple bond correlation (HMBC) techniques. The ^{31}P signal belongs to n^{th} step shows strong correlation with three bond scalar coupled $(H3')_n$ and $(H5'/H5'')_{n+1}$ protons and a weak correlation with four bond scalar coupled $(H4')_n$ and $(H4')_{n+1}$ protons. The ^{31}P signals were named as d-(T1pT2pG3pG4pG5pG6pT7) for the sin ^{31}P signals belongs to d-$(TTGGGGT)_4$ quadruplex sequence. The 31P resonances were assigned using ^{1}H-^{31}P HMBC spectra of d-$(TTGGGGT)_4$ at 298 K. The assignment of protons of d-$(TTGGGGT)_4$ at 298 K aids in the assignment of 31P resonances by providing the exact position of H3'/H4'/H5'/H5' signals. The terminal ^{31}P resonances of T1pT2 and G6pT7 resonates at -0.437 and -0.712 ppm, respectively. The remaining four signals belong to T2pG3, G3pG4, G4pG5 and G5pG6 resonates at -0.619, -0.861, -0.733 and -0.831 ppm, respectively. As TTGGGGT sequence forms tetramolecular parallel quadruplex structure, with C4 symmetry, we observe six phosphorous signals for the quadruplex structure. The observed ^{31}P chemical shift range between -0.43 ppm to -0.861 ppm, clearly indicates that quadruplex adopts right handed helical geometry.

6.1.5.2 Phosphorous-31 NMR of rutin-d-$(TTGGGGT)_4$ quadruplex DNA.

Addition of rutin to d-$(TTGGGGT)_4$ quadruplex DNA to reach D/N ratios (Fig 6. 18) of 0.25, 0.5, 0.75 and 1.0 doesnot results in the development of any extra peak in the down-field region of the existing peaks. Only six ^{31}P resonances were observed even after the addition of two equivalent mol of rutin to quadruplex DNA, which confirms the quadruplex DNA doesn't open up to accommodate the ruin molecule. Hence quadruplex structure along with its C4 symmetry is maintained at this D/N ratio. Change in the chemical shifts positions of ^{31}P signals upon complex formation as a function of D/N ratios were given in Table 6.12. Complex formation results in the downfield shift of ^{31}P signals belong to all the steps except for G5pG6, which shows downfield shift of -0.025 ppm. G6pT7 and G4pG5 step ^{31}P signals shows maximum up-field shift by 0.194 and 0.189 ppm, respectively. Whereas T1pT2, G3pG4 and T2pG3 step signals shift by 0.114, 0.105, 0.084 ppm respectively. The magnitude of chemical shift change in ^{31}P signals upon rutin binding is less when compared to classical intercalative binding, which shows downfield shift of ^{31}P signals by >1.5 ppm (*Searle et al. 1988, Mazzini et al. 1998*). On the other hand less than 0.5 ppm change in

chemical shift position upon binding of a ligand indicates the external binding like groove binding or end stacking, which doesnot require opening of base quartet. Hence obtained chemical shift changes suggests that rutin binds to d-(TTGGGGT)$_4$ quadruplex by external binding mode.

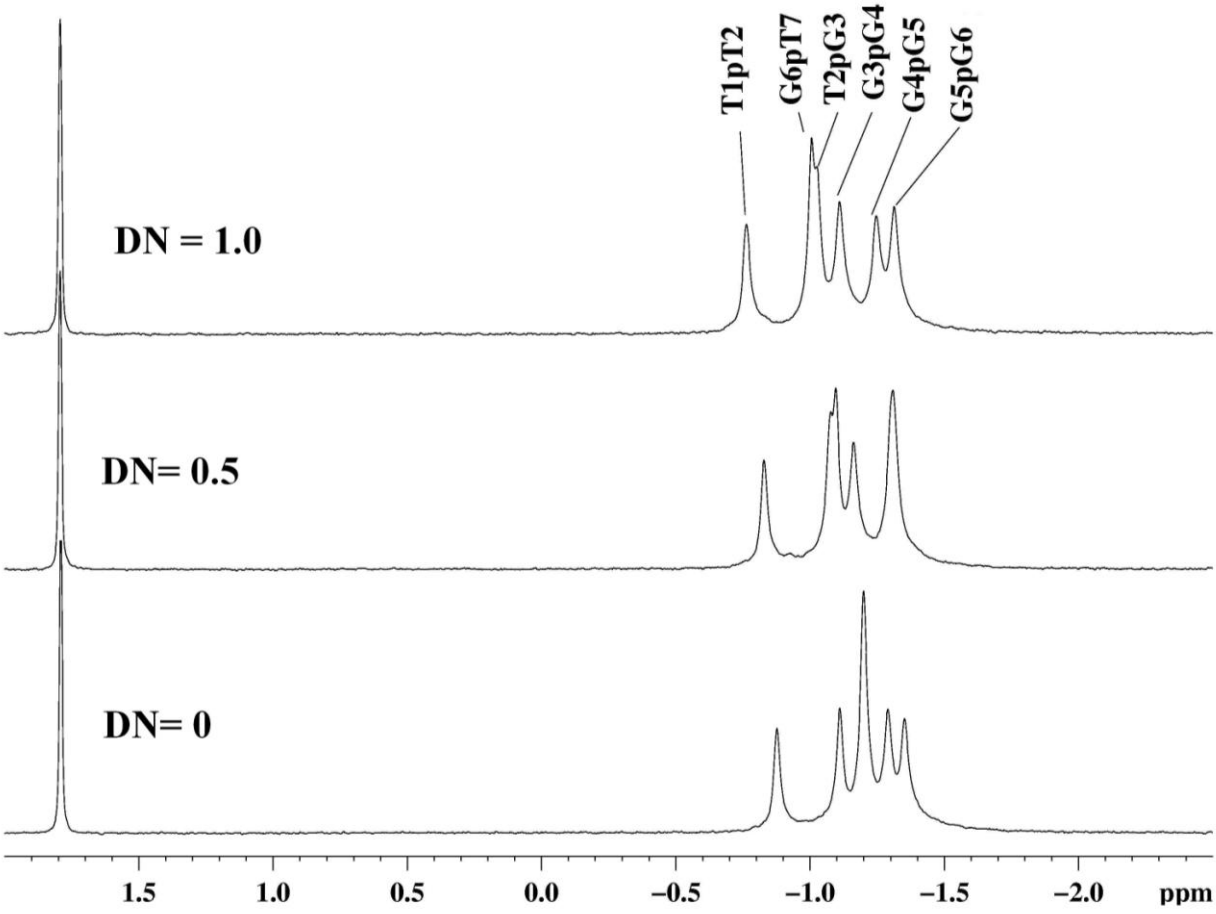

Fig 6.18 Stack of ^{31}P spectra of uncomplexed d-(TTGGGGT)$_4$ and rutin complexed d-(TTGGGGT)$_4$ at D/N ratios 0.5 and 1.0 at 298 K.

Table 6.12 ^{31}P chemical shift of d-(TTGGGGT)$_4$ protons in d-(TTGGGGT)$_4$-rutin complex at 298 K as a function of D/N. $\Delta\delta = \delta b_{(D/N\ 1.0)} - \delta f_{(D/N\ 0.0)}$. +ve $\Delta\delta$ downfield shift and -ve $\Delta\delta$ upfield shift.

	T1pT2	T2pG3	G3pG4	G4pG5	G5pG6	G6pT7
0.0	-0.875	-1.109	-1.351	-1.198	-1.289	-1.198
0.25	-0.851	-1.097	-1.326	-1.184	-1.306	-1.151
0.5	-0.828	-1.076	-1.307	-1.162	-1.306	-1.095
0.75	-0.794	-1.051	-1.275	-1.136	-1.317	-1.005
1.0	-0.761	-1.025	-1.246	-1.109	-1.314	-1.004
Δδ	0.114	0.084	0.105	0.189	-0.025	0.194

6.1.6 Resonance assignment of rutin-d-(TTGGGGT)$_4$ complex.

Two dimensional ^{1}H-^{1}H NOESY, ^{1}H-^{1}H COSY, ^{1}H-^{1}H TOCSY and ^{1}H-^{13}C HSQC techniques were used to unambiguously assign resonances of rutin-d(TTGGGGT)$_4$ complex at D/N 1.0 at 298 K. The resonances were assigned using strategies mentioned in the section 6.1.2. Fig. 6.21 shows the NOESY expansion of aromatic base H8/H6 and sugar H1'/H2'/H" protons region, all the sequential correlations between intra base H8/H6 protons with its sugar H1'/H2'/H" protons were present. This shows that d-(TTGGGGT)$_4$ structure doesnot open up to accommodate rutin, hence ruling out the possibility of intercalation. The observation of NOE cross peak between imino resonances of the two successive G-quartet steps also confirms that rutin doesnot intercalate into any of the G-quartet steps (Fig.6.20).

After the assignment of resonances of quadruplex DNA, rutin resonances were assigned using the correlations present in ^{1}H-^{1}H NOESY and ^{1}H-^{13}C HSQC experiments of complex at D/N 2.0. The monitoring of titration data helps in the identifying the rutin protons, as resonances of these protons grow in intensity with each increasing DN ratio. The utilization of ^{1}H-^{13}C HSQC experiment to assign rutin proton helps in the fact that, the aromatic ^{13}C resonances of rutin molecule resonate between ~ 95 – 126 ppm while that of quadruplex heterocyclic aromatic ring ^{13}C resonances resonates in the region downfield of ~ 135 ppm and anomeric sugar H1' attached ^{13}C resonances resonates in the region upfield of ~ 89 ppm. Hence the correlation peaks in ^{1}H-^{13}C HSQC experiment which appears in the region ~ 95 – 130 ppm was attributed to the ^{13}C resonances of the rutin attached to its aromatic protons. Fig.6.19 shows the overlap of uncomplexed ^{1}H-^{13}C HSQC of d-(TTGGGGT)$_4$ (red) with that of two molar equivalents rutin complexed d-(TTGGGGT)$_4$ (black), five ^{1}H-^{13}C correlations belongs to H2', H6', H5', H6 and H8 protons and their respective 13-carbons were clearly observed in the aromatic region.

The 13-carbons attached to anomeric protons H1" and H1'" resonates around ~ 101-107 ppm, where no other quadruplex signals were observed, hence these two correlations were assigned easily. The downfield resonating signal at ~ 107.3 ppm was assigned to ^{13}C attached to H1" proton of glucose sugar and upfield signal at ~ 103.5 ppm was assigned ^{13}C attached to H1'" proton of rahmnose sugar. The assignment of 13-carbon signals attached to H6'" proton of rahmnose sugar was straightforward as this proton signal resonates in the most upfield region and hence the signal at ~ 19.0 ppm was assigned to the ^{1}H-^{13}C correlation because of it.

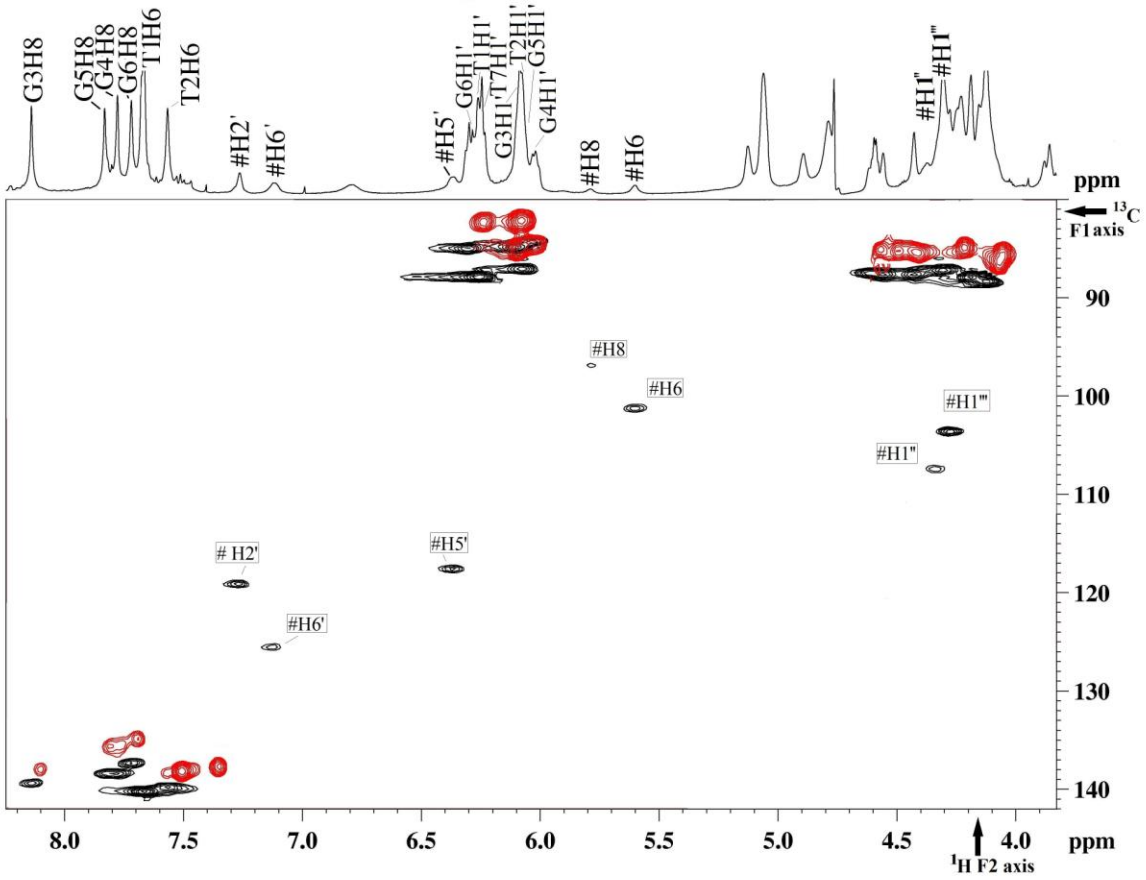

Figure 6.19: Overlap of ^{1}H-^{13}C HSQC spectrum of 2:1 rutin complexed d-(TTGGGGT)$_4$ (black) and alone d-(TTGGGGT)$_4$ at 298 K, showing rutin ^{1}H and ^{13}C correlations after complex formation.

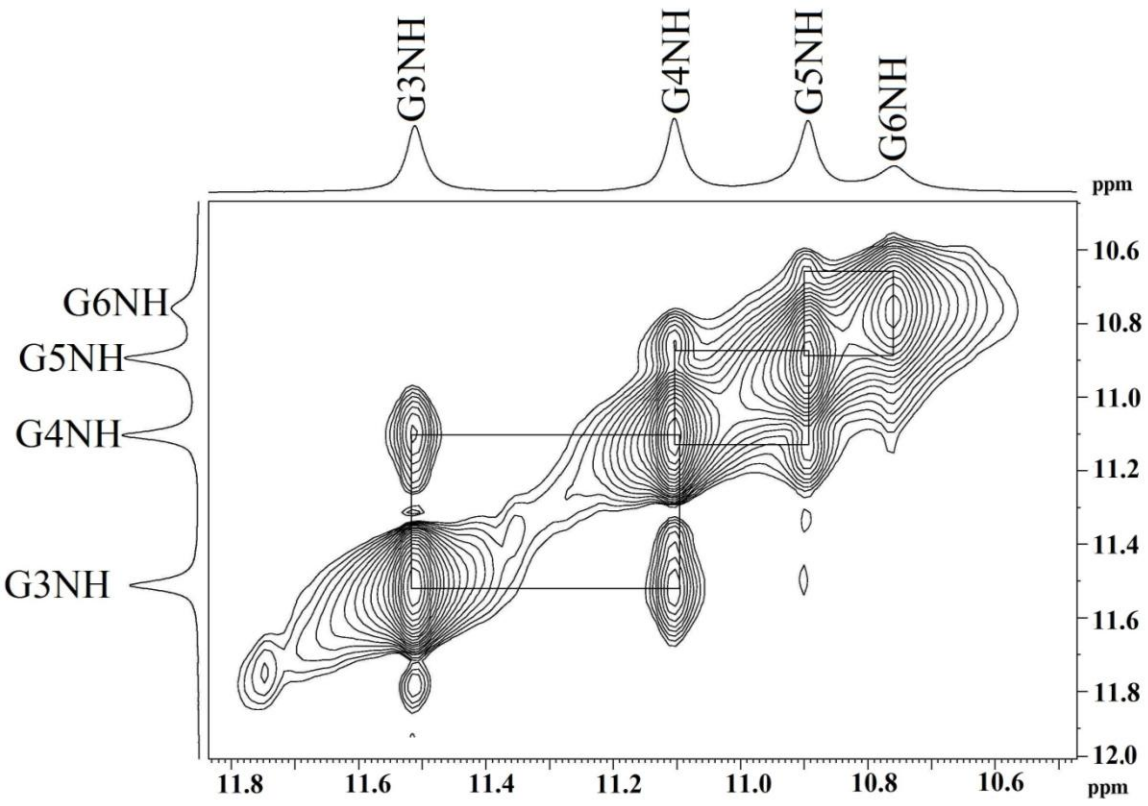

Figure 6.20: Expansion of 200ms NOESY spectrum of 1:1 rutin-d-(TTGGGGT)$_4$ complex at 298 K showing connectivities between guanine NH-NH protons of successive G-quartet steps in d-(TTGGGGT)$_4$.

The remaining ^{13}Csignals of glucose and rahmnose sugar resonate in the region between ~ 64 – 80 ppm on the ^{13}C axis, this region overlaps with the resonances form ^{13}C attached to H5'/H5" of pentose sugars of quadruplex DNA. But on the ^{1}H axis these signals separate out, as quadruplex sugar H5'/H" resonates downfield of ~ 3.77 ppm while ring protons of the rutin sugars resonate upfield of ~3.77 ppm. Hence these signals are easily identified and assigned on the ^{1}H-^{13}C HSQC spectra.

The NOESY overlap of expansion of uncomplexed d-(TTGGGGT)$_4$ and 2:1 rutin complexed d-(TTGGGGT)$_4$ at 298 K (Fig.6.23) shows NOE correlation between aromatic H6' and H5' protons of rutin molecule and the scalar (^{3}J) coupling between these two protons. As there is no scalar coupled proton correlation can be expected in this region of d-(TTGGGGT)$_4$, this peak can be assigned unambiguously to H5' and H6' protons. This can be further confirmed by TOCSY experiments, as the protons H2', H6' and H5' of ring A show TOCSY correlation between

themselves and H6 and H8 protons of ring B show correlation between them. Hence by this way aromatic protons of rutin in complexation with d-(TTGGGGT)$_4$ has been identified.

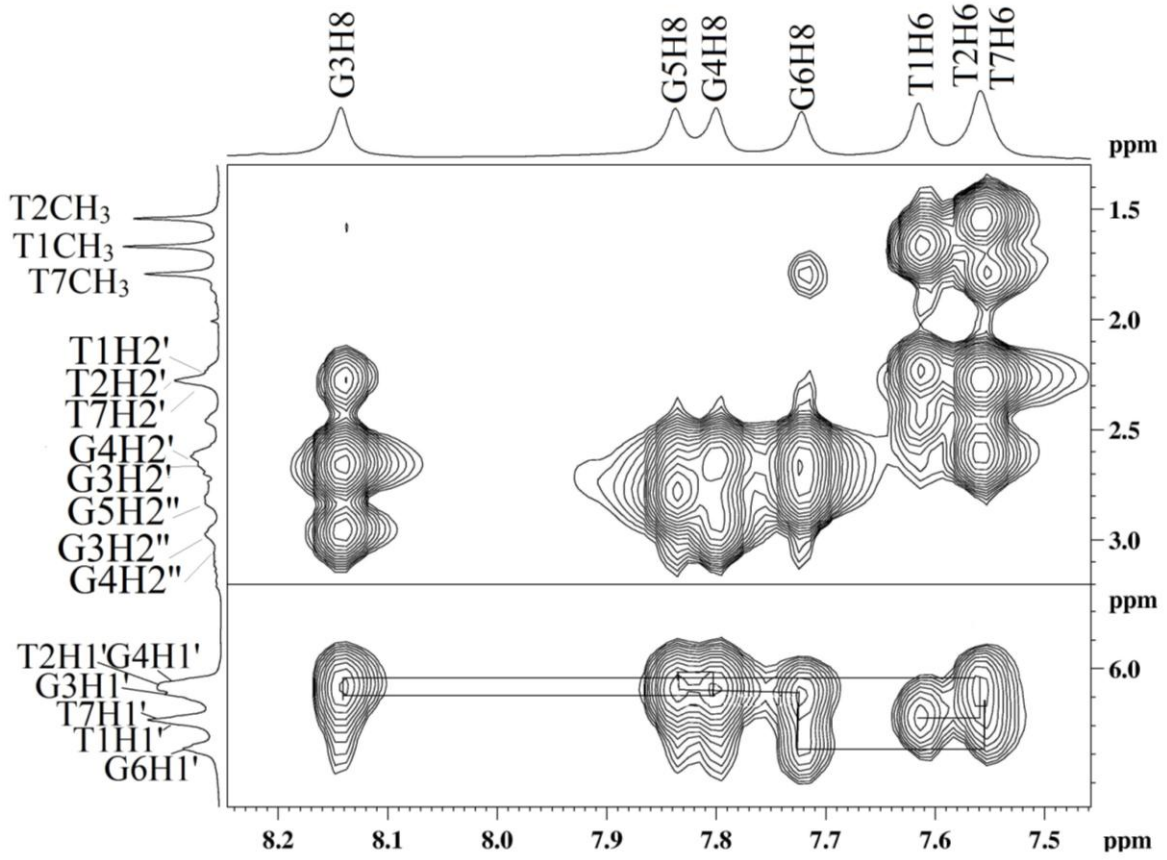

Figure 6.21: Expansion of 200ms NOESY spectrum of 2:1 rutin-d-(TTGGGGT)$_4$ complex at 298 K showing sequential connectivities between aromatic H8/H6 protons with sugar H1'/H2'/H2'' protons of d-(TTGGGGT)$_4$ proton.

Similarly, a combination of NOESY, TOCSY and ^{1}H-^{13}C HSQC experiments were used to identify the sugar protons of 2:1 complex rutin. TOCY experiment helps in identifying sugar resonances of glucose and rahmnose moieties present in rutin molecule, as these protons of these two sugars give separate TOCSY correlations like the resonances of deoxy-ribose sugar of d-(TTGGGGT)$_4$.

The NOESY spectra of rutin-d-(TTGGGGT)$_4$ complex at D/N ratio 2.0 show intramolecular NOEs between aromatic and sugar ring protons of rutin, apart from these dipolar coupled protons, NOEs

between scalar coupled protons were also observed (Fig. 6.22). These NOEs helps in the understanding of spatial arrangement of rutin sugar with respect to aromatic flavonol ring. The NOEs obtained were used in restrained molecular dynamics to build the structure adopted by rutin molecule upon quadruplex interaction. A total of 18 intermolecular intramolecular peaks were observed between rutin protons (Table 6.13), which were used during restrained molecular dynamics simulation studies.

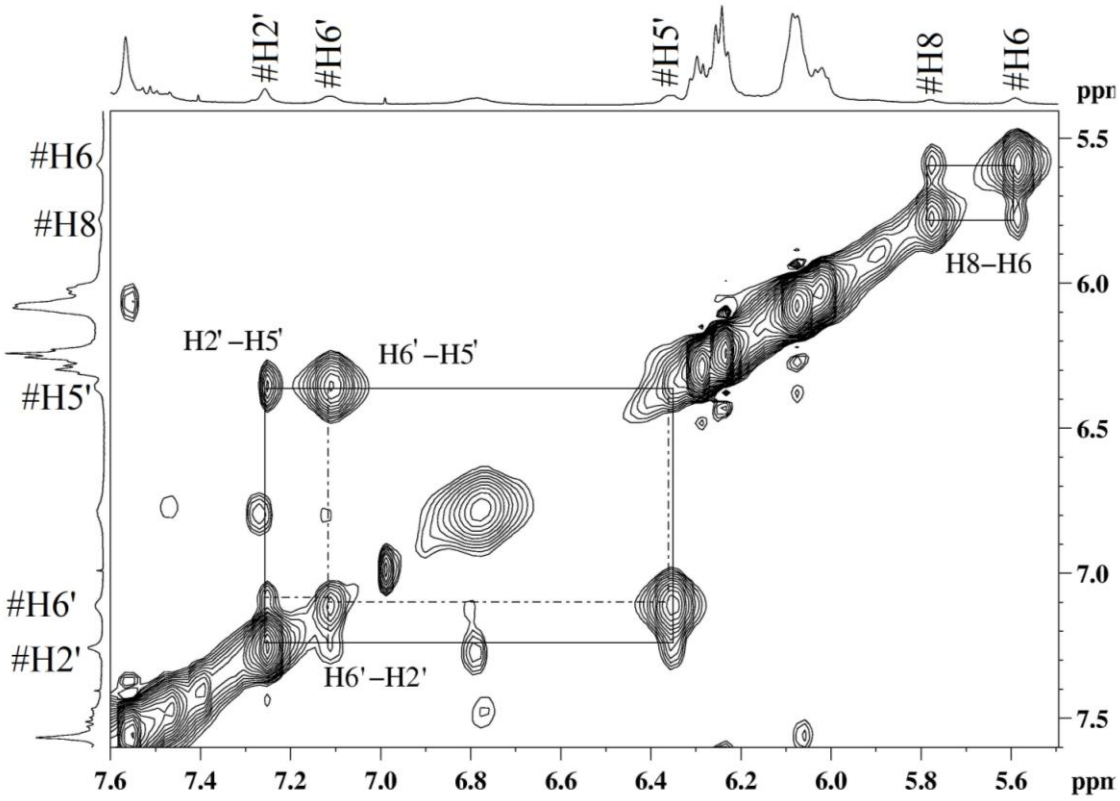

Figure 6.22: Expansion of TOCSY spectrum of 2:1 rutin-d-(TTGGGGT)$_4$ at 298 K complex showing correlations between aromatic ring A (H2'-H5', H6'-H5' and H6'-H2') and ring B (H8-H6) protons of complexed rutin.

The NOESY expansion of rutin- d-(TTGGGGT)$_4$ complex D/N 2.0 at 298 K (Fig.6.24) show NOE correlations (intermolecular contacts) between rutin and d-(TTGGGGT)$_4$ protons (labeled as #). The spectra of rutin-d-(TTGGGGT)$_4$ complex at D/N ratio 1.0 shows intermolecular NOEs between rutin and d-(TTGGGGT)$_4$ protons. The rutin H2', H6' and H8 aromatic protons shows intermolecular NOE connectivities with G6NH, G6H8 protons of d-(TTGGGGT)$_4$ quadruplex (Table 6.14). Increase in the rutin concentration to reach molar equivalent ratio (D/N 2.0) of 2.0

results in the appearance of new NOE correlations between rutin and d-(TTGGGGT)$_4$ protons. The new NOEs at D/N correspond to the sugar protons belong to T1and T2 step. i.e. T1H2', T2CH$_3$ and T2H2' protons. No NOE correlations were observed for rutin with G3:G4:G5 step protons of d-(TTGGGGT)$_4$ quadurplex.

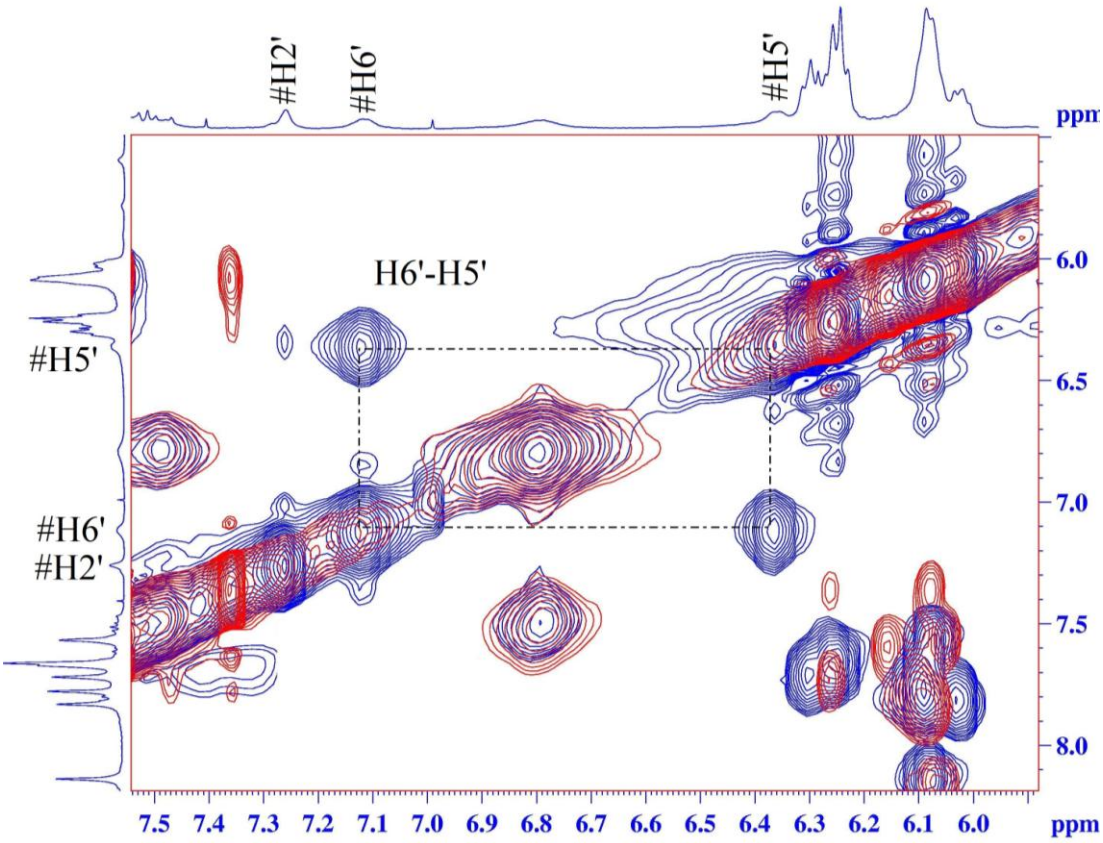

Figure 6.23: Expansion of 200 ms NOESY spectrum of uncomplexed (red) and 2:1 rutin complexed d-(TTGGGGT)$_4$ (blue) at 298 K complex showing intra-molecular contact between rutin aromatic protons H5' and H6'.

Due to the overlapping with G6H1' proton resonance of quadruplex DNA, intermolecular NOE contacts between H5' proton or rutin and protons of quadruplex DNA could not be assigned properly. The NOE cross peaks were observed between the aromatic protons of quercetin with T1 and T2 step methyl and sugar H2'/H2'' protons. The A ring aromatic H6 proton gives medium intensity NOE correlation with G3H2' proton.

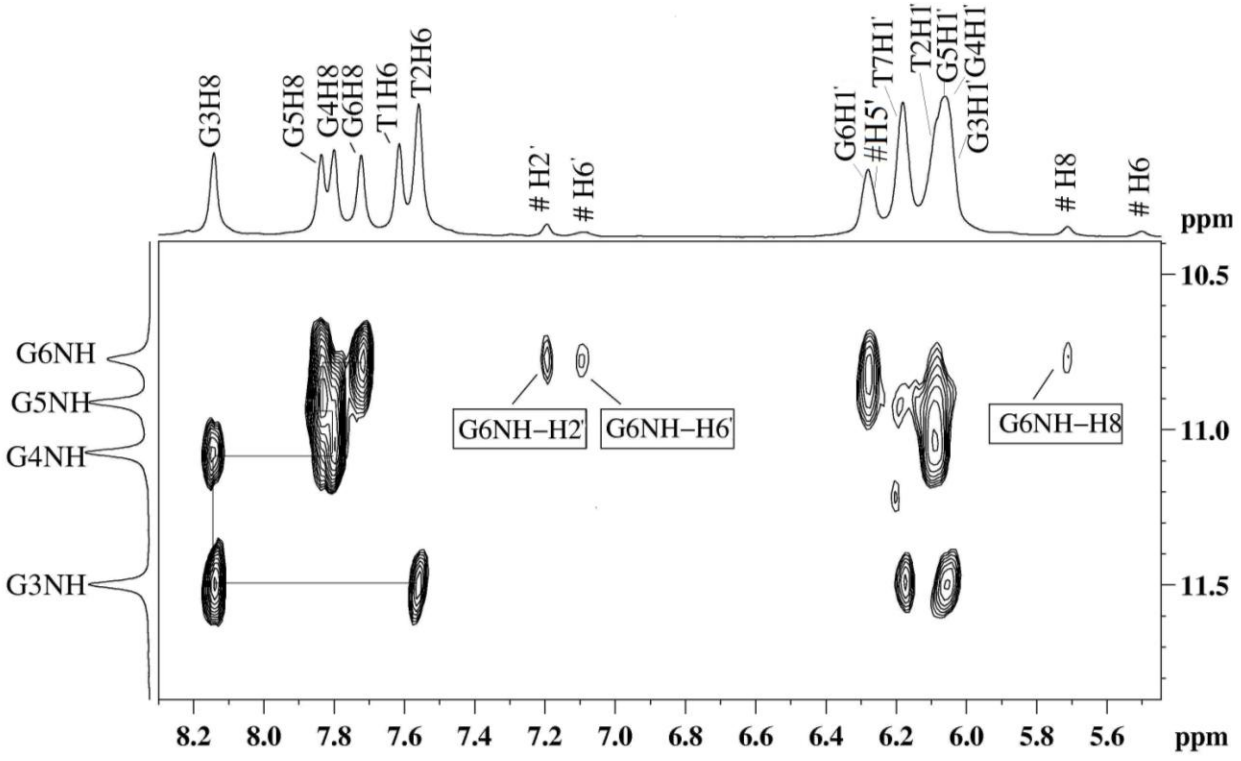

Figure 6.24: Expansion of 200ms NOESY spectrum of 1:1 rutin-d-(TTGGGGT)$_4$ complex at 298 K showing intermolecular contacts between rutin protons and d-(TTGGGGT)$_4$ protons (denoted as #).

Total 11 intermolecular NOE contacts were observed between rutin and d-(TTGGGGT)$_4$ quadruplex protons. The intermolecular NOEs were separated into two groups, one set of NOEs between rutin and T1pT2 step protons and second set of NOEs between rutin and G6pT7 step protons. Analysis of observed NOEs, clearly shows that d-(TTGGGGT)$_4$ has two binding sites for rutin. The first site at G6pT7 step is high affinity one, as intermolecular peaks were observed at D/N 1.0 and the second low affinity site at T1pT2 step, which shows intermolecular peaks at D/N 2.0. Since single molecule of rutin cannot give intermolecular peaks with both T1pT2 step and G6pT7 step protons simultaneously, this establishes that two molecules of rutin bind to d-(TTGGGGT)$_4$ quadruplex structure in a stoichiometric ratio of 2:1.

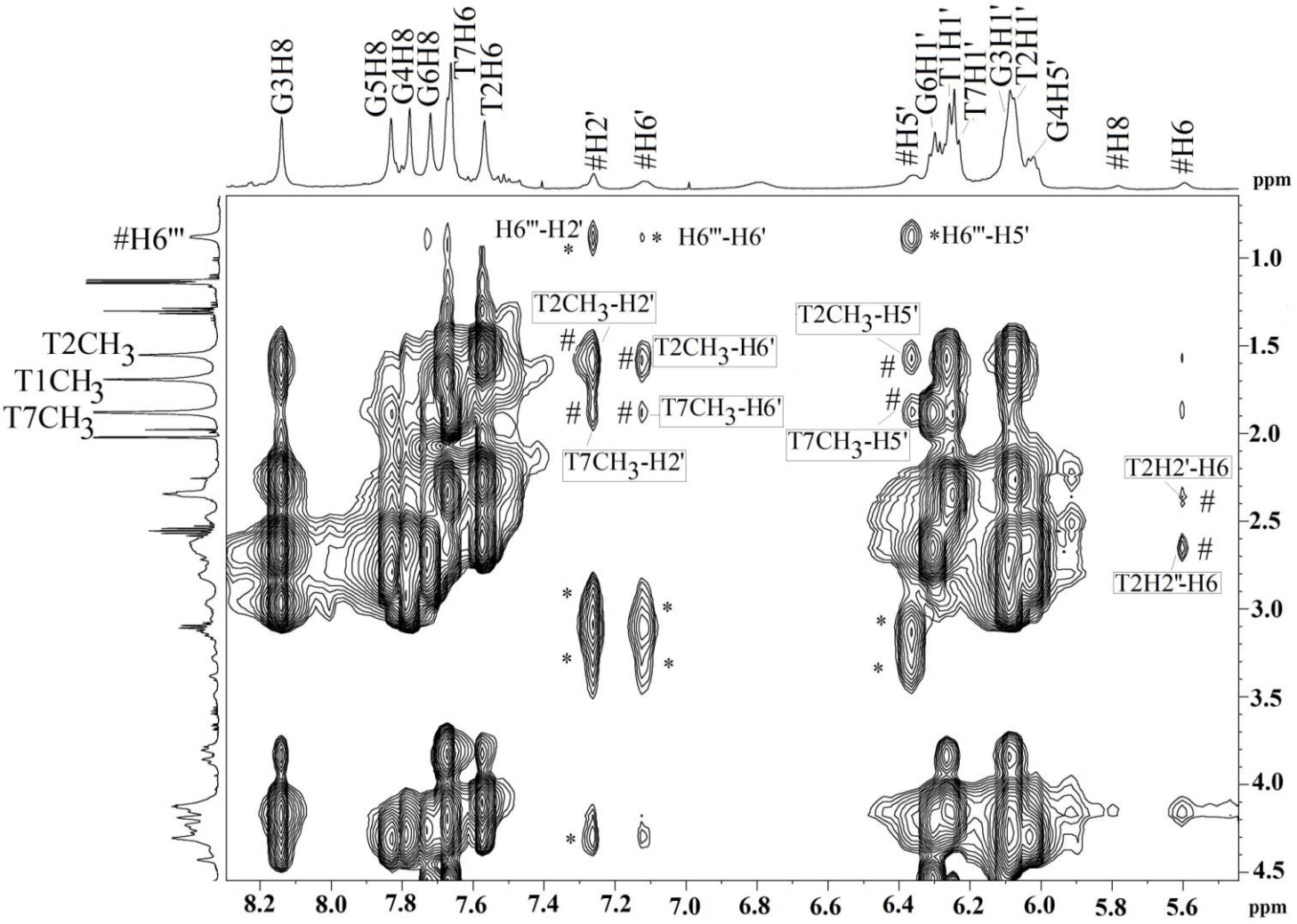

Figure 6.25: Expansion of 200ms NOESY spectrum of 2:1 rutin-d-(TTGGGGT)$_4$ at 298 K complex showing intermolecular contacts between rutin protons and d-(TTGGGGT)$_4$ protons (denoted as #) and intramolecular contacts with in rutin molecule (denoted as *).

Table 6.13: Rutin-rutin intra-molecular contacts in rutin-d-$(TTGGGGT)_4$ complex at D/N 2.0 at 298 K, also shown intensities of cross peaks (m= medium, w= weak, ww=very weak), distance obtained from NOESY cross peaks and distance obtained after rMD simulations.

Sl. no	Rutin protons	Intensity	Distance from NOE (Å)	Distance from rMD (Å)
1	H2'-H5'	ww	4.9	4.9
2	H2'-H6'	ww	4.6	4.7
3	H2'-H1"	w	4.2	4.1
4	H2'-H1"'	w	4.1	4.0
5	H2'- H4"'	m	3.5	3.6
6	H2'- H5"'	m	3.4	3.5
7	H2'-H6"'	w	4.0	3.9
8	H6'- H5'	s	2.4	2.45
9	H6'-H1"'	w	3.9	3.8
10	H6'-H4"'	m	3.1	3.15
11	H6'-H5"'	m	3.5	3.6
12	H6'- H6"'	w	4.3	4.3
13	H5'- H1"'	m	3.6	3.7
14	H5'- H4"'	m	3.4	3.45
15	H5'- H5"	m	3.5	3.6
16	H5'- H6"'	m	3.1	3.2
17	H6-H1"'	w	4.5	4.5
18	H6"'-H5"'	s	2.8	2.5

Table 6.14: Rutin-d-$(TTGGGGT)_4$ intermolecular contacts obtained at D/N 2.0 complex at 298 K, also shown intensities of cross peaks (m= medium, w= weak, ww=very weak), distance obtained from NOESY cross peaks and distance obtained after rMD simulations.

Sl No	Rutin protons	d-$(TTGGGGT)_4$ protons	Intensity of NOE	Distance from NOESY (Å)	Distance from rMD (Å)
I1	H6'	G6NH	m	3.6	3.5
I2	H2'	G6NH	w	4.2	4.2
I3	H8	G6NH	ww	4.6	4.5
I4	H2'	$G6NH_2^{nb}$	ww	4.7	4.6
I5	H8	G6H8	ww	4.6	4.6
I6	H5'	$T7CH_3$	w	4.1	4.0
I7	H5'	$T2CH_3$	m	3.6	3.5
I8	H2'	$T2CH_3$	m	3.80	4.1
I9	H6'	$T2CH_3$	w	4.0	3.8
I10	H6	T2H2'	w	4.25	4.2
I11	H6	T2H2"	w	4.1	4.0

The observed intermolecular contacts (I peaks) were listed in table 6.14 with distances obtained from integration of NOE volume. The interproton distances present were divided into weak, medium and strong based on the intensity of the cross peaks. All the observed NOE cross peaks were in the range of medium to weak. These intermolecular contacts provide the direct insight into the possible orientation of rutin molecule in the binding site. The $T1CH_3$, $T2CH_3$ and T2 H2'/H2" protons occupy the groove region of the d-$(TTGGGGT)_4$ quadruplex structure, the observed NOEs between rutin and d-$(TTGGGGT)_4$ indicates the possibility of rutin binding to the groove region of quadruplex.

The presence of base H8/H6 - sugar H1' /H2'/H2" sequential connectivities and guanine imino-imino (GNH) connectivities between successive G-quartet planes (G3:G4:G5:G6) in the NOESY spectrum of 2:1 rutin complexed d-$(TTGGGGT)_4$ excludes intercalative mode of binding by rutin. The absence of extra bound resonances in the downfield region of phosphorous-31 spectrum along with very little (less than $\Delta\delta$ = 0.5 ppm) change in position of ^{31}P signals also supports this conclusion.

The shifts in the position of guanine imino protons involved in the G-quartet formation are the important indicators of type of ligand binding to the quadurplex DNA. In the present study GNH protons show large upfield shift ($\Delta\delta_{max}$ = 0.24 ppm, for G6NH) which is similar to the observed shifts of well known quadruplex end stackers like TMPyP4 ($\Delta\delta_{max}$ = 0.21 ppm) (*Mita et al. 2006*) and RHPS4 ($\Delta\delta_{max}$ = 0.45 ppm) (*Gavathiotis et al. 2003*). Magnitude of chemical shift change observed in quadruplex protons upon quercetin binding is also very less. The chemical shift changes of G-imino protons in our studies ($\Delta\delta_{max}$ = 0.24 ppm upfield shift) is less when compared to the the changes observed in d-(TGGGGT)4-distamycin complex ($\Delta\delta_{max}$ = 0.18 ppm upfield shift) and also in d-(TGGGGT)4-distamycin analogue/derivative complex ($\Delta\delta_{max}$ = 0.15 ppm upfield shift) (*Martino et al. 2007; Cosconati et al. 2010*). Distamycin and its derivatives interact with tetramolecular quadruplex structure via a groove binding mode. This clearly shows that rutin binds to G6pT7 step by partial end-stacking mode, with rutin aromatic chromophore inserting between G6pT7 step and bulky sugar groups present in the groove region. In the second binding site of T1pT2, rutin binds in the groove region, with its aromatic ring giving NOE correlations with groove protons of T1pT2 step, i.e. H6 proton with T2H2'/H2" protons, H6' proton with $T2CH_3$ protons, H2' proton with $T2CH_3$ protons. These results were similar to that of observed by Sun et

al., (Sun et al., 2007) as they predicted rutin forms a structure of hammer and blade, the aromatic rings acts as blade and stacks on G-quartet, whereas the torsional flexible sugars act as hammer. Hence we can say by observed NOEs that ruitn aromatic ring stacks on the 3' terminal G-quartet, stabilized by π-π aromatic surface of both rutin and terminal G-tetrad plane. And due to the puckering effect and non planar rings both sugars cannot insert into the quadruplex DNA.

The presence of intramolecular NOEs within the rutin molecule clearly shows that change in conformation of the rahmnose sugar ring upon binding to DNA (Table 6.13).

6.1.7 Restrained molecular dynamics

The NOESY cross peaks at D/N ratio 2.0 at 298 K were used to obtain distances using SPARKY software (*Goddard and Kneller, University of California, San Francisco*). The distances were used as restraints to for the energy minimization using rMD simulations. Apart from NOEs obtained from our studies planar constraints between guanines in G-quartet planes were used in order to stabilize the repulsion due to centrally located four oxygen atoms of a G-quartet. The detailed protocol of simulated annealing and rMD simulations were given in section 2.14.

The distance between aromatic H5'-H6' protons of rutin (2.44 Å) which were well separated at D/N ration 2.0 at 298 K was use as a standard reference distance to calculate the distances. Distances obtained by above mentioned step can be cross verified using the distance of T7CH_3-H6 (2.99 Å) of d-$(TTGGGGT)_4$.

The inter and intra molecular distances obtained in rutin- d-$(TTGGGGT)_4$ complex were classified into three categories, namely i) intermolecular distances between rutin and d-$(TTGGGGT)_4$ protons, ii) intra molecular distances obtained between protons of rutin molecule and iii) intra molecular distances between protons of d-$(TTGGGGT)_4$. Based on this, obtained NOE restraints were classified into quadruplex-rutin constraints, rutin-rutin constraints and quadruplex-quadruplex constraints. These distances were used as NOE restraints to build a structure using restrained molecular dynamics simulation protocol. The tetramolecular quadruplex d-$(TTGGGGT)_4$ PDB structure (139D) (*Wang and Patel, 1994*) was used for quadruplex structures. The potentials of the atoms were changed to suit the potential setup of CVFF force field provided by INSIGHT II. Initial rutin glycoside structure was built using the builder module of INSIGHT II, version 2005 (Accelyrs Inc., San Diego, California) on Silicon Graphics Fuel (SGI)

workstation and energy minimized using biopolymer module. The energy minimized structures were used as starting templates to build a final model.

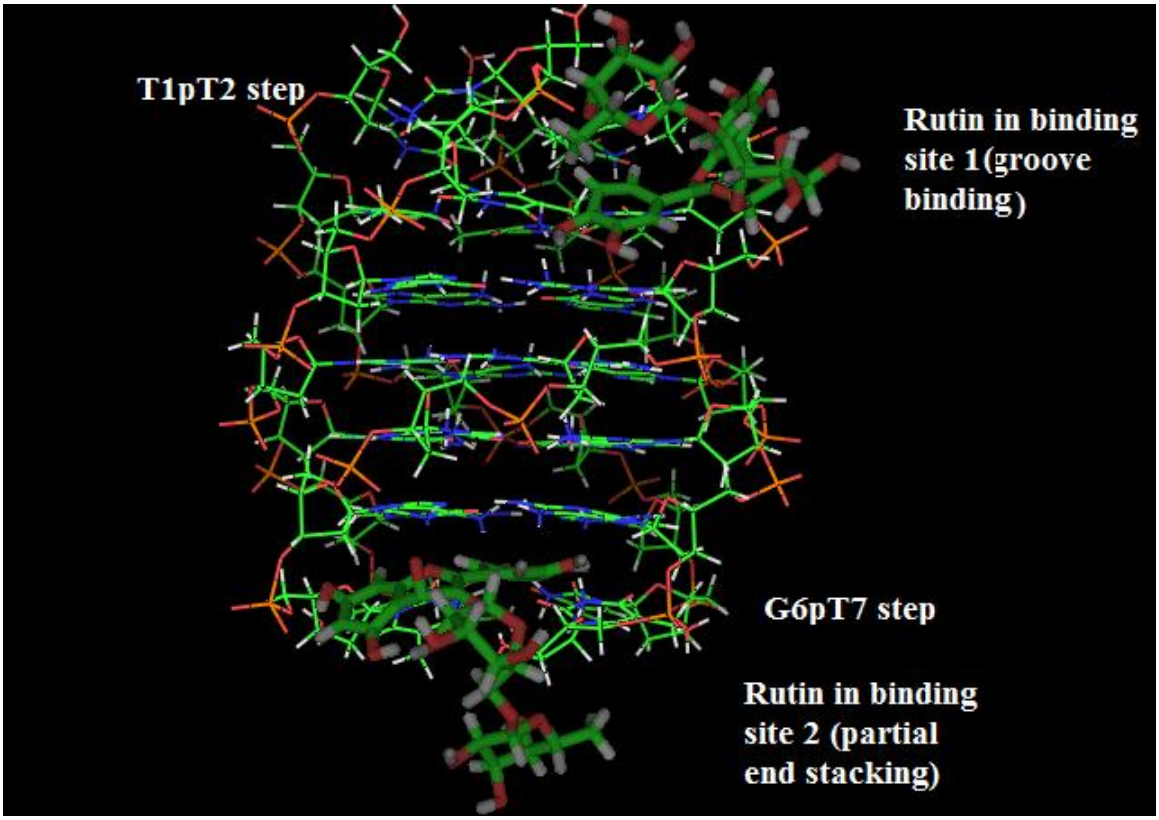

Figure 6.26: Model of final complex of rutin with d-(TTGGGGT)$_4$ after rMD simulations using constraints showing groove binding of rutin to T1pT2pG3 step and G6pT7 step of quadruplex.

The obtained 18 intramolecular rutin NOE distances were used to build initial structure of rutin. The energy minimized rutin molecule was placed in the two binding sites i.e. G6pT7 and T1pT2pG3 step and G6pT7 step of the quadruplex DNA such that all the intermolecular constraints between rutin and d-(TTGGGGT)$_4$ were satisfied. After the orientation of rutin molecule in the binding sites, the intermolecular rutin-quadruplex, intramolecular rutin-rutin and quadruplex-quadruplex NOE restraints were incorporated using generic distance option of the Discover module with a force constant of 25, 15, 10 Kcal mol^{-1} Å^{-2} for strong, medium and weak interactions, respectively. Apart from NOEs obtained from our studies planar constraints between guanines in G-quartet planes were used in order to stabilize the repulsion due to centrally located four oxygen atoms of a G-quartet.

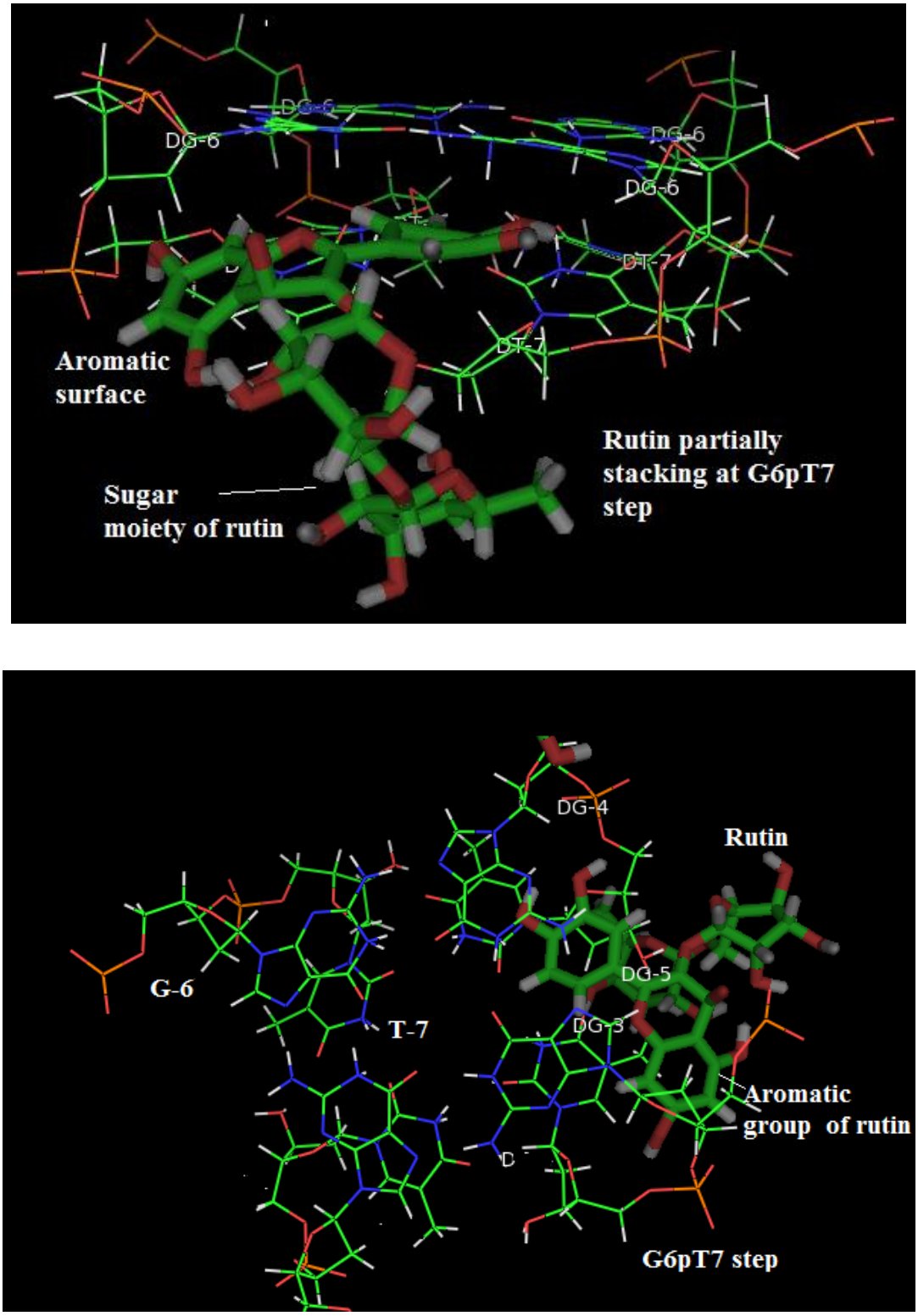

Figure 6.27: (a-b) Model of final complex of rutin with d-(TTGGGGT)$_4$ after rMD simulations showing partial stacking of rutin at G6pT7 step of quadruplex.

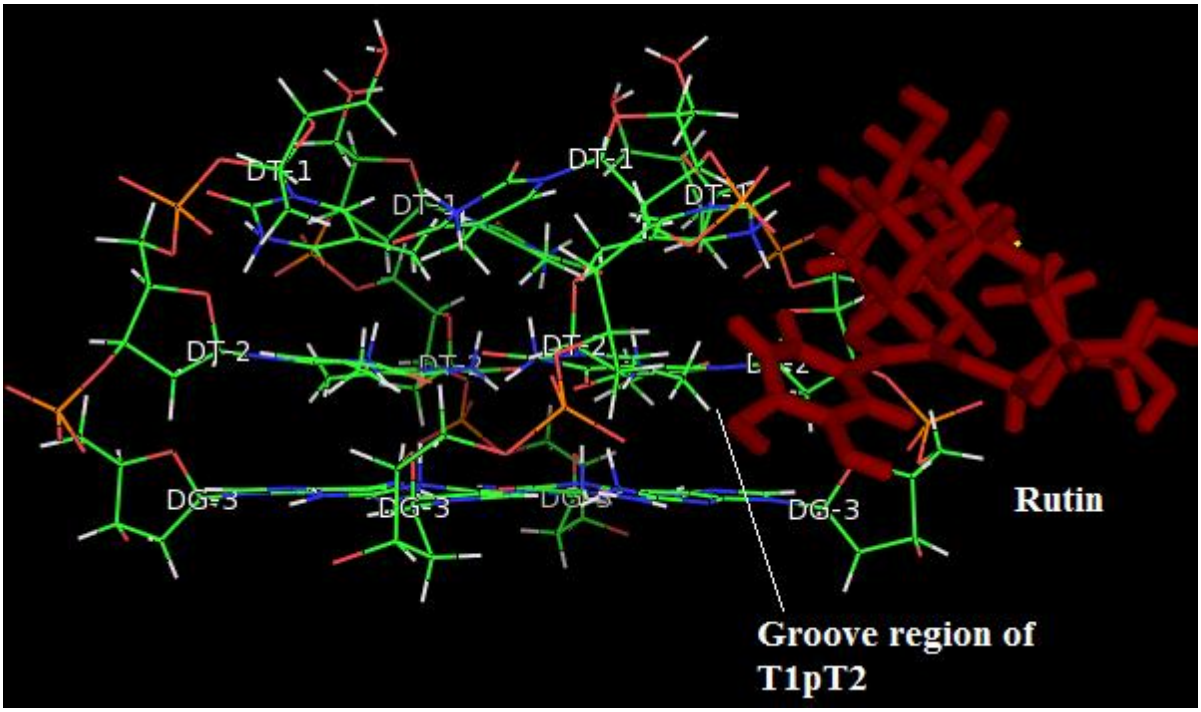

Figure 6.28: Model of final complex of rutin with d-(TTGGGGT)$_4$ after rMD simulations showing groove binding of rutin at T1pT2pG3 step of quadruplex.

Table 6.11: Structural data and energy terms of the final rutin-d-(TTGGGGT)$_4$ complex.

Experimental Restraints	
Intramolecular	
Rutin-rutin	18
Quadruplex-quadruplex	240
Intermolecular	
Rutin-quadruplex	11
CVFF energy (kcal mol^{-1}) of the minimized structures	
Total	586.5
Torsional	523.4
Electrostatic	-254.9
Restraint	185.3
Average r.m.s.d	0.2Å
Restraint Violations	
Distance (>0.5Å)	14

The final structure (Fig. 6.26 – Fig. 6.28) shows the rutin interacts at two binding sites in different orientations, at G6pT7 step rutin binds with partial stacking of its aromatic B ring on the terminal (G6) G-quartet plane, with its glucose and rahmnose sugar moieties adopting a stage like structure for this stacking interaction (Fig. 6.27 a-b). This interaction was favorable as rutin aromatic ring stacks upon terminal G-quartet aromatic surface by π-π interaction.

Fig 6.28 shows the binding of rutin to its second binding site in d-$(TTGGGGT)_4$ quadruplex structure i.e. T1pT2pG3 step. Rutin binds in the groove region of this site, with its B-ring forming close contact with T2 residue of the quadruplex. The tetramolecular quadruplex structure formed by d-$(TTGGGGT)_4$ sequence has more ordered 5'-terminal T1pT2 residues when compared to tetramolecular structure formed by human single repeat telomeric sequence d-$(TTAGGGT)_4$ (Gavathiotis et al., 2003). Hence binding of rutin to the groove region of d-$(TTGGGGT)_4$ is energetically favorable. The obtained ΔT_m value of ~ 15 K from imino proton melting studies and melting profiles supports the binding of rutin to quadruplex by end stacking and groove binding mode. As at higher temperatures G3NH starts disappearing when compared to G6NH proton, this indicates the G-quartet step at G6NH is more stabilized than imino proton G3 step. Therefore based on the detailed one and two-dimensional NMR experiments, we are proposing that rutin binds to the tetramolecular G-quadruplex structure by partial end stacking at G6pT7 step and external groove binding at T1pT2pG3 step, which ultimately results in stabilization of the quadruplex structure.

6.1.8 TRAP assay

In-vitro biological activity of rutin against the telomerase enzyme was done by using PCR based telomeric repeat amplification protocol (TRAP) assay (Kim et al., 1994, Wright et al., 1995). After the telomerase elongation step, the rutin was added prior to that of PCR elongation. This effectively reduces the ligand inhibiting the telomerase or polymerase enzyme. The modified protocol helps in ligand interacting with G-quartet structures formed prior to PCR step. Telomerase extract from MCF-7 cell lines were selected as it has more telomerase activity than available cancer cell types, and has been well documented in literature (*Ramachandran et al., 2002, Herbert et al., 2006*). The detailed protocol was given in section 2.9. The quercetin concentration in the range of 0.1 μM to 100 μM was used to check the telomerase inhibition activity.

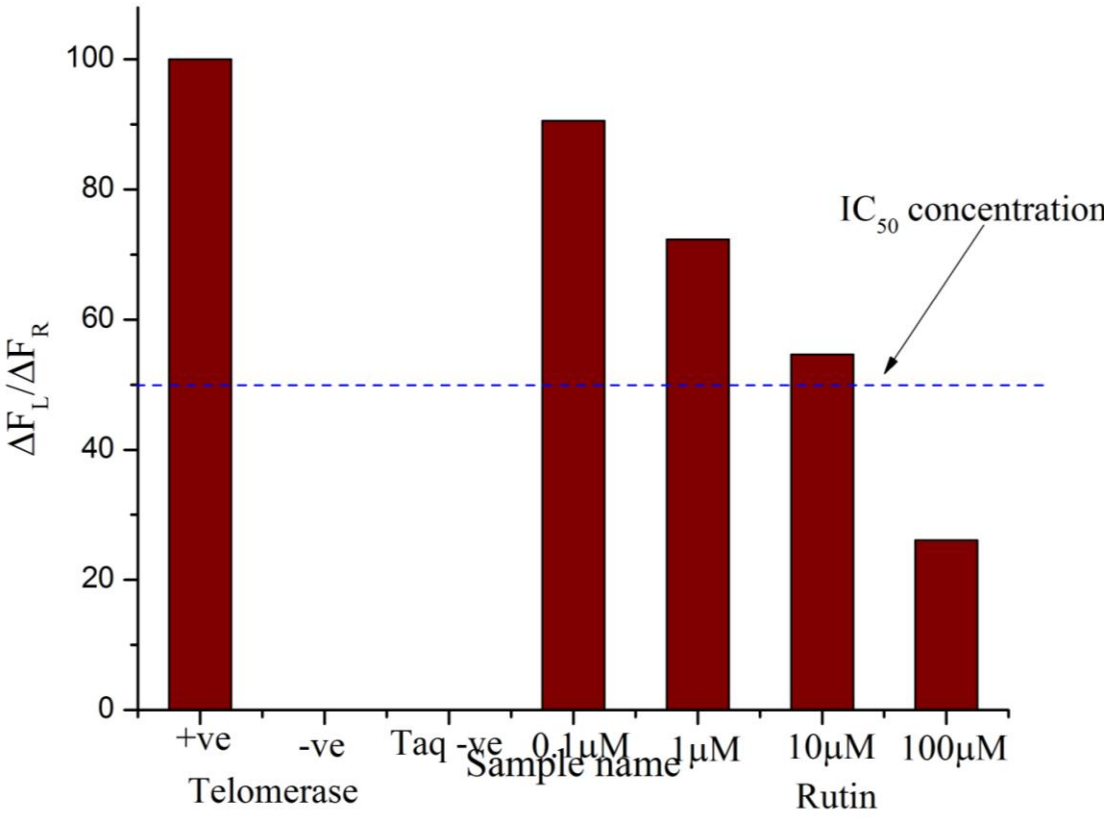

Figure 6.29: TRAP assay of rutin, showing $\Delta F_L/\Delta F_R$ values from fluorescence based assay.

The $\Delta F_L/\Delta F_R$ value of untreated telomerase positive cells were used as positive control and the vales of control without telomerase used as negative control. Rutin in the concentration range of 0.1 μM to 100 μM was used in the present study. Analysis of the results (Fig 6.29) shows that rutin at concentration of 10 μM shows ~ 45 % inhibition of telomerase activity, but at 100 μM concentrations it shows ~ 75 % inhibition. Hence the effective IC_{50} value of quercetin is about ~ 20 μM. Our result clearly shows that rutin binds to G-quadruplex structure more efficiently than its aglycone counterpart quercetin.

6.2 Summary and conclusions

Rutin shows five aromatic resonances with characteristic splitting patterns, five hydroxyl proton (-OH) resonances appear in the downfield region to these protons, with -OH5 proton resonating in the most downfield region of the spectrum. This confirms the presence of quercetin flavonol backbone. The sugar protons appear on the upfield region of the spectrum, they show characteristic TOCSY and COSY correlations. The glucose sugar ring is attached to the 3'-O atom of the

quercetin C ring. The H6''' (methyl) proton attached to the rahmnose sugar resonates in the most upfield (δ 0.9 ppm) region, and shows characteristic doublet pattern due to the presence of H5''' proton.

Presence of single set of four signals in the Hoogsteen hydrogen bonded region (12-10.5 ppm), confirms the existence of single predominant species with guanines involved in Hoogsteen hydrogen bonding scheme. Existence of NOESY correlations between guanine H8 protons with its adjacent guanine NH proton with in a quartet, and with 3' flanking GNH proton confirms the presence of G-quartet structures and which helps in the formation of tetramolecular G-quadruplex structure. The intensities of H8/H6 with sugar H1'/H2'/H2'' sequential connectivities confirms that backbone adopts right handed geometry. The presence of six ^{31}P signals in phosphorous-31 spectrum also confirms the existence of single predominant species.

Upon successive addition of rutin to d-$(TTGGGGT)_4$, all aromatic protons show upfield shift. The anomeric H1'' proton of glucose sugar shifts up-field by 1.01 ppm, whereas rahmnose anomeric H1''' proton shifts upfield by 0.1 ppm. All other sugar ring protons show little change in position. All four G-quartet NH protons shifts upfield, maximum shift observed for G6NH (0.24 ppm) followed by G5NH. After complexation, all intra base and inter base sequential connectivities between aromatic H8/H6 protons and sugar H1'/H2'/H2'' protons were clearly observed. The presence of guanine imino NOEs between successive G-quartet planes of G3:G4:G5:G6 clearly confirms that G-quadruplex doesnot open up to accommodate the rutin. Total of 14 inter molecular NOEs were observed between rutin protons and d-$(TTGGGGT)_4$ protons. Rutin H2' and H6' proton shows NOE cross peak with G6NH proton in D/N 1.0, whereas the at D/N 2.0 new NOEs appear between rutin aromatic and T1pT2 step protons. This confirms that rutin has two binding sites for d-$(TTGGGGT)_4$ one at G6pT7 step and another at T1pT2 step. Studies of restrained molecular simulations shows that aromatic ring B of the rutin molecule inserts into the G6pT7 step, which explains the observed NOEs between C ring protons of rutin with GNH and GH1' proton of d-$(TTGGGGT)_4$. In the second binding site rutin binds rather in the groove region as this segment of DNA is not properly ordered due to motions of T1 and T2 residues. Hence the second rutin molecule binds to the groove region of T1pT2 segment of d-$(TTGGGGT)_4$ DNA.

Our studies clearly shows that rutin with its bulky group cannot intercalate into the G-quadruplex segment, as energy penalty for ordering of sugar endocyclic torsional angles is also more along

with the replacement of co-ordination metal ion from central cavity of G-tetrads. Hence rutin binds externally in both sites. The TRAP assay results show that rutin has IC_{50} value of about 25 μM. Therefore rutin binds to G-quadruplex structure more efficiently than quercetin, its aglycone counterpart.

Chapter 7

Final summary and conclusions on interaction of mitoxantrone, flavonol quercetin and flavonol glycoside rutin with d-(TTGGGGT)$_4$ tetramolecular G-quadruplex.

The UV-Vis studies show the multiple mode of binding of MTX to d-(TTGGGGT)$_4$ quadruplex sequence. Both monomer and dimer peaks of MTX shows bathochromic shift with initial hypochromism till D/N ratio 2.0 and hyperchromism after this molar ratio. The apparent binding constant K = 3.53 x 10^6 M^{-1} and 3.73 x 10^6 M^{-1} for D/N = 0.5 to 2.0 and D/N = 2.0 to 4.0 shows that MTX binds strongly with d-(TTGGGGT)$_4$. The UV-Vis thermal melting study gives the ΔT_m of ~ 25 K; the melting temperature of MTX bound d-(TTGGGGT)$_4$ increases till D/N 4.0 and saturates after this D/N ratio. The method of continuous variation studies also confirms the stoichiometric ratio of 4.0, as multiple inflection points were observed due to the formation of more than one MTX-d-(TTGGGGT)$_4$ complexes. The steady state and time resolved fluorescence studies show that the environment of MTX changes upon binding to quadruplex structure. The binding constant of K = 6.6 x 10^5 M^{-1} and n = 0.9 for D/N ratio in the range 2.1- 4.0 and K = 5.4 x 10^5 $M^{-1}$and n = 1.89 for lower D/N values of 0.79 - 2.1 were obtained.

Binding of MTX doesnot induce changes in quadruplex structure till D/N 4.0. Plot of changes in CD of quadruplex versus D/N ratio shows inflection point at 2.0. Weak induced bands were observed upon binding of MTX to d-(TTGGGGT)$_4$. The two SPR runs give affinity constant K_A as 1.037 x 10^4 M^{-1} and 1.142 x 10^4 M^{-1}, with an average value of 1.086 x 10^4 M^{-1}. Both runs show MTX binds with two distinct binding affinities, while one is stronger and other is weaker (10 times weak). The binding affinity constants obtained by SPR and UV-Vis were in agreement with the change in T_m value obtained by thermal melting studies. Thus the results reported in present study prove that mitoxantrone binds to quadruplex with high selectivity and stabilizes the structure. The TRAP assay results give the IC_{50} value of ~2 μM for MTX.

Multi spectroscopic studies on interaction of mitoxantrone (MTX) with tetramolecular G-quadruplex sequence d-(TTGGGGT)$_4$ gives the binding stoichiometry of four MTX molecules binding to one d-(TTGGGGT)$_4$ quadruplex structure.

The detailed solution NMR studies of d-(TTGGGGT)$_4$ shows that, The G3:G4:G5:G6 imino protons resonante in the Hoogsteen hydrogen bonding region of 12-10.5 ppm, along with characteristic connectivities in 200 ms NOESY spectra at 298 K which confirms the formation of G-quadruplex structure. The sequential connectivities between aromatic H8/H6 protons with sugar H1'/H2'/H2" protons confirms that d-(TTGGGGT)$_4$ adopts a right handed backbone geometry. Presence of only single set of resonances confirms that molecule adopts C4 symmetry upon quadruplex formation.

The mitoxantrone (MTX) shows usual characteristic ^{1}H and ^{13}C chemical shifts, whereas MTX protons shifts upfield after forming complex with d-(TTGGGGT)$_4$. The presence of single set of resonances for at all D/N ratios till 4.0 suggests that quadruplex structure maintains its C4 symmetry. The G6NH, T7H6, T7CH$_3$ protons of d-(TTGGGGT)$_4$ shows broadening of resonances till D/N ratio 1.0, and addition of MTX to reach higher molar ratio D/N 2.0 results in the sharpening of these resonances. All four G-quartet imino protons shifts upfield gradually. The G6NH shows maximum upfiled shift of 0.26 ppm, which is comparable with the well known G-quadruplex binders like RHPS4, TMPyP4. The presence of imino-imino NOE correlation between successive G-quartet steps, and sequential connectivities between aromatic H6/H8 with sugar H1'/H2'/H2" protons confirms that MTX does not intercalate between G-quartets. The thermal melting studies of imino protons illustrate ΔT_m of ~ 25 K thus validating the stabilization of quadruplex structure by d-(TTGGGGT)$_4$ structure. This melting temperature was independently confirmed by melting studies using UV-Vis, which shows ΔT_m of ~ 24 K in complex D/N 4.0. ^{31}P resonances doesnot show any significant shift and no correlation peak is observed in ^{31}P-^{31}P NOESY exchange spectra upon complex formation and no extra signal was observed in the downfield region of the spectra.

Presence of NOE connectivities between 2/3H proton of MTX with 11CH$_2$ and 12CH$_2$ protons confirms the formation of MTX-MTX head-to-tail dimer. Seven MTX-MTX dimer NOE connectivities and nine MTX intra molecular connectivities were observed which aids in the restrained molecular simulations (rMD). The MTX protons show NOEs with protons of G6pT7 and T1pT2 step and 38 inter molecular NOE connectivities were observed between MTX dimer and d-(TTGGGGT)$_4$ of D/N 4.0 at 298 K. The final model of MTX bound to d-(TTGGGGT)$_4$ after rMD simulations confirms that MTX dimer binds to d-(TTGGGGT)$_4$ quadruplex structure at

G6pT7 step with alkyl amine side chains in the groove region while the second dimer binds externally to T1pT2 step in the groove region. The results obtained in this chapter supports extensively that the well known anti-cancer drug MTX interacts with d-(TTGGGGT)$_4$ quadruplex structure and stabilizes it. These results augment well with the results obtained in chapter 3, and hence clearly prove that MTX effectively binds and stabilizes G-quadruplex structure inhibiting the activity of telomerase enzyme, a well known tumor marker.

Addition of two mol equivalents of quercetin to d-(TTGGGGT)$_4$ quadruplex DNA results in development of new intermolecular and intra molecular NOEs between quercetin and quercetin-d-(TTGGGGT)$_4$ protons. Total of 15 inter molecular NOE peaks were observed between quercetin and d-(TTGGGGT)$_4$ protons, most of which were with the T2CH$_3$, T2H2' and T2H2" which forms the groove region of quadruplex. Further absence of inter molecular NOEs between quercetin and any G step protons, and presence of GNH-GNH NOE correlation and all sequential connectivities proves that G-quartet doesnot open up. Hence, discarding the intercalation mode of binding by quercetin to d-(TTGGGGT)$_4$ quadruplex structure. Moreover, the final energy minimized structure shows that quercetin binds to the T1pT2pG3 step groove region of d-(TTGGGGT)$_4$ quadruplex structure.

Five aromatic quercetin protons show characteristic splitting pattern at 298 K, upon binding to d-(TTGGGGT)$_4$ quadruplex structure and all quercetin protons shift upfield. The ^{31}P exchange spectra doesnot showy any extra peak. Uncomplexed d-(TTGGGGT)$_4$ shows melting temperature of (T_m) of 348 K and addition of two mol equivalents of quercetin results in the increase in meting temperature to 353 K. Hence, ~ΔT_m of 5 K suggests that quercetin molecule stabilizes the G-quadurplex structure. The TRAP assay results showed that quercetin inhibits telomerase activity at effective IC50 value of ~ 45 μM.

Rutin shows five aromatic resonances with characteristic splitting patterns, five hydroxyl proton (-OH) resonances appear in the downfield region to these protons, with -OH5 proton resonating in the most downfield region of the spectrum. This confirms the presence of quercetin flavonol backbone. The sugar protons appear on the upfield region of the spectrum and show characteristic TOCSY and COSY correlations.

All aromatic protons of rutin show upfield shift upon complexation. All other sugar ring protons show little change in position. All four G-quartet NH protons shifts upfield, maximum shift observed for G6NH (0.24 ppm) followed by G5NH. Total of 14 inter molecular NOEs were observed between rutin protons and d-(TTGGGGT)$_4$ protons. Rutin H2' and H6' proton shows NOE cross peak with G6NH proton in D/N 1.0, whereas at D/N 2.0 new NOEs appear between rutin aromatic and T1pT2 step protons. This confirms that rutin has two binding sites for d-(TTGGGGT)$_4$; one at G6pT7 step and another at T1pT2 step. Studies of restrained molecular simulations shows that aromatic ring B of the rutin molecule inserts into the G6pT7 step, which explains the observed NOEs between C ring protons of rutin with GNH and GH1' proton of d-(TTGGGGT)$_4$. In the second binding site, rutin binds rather in the groove region as this segment of DNA is not properly ordered due to motions of T1 and T2 residues. Hence the second rutin molecule binds to the groove region of T1pT2 segment of d-(TTGGGGT)$_4$ DNA. Our studies clearly shows that rutin with its bulky group cannot intercalate into the G-quadruplex segment, as energy penalty for ordering of sugar endocyclic torsional angles is also more along with the replacement of co-ordination metal ion from central cavity of G-tetrads. Hence rutin binds externally in both sites.

Upon complexation, all intra base and inter base sequential connectivities between aromatic H8/H6 protons and sugar H1'/H2'/H2" protons were clearly observed. The presence of guanine imino NOEs between successive G-quartet planes of G3:G4:G5:G6 clearly confirms that G-quadruplex doesnot open. Quadruplex structure doesnot open to accommodate any one of the three ligands used in our present study.

The imino melting studies show that rutin stabilizes d-(TTGGGGT)$_4$ quadruplex structure more effectively when compared to quercetin. Rutin has ΔT_m ~ 15 K, whereas quercetin shows ΔT_m ~ 5 K stabilization of quadruplex structure. Moreover the imino proton shift is also more in rutin-d-(TTGGGGT)$_4$ complex when compared to quercetin bound d-(TTGGGGT)$_4$.

The TRAP assay results shows that show that Rutin has IC_{50} value of ~25 μM, whereas quercetin has IC_{50} value of ~45 μM. Comparison of results obtained between flavonol quercetin with its O-3 glycoside, rutin offers an interesting detail of how a structure activity of a molecule depends upon its target structure. As quercetin is a small aromatic flavonoid, it shows very potent intercalation activity among duplex nucleic acids (*Solimai, 1996*) but it cannot effectively stack or intercalate to

G-quadruplex structure, owing to the energy barrier. Whereas rutin is a large molecule with rutinose sugar attached to quercetin moiety, it has less binding affinity with duplex nucleic acids, but it is a better binder to higher order nucleic acid structure like triplex DNA (*Wan et al., 2009*) or quadruplex DNA (our present study). Therefore rutin binds to G-quadurplex structure more efficiently than quercetin, its aglycone counterpart.

The results of our present study clearly concludes that anti-cancer drug mitoxantrone has higher affinity for d-$(TTGGGGT)_4$ G-quadruplex DNA, followed by rutin, which shows higher affinity than its aglycone counterpart quercetin. The information gleaned from these structural studies of G-quadruplex and three ligand complexes aids greatly in rational anti-cancer drug design based on the telomerase inhibition strategy.

References

1. Aboul-Ela, F., Murchie, A.I. and Lilley, D.M. NMR study of parallel-stranded tetraplex formation by the hexadeoxynucleotide d (TG_4T). Nature, 19, 280-282, 1992.
2. Aboul-ela, F., Murchie, A.I., Norman, D.G. and Lilley, D.M. Solution Structure of a Parallel-stranded Tetraplex Formed by d (TG_4T) in the Presence of Sodium Ions by Nuclear Magnetic Resonance Spectroscopy. *J. Mol. Biol.* 243, 458-471, 1994.
3. Ahmed, M.S., Ramesh, V., Nagaraja, V., Parish, J. and Hadi, S. Mode of binding of quercetin to DNA. *Mutagenesis*. 9, 193-197, 1994.
4. Alvi, N., Rizvi, R. and Hadi, S. Interaction of quercetin with DNA. *Bioscience reports*, 6, 861-868, 1986.
5. Ambrus A., Chen D., Dai J., Jones R.A. and Yang D. Solution structure of the biologically relevant G-Quadruplex element in the human c-MYC promoter. Implications for G-quadruplex stabilization. *Biochemistry*. 44, 2048 – 2058, 2005.
6. Anantha, N.V., Azam, M. and Sheardy, R.D. Porphyrin binding to quadruplexed T4G4. *Biochemistry*. 37, 2709-2714, 1998.
7. Antanasijevic, A., Ramirez, B. and Caffrey, M. Comparison of the sensitivities of Water LOGSY and saturation transfer difference NMR experiments. *J. Biomol. NMR.* 60, 37-44, 2014.
8. Arnott, S., Chandrasekaran, R. and Marttila, C.M. Structures for polyinosinic acid and polyguanylic acid. *Biochem. J*. 141, 537-543, 1974.
9. Antanasijevic, A., Ramirez, B. and Caffrey, M. Comparison of the sensitivities of WaterLOGSY and saturation transfer difference NMR experiments. *Journal of biomolecular NMR*, 60, 37-44, 2014
10. Awasthi, P., Dogra, S., Awasthi, L.K. and Barthwal, R. Molecular Modeling Study of Interaction of Anthracenedione Class of Drug Mitoxantrone and Its Analogs with DNA Tetrameric Sequences. Software Tools and Algorithms for Biological Systems, Springer: 385-400, 2011.
11. Awasthi, P., Dogra, S. and Barthwal, R. Multispectroscopic methods reveal different modes of interaction of anti cancer drug mitoxantrone with Poly (dG-dC). Poly (dG-dC) and Poly (dA-dT). Poly (dA-dT). *J. Photochem. Photobiol. B: Biol.* 127: 78-87, 2013.

12. Baleja, J.D., Germann, M.W., van de Sande, J.H. and Sykes, B.D. Solution conformation of purine-pyrimidine DNA octamers using nuclear magnetic resonance, restrained molecular dynamics and NOE-based refinement. *J. Mol. Biol.* 215, 411-428, 1990.
13. Bandele, O.J. and Osheroff, N. Bioflavonoids as poisons of human topoisomerase IIα and IIβ. *Biochemistry*, 46, 6097-6108, 2007.
14. Baumann, P. and Cech, T.R. Pot1, the putative telomere end-binding protein in fission yeast and humans. *Science*, 292, 1171-1175, 2001.
15. Benesi, H.A. and Hildebrand, J.H. A Spectrophotometric Investigation of the Interaction of Iodine with Aromatic Hydrocarbons. *J. Am. Chem. Soc.* 71, 2703- 2707, 1949.
16. Bhadra, K. and G. S. Kumar Interaction of berberine, palmatine, coralyne, and sanguinarine to quadruplex DNA: A comparative spectroscopic and calorimetric study. *Biochim. Biophys. Acta (BBA)-General Subjects*. 1810, 485-496, 2011.
17. Bhavesh, N.S., Patel, P.K., Karthikeyan, S. and Hosur, R.V. Distinctive features in the structure and dynamics of the DNA repeat sequence GGCGGG. *Biochem. Biophys. Res. Commun.*, 317, 625-633, 2004.
18. Blackburn, E.H. Switching and signaling at the telomere. *Cell*, 106, 661-673, 2001.
19. Boyle, S., Dobson, V., Duthie, S., Hinselwood, D., Kyle, J. and Collins, A. Bioavailability and efficiency of rutin as an antioxidant: a human supplementation study. *Eur J. Clin. Nutri.* 54, 774-782. 2000.
20. Brett, A., Macedo, T., Raimundo, D., Marques, M. and Serrano, S. Voltammetric behaviour of mitoxantrone at a DNA-biosensor. *Biosens. Bioelectron.* 13, 861-867, 1998.
21. Broccoli, D., Smogorzewska, A., Chong, L. and de Lange, T. Human telomeres contain two distinct Myb-related proteins, TRF1 and TRF2. *Nature genetics*, 17, 231-235, 1997.
22. Burda, S., and Oleszek, W. Antioxidant and antiradical activities of flavonoids, *J. Agric. Food Chem.* 49, 2774-2779, 2001.
23. Campbell N.H., Parkinson G.N., Reszka A.P. and Neidle S. Structural basis of DNA quadruplex recognition by an acridine drug. *J.Am.Chem.Soc*., 130, 6722 – 6724, 2008.
24. Chakraborty, T., Jayaprakash, S., Srinivasu, P., Madhavendra, S., Ravi Sankar, A. and Kunwar, A. Furanoid sugar amino acid based peptidomimetics: well-defined solution conformations to gel-like structures. *Tetrahedron*, 58, 2853-2859, 2002.

25. Chakraborty, T., Jayaprakash, S., Diwan, P., Nagaraj, R., Jampani, S. and Kunwar, A. Folded conformation in peptides containing furanoid sugar amino acids. *J. Am. Chem. Soc.*, 120, 12962-12963, 1998.
26. Chaput, J.C. and Switzer, C. A DNA pentaplex incorporating nucleobase quintets. *Proc. Nat. Acad. Sci.* 96, 10614-10619, 1999.
27. Cherezov, V., Qiu, H., Pector, V., Vandenbranden, M., Ruysschaert, J.-M. and Caffrey, M. (2002) Biophysical and Transfection Studies of the diC14 Amidine/DNA Complex. *Biophys. Journal*, 82, 3105-3117, 2002.
28. Cheong C. and Moore P.B. Solution structure of an unusually stable RNA tetraplex containing G- and U-quartet structures. *Biochemistry*. 31, 8406 – 8414, 1992.
29. Chowdhury, A., Sharma, S., Mandal, S., Goswami, A., Mukhopadhyay, S. and Majumder, H. Luteolin, an emerging anti-cancer flavonoid, poisons eukaryotic DNA topoisomerase I. *Biochem. J*, 366, 653-661, 2002.
30. Chunying W., Gaoyi H., Guoqing J., Jun Z., Can L. Study on the interaction of porphyrin with G-quadruplex DNAs. *Biophysial Chemistry*, 137, 19-23, 2008
31. Clark G.R., Pytel P.D., Squire C.J. and Neidle S. Structure of the First Parallel DNA Quadruplex-drug Complex. *J.Am.Chem.Soc*. 125, 4066 – 4067, 2003
32. Clark, G.R., Pytel, P.D. and Squire, C.J. The high-resolution crystal structure of a parallel intermolecular DNA G-4 quadruplex/drug complex employing syn glycosyl linkages. *Nuc. Acid. Res.* 40, 5731-5738, 2012.
33. Cosconati, S., Marinelli, L., Trotta, R., Virno, A., De Tito, S., Romagnoli, R., Pagano, B., Limongelli, V., Giancola, C. and Baraldi, P.G. Structural and conformational requisites in DNA quadruplex groove binding: another piece to the puzzle. *J. Am. Chem. Soc*. 132, 6425-6433, 2010.
34. Counter, C.M., Avilion, A.A., LeFeuvre, C.E., Stewart, N.G., Greider, C.W., Harley, C.B. and Bacchetti, S. Telomere shortening associated with chromosome instability is arrested in immortal cells which express telomerase activity. *The EMBO journal*, 11, 1921, 1992.
35. Damm, K., Hemmann, U., Garin-Chesa, P., Hauel, N., Kauffmann, I., Priepke, H., Niestroj, C., Daiber, C., Enenkel, B. and Guilliard, B. A highly selective telomerase inhibitor limiting human cancer cell proliferation. *The EMBO journal*, 20, 6958-6968, 2001.

36. Davies, D.B., Veselkov, D.A., Evstigneev, M.P. and Veselkov, A.N. Self-association of the antitumour agent novatrone (mitoxantrone) and its hetero-association with caffeine. *J. Chem. Soc, Perkin Transactions 2*. 61-67, 2001.
37. Davis, D.G. and Bax, A. Assignment of complex proton NMR spectra via two-dimensional homonuclear Hartmann-Hahn spectroscopy. *J. Am. Chem. Soc*, 107, 2820-2821, 1985.
38. De Cian, A. and J.-L. Mergny. Quadruplex ligands may act as molecular chaperones for tetramolecular quadruplex formation. *Nucleic. Acid. Res*. 35, 2483-2493, 2007.
39. De Lange, T. Shelterin: the protein complex that shapes and safeguards human telomeres. *Genes & development*, 19, 2100-2110, 2005.
40. Dogra, S., Awasthi, P., Tripathi, S., Pradeep, T., Nair, M.S. and Barthwal, R. NMR-based structure of anticancer drug mitoxantrone stacked with terminal base pair of DNA hexamer sequence d-(ATCGAT)2. *J. Biomol. Struc. Dyn.* 1-20., 2013
41. Donohue, J. and Trueblood, K.N. Base pairing in DNA. *Journal of molecular biology*, 2, 363-371, 1960.
42. Duthie, S., Collins, A., Duthie, G. and Dobson, V. Quercetin and myricetin protect against hydrogen peroxide-induced DNA damage (strand breaks and oxidised pyrimidines) in human lymphocytes. *Mutation Research/Genetic Toxicol. Environ. Mutagen.* 393, 223-231, 1997.
43. Errington, F., Willmore, E., Tilby, M., Li, L., Li, G., Li, W., Baguley, B. and Austin, C. Murine transgenic cells lacking DNA topoisomerase IIβ are resistant to acridines and mitoxantrone: analysis of cytotoxicity and cleavable complex formation. *Mol. Pharmacol.* 56, 1309-1316, 1999.
44. Fathiazada, F., Azarmib, Y. and Khodaie, L. Pharmacological Effects of Peganum harmala seeds extract on isolated rat uterus. *Iran. J. Pharm. Sci.* 2, 81-86, 2006.
45. Fathiazad, F., Delazar, A., Amiri, R. and Sarker, S.D. Extraction of flavonoids and quantification of rutin from waste tobacco leaves. *Iran. J. Pharm. Res.* 222-227, 2010.
46. Fedoroff, O.Y., Salazar, M., Han, H., Chemeris, V.V., Kerwin, S.M. and Hurley, L.H. NMR-based model of a telomerase-inhibiting compound bound to G-quadruplex DNA. *Biochemistry*, 37, 12367-12374, 1998.
47. Felsenfeld, G., Davies, D.R. and Rich, A. Formation of a three-stranded polynucleotide molecule. *J. Am. Chem. Soc.* 79, 2023-2024, 1957.

48. Fiorani, M. and Accorsi, A. Dietary flavonoids as intracellular substrates for an erythrocyte trans-plasma membrane oxidoreductase activity. *British journal of nutrition*, 94, 338-345, 2005.
49. Franceschin, M., Rossetti, L., D'Ambrosio, A., Schirripa, S., Bianco, A., Ortaggi, G., Savino, M., Schultes, C. and Neidle, S. Natural and synthetic G-quadruplex interactive berberine derivatives. *Bioorg. Med. Chem. Letters*, 16, 1707-1711, 2006.
50. Freyer, M.W., Buscaglia, R., Kaplan, K., Cashman, D., Hurley, L.H. and Lewis, E.A. Biophysical Studies of the c-MYC NHE III Promoter: Model Quadruplex Interactions with a Cationic Porphyrin. *Biophys. J.*, 92, 2007
51. Gai, W., Yang, Q., Xiang, J., Jiang, W., Li, Q., Sun, H., Guan, A., Shang, Q., Zhang, H. and Tang, Y. A dual-site simultaneous binding mode in the interaction between parallel-stranded G-quadruplex d $(TGGGGT)_4$ and cyanine dye 2, 2′-diethyl-9-methyl-selenacarbocyanine bromide. *Nucl. Acid. Res.* 41, 2709-2722, 2013.
52. Gavathiotis, E., Heald, R.A., Stevens, M.F. and Searle, M.S. Drug Recognition and Stabilisation of the Parallel-stranded DNA Quadruplex d $(TTAGGGT)_4$ containing the Human Telomeric Repeat. *J. Mol. Biol.*, 334, 25-36, 2003.
53. Gefter, M.L. and Russell, R.L. Role of modifications in tyrosine transfer RNA: a modified base affecting ribosome binding. *J. Mol. Biol.* 39, 145-157, 1969.
54. Gehring, K., Leroy, J.-L. and Guéron, M. A tetrameric DNA structure with protonated cytosine-cytosine base pairs. Nature, 363,561-565, 1993
55. Gellert, M., Lipsett, M.N. and Davies, D.R. Helix formation by guanylic acid. *Proc. Nat. Aca. Sci.* 48, 2013-2015, 1962.
56. Gellert, G.C., Jackson, S.R., Dikmen, Z.G., Wright, W.E. and Shay, J.W. Telomerase as a therapeutic target in cancer. *Drug Discovery Today: Disease Mechanisms*, 2, 159-164, 2005.
57. Germann, M.W., Kalisch, B.W. and van de Sande, J.H. Relative stability of parallel-and anti-parallel-stranded duplex DNA. *Biochemistry*. 27, 8302-8306, 1998.
58. Germann, M.W., Pon, R.T. and van de Sande, J.H. A general method for the purification of synthetic oligodeoxyribonucleotides containing strong secondary structure by reversed-phase high-performance liquid chromatography on PRP-1 resin. *Anal. Biochem.*, 165, 399-405, 1987.

59. Ghiasi M and Majid M. H. Quantum mechanical study of antioxidative ability and antioxidative mechanism of rutin (vitamin P) in solution. *Carbohydrate Res.* 346, 739-744, 2011.
60. Goddard. T. D and Kneller. D. G, University of California, San Francisco, SPARKY software.
61. Gorenstein, D.G. ^{31}P NMR of DNA. *Methods in enzymology*, 211, 254-286, 1992.
62. Gornall, K.C., Samosorn, S., Talib, J., Bremner, J.B. and Beck, J.L. Selectivity of an indolyl berberine derivative for tetrameric G-quadruplex DNA. *Rapid Commun. Mass Spectro.* 21, 1759-1766, 2007.
63. Gray, R.D. and Chaires, J.B. Kinetics and mechanism of K+-and Na+-induced folding of models of human telomeric DNA into G-quadruplex structures. *Nucleic. Acids. Res.*, 36, 4191-4203, 2008.
64. Gavathiotis, E. and Searle, M.S. Structure of the parallel-stranded DNA quadruplex d $(TTAGGGT)_4$ containing the human telomeric repeat: evidence for A-tetrad formation from NMR and molecular dynamics simulations. *Org. Biomol. Chem.*, 1, 1650-1656, 2003.
65. Gray, R.D., Li, J. and Chaires, J.B. Energetics and Kinetics of a Conformational Switch in G-Quadruplex DNA. *J. Phys. Chem. B*, 113, 2676-2683, 2009.
66. Gros, J., Aviñó, A., de la Osa, J.L., González, C., Lacroix, L., Pérez, A., Orozco, M., Eritja, R. and Mergny, J.-L. 8-Amino guanine accelerates tetramolecular G-quadruplex formation. *Chem. Comm.* 22, 2926-2928, 2008.
67. Guo et al., Int. J. Gynecol. Cancer, 2004
68. Gupta, G., Garcia, A.E., Guo, Q., Lu, M. and Kallenbach, N.R. Structure of a parallel-stranded tetramer of the Oxytricha telomeric DNA sequence dT_4G_4. *Biochemistry*, 32, 7098-7103, 1993.
69. Haider, S.M., Parkinson, G.N. and Neidle, S. Structure of a G-quadruplex–ligand complex. *J. Mol. Biol.* 326, 117-125, 2003.
70. Han, H., Cliff, C.L. and Hurley, L.H. Accelerated assembly of G-quadruplex structures by a small molecule. *Biochemistry*, 38, 6981-6986, 1999.
71. Han, H. and L. H. Hurley. G-quadruplex DNA: a potential target for anti-cancer drug design. *Trend. Pharmacol. Sci.* 21, 136-142, 2000.
72. Han, H., D. R. Langley, et al. (2001). Selective interactions of cationic porphyrins with G-quadruplex structures. *J. Am. Chem. Soc.* 123, 8902-8913, 2001.

73. Han, H., Hurley, L.H. and Salazar, M. A DNA polymerase stop assay for G-quadruplex-interactive compounds. *Nucleic. Acids. Res.*, 27, 537-542, 1999.

74. Hayward, W.S., Neel, B.G. and Astrin, S.M. Activation of a cellular *onc* gene by promoter insertion in ALV-induced lymphoid leukosis. 1981.

75. Herbig, U., Jobling, W.A., Chen, B.P., Chen, D.J. and Sedivy, J.M. Telomere Shortening Triggers Senescence of Human Cells through a Pathway Involving ATM, p53, and $p21^{CIP1}$,but Not $p16^{INK4a}$. *Mol. cell*, 14, 501-513, 2004.

76. Horvath, M.P. and Schultz, S.C. DNA G-quartets in a 1.86 Å resolution structure of an *Oxytricha nova* telomeric protein-DNA complex. *J. Mol. Biol.*, 310, 367-377, 2001.

77. Hosur, R, Govil, G. and Miles, H.T Application of two-dimensional NMR spectroscopy in the determination of solution conformation of nucleic acids. *Mag. Reson. Chem.* 26, 927-944, 1998.

78. Hounsou, C., Guittat, L., Monchaud, D., Jourdan, M., Saettel, N., Mergny, J.L. and Teulade-Fichou, M.P, G-Quadruplex Recognition by Quinacridines: a SAR, NMR, and Biological Study. *ChemMedChem*. 2, 655-666, 2007.

79. Huppert, J.L. and Balasubramanian, S. G-quadruplexes in promoters throughout the human genome. *Nucleic. Acid. Res.* 35, 406-413, 2007.

80. Incles, C.M., Schultes, C.M., Kempski, H., Koehler, H., Kelland, L.R. and Neidle. S. A G-quadruplex telomere targeting agent produces p16-associatedsenescence and chromosomal fusions in human prostate cancer. *Mol. Cancer Ther.* 3, 1201–1206, 2004.

81. Islam, M.M., Pandya, P., Kumar, S. and Kumar, G.S. RNA targeting through binding of small molecules: Studies on t-RNA binding by the cytotoxic protoberberine alkaloid coralyne. *Mol. Biosyst.* 5, 244-254, 2009.

82. Jeener, J., Meier, B., Bachmann, P. and Ernst, R. Investigation of exchange processes by two-dimensional NMR spectroscopy. *J. Chem. Phy.* 71, 4546-4553, 1979.

83. Kapuscinski, J., Darzynkiewicz, Z., Traganos, F. and Melamed, M.R. Interactions of a new antitumor agent, 1, 4-dihydroxy-5, 8-bis [[2-[(2-hydroxyethyl) amino]-ethyl] amino]-9, 10-anthracenedione, with nucleic acids. Biochem. Pharmocol. 30, 231-240, 1981.

84. Kaushik, M., Prasad, M., Kaushik, S., Singh, A. and Kukreti, S. Structural transition from dimeric to tetrameric i-motif, caused by the presence of TAA at the 3′-end of human telomeric C-rich sequence. *Biopolymers.* 93, 150-160, 2010.

85. Khetrapal, C., Govil, G. and Yeh, H. The preferred conformation (s) of trimethyl phosphate as derived from NMR spectra of partially oriented molecules and potential energy calculations. *Journal of Molecular Structure*, 116, 303-311, 1984.
86. Khetrapal, C. and Kunwar, A. Determination of chemical shift anisotropy without a reference and of direct and indirect spin-spin couplings between heteronuclei. *Chemical Physics Letters*, 82, 170-171, 1981.
87. Kieper, I., Schmidt, T., Fera, B. and Rüterjans, H. ^{15}N-Labeled Oligodeoxynucleotides - Useful Probes for 1H-NMR Investigations. *Nucleosides & nucleotides*, 7, 821-825, 1998.
88. Kim, N.W., Piatyszek, M.A., Prowse, K.R., Harley, C.B., West, M.D., Ho, P.d.L., Coviello, G.M., Wright, W.E., Weinrich, S.L. and Shay, J.W. Specific association of human telomerase activity with immortal cells and cancer. *Science*, 266, 2011-2015, 1994.
89. Kim, S.-h., Kaminker, P. and Campisi, J. TIN2, a new regulator of telomere length in human cells. *Nature genetics*, 23, 405-412, 1999.
90. Kostyuk, V., Potapovich, A., Strigunova, E., Kostyuk, T. and Afanas' ev, I. Experimental evidence that flavonoid metal complexes may act as mimics of superoxide dismutase. *Arch. Biochem. Biophys.* 428, 204-208, 2004.
91. Kotovych, G., Lown, J.W. and Tong, J.P. High-field 1H and 31P NMR studies on the binding of the anticancer agent mitoxantrone to d [CpGpApTpCpG] 2. *J. Biomol. Struc. Dyn.* 4, 111-125, 1986.
92. Kovaleva, O., Shchyolkina, A., Mamaeva, O., Ol'shevskaya, V., Makarenkov, A., Semeikin, A., Shtil, A., Borisova, O. and Kaluzhny, D. Complexes of antiparallel telomeric G-quadruplex d $(TTAGGG)_4$ with carboxymethyl tetracationic porphyrins. *Molecular Biology*, 47, 453-460, 2013.
93. Kumar, S., Foti, M., West, J., Schweitzer, B.I., Reed, M.W., Gamper, H.B., Gorn, V.V., Lukhtanov, E.A. and Meyer, R.B. Solution structure of a highly stable DNA duplex conjugated to a minor groove binder. *Nucleic. Acids. Res.*, 26, 831-838, 1998.
94. Kypr, J., Kejnovská, I., Renčiuk, D. and Vorlíčková, M. Circular dichroism and conformational polymorphism of DNA. *Nuc. Acid. Res.* 37, 1713-1725, 2009.
95. Lakowicz, J.R., Principles of Fluorescence Spectroscopy, third ed., Springer, New York, 2006.
96. Lane, A.N., Chaires, J.B., Gray, R.D. and Trent, J.O. Stability and kinetics of G-quadruplex structures. *Nucleic. Acids. Res.*, 36, 5482-5515, 2008.

97. Lee, S., Park, H.S., Notsu, Y., Ban, H.S., Kim, Y.P., Ishihara, K., Hirasawa, N., Jung, S.H., Lee, Y.S. and Lim, S.S. Effects of hyperin, isoquercitrin and quercetin on lipopolysaccharide-induced nitrite production in rat peritoneal macrophages. *Phytother. Res.*, 22, 1552-1556, 2008.
98. Levy, M.Z., Allsopp, R.C., Futcher, A.B., Greider, C.W. and Harley, C.B. Telomere end-replication problem and cell aging. *J. Mol. Biol.*, 225, 951-960, 1992.
99. Li, B., Oestreich, S. and de Lange, T. Identification of human Rap1: implications for telomere evolution. *Cell*, 101, 471-483, 2000.
100. Li, N., Ma, Y., Yang, C., Guo, L. and Yang, X. Interaction of anticancer drug mitoxantrone with DNA analyzed by electrochemical and spectroscopic methods. *Biophys. Chem.*, 116, 199-205, 2005.
101. Li, W., Zhang, M., Zhang, J.-l., Li, H.-q., Zhang, X.-c., Sun, Q. and Qiu, C.-m. (2006) Interactions of daidzin with intramolecular G-quadruplex. *FEBS letters*, 580, 4905-4910, 2006.
102. Li, Q., Xiang, J., Li, X., Chen, L., Xu, X., Tang, Y., Zhou, Q., Li, L., Zhang, H. and Sun, H. Stabilizing parallel G-quadruplex DNA by a new class of ligands: two non-planar alkaloids through interaction in lateral grooves. *Biochimie*. 91, 811-819, 2009.
103. Lin, S. and Struve, W.S. Solvatochromism and time-resolved fluorescence of the antitumor agent mitoxantrone and its analogs in solution and in DNA. *J. Phys. Chem.* 95, 2251-2256, 1991.
104. Lown, J.W. and Hanstock, C.C. High field 1H-NMR analysis of the 1: 1 intercalation complex of the antitumor agent mitoxantrone and the DNA duplex d $(CpGpCpG)_2$. *J. Biomol. Str. Dyn.* 2, 1097-1106, 1985.
105. Makarov, V.L., Hirose, Y. and Langmore, J.P. Long G tails at both ends of human chromosomes suggest a C strand degradation mechanism for telomere shortening. *Cell*, 88, 657-666, 1997.
106. Marathias, V.M., Wang, K.Y., Kumar, S., Pham, T.Q., Swaminathan, S. and Bolton, P.H. Determination of the number and location of the manganese binding sites of DNA quadruplexes in solution by EPR and NMR in the presence and absence of thrombin. *J. Mol. Biol.*, 260, 378-394, 1996.
107. Martino, L., Virno, A., Pagano, B., Virgilio, A., Di Micco, S., Galeone, A., Giancola, C., Bifulco, G., Mayol, L. and Randazzo, A.Structural and thermodynamic studies of the

interaction of distamycin A with the parallel quadruplex structure [d (TGGGGT)] $_4$. *J. Amer. Chem. Soc.*, 129, 16048-16056, 2007.

108. Masiero, S., Trotta, R., Pieraccini, S., De Tito, S., Perone, R., Randazzo, A. and Spada, G.P. A non-empirical chromophoric interpretation of CD spectra of DNA G-quadruplex structures. *Org. Biomol. Chem.*, 8, 2683-2692, 2010.
109. Mazzini, S., Mondelli, R. and Ragg, E. Structure and dynamics of intercalation complexes of anthracyclines with d $(CGATCG)_2$ and d $(CGTACG)_2$. 2D-^{1}H and ^{31}P NMR investigations. *J. Chem. Soc., Perkin Trans. 2*, 1983-1992, 1998.
110. Menichincheri, M., Ballinari, D., Bargiotti, A., Bonomini, L., Ceccarelli, W., D'Alessio, R., Fretta, A., Moll, J., Polucci, P. and Soncini, C. (2004) Catecholic flavonoids acting as telomerase inhibitors. *J. Med.Chem.* 47, 6466-6475, 2004.
111. Mergny, J.-L., Mailliet, P., Lavelle, F., Riou, J.-F., Laoui, A. and Hélène, C. The development of telomerase inhibitors: the G-quartet approach. *Anti-Cancer Drug Des.*, 14, 327-339, 1999.
112. Mita, H., Ohyama, T., Tanaka, Y. and Yamamoto, Y. Formation of a complex of 5, 10, 15, 20-tetrakis (N-methylpyridinium-4-yl)-21 H, 23 H-porphyrin with G-quadruplex DNA. *Biochemistry*, 45, 6765-6772, 2006.
113. Mitrasinovic, P., T Palakshan, P., Tripathi, S. and N Tripathi, A. On the Affinity and Specificity of Quercetin for DNA. *Medicinal Chemistry*, 9, 193-202, 2013.
114. Moore, M.J., Schultes, C.M., Cuesta, J., Cuenca, F., Gunaratnam, M., Tanious, F.A., Wilson, W.D. and Neidle, S. Trisubstituted acridines as G-quadruplex telomere targeting agents. Effects of extensions of the 3, 6-and 9-side chains on quadruplex binding, telomerase activity, and cell proliferation. *J. Med. Chem.*, 49, 582-599, 2006.
115. Monchaud, D., Allain, C., Bertrand, H., Smargiasso, N., Rosu, F., Gabelica, V., De Cian, A., Mergny, J.-L. and Teulade-Fichou, M.-P. Ligands playing musical chairs with G-quadruplex DNA: a rapid and simple displacement assay for identifying selective G-quadruplex binders. *Biochimie*, 90, 1207-1223, 2008.
116. Murat, P., Singh, Y. and Defrancq, E. Methods for investigating G-quadruplex DNA/ligand interactions. *Chem. Soc. Rev.*, 40, 5293-5307, 2011.
117. Nambiar, M., Goldsmith, G., Moorthy, B.T., Lieber, M.R., Joshi, M.V., Choudhary, B., Hosur, R.V. and Raghavan, S.C. Formation of a G-quadruplex at the BCL2 major

breakpoint region of the t (14; 18) translocation in follicular lymphoma. *Nucleic. Acids. Res.*, 39, 936-948, 2011.

118. Napolitano, J.G., Lankin, D.C., Chen, S.N. and Pauli, G.F. Complete 1H NMR spectral analysis of ten chemical markers of Ginkgo biloba. *Mag. Res. Chem.* 50, 569-575, 2012.
119. Nanjunda, R., Owens, E.A., Mickelson, L., Dost, T.L., Stroeva, E.M., Huynh, H.T., Germann, M.W., Henary, M.M. and Wilson, W.D. Selective G-Quadruplex DNA Recognition by a New Class of Designed Cyanines. *Molecules*, 18, 13588-13607, 2013.
120. Neidle, S. The structures of quadruplex nucleic acids and their drug complexes. *Curr. Opin. Struct. Biol.*, 19, 239-250, 2009.
121. Neidle, S. and Parkinson, G.N. Quadruplex DNA crystal structures and drug design. *Biochimie*, 90, 1184-1196, 2008.
122. Nickavar, B. and Amin, G.Enzyme assay guided isolation of an α-Amylase inhibitor flavonoid from Vaccinium arctostaphylos leaves. *Iran. J. Pharm. Res: IJPR*, 10, 849, 2011.
123. Norton, J.C., Piatyszek, M.A., Wright, W.E., Shay, J.W. and Corey, D.R. Inhibition of human telomerase activity by peptide nucleic acids. *Nature biotechnology*, 14, 615-619, 1996.
124. Otter, A., Lown, J.W. and Kotovych, G. Sequential assignments in deoxyribonucleotide tetramers by $^{31}P/^{1}H$ two-dimensional shift correlation NMR spectroscopy. *Magn. Reson. Chem.*, 24, 251-254, 1986.
125. Otter, A., Hanstock, C.C., Kotovych, G., Rayner, B., Vasseur, J.J., Imbach, J.-L. and Lown, J.W. *Mechanisms of DNA Damage and Repair*. Springer, pp. 211-218. 1996.
126. Ou, T.-M., Lu, Y.-J., Zhang, C., Huang, Z.-S., Wang, X.-D., Tan, J.-H., Chen, Y., Ma, D.-L., Wong, K.-Y. and Tang, J.C.-O. Stabilization of G-quadruplex DNA and down-regulation of oncogene c-myc by quindoline derivatives. *J. Med. Chem.*, 50, 1465-1474, 2007.
127. Paramasivan, S., Rujan, I. and Bolton, P.H. Circular dichroism of quadruplex DNAs: applications to structure, cation effects and ligand binding. *Methods*, 43, 324-331, 2007.
128. Parker, B.S., Cullinane, C. and Phillips, D.R. Formation of DNA adducts by formaldehyde-activated mitoxantrone. *Nucleic. Acids. Res.*, 27, 2918-2923, 1999.
129. Patel, D.J. Peptide antibiotic-oligonucleotide interactions. Nuclear magnetic resonance investigations of complex formation between actinomycin D and d-ApTpGpCpApT in aqueous solution. *Biochemistry*, 13, 2396-2402, 1974.

130. Patel, P., Bhavesh, N.S. and Hosur, R. NMR observation of a novel C-tetrad in the structure of the SV40 repeat sequence GGGCGG. *Biochem. Biophys. Res. Commun.*, 270, 967-971, 2000.

131. Patel, P. and Hosur, R. NMR observation of T-tetrads in a parallel stranded DNA quadruplex formed by Saccharomyces cerevisiae telomere repeats. *Nucleic. Acids. Res.*, 27, 2457-2464, 1999.

132. Patel, P.K., Koti, A. and Hosur, R. NMR studies on truncated sequences of human telomeric DNA: observation of a novel A-tetrad. *Nucleic. Acids. Res.*, 27, 3836-3843, 1999.

133. Perry, P.J., Read, M.A., Davies, R.T., Gowan, S.M., Reszka, A.P., Wood, A.A., Kelland, L.R. and Neidle, S. 2, 7-Disubstituted amidofluorenone derivatives as inhibitors of human telomerase. *J. Med. Chem.*, 42, 2679-2684, 1999.

134. Phan, A.T., Kuryavyi, V., Gaw, H.Y. and Patel, D.J. Small-molecule interaction with a five-guanine-tract G-quadruplex structure from the human MYC promoter. *Nat. Chem. Biol*, 1, 167-173, 2005.

135. Phan, A.T., Modi, Y.S. and Patel, D.J. Two-repeat *Tetrahymena* Telomeric d (TGGGGTTGGGGT) Sequence Interconverts Between Asymmetric Dimeric G-quadruplexes in Solution. *J. Mol. Biol.*, 338, 93-102, 2004.

136. Pristovšek, P., Sengupta, K., Löhr, F., Schäfer, B., von Trebra, M.W., Rüterjans, H. and Bernhard, F. Structural Analysis of the DNA-binding Domain of theErwinia amylovora RcsB Protein and Its Interaction with the RcsAB Box. *J. Biol. Chem.*, 278, 17752-17759, 2003

137. Ragazzon, P. and Chaires, J.B. Use of competition dialysis in the discovery of G-quadruplex selective ligands. *Methods*, 43, 313-323, 2007.

138. Ramirez, B.E., Antanasijevic, A. and Caffrey, M. Ligand Screening using NMR *Structural Genomics and Drug Discovery*. Springer, pp. 305-313, 2014.

139. Rangan, A., Fedoroff, O.Y. and Hurley, L.H. Induction of duplex to G-quadruplex transition in the c-myc promoter region by a small molecule. *J. Biol. Chem.*, 276, 4640-4646, 2001.

140. Ravindranath, M.H., Muthugounder, S., Presser, N. and Viswanathan, S. *Complementary and Alternative Approaches to Biomedicine*. Springer, pp. 121-165, 2004

141. Read, M., Harrison, R.J., Romagnoli, B., Tanious, F.A., Gowan, S.H., Reszka, A.P., Wilson, W.D., Kelland, L.R. and Neidle, S. Structure-based design of selective and potent

G quadruplex-mediated telomerase inhibitors. *Proc. Natl. Acad. Sci. U.S.A.*, 98, 4844-4849, 2001.

142. Read, M.A., Wood, A.A., Harrison, J.R., Gowan, S.M., Kelland, L.R., Dosanjh, H.S. and Neidle, S. Molecular modeling studies on G-quadruplex complexes of telomerase inhibitors: structure-activity relationships. *J. Med. Chem.* 42, 4538-4546, 1999.
143. Rezler, E.M., Seenisamy, J., Bashyam, S., Kim, M.-Y., White, E., Wilson, W.D. and Hurley, L.H. Telomestatin and diseleno-sapphyrin bind selectively to two different forms of the human telomeric G-quadruplex structure. *J. Am. Chem. Soc.* 127, 9439-9447, 2005.
144. Rosu, F., Gabelica, V., Poncelet, H. and De Pauw, E. Tetramolecular G-quadruplex formation pathways studied by electrospray mass spectrometry. *Nucleic. Acids. Res.*, 38, 5217-5225, 2010.
145. Saito, K., Tai, H., Hemmi, H., Kobayashi, N. and Yamamoto, Y.Interaction between the heme and a G-quartet in a heme–DNA complex. *Inorg. Chem.* 51, 8168-8176, 2012.
146. Searle, M.S., Hall, J.G., Denny, W.A. and Wakelin, L.P. NMR studies of the interaction of the antibiotic nogalamycin with the hexadeoxyribonucleotide duplex d (5'-GCATGC)$_2$. *Biochemistry*, 27, 4340-4349, 1988.
147. Shin-ya, K., Wierzba, K., Matsuo, K.-i., Ohtani, T., Yamada, Y., Furihata, K., Hayakawa, Y. and Seto, H. Telomestatin, a novel telomerase inhibitor from Streptomyces anulatus. *J. Am. Chem. Soc.* 123, 1262-1263, 2001.
148. Schultze, P., Macaya, R.F. and Feigon, J. Three-dimensional solution structure of the thrombin-binding DNA aptamer d (GGTTGGTGTGGTTGG). *J. Mol. Biol.* 235, 1532-1547, 1994.
149. Schultheiss, J., Kunert, O., Gase, U., Scharf, K.D., Nover, L. and Rüterjans, H. Solution Structure of the DNA-Binding Domain of the Tomato Heat-Stress Transcription Factor HSF24. *Eur. J. Biochem.* 236, 911-921, 1996.
150. Sen, D. and Gilbert, W. Formation of parallel four-stranded complexes by guanine-rich motifs in DNA and its implications for meiosis. Nature, 334, 364-366, 1988.
151. Sengupta, B., Pahari, B., Blackmon, L. and Sengupta, P.K. Prospect of bioflavonoid fisetin as a quadruplex DNA ligand: a biophysical approach. *PloS one*, 8, 65383., 2013
152. Seenisamy, J., Bashyam, S., Gokhale, V., Vankayalapati, H., Sun, D., Siddiqui-Jain, A., Streiner, N., Shin-Ya, K., White, E. and Wilson, W.D. Design and synthesis of an expanded

porphyrin that has selectivity for the c-MYC G-quadruplex structure. *J. Am. Chem. Soc.*127, 2944-2959, 2005.

153. Seenisamy, J., Rezler, E.M., Powell, T.J., Tye, D., Gokhale, V., Joshi, C.S., Siddiqui-Jain, A. and Hurley, L.H. The dynamic character of the G-quadruplex element in the c-MYC promoter and modification by TMPyP4. *J. Am. Chem. Soc.*, 126, 8702-8709, 2004.
154. Shafer R.H. Spectroscopic studies of the interaction of daunomycin with transfer RNA. *Biochem. Pharmacol*. 26, 1729, 1977.
155. Siddiqui-Jain, A., Grand, C.L., Bearss, D.J. and Hurley, L.H. Direct evidence for a G-quadruplex in a promoter region and its targeting with a small molecule to repress c-MYC transcription. *Proc. Nat. Acad. Sci.* 99, 11593-11598, 2002.
156. Sidhu, O., Annarao, S., Chatterjee, S., Tuli, R., Roy, R. and Khetrapal, C. Metabolic alterations of Withania somnifera (L.) Dunal fruits at different developmental stages by NMR spectroscopy. *Phytochem. Anal.*. 22, 492-502, 2011.
157. Singh, M.P., Joseph, T., Kumar, S., Bathini, Y. and Lown, J.W. Synthesis and sequence-specific DNA binding of a topoisomerase inhibitory analog of Hoechst 33258 designed for altered base and sequence recognition. *Chem. Res. Toxicol.* 5, 597-607, 1992
158. Singh, S., Patel, P. and Hosur, R. Structural polymorphism and dynamism in the DNA segment GATCTTCCCCCCGGAA: NMR investigations of hairpin, dumbbell, nicked duplex, parallel strands, and i-motif. *Biochemistry*. 36, 13214-13222, 1997.
159. Singhal, G. and Rajeswari, M.R. Interaction of Actinomycin D with Promoter Element of c-met and Its Inhibitory Effect on the Expression of c-Met. *J. Biomol. Struct. Dyn.* 26, 625-636, 2009.
160. Singhal, G. and Rajeswari, M.R. Molecular Aspects of the Interaction of Hoechst-33258 with GC-Rich Promoter Region of c-met. *DNA and cell biology*, 29, 91-100, 2010.
161. Singhal, G. and Rajeswari, M.R. Preferential binding of anti-cancer drug adriamycin to the Sp1 binding site in *c-met* promoter region: A spectroscopic and molecular modeling study. *Journal of Molecular Structure*, 920, 208-213, 2009.
162. Smith, F.W. and Feigon, J. Strand orientation in the DNA quadruplex formed from the *Oxytricha* telomere repeat oligonucleotide d (G4T4G4) in solution. *Biochemistry*, 32, 8682-8692, 1993.

163. Smith, P.J., Morgan, S.A., Fox, M.E. and Watson, J.V. Mitoxantrone-DNA binding and the induction of topoisomerase II associated DNA damage in multi-drug resistant small cell lung cancer cells. *Biochem. Pharmacol.* 40, 2069-2078, 1990.

164. Smith, F.W., Schultze, P. and Feigon, J. Solution structures of unimolecular quadruplexes formed by oligonucleotides containing Oxytricha telomere repeats. *Structure*, 3, 997 – 1008, 1995.

165. Solimani, R. Quercetin and DNA in solution: analysis of the dynamics of their interaction with a linear dichroism study. *Int. J Biol. Macromol.* 18, 287-295, 1996.

166. Solimani, R., Bayon, F., Domini, I., Pifferi, P.G., Todesco, P.E., Marconi T.G. and Samori, B. Flavonoid-DNA interaction studied with flow linear dichroism technique. *J. Agric. Food Chem.* 43, 876-882, 1995.

167. Spencer, J., Kuhnle, G., Williams, R. and Rice-Evans, C. Intracellular metabolism and bioactivity of quercetin and its in vivo metabolites. *Biochem. J*, 372, 173-181, 2003.

168. Strahl, C. and Blackburn, E.H. Effects of reverse transcriptase inhibitors on telomere length and telomerase activity in two immortalized human cell lines. *Mol. Cell. Biol.* 16, 53-65, 1996.

169. Sun, D., Thompson, B., Cathers, B.E., Salazar, M., Kerwin, S.M., Trent, J.O., Jenkins, T.C., Neidle, S. and Hurley, L.H. Inhibition of human telomerase by a G-quadruplex-interactive compound. *J. Med. Chem.*, 40, 2113-2116, 1997.

170. Sun, H., Tang, Y., Xiang, J., Xu, G., Zhang, Y., Zhang, H. and Xu. L. Spectroscopic studies of the interaction between quercetin and G-quadruplex DNA. *Bioorg. Med. Chem. Lett.*, 16, 3586-3589, 2006.

171. Sun, H., Xiang, J., Tang, Y. and Xu, G. Regulation and recognization of the extended G-quadruplex by rutin. *Biochem. Biophys. Res. Commun*. 352, 942–946, 2007.

172. Topal, M.D. and Fresco, J.R. Complementary base pairing and the origin of substitution mutations. 1976

173. van de Sande, J.H., Ramsing, N.B., Germann, M.W., Elhorst, W., Kalisch, B.W., Von Kitzing, E., Pon, R.T., Clegg, R.C. and Jovin, T.M. Parallel stranded DNA. *Science*, 241, 551-557, 1988.

174. Wallace, R.E., Murdock, K., Angier, R.B. and Durr, F.E. Activity of a novel anthracenedione, 1, 4-dihydroxy-5, 8-bis {{{2-[(2-hydroxyethyl) amino] ethyl} amino}}-9,

10-anthracenedione dihydrochloride, against experimental tumors in mice. *Can. Res.*, 39, 1570-1574, 1979.

175. Wan, C., Cui, M., Song, F., Liu, Z. and Liu, S. A study of the non-covalent interaction between flavonoids and DNA triplexes by electrospray ionization mass spectrometry. *Int. J. Mass Spec.*, 283, 48-55, 2009.
176. Wang, Y. and Patel, D.J. Solution structure of the *Tetrahymena* telomeric repeat d $(T_2G_4)_4$ G-tetraplex. *Structure*, 2, 1141-1156, 1994.
177. Wang, Y. and Patel D.J. Solution structure of a parallel-stranded G-quadruplex DNA. *J. Mol. Biol.* 1993, 234, 1171 - 1183.
178. Wang, Y. and Patel, D.J. Guanine residues in d (T2AG3) and d (T2G4) form parallel-stranded potassium cation stabilized G-quadruplexes with anti glycosidic torsion angles in solution. *Biochemistry*, 31, 8112-8119, 1992.
179. Webb, M. and Ebeler, S. Comparative analysis of topoisomerase IB inhibition and DNA intercalation by flavonoids and similar compounds: structural determinates of activity. *Biochem. J*, 384, 527-541, 2004.
180. Webba da Silva M. Association of DNA quadruplexes through G,C,G,C tetrads. Solution structure of d(GCGGTGGAT). *Biochemistry*, 2003, 42, 14356 - 14365.
181. Wei, C., Han, G., Jia, G., Zhou, J. and Li, C. Study on the interaction of porphyrin with G-quadruplex DNAs. *Biophys. Chem.*, 137, 19-23, 2008.
182. Wheelhouse, R.T., Sun, D., Han, H., Han, F.X. and Hurley, L.H. Cationic porphyrins as telomerase inhibitors: the interaction of tetra-(N-methyl-4-pyridyl) porphine with quadruplex DNA. *J. Am. Chem. Soc.* 120, 3261-3262, 1998.
183. White, E.W., Tanious, F., Ismail, M.A., Reszka, A.P., Neidle, S., Boykin, D.W. and Wilson, W.D. Structure-specific recognition of quadruplex DNA by organic cations: influence of shape, substituents and charge. *Biophys. Chem.*, 126, 140-153, 2007.
184. Williamson, J.R., Raghuraman, M. and Cech, T.R. Monovalent cation-induced structure of telomeric DNA: the G-quartet model. *Cell*, 59, 871-880, 1989.
185. Williamson, J.R. G-quartet structures in telomeric DNA. *Ann. Rev. Biophy. Biomol. Struc.* 23, 703-730, 1994.
186. Williamson. M. P, Use of chemical shift perturbation to characterize ligand binding. *Prog. Nucl. Mag. Res. Spectroscopy*, 13, 1-16, 2013.
187. Wilson and Jones, Biopolymers 1986

188. Wilson, W.D., Ratmeyer, L., Zhao, M., Strekowski, L. and Boykin, D. The search for structure-specific nucleic acid-interactive drugs: effects of compound structure on RNA versus DNA interaction strength. *Biochemistry*, 32, 4098-4104, 1993.

189. Wilson, W.D., Tanious, F.A., Barton, H.J., Jones, R.L., Fox, K., Wydra, R.L. and Strekowski, L. DNA sequence dependent binding modes of 4', 6-diamidino-2-phenylindole (DAPI). *Biochemistry*, 29, 8452-8461, 1990.

190. Wilson, W.D. and Jones, R.L. Interaction of actinomycin D, ethidium quinacrine daunorubicin, and tetralysine with DNA: ^{31}P NMR chemical shift and relaxation investigation. *Nucleic Acids. Res*. 10, 1399-1410. 1982.

191. Wright, W.E., Tesmer, V.M., Huffman, K.E., Levene, S.D. and Shay, J.W. Normal human chromosomes have long G-rich telomeric overhangs at one end. *Genes Develop*. 11, 2801-2809, 1997.

192. Xue, Y., Kan, Z.-y., Wang, Q., Yao, Y., Liu, J., Hao, Y.-h. and Tan, Z. Human telomeric DNA forms parallel-stranded intramolecular G-quadruplex in K+ solution under molecular crowding condition. *J. Am. Chem. Soc.*, 129, 11185-11191, 2007.

193. Ye, J.Z.-S., Hockemeyer, D., Krutchinsky, A.N., Loayza, D., Hooper, S.M., Chait, B.T. and de Lange, T. POT1-interacting protein PIP1: a telomere length regulator that recruits POT1 to the TIN2/TRF1 complex. *Genes & development*, 18, 1649-1654, 2004.

194. Zahler, A.M., Williamson, J.R., Cech, T.R. and Prescott, D.M. Inhibition of telomerase by G-quartet DMA structures. *Nature*, 350, 718-720, 1991.

195. Zhang, J.-l., Fu, Y., Zheng, L., Li, W., Li, H., Sun, Q., Xiao, Y. and Geng, F. Natural isoflavones regulate the quadruplex–duplex competition in human telomeric DNA. *Nucl. Acid. Res.* 37, 2471-2482, 2009.

196. Zhang, H., Wang, X., Wang, P., Pang, S., Ai, X. and Zhang, J. Interactions between meso-tetrakis (4-(N-methylpyridiumyl)) porphyrin TMPyP4 and DNA G-quadruplex of telomeric repeated sequence TTAGGG. *Science in China Series B: Chemistry*, 51, 452-456, 2008.

197. Zhang, W.-J., Ou, T.-M., Lu, Y.-J., Huang, Y.-Y., Wu, W.-B., Huang, Z.-S., Zhou, J.-L., Wong, K.-Y. and Gu, L.-Q. 9-Substituted berberine derivatives as G-quadruplex stabilizing ligands in telomeric DNA. *Bioorg. Med. Chem.* 15, 5493-5501, 2007.

198. Zheng, S., Chen, Y., Donahue, C.P., Wolfe, M.S. and Varani, G. Structural basis for stabilization of the tau pre-mRNA splicing regulatory element by novantrone (mitoxantrone). *Chem. biol.* 16, 557-566, 2009.

199. Zhong, Z., Shiue, L., Kaplan, S. and de Lange, T. A mammalian factor that binds telomeric TTAGGG repeats in vitro. *Mol. Cell. Bio.* 12, 4834-4843, 1992.